Stem cell-derived Retinal Pigment Epithelium Models of Lysosomal Dysfunction in Disease

MARIA HELENA SEQUEIRA CARDOSO

Tese para obtenção do grau de Doutor em Mecanismos de Doença e Medicina Regenerativa

na NOVA Medical School | Faculdade de Ciências Médicas

Junho de 2018

STEM-CELL DERIVED RETINAL PIGMENT EPITHELIUM MODELS OF LYSOSOMAL DYSFUNCTION IN DISEASE

Maria Helena Sequeira Cardoso

Orientador: Miguel Seabra, Professor MD PhD

Orientadora: Sara Maia; PhD

Orientadora: Teresa Barona, PhD

Tese para obtenção do grau de Doutor em Mecanismos de Doença e Medicina Regenerativa

Junho de 2018

Stem cell-derived Retinal Pigment Epithelium Models of Lysosomal Dysfunction in Disease

Most of this work was developed at CEDOC, Chronic Diseases Research Centre, NOVA Medical School|Faculdade de Ciências Médicas, Universidade NOVA de Lisboa, Portugal, under supervision of Miguel Seabra, Sara Maia, and Teresa Barona. Part of the work was developed together with Michael Hall and Clare Futter, at the UCL Institute of Ophthalmology, London, UK.

The opinions expressed in this publication are from the exclusive responsibility of the author. Mª Helena Cardoso was financially supported through a scholarship from ProRegeM, doctoral program on Mechanisms of Disease and Regenerative Medicine, a collaboration between CEDOC|NMS UNL and CBMR-UAlg, by the Portuguese Foundation for Science and Technology (PD/BD/52422/2013).

Se podes olhar, vê. Se podes ver, repara.
José Saramago

Acknowledgements

This thesis would not be possible without the contribution, support and friendship of many people:

First and foremost, to my supervisors, Sara and Miguel. To Sara, for all that you taught me and for all your support, and to Miguel for all the reassurance, guidance and scientific insight. Thank you for all the opportunities and encouragement to go learn at other labs, not just for the science, but also for the personal growth that comes with those experiences. And thank you for making me feel welcome back too. Your infectious enthusiasm about cell biology effectively turned me into an RPE engineer.

To FCT (Fundação para a Ciência e Tecnologia), my fellowship and the six months abroad were essential for this project to be possible.

To all the people who composed the initial group I integrated: José Ramalho, Catarina Sequeira, Firmina Lebre, Melissa Rocha and Augusta Marques. Thank you for all your help, for all you taught me and for showing me around the lab. For the companionship over coffee or serial PCRs and westerns, for the support and complicity on bad-mood days and inspirational everlasting strength.

To all the people who compose the Molecular Mechanisms of Disease group now, specially to Sandra Tenreiro, Ana Sofia Falcão, Cristina Escrevente, Gabriela Santos and Teresa Barona. Thank you for all the important input and suggestions, for all the experiments we did together, for the great group environment and for our team-building meetings. I truly believe great work and long-lasting friendship will come out of this group.

To Clare Futter, for welcoming me at the IoO UCL, and to Michael Hall for showing me around the lab. Thank you for all your contributions to this work, for your scientific insight and helpful discussions. And to all people who provided such a good working environment there.

To the people at the Clegg Lab at UCSB, specially to Cassidy Arnold, for all you taught me about stem cell culture and RPE differentiation.

To all.CEDOC, for the institutional support (though not always straight forward), but most importantly to all the researchers that make it work by the end of the day. Research in Portugal is taken for granted - we do have genuine reason to protest. Still, inspirational people continue to endure and persist, effectively uprising Universities' rankings and teaching future researchers that science is worth doing, even in a sometimes hostile environment.

To the ProRegeM direction, thank you for this PhD opportunity, for all the encouragement along the way and for the help in mediating conversations with NMS.

To my PhD external advisors, for the helpful suggestions and support.

To the CEDOC PhD students and to the Post-Docs for all the shared moments at the students retreat, at casual fridays and for the occasional hallway discussions.

Às minhas amigas dos almoços e das conversas no lab ou na mosca: Ana Soares e Cláudia Pereira, aquelas que procuro na hora de ir embora porque já chega de CEDOC por hoje. Aos ProRegeMies 10%, os mais promissores. Às minhas Toxscreen business partners Aline Marinho, Margarida Correia e Susana Rodrigues. Por todas as frustrações partilhadas, por todo o drama e bom humor gerado nos passeios pela Ria Formosa.

Aos meus amigos de antes e de sempre, por todo o apoio e por todos os nossos momentos partilhados, mesmo quando separados. Àqueles que agora reencontro nas férias, nas defesas de doutoramento e nos casamentos e que tornam bons até esses eventos demasiado formais.

À minha família. Continuo feliz por ter nascido. E tomar conta de células não tem a mesma piada que correr atrás do sobrinho. Obrigada por todo o apoio e incentivo.

Ao Zé Catota, como sempre: obrigada pela paciência, pelo companheirismo e cumplicidade e por tudo o resto.

É bom também ter contrariedades,

Sem nunca perder a fantasia.

Tentar,

Falhar,

Sofrer,

Perder um tempo a duvidar. . .

Dobrar o empenho e a humildade.

É, pintar cada momento de alegria!

Ver que a chuva parou, o melro assobiou

Vá, deixem lá contagiar-se, que eu estou pronto pra ganhar o dia!

Diabo na Cruz

Abstract

Retinal degenerative disorders are the leading cause of vision impairment in developed countries. In many cases, photoreceptor degeneration occurs as a consequence of Retinal Pigment Epithelium (RPE) dysfunction. This is the case of Age-related Macular Degeneration (AMD) where progressive degeneration typically occurs, stemming from inadequate maintenance of the RPE cells. A crucial feature of this internal preservation is the ability to properly degrade and/or recycle the protein- and lipid- content which result from daily processing of Photoreceptor Outer Segments (POS). Degradation and recycling of cellular components are the main responsibilities attributed to lysosomes and remarkably, many age-related diseases stem from improper lysosomal health.

Human Pluripotent Stem cells (hPSc) can be used as starting material to obtain reliable *in vitro* models of human RPE, providing direct access to identification of the initial events of many retinal degenerative diseases. Stem cell proliferation potential is virtually limitless, therefore hPSc differentiation into RPE paves the way for the standard production of reliable human RPE lines, without the hurdles of available, but unreliable RPE cell lines or the hardships of establishing RPE primary cultures.

The present work focuses on the development and characterization of a human RPE *in vitro* model, derived from pluripotent stem cells, with the ultimate goal of studying retinopathies' early events. This model was then used to explore the importance of the lysosome in intracellular cargo processing and the role of lysosomal dysfunction in age-related disorders, in particular in the case of AMD.

Accordingly, a stem cell differentiation protocol was optimized and a comprehensive characterization of the obtained hPSc-RPE cells was performed. Based on this cellular model, POS-induced lysosomal dysfunction is proposed as a tool, which can be used to recapitulate AMD disease features.

Furthermore, a drug-based model featuring chloroquine-induced hPSc-RPE degeneration through lysosomal dysfunction was establish and characterized. In particular, cells were subjected to extended time-course chloroquine treatments and lysosomal function was thoroughly characterized. Specifically, cells were submitted to acute, continued and chronic treatments and shown to respond differently throughout these time courses. Firstly, chloroquine (CQ) dosage was titrated, based on viability assays, in order to establish under-lethal regimens considering experimental temporal settings. Nuclear translocation of lysosome-regulator transcription factors was verified. Moreover, a thorough characterization featuring relevant lysosomal properties was covered, including

their ability to degrade phagocytic, endocytic and autophagy cargoes, their cathepsin proteolytic activity and luminal acidity. Furthermore, lysosomal exocytosis was verified upon CQ treatment and, upon study of the RPE ultrastructure, is suggested as a key disease initiation event. Whenever possible, results obtained with hESc-RPE were repeated using primary RPE cell lines, human and porcine, reinforcing and extrapolating crucial findings to general RPE cell biology.

Ultimately, RPE cellular models were shown to recapitulate crucial features of age-related retinal degeneration, in particular, subcellular deposit formation, which constitutes the defining feature underlying AMD's early events.

Additionally, in the supplementary material, a side-project developed throughout the course of the PhD is presented. Specifically, this study regards VEGF regulation in a mouse RPE line, and in particular VEGF titration by Rab-regulated endocytic trafficking of the $VEGFR_2$.

Overall, this study opens new avenues to explore *in vitro* cellular models of RPE to dissect the molecular mechanisms of degeneration and also to explore new therapeutic approaches aiming to restore lysosomal function and ultimately pave the way for *in vivo* studies.

Keywords: Retinal Pigment Epithelium, differentiation, pluripotent stem cells, degeneration, cell-based models, lysosome dysfunction.

Resumo

As doenças degenerativas da retina são as principais responsáveis pela perda de visão, nos países desenvolvidos. Frequentemente, a degeneração dos fotorrecetores ocorre devido à perda de função do Epitélio Pigmentar da Retina (RPE). A Degenerescência Macular relacionada com a idade (DMI) é uma doença degenerativa da área central da retina (mácula) que provoca uma perda progressiva da visão central. Pensa-se que a disfunção do RPE está na origem desta doença. Em particular, pensa-se que a conservação da função lisossomal destas células é de extrema importância no contexto de doença. O RPE é responsável por degradar e reutilizar componentes celulares, como proteínas e lípidos, que resultam do processamento diário dos terminais dos fotorrecetores, necessários ao bom funcionamento celular e ao processo visual. O declínio da função lisossomal tem sido apontado como estando envolvido numa série de doenças crónicas relacionadas com a idade.

As células estaminais pluripotentes (hPSc) podem ser usadas como matéria prima para obter modelos de RPE *in vitro* fiáveis, que permitem ter acesso direto para identificar os mecanismos iniciais de doenças degenerativas da retina. O potencial de proliferação das células estaminais é praticamente ilimitado, pelo que a diferenciação destas células para RPE permite estabelecer uma produção sistemática de linhas humanas de RPE. Isto permite ultrapassar obstáculos existentes com as linhas de RPE disponíveis menos fiáveis ou mais difíceis de obter por culturas primárias.

O trabalho aqui apresentado visou o desenvolvimento e a caracterização de um modelo *in vitro* de RPE derivado de células estaminais pluripotentes, com o objetivo final de estudar os eventos que estão na origem das retinopatias. Este modelo foi usado para explorar a importância da função lisossomal no processamento de material intracelular e, sobretudo, o papel da disfunção lisossomal em doenças do envelhecimento, com particular ênfase na DMI.

Assim, foram otimizados protocolos de diferenciação de células estaminais em RPE e as células obtidas (hPSc-RPE) foram caracterizadas em detalhe. Baseado neste modelo celular, a disfunção lisossomal causada pelo processamento dos terminais externos dos fotorrecetores é proposta aqui como ferramenta de estudo, por reproduzir características chave da DMI.

Para além disso, foi também implementado e caracterizado um modelo de disfunção lisossomal farmacológico, com base no tratamento de hPSc-RPE com cloroquina. Em

particular, as células foram submetidas a regimes prolongados de exposição a este fármaco e a função lisossomal foi avaliada em vários períodos de estímulo. Nomeadamente, as células foram sujeitas a tratamentos agudos, continuados ou crónicos e foram demonstradas respostas diferenciadas, consoante os intervalos avaliados. Em primeiro lugar, as doses de cloroquina foram estabelecidas, com base em ensaios de viabilidade, de forma a escolher um regime não letal para as células, durante os tempos de estudo. Posteriormente, foi verificada a translocação nuclear de fatores de transcrição reguladores da função lisossomal. De seguida, as propriedades características dos lisossomas foram avaliadas, incluindo a capacidade de degradação de cargas fagocíticas, endocíticas e provenientes de autofagia, a atividade proteolítica das catepsinas e a acidez luminal. Para além disso, observou-se exocitose de lisossomas após tratamento com cloroquina, e com base na ultraestrutura do RPE, foi proposto que este seja um evento chave no desenvolvimento de doença. Vários dos resultados obtidos com hPSc-RPE foram confirmados em linhas primárias de RPE, humanas e de porco, de forma a reforçar e extrapolar as conclusões do estudo e relacionar com a biologia celular do RPE em geral.

Por fim, os modelos celulares de RPE demonstraram reproduzir caraterísticas fundamentais de doenças degenerativas da retina relacionadas com o envelhecimento, nomeadamente com o aparecimento de depósitos subcelulares, tipicamente usados como identificadores de DMI.

Adicionalmente, na secção de material suplementar, é apresentado um trabalho complementar, desenvolvido durante o percurso do doutoramento. Este trabalho consiste em estudos sobre o fator de crescimento endotelial vascular (VEGF) e sobre a sua regulação por parte de proteínas Rab do tráfego intracelular do recetor $VEGFR_2$.

Globalmente, este estudo abre portas a novas perspetivas para explorar modelos celulares de RPE, de forma a dissecar os mecanismos moleculares de degeneração por detrás das doenças da retina. Para além disso, os modelos aqui desenvolvidos têm o potencial para serem utilizados para estudar novas abordagens terapêuticas, de forma a restaurar a função lisossomal, e abrir caminho para estudos *in vivo*.

Palavras-chave: Epitélio Pigmentar da Retina, diferenciação, células estaminais pluripotentes, modelos celulares de doença, disfunção lisossomal.

Publications

The work described herein resulted in the following outputs.

Presenting author is highlighted in bold. Contributions from this thesis's author are underlined.

Papers in Peer-reviewed International Scientific Journals

Cardoso MH, Hall M, Falcão AS, Escrevente C, Santos G, Tenreiro S, Futter CE, Seabra MC, *Chloroquine-induced hESc-RPE Model of Lysosomal Dysfunction* (Manuscript in preparation)

Cardoso MH, Rodrigues IP, Maia S, Pires CF, Portal MD, Strauss O, Seabra MC, Ramalho JS, *VEGF titration by RabGTPase-regulated trafficking of VEGFR2 in RPE* (Manuscript in preparation)

Oral Communications

Hall M, Cardoso MH, Falcão AS, Escrevente C, Tenreiro S, Wavre S, Meschede I, Burgoyne T, Seabra MC, **Futter CE**, *Modelling lysosome dysfunction in the retinal pigment epithelium in early AMD*, Pro-retina Meeting 2018, Germany, Apr 2018

Cardoso MH, Tenreiro S, Falcão AS, Escrevente C, Seabra MC. *Planning WP4 – Biological validation of BrM and CVN models*, Biomembrane Consortium Meeting, Warsaw, Poland, Mar 2018

Cardoso MH, Hall M, Futter CE, Seabra MC. *hESc-derived RPE: model of Lysosome Dysfunction*, ProRegeM Annual Meeting, CEDOC/NMS UNL, Dec 2017.

Cardoso MH, Hall M, Futter CE, Seabra MC. *hESc-derived RPE: model of Lysosome Dysfunction*, CEDOC Casual Friday with Science Seminar, Nov 2017.

Cardoso MH, Hall M, Futter CE, Seabra MC. *Retinal Pigment Epithelium cell-based therapies and Disease Mechanisms*, II Retiro de Estudantes de Doutoramento do CEDOC, Sep 2017

Cardoso MH, Tenreiro S, Falcão AS, Escrevente C, Seabra MC. *Biological validation of BrM and CVN models*, Biomembrane Consortium Meeting, Pisa, Italy, Sep 2017

Cardoso, MH, *Retinal Pigment Epithelium cell-based therapies and Disease Mechanisms*, ProRegeM Annual Meeting, CEDOC/NMS UNL, Jan 2017

Cardoso, MH, *Retinal Pigment Epithelium cell-based therapies and Disease Mechanisms*, II Retiro de Estudantes de Doutoramento do CEDOC, Sep 2016

Cardoso MH, Maia S, Ramalho J, Barona T, Seabra MC, *Differentiation Of Human Embryonic Stem Cells Into Retinal Pigment Epithelium*, 19th Symposium of Biology Students in Europe – SymBioSE, Jul 2016, Vila Real, Portugal

M. Rocha, S. Maia, D. Santos, MH. Cardoso, J. Ramalho, M. Martins, M. Seabra & T. Barona, *Image software and statistical analysis applied to expression of RAB25 in breast cancer,* International Conference on Clinical and BioEngineering for Women's Health, Porto, Portugal, 2015

Cardoso MH, *Reprogramming Fibroblasts into Retinal Pigment Epithelium cells*, ProRegeM Annual Meeting, University of Algarve, Portugal, 2015

Poster Presentations

Cardoso MH, Hall M, Falcão AS, Escrevente C, **Tenreiro S**, Futter CE, Seabra MC, *Lysosomal dysfunction in the retinal pigmented epithelium and the pathogenesis of age-related macular degeneration,* 2nd Small Meeting on Endocytic Trafficking and Signaling, Braga, Portugal, July 2018

Hall M, Falcão AS, Escrevente C, Cardoso MH, Santos G, Tenreiro S, Futter CE, **Seabra MC**, *Lysosomal dysfunction in the retinal pigmented epithelium and the pathogenesis of age-related macular degeneration*, Gordon Research Conference on Lysosomes and Endocytosis, Andover, United States, Jun 2018

Cardoso MH, Hall M, Falcão AS, Escrevente C, Tenreiro S, Futter CE, Seabra MC, *hESc-derived RPE model of chronic lysosome dysfunction*, Embo Lysosomes and Metabolism workshop, Naples, Italy, May 2018

Falcão AS, Escrevente C, Cardoso MH, Santos G, Tenreiro S, Seabra MC, *Using photoreceptor outer segments autofluorescence to measure lysosomal dysfunction in pig and human retinal pigmented epithelial cells*, Embo Lysosomes and Metabolism workshop, Naples, Italy, May 2018

Hall M, Cardoso MH, Falcão AS, Escrevente C, Tenreiro S, Seabra MC, Futter CE, *Modelling lysosome dysfunction in the retinal pigment epithelium in the development of early AMD*, Institute of Ophthalmology Meeting 2018, London, UK, Apr 2018

Contents

CHAPTER 2

CHAPTER 3

List of Figures

List of Tables

Abbreviations

AD	Alzheimer´s Disease
AMD	Age-related Macular Degeneration
AMPK	AMP-activated protein kinase
Atg	Autophagy-related Protein
ATP	Adenosine Triphosphate
b-hex	ß-hexosaminidase
Baf/ Baf A1	Bafilomycin A1
Best	Bestrophin
BMP	Bone Morphogenic Protein
BrM	Bruch's Membrane
BSA	Bovine Serum Albumin
CatB/L/D	Cathepsin B/L/D
CHM	Choroideremia
CLEAR	Coordinated Lysosomal Expression and Regulation
CNS	Central Nervous System
CNV	Choroidal Neovascularization
ConcA	Concanamycin A
CQ	Chloroquine
CRALBP (or RLBP1)	Retinaldehyde-Binding Protein 1
DKK1	Dickkopf-related protein 1
DMEM	Dulbecco's Modified Eagle Medium
DNA	Deoxyribonucleic Acid
ECM	Extracellular Matrix
EE	Early Endosomes
ELISA	Enzyme-linked Immunosorbent Assay
EM	Electron Microscopy

FBS	Fetal Bovine Serum
FGF	Fibroblast Growth Factor
GA	Gluteraldehyde
GFP	Green Fluorescent Protein
hESc	human Embryonic Stem cells
HIF1α	Hypoxia-inducible factor 1-alpha
hiPSc	induced Pluripotent Stem cells
hPSc	human Pluripotent Stem cells
IF	Immunofluorescence
IGF1	Insulin Growth Factor 1
LAMP	Lysosome-associated Membrane Protein
LAP	LC3 Associated Phagocytosis
LC3	Microtubule-associated Proteins 1A/1B light chain 3
LDH	Lactate Dehydrogenase
LE	Late Endosomes
Lonza hRPE	human fetal RPE purchased from Lonza
LROs	Lysosome-related Organelles
LSD	Lysosomal Storage Disorder
LT	LysoTracker
LYNUS	Lysosomal Nutrient Sensing
M6PR	Mannose-6-Phosphate Receptors
MAPK1/ERK2	Mitogen-activated protein kinase 1
MEFs	Mouse Embryonic Fibroblasts
MerTK	tyrosine-protein kinase Mer
miRNA	micro Ribonucleic acid
MiT/TFE	Microphthalmia Family of Transcription Factors.
MITF	Microphthalmia-associated Transcription Factor
MRed	Magic Red
mTORC	mammalian Target of Rapamycin Complex
MVBs	Multivesicular Bodies
NIC	Nicotinamide
NPC	Niemann-Pick Type C
OTX1/2	Homeobox protein1/2

PAX6	Paired box protein Pax-6
PBS	Phosphate Buffered Saline
PD	Parkinson´s disease
PEDF	Pigment Epithelium Derived Factor
PenStrep	Penicillin Streptomycin
PFA	Paraformaldehyde
Pi(n)P	Phosphoinositide (n) Phosphate
POS	Photoreceptor Outer Segments
pRPE	porcine RPE
RA	Retinoic Acid / Rheumatoid Arthritis
Rap	Rapamycin
RCS	Royal College of Surgeons
RDM	Retinal Differentiation Medium
RNA	Ribonucleic acid
RPE	Retinal Pigment Epithelium
SD	Standard Deviation
SFEB	Serum-free Embryoid Body
Shh	Sonic Hedgehog
SLE	Systemic Lupus Erythematosus
SNARE	SNAP (Soluble NSF(N-ethylmaleimide-sensitive factor) Attachment Protein) REceptor
SQSTM1	Sequestosome 1
TEER or TER	Transepithelial Electrical Resistance
TFEB	Transcription Factor EB
TFs	Transcription Factors
TGFβ	Transforming growth factor beta
TRPML	transient receptor potential cation channel, mucolipin
TYR	Tyrosinase
TYRP1	Tyrosinase-related Protein 1
vATPase	vacuolar ATPase
VEGF	Vascular Endothelial Growth Factor
VIP	Vasoactive Intestinal Peptide
ZO-1	Zonula Occludens 1

CHAPTER 1

Introduction

Age-related disorders often result from a combination of factors, still many chronic and late onset diseases share common mechanisms of cellular homeostasis dysregulation. Many times these diseases manifest in post-mitotic cells, due to accumulation of problems through time, up to a state with which the cell can no longer cope.

This thesis focuses on a particular post-mitotic cell type – the Retinal Pigment Epithelium – and on the molecular mechanisms of disease associated with age-related blinding disorders, namely Age-related Macular Degeneration. Human Pluripotent Stem cells were used to generate an in-vitro *model of RPE. This model was then used to study Lysosomal Dysfunction, which is proposed here as a key mechanism for retinal degenerative disease onset and progression.*

1.1 Eye structure and visual function

The vertebrate eye represents an inspiring structure, when it comes to demonstrate the great importance of vision as a selective evolutionary advantage. Comprehensive studies across a wide range of vertebrate species have demonstrated the conservation of traits from the last common ancestor of all jawed vertebrates ~400 million years ago (Kevany et al. 2010; Fuhrmann 2010).

The vertebrate eye is composed by the optic apparatus (cornea, lens and iris), the photosensitive layer (photoreceptors: rods and cones), and a light absorbing and nurturing layer (Retinal Pigment Epithelium or RPE and choroid). The cornea functions as a window to the eye, allowing light to penetrate; smooth muscle constitutes the iris and allows for a regulated opening of the pupil, and consequently more or less light to enter; light is then focused by the lens, passes through the eye ball filling vitreous humor and hits the retina, at the back of the eye.

1.1.1 The retina and the Retinal Pigment Epithelium

The human retina is constituted by an inner neural layer, with millions of photoreceptors which convert light energy into nerve impulses, and an outer pigmented layer, composed of RPE cells, which absorbs scattered light. Besides the photoreceptors, the neural layer contains other neurons: ganglion cells, whose axons weave together to form the optic nerve; bipolar cells, which have synapses at both ends and establish a bridge between photoreceptors and ganglion cells; amacrine cells, which connect with bipolar and ganglion cells; and horizontal cells, connected laterally to adjust photoreceptors' outputs in order to adapt vision to both bright and dim light. Glia cells, namely müller cells are also present in the neural retina, maintaining homeostasis of the retina, by controlling angiogenesis and releasing neurotrophic factors. A schematic representation of the retina, depicted in Figure 1. 1.

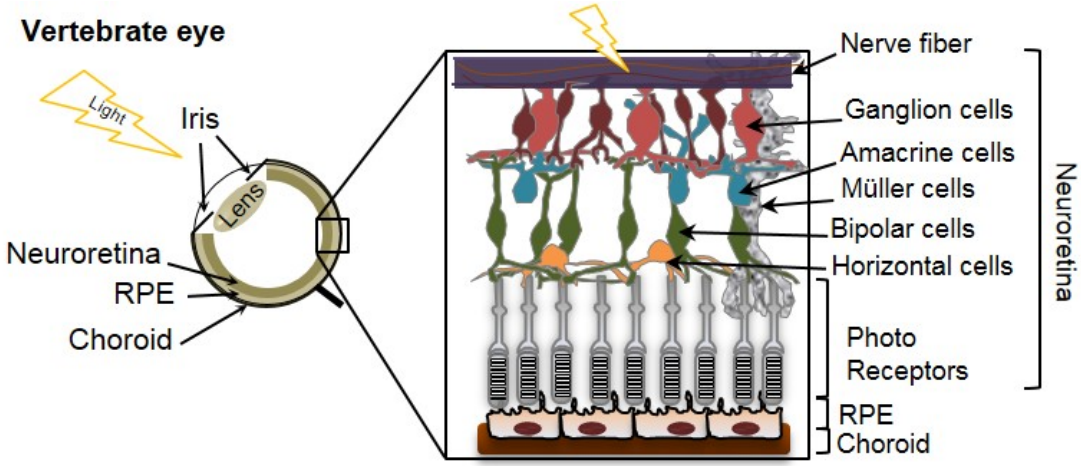

Figure 1. 1 - Schematic representation of eye structure with focus on the retina. Adapted from (Kolb 1995).

The visual process starts with light collection by photoreceptor cells: rods and cones. Rods relay exquisite sensitivity in low-light settings, conveying contrast and definition, whereas cones govern ambient light collection and distinction of the different colors, but with relatively low sensitivity (Kevany et al. 2010). Each rod and cone is composed of a synaptic terminal, an outer segment, an inner segment and a cilium connecting the outer and inner segments. The photo pigment opsin (also referred to as rhodopsin) comprises >95% of the rods outer segments' membrane protein. Opsins are G protein-coupled receptors that require a bound chromophore 11-cis-retinal to absorb photons. Upon absorption of a photon, 11-cis-retinal is converted to all-trans-retinal, conveying the pigment its "active" state (Kevany et al. 2010). This photo-excited opsin triggers a signal transduction cascade, which amplifies the signal and leads to the shutdown of cation channels, thereby hyperpolarizing photoreceptor membrane. This change in membrane potential is then sensed by the synapses, resulting in neurotransmitters release, which in turn relay information to bipolar and ganglion cells, with lateral interaction of horizontal and amacrine cells (Sung & Chuang 2010). Photoreceptors are exposed to photo-oxidative products with consequent damage of proteins and lipids. However, they undergo continuous daily renewal, with the distal portion of Photoreceptor Outer Segments (POS)

discs being shed and replenished at the Inner Segment region, in a mechanism which involves transport through the connecting cilium (Burgoyne et al. 2016; Young 1971). At the terminal end of POS, the RPE closely contacts and phagocytoses the shed material, taking part in the visual cycle. In the RPE, the visual pigment is recycled from all-trans-retinal back to 11-cis-retinal, which is returned to the outer segments, thus completing the visual cycle (Bharti et al. 2010).

1.1.2 Function of the RPE

The RPE is a single layer of tightly packed and polarized pigmented cells responsible for several functions necessary for retinal health (Figure 1. 2).

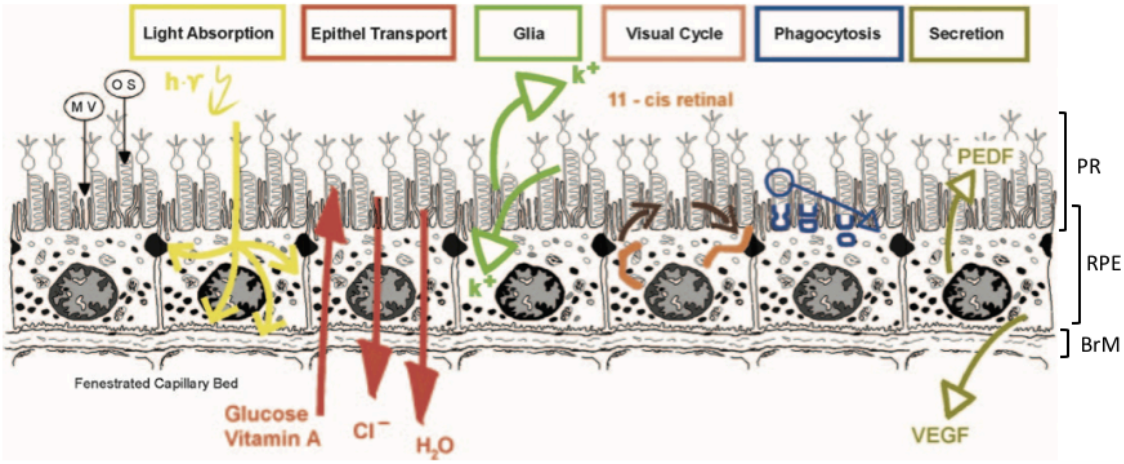

Figure 1. 2 - Schematic representation of the RPE main functions. PR: Photoreceptors, RPE: Retinal Pigment Epithelium; BrM: Bruch's membrane; O.S.: Outer Segment; M.V.: microvilli (Strauss 2005a).

In particular, RPE cells display high functioning preventive mechanisms against photo oxidation: pigment-mediated absorption of scattered light, maintenance of high levels of antioxidants which remove chemically reactive species, and also repair of damaged DNA, proteins and lipids. These mechanisms allow the RPE to assure structural integrity, while balancing photo oxidation from the retinal side and overflow of oxygen from the choroid side (Strauss 1995).

The RPE is responsible for the nourishment of the adjacent neural retina layers and is able to efficiently transport nutrients and ions between the retina and choriocapillaris, through highly convoluted basal infolds, which convey increased contact surface (Kevany et al. 2010; Strauss 1995; Sparrow et al. 2010). At the RPE basal side, establishing a selective blood/retina barrier with the choriocapillaris, lays the Bruch's Membrane (BrM), through which metabolic waste products and water excess are removed transcellularly towards the bloodstream. This barrier property is essential to maintain the immune privilege of the eye. Also, the RPE is responsible for the transport of essential metabolites, including glucose, fatty acids and new retinoids from the bloodstream into the retina and it is absolutely required for the regeneration of 11-cis-retinal, during the visual cycle (Kevany et al. 2010; Keeling et al. 2018).

The RPE actively phagocytosis and recycles the POS, on a daily basis. This process is regulated by the circadian rhythm and triggered by morning light, even in nocturnal animals. It is estimated that the whole length of POS is completely renewed every 10 days, a process coordinated by both photoreceptors and RPE (Law et al. 2010; Strauss 2005a).

Finally, RPE cells secrete important growth factors, such as Pigment Epithelium Derived Factor (PEDF) and Vascular Endothelial Growth Factor (VEGF), the latter being a crucial survival factor and modulator of vascular permeability and angiogenesis (Sparrow et al. 2010; Penn et al. 2008; Strauss 2005a).

Together, RPE and photoreceptors work as a functional unit, each depending on the other. For instance, genetic defects affecting the photoreceptors lead to RPE degeneration and *vice-versa*. In order to allow this close interaction, a tight coordination and structure maintenance are necessary. When this balance is not kept, degeneration of both layers ensues, jeopardizing the whole visual function.

1.2 Age-related Macular Degeneration

Age-related macular degeneration (AMD) is a retinal degenerative disorder, characterized by progressive visual impairment, caused by late-onset degeneration of the photoreceptors and retinal pigment epithelium (Al-Zamil & Yassin 2017). It is the leading cause of blindness in the developed world. In fact, AMD affects 0.2% of the population aged 55 to 64, rising to 11-13% of the population older than 85 years (Evans 2001; de Jong 2006).

As the designation suggests, AMD affects primarily the macula region, which constitutes the central area of the retina, approximately 4% of the total retina area. It is in that central region that the fovea is located, representing an area of tightly packed cone photoreceptors. For this reason, the macula is responsible for high-resolution central vision, sensible to color upon day light. Remarkably, this area of the retina has arguably the highest metabolic burden of the whole human body (Hageman et al. 1995; Biasutto et al. 2013). AMD typically progresses into one of two forms: dry AMD, with macular RPE atrophy and consequent photoreceptor loss, and wet AMD, characterized by neovascularization from the choroid into the retinal space (Figure 1. 3).

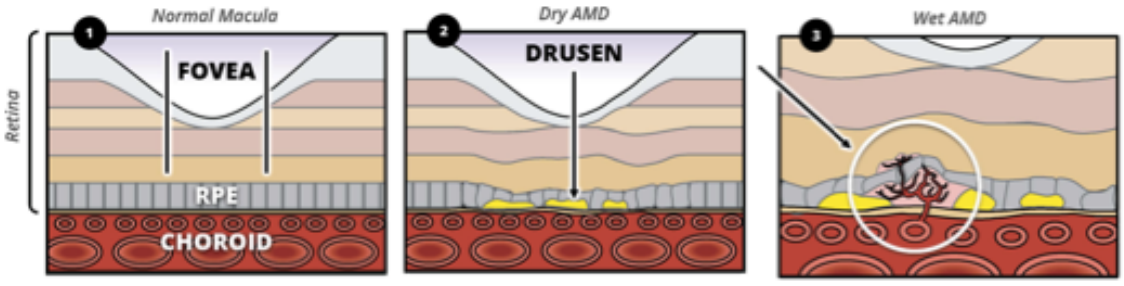

Figure 1. 3 - Schematic representation of 1: normal macula, 2: dry AMD and 3: wet AMD. Adapted from ClipArt.

1.2.1 Clinical standpoint

AMD is often considered as a multifactorial disease, without a fully understood pathophysiology. Pathogenesis of AMD is regarded as the result of a combination of metabolic, functional, genetic and environmental factors (Hamdi & Kenney 2003). On the one hand, with aging, the RPE starts accumulating residual material containing lipofuscin, which would normally be eliminated through the choriocapillaris (Guha, Liu, et al. 2014). On the other hand, changes of Bruch's membrane permeability have been associated with the accumulation of extruded material (Bhutto & Lutty 2012). Specifically, focal yellow deposits termed drusen build up in the extracellular matrix, at the interphase between RPE and the inner collagenous layer of the Bruch's membrane (Figure 1. 3). Besides thickening of the Bruch's membrane, with degeneration of elastin and collagen layers within the membrane, it has further been observed that choriocapillaris become thinner, which may contribute to the decline in the removal of extracellular material. The elastic layer of the Bruch's membrane is thinner in the foveal region, potentially conveying lowered tissue resistance to neovascularization in that area (de Jong 2006). Furthermore, blood/retina barrier failure induces local incitement of the innate immunity and disturbs fundamental RPE functions (Guha, Liu, et al. 2014). It is also typical to find pigmentary disturbances, such as hypo- and hyperpigmentation in AMD patients, still the presence of drusen in the macula region is considered to be the hallmark sign of AMD (Al-Zamil & Yassin 2017).

Dry AMD, also called geographic atrophy, is characterized by a demarcated area of hypopigmentation, in which large choroidal vessels are visible and patients experience loss of vision as gaps in an image. On the other hand, the wet form of AMD, also called exudative, appears as hemorrhagic fluid, originating from choroidal neovascularization (CNV). CNV originates from normal choriocapillaris, but invades the subretinal space, the RPE and neuroretina, causing retinal detachment (de Jong 2006). If left untreated, wet AMD usually causes legal blindness within months after the second eye becomes affected, while in the case of dry AMD these events may take years (de Jong 2006; Arunkumar et al. 2018; Hageman et al. 1995). Ultimately, patients suffer visual image distortion and, as the hemorrhages and scaring continue in the foveal area, progressive vision loss (Figure 1. 4).

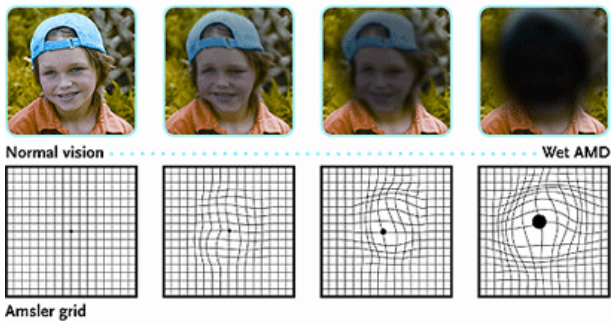

Figure 1. 4 - Progressive image distortion and central vision loss, caused by wet AMD (aoa.org 2017).

AMD can be considered at early stage when visual symptoms are inconspicuous, but drusen and pigmentary changes are present. When areas of abnormal pigmentation expand, associated with larger drusen, the patient is considered at higher risk of developing late forms of AMD (de Jong 2006; Mehta 2015). Late AMD may present in both dry or wet forms; however, one patient may present a different form in each eye or even both in the same eye. Because of similarities with other retinal diseases, AMD is considered to be a diagnosis of exclusion. For this reason, and because progression is gradual, research into AMD focuses mostly on the development of therapies for the advanced stages, rather than initiating events. Diagnosis relies on the identification of macular signs, namely the detection of pigmentation alterations and most notably of drusen, whose origin remains unknown (de Jong 2006; Mehta 2015).

1.2.2 AMD cell biology

As previously discussed, the RPE plays a pivotal role in the daily uptake of POS and their recycling, taking part in the visual cycle. Photoreceptors are particularly susceptible to photo oxidation and formation of reactive oxygen species, with consequent peroxidation of proteins and lipids. Exposure to bright light has been shown to cause irreversible lesions in the central retina, related to the rate of rhodopsin regeneration by the RPE (Frost et al. 2014). POS phagocytosis and recycling of visual pigment within the RPE leads to the appearance of residual undigested bodies, which become substrates for lipofuscin formation. Lipofuscin is an autofluorescent cellular waste product, formed by the condensation of all-trans-retinal and phosphatidylethanolamine, becoming virtually undegradable (Krohne et al. 2010). Aging leads to an accumulation of lipofuscin granules which gradually worsens the RPE digestive burden and this is more pronounced at the macula region (Kevany et al. 2010; de Jong 2006) (Figure 1. 5).

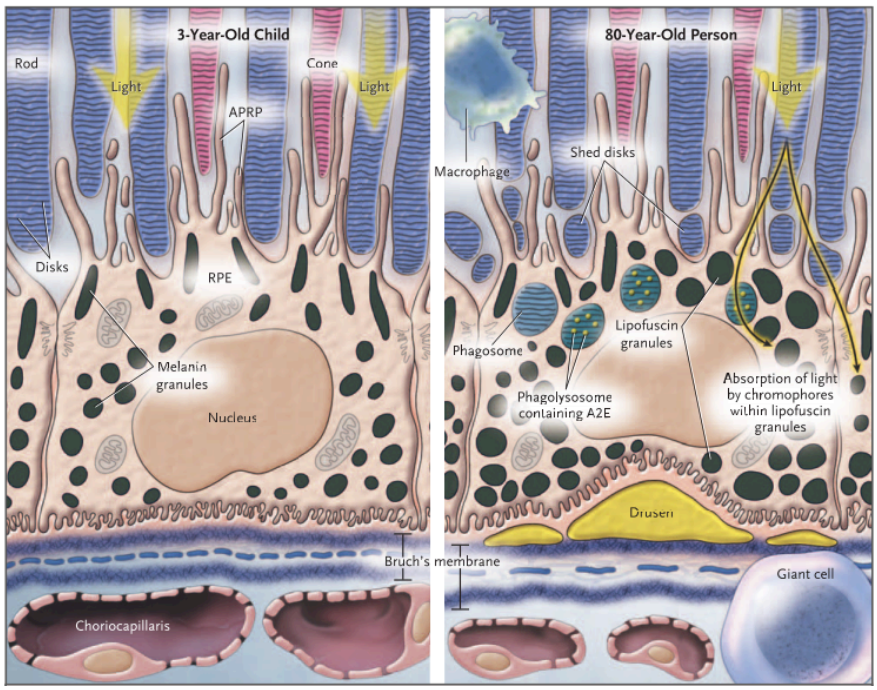

Figure 1. 5 - Schematic representation of young and aged RPE (de Jong 2006).

As depicted, a feature of the aged retina is the thickening of the Bruch's membrane, which accumulates lipids and glycoproteins throughout time (Figure 1. 5). Due to increased lipid content, this membrane becomes less permeable, causing a depletion of fluid and nutrient transport across and into the retina. Drusen deposits prompt local chronic inflammation with dendritic and macrophage invasion from the choroid and consequent release of pro-inflammatory cytokines and angiogenic factors (de Jong 2006). Choroidal fenestrated vessels also reduce in thickness, decreasing transport of macromolecules and causing hypoxia. Local hypoxia stabilizes Hypoxia-inducible factor 1-alpha (HIF1α), resulting in pro-angiogenic gene up-regulation, most notably VEGF secretion increase by the RPE with consequent neovascularization (de Jong 2006; Ablonczy et al. 2014).

It is important to mention that membrane-bound residual bodies appear naturally, in healthy individuals, with age. These drusen form at the basement membrane of the RPE starting at the third-fourth decades of life and basal laminar deposits accumulation follows (Hageman et al. 2001). It remains undetermined how or why drusen composition and localization may vary, or why some people are more prone to progress to AMD disease than others. In aged mice and more severely in mice models of retinal degeneration, RPE cells develop some characteristic changes resembling some aspects of AMD: lipofuscin, melanolipofuscin, extracellular deposits in the baso-lateral area and loss of basal infoldings (Wavre-Shapton et al. 2013; Chen et al. 2009).

Several risk factors have been linked to AMD, especially age (>60 years), but also family history and lifestyle (smoking and diet). Moreover, genetic studies have found evidence that polymorphisms in genes that encode complement factors can affect AMD risk either by increasing the likelihood of developing it or by protecting against disease progression (Evans 2001; de Jong 2006).

1.2.3 Treatment options

There are currently few therapeutic options for patients with wet AMD, consisting mainly of intraocular injections of VEGF inhibitors. These, however, do not target the underlying degeneration, thus the disease is only delayed and there is a high rate of recurrence when treatment is discontinued (Aboul Naga et al. 2015; Saeed et al. 2013; Penn et al. 2008; Kami et al. 2008; Mandai et al. 2017). The dry form of AMD, which constitutes the majority of cases (80-90%), has no current treatment option (Al-Zamil & Yassin 2017).

Research is being directed towards finding and managing AMD's early events, with the ultimate goal of avoiding loss of RPE, a critical step for disease progression. The fact that this unique cell type is affected makes AMD a target for cell-based therapy. Consequently, a massive effort has been engaged in the latest years to differentiate RPE from human Pluripotent Stem Cells (hPSc) for both *in vitro* studies and transplantation.

1.3 Pluripotent Stem cell-derived RPE

The emergence of human Embryonic Stem cells (hESc) in 1998 and induced Pluripotent Stem cells (hiPSc) in 2006 revolutionized cell-based therapies and was a stepping stone for the development of reliable models of disease (Leach & Clegg 2015; Song & Bharti 2016; Bharti et al. 2010).

hES cells are derived from blastocysts and are characterized by their ability to self-renew indefinitely and to generate differentiated cells of all three germ layers. iPS cells, on the other hand, are derived by transdifferentiation or reprogramming of somatic cells, by forced expression of pluripotency factors (such as OCT4, SOX2, KLF4 and c-MYC) (Takahashi & Yamanaka 2006). iPS cells are also characterized by their competence to self-renew and differentiate into all three germ layers.

Therapeutic approaches to treat and study the mechanisms of retinal degeneration, in particular early AMD, are largely lacking. There are models for some types of retinal degeneration, but they are not able to fully represent the degeneration mechanism (Jin et al. 2012; Housset et al. 2013; Cano et al. 2010; Meyer et al. 2009; Wang & Neufeld 2010; Singh, Shen, et al. 2013; Song & Bharti 2016). In order to bridge this need, Pluripotent Stem cells come as a revolutionizing concept, as they can be differentiated into retinal cells, namely RPE (Reynolds & Lamba 2014; Leach & Clegg 2015). And, because differentiation protocols are devised to mimic known developmental cues, they also provide valuable information about RPE specification steps in a shorter time frame relative to *in vivo* ocular development (Meyer et al. 2009).

1.3.1 Development and patterning of the eye

Vertebrate eye patterning occurs early in embryonic development. During that time, the anterior neural tube ectoderm originates the retina, the iris and ciliary body epithelia, as well as the optic nerve, while surface ectoderm gives rise to the exterior components of the eye: lens, conjunctival, cornea epithelia, eyelids and lacrimal apparatus. A complex conjugation of inductive or inhibitory signals coming from tissue-tissue interaction, cell intrinsic factors and activation of transcription factors (TFs) has to occur in a timely combination, to ensure correct determination and maintenance of specific cell fate (Fuhrmann 2010).

Initially, the forebrain specifies to become the eye field, located centrally. By morphogenic movement of cells, the single eye field is divided, forming bilateral neural folds, called optic grooves or sulci. As the neural tube closes, these outgrowing grooves become the optic vesicles and their connections to the forebrain form the optic stalk, which eventually grows into the optic nerve (Fuhrmann 2010). The stages of eye development are depicted in Figure 1. 6.

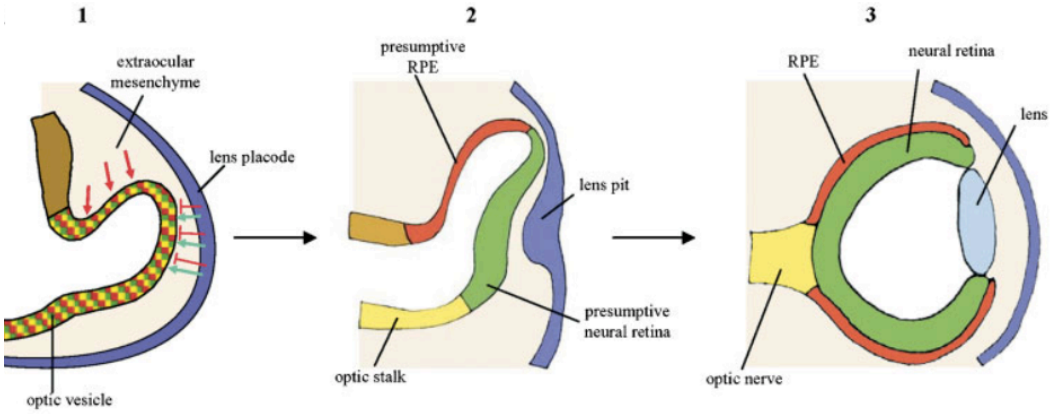

Figure 1. 6 - Schematic representation of eye developmental stages. 1: early unpatterned cells, 2: optic vesicle, 3: optic cup (Martínez-Morales et al. 2004).

The exterior portion of each optic vesicle interacts with the surface ectoderm and induces that area to form a thickening, called the lens placode, a precursor of the lens (Figure 1. 6). At the same time, the optic vesicle also invaginates into a double layered structure, called optic cup, which will form the posterior part of the eye and give rise to the retina (Kwan et al. 2012). The anterior layer of the optic cup will eventually become the iris and ciliary body; the posterior thicker layer will be divided into an inner neural retina and outer pigmented coating. The surrounding structures of the eye develop from the condensation of the external surface of the optic cup into two layers: the inner pigmented and vascular layer, known as the choroid, and the outer fibrous layer, called sclera (Martínez-Morales et al. 2004; Fuhrmann 2010).

In the pre-retina, melanin granules start to appear in the retinal epithelium at four and a half weeks of human embryonic development. At about week six, the cells in the innermost posterior layer of the optic cup begin to differentiate gradually into photoreceptors, after which müller cells and bipolar cells become differentiated, and finally retinal ganglion cells. Ganglion cells' axons tangle together and fill the lumen of the optic stalk as it becomes the optic nerve. By eight months of development, all retinal layers are recognizable. However, photoreceptor maturation continues after birth, accompanied by corresponding improvement of visual acuity (Fuhrmann et al. 2014; Fuhrmann 2010).

1.3.2 Signaling pathways in eye development

Eye patterning progresses depending on signaling cascades driven by Fibroblast Growth Factor (FGF), Bone Morphogenic Proteins (BMP), Wnt and retinoic acid. For early eye patterning events to occur, Wnt/βcatenin antagonists, such as Dickkopf-related protein 1 (DKK1), as well as direct suppressors of Wnt ligand transcription, such as Homeobox protein SIX3, are present and stimulate forebrain development. If this inhibition of Wnt/βcatenin is lost or inefficient, there is suppression of eye development, giving rise to eyeless or headless embryos, in severe cases (Lagutin et al. 2003; Fuhrmann et al. 2014).

Signaling molecules from neighboring tissues can activate or repress a network of TFs, which imprint the differentiated state of the retinal layers. A large number of eye development regulators are now known, most importantly Microphthalmia-associated transcription factor (MITF), Homeobox protein OTX1, OTX2 and Paired box protein Pax-6 (PAX6) have been proven to be essential (Martínez-Morales et al. 2004).

One of the earliest RPE specification markers is MITF. Mitf transactivates genes related to pigmentation and RPE maturation, such as Tyrosinase (TYR), Tyrosinase-related proteins (TYRP), melanosomal proteins and Bestrophin (Best) (Fuhrmann 2010; Fuhrmann et al. 2014; Martínez-Morales et al. 2004). Mitf also transactivates expression of miRNAs, such as miR-204 and miR211, tightly regulating RPE differentiation and homeostasis (Raghunath & Perumal 2015). Without Mitf, pigmentation defects occur and RPE transdifferentiates into neural retina (Fuhrmann et al. 2014; Martínez-Morales et al. 2004). In fact, regulation of MITF is crucial and relies on a combination of several factors, for instance Otx2. Low levels of Otx2 result in a decrease of Mitf and consequent transdifferentiation. During development, Otx2 is expressed throughout the whole optic vesicle, but in the optic cup it regulates RPE specification by interacting with and regulating a set of genes involved in such specific RPE functions as melanogenesis (MITF and TYR, TYRP1), retinol metabolism, pH regulation and metal concentration (Martinez-Morales et al. 2001; Housset et al. 2013; Martínez-Morales et al. 2004). Downregulation of OTX2 affects these functions and results in neural retina degeneration and vision loss. Ultimately, there is evidence suggesting OTX2 expression in RPE to be both necessary and sufficient to prevent photoreceptor degeneration onset in some cases (Housset et al. 2013).

PAX6 expression is distributed over the entire optic vesicle and early optic cup. It is, however, downregulated upon developing RPE at the late optic cup stage (Martínez-Morales et al. 2004). When PAX6 expression is impaired, differentiation of RPE is delayed or reduced. It has also been shown that PAX6 acts together with MITF, by binding and activating it, to promote RPE-specification, adapting its effect depending on tissue-specific context (Bharti et al. 2012). We know now that there is a tight interplay to control fundamental factors' expression levels, such as MITF, OTX2 and PAX6, during optic cup formation. Without MITF, for instance, phenotypes as severe as anophtalmia can occur (Martínez-Morales et al. 2004; Fuhrmann 2010; Fuhrmann et al. 2014). Mutations/loss of OTX2 in humans have been linked to ocular malformation and degenerations of RPE, photoreceptors, bipolar and müller cells (Housset et al. 2013). PAX6 plays a crucial role in eye induction, as we have learned by the eyeless phenotype observed in animal models depleted of it. Conversely, ectopic expression of PAX6 has been shown to induce eye formation in Drosophila's antennae and legs (Halder et al. 1995).

Other than intrinsic factors, external signals can shift the balance and influence regionalization of the patterning eye. For instance, Transforming growth factor beta (TGFβ) family members from the extraocular mesenchyme favor cells of the optic vesicle to become RPE, whereas FGF signals from the lens placode suppress RPE and reinforce neural retina identity (Fuhrmann et al. 2014; Martínez-Morales et al. 2004) (Figure 1. 7).

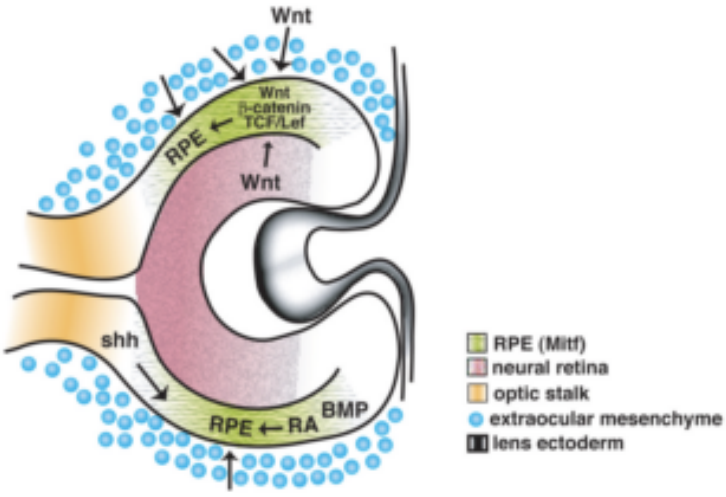

Figure 1. 7 - Representation of the signaling pathways regulating RPE patterning: Sonic Hedgehog Signaling (shh), Bone Morphogenic Protein (BMP), Retinoic Acid (RA), Wnt/βcatenin, TCF/Lef TFs (Fuhrmann 2010).

Finally, cell proliferation is terminated postnatally and the RPE matures acquiring an apical-basal polarity and becoming a monolayer sheet epithelium. Unlike other epithelia, the RPE maintains tissue homeostasis through long-term survival, with little evidence of cell turnover and no evidence for *de novo* cell production (Fuhrmann et al. 2014). A cumulative understanding of developmental processes driving specification and differentiation of RPE is providing more insight into the mechanisms that underlie plasticity of the RPE. Yet, a comprehensive explanation covering all molecular networks that drive these processes is still being built. Ultimately, the RPE has a limited self-renewal and repair ability, which is thought to be tightly conditioned by its extracellular environment.

Since birth, density of RPE cells decreases over time, due to continued growth of the eye during the juvenile period, but also due to cell loss related with aging. To maintain the barrier epithelium, cells undergo hypertrophy without loss of contact with neighboring cells. The RPE has a remarkable intrinsic capacity to cope with damage, being able to restore itself (by hypertrophy) even after 60-80% cell loss. Still, upon retinal damage or disease, cell loss may cause an over burden of the remainder RPE, which ultimately leads to photoreceptor degeneration (Longbottom et al. 2009).

1.3.3 The promise of hPSc-RPE's therapeutic potential

Autologous RPE replacement surgery has been performed with success, in proof-of-principle procedures, with some improvement of AMD patients' visual responses. On a first approach, surgical techniques consisting on macular translocation or on substitution of macular RPE, using small patches of healthy RPE from the peripheral regions of the eye of the same patient, were attempted, with moderate success. However, due to the high number of patients with AMD and to the complexity and complications of these surgical approaches, tissue transplantation is now considered as a better alternative (Carr et al.

2013). Different sources of RPE have been proposed as starting material for transplant, for instance fetal or neonatal RPE, as well as spontaneously generated or engineered RPE cell lines. Alas, maintaining a supply of fresh neonatal or fetal RPE is difficult and controversial, whereas RPE cell lines are known to have a limited propagation capacity and lose essential characteristics, ultimately dedifferentiating (Carr et al. 2013).

Based on collectively built knowledge regarding eye development and RPE specification, it is now possible to differentiate RPE from human Pluripotent Stem cells (Figure 1. 8).

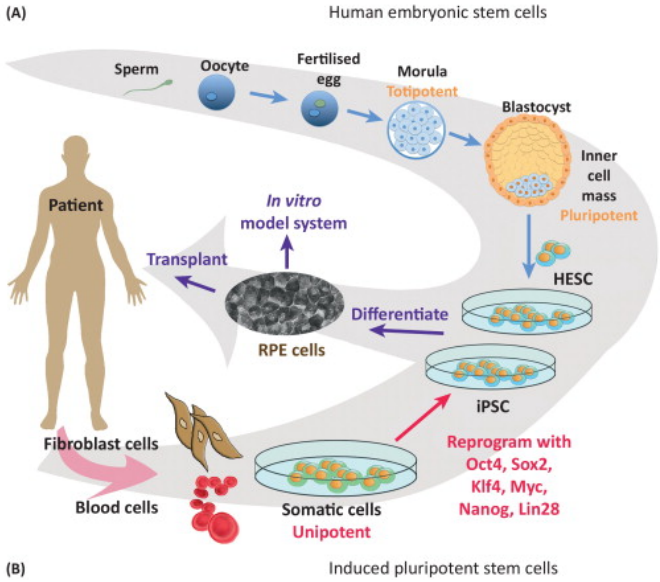

Figure 1. 8 - RPE can be obtained through differentiation of hES cells or of reprogrammed hiPS cells (Carr et al. 2013).

Since hiPS cells can be derived from somatic cells of a patient, they can more promptly be used for cell replacement therapies (for the same donor patient) as cells and host would carry the same histocompatibility antigens. When it comes to studying the visual system in particular, it is a challenge to obtain samples from patients' eyes, without causing vision impairment, thus induced pluripotent stem cell technology is, in this case, invaluable. Nevertheless, iPS cells' weakness is that they carry the same genetic landscape which may have originated the patient's disorder in the first place. For basic research purposes, patient-specific iPS cells are an ideal source to investigate genetic mechanisms of disease *in vitro* as well as study disease risk factors or perform drug screening.

Still, if on the one hand, it is possible to obtain "individual-type RPE" by differentiating patient-specific iPS cells, on the other hand, by starting from hES cells it is possible to obtain healthy "standard" RPE. In fact, while hES cells are directly recovered from the blastocyst, iPS cells require the additional reprogramming necessary to become pluripotent, since they are derived from patients' somatic cells. Ultimately, the use of hES cells may be considered more standardized than hiPS cells, in the sense that it requires less manipulation, thus allowing a more readily production of similar hPSc-RPE lines. Starting from one original hES cell line - with everlasting potential - and using the same protocol to differentiate them, it would be, in theory, possible to establish a standard, unremitting

RPE line. Additionally, studies aiming at engineering histocompatible embryonic stem cells are proceeding with the ultimate goal of surpassing the disadvantages of iPS cells: high cost for each patient and prolonged cell culture for reprogramming and differentiation, validation and regulatory approval (Riolobos et al. 2013).

Importantly, a thorough characterization of newly-obtained human Pluripotent Stem cell-derived RPE (hPSc-RPE) is prerequisite, whether these cells are used for laboratory-based cell biology research or for clinical settings, in cell-replacement therapies. hPSc-RPE are usually compared to RPE primary cultures (fetal and adult) and to standard RPE cell lines, namely to assure specific RPE markers expression and functional similarities. Transcriptional profiling indicates that hPSc-RPE is more similar to fetal than adult RPE, expressing many essential RPE markers, such as RPE65, Retinaldehyde-binding protein 1 (CRALBP), Bestrophin (Best) and Zonula Occludens 1 (ZO-1), some of which are lost in RPE cell lines. Furthermore, hPSc-RPE is able to polarize, exhibiting comparable transepithelial electrical resistance (TEER or TER) values to those of RPE obtained from primary cultures. hPSc-RPE are also able to secrete such essential growth factors as VEGF and PEDF in a polarized fashion and, most notably, they are capable of phagocytosing POS. Additionally, hESc-RPE and hiPSc-RPE usually present similar expression profiles compared to one another, as well as typical RPE functions (Carr et al. 2013; David E. Buchholz 2009; A. J. Carr et al. 2009).

In the end, whether derived from embryonic or induced pluripotent stem cells, hPSc-RPE cells have been obtained successfully and used for transplantation studies in animal models. These experiments were shown prolific: hPSc-RPE displayed phagocytic ability *in vivo* and most importantly, visual performance of transplanted animals was improved (Carr et al. 2013; Forest et al. 2015; Kamao et al. 2014).

Following animal testing, clinical trials directed towards the treatment of macular degeneration patients by cell replacement therapies are proceeding (Figure 1. 9).

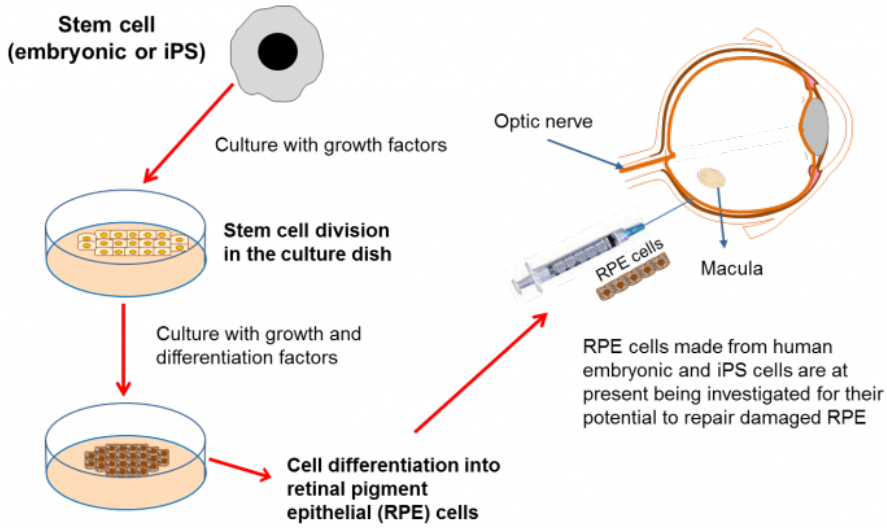

Figure 1. 9 - Representation showing stem cell research for RPE replacement therapies (Astrid Limb n.d.).

Fundamentally two types of cell-replacement therapies have been tested: injection of single-cell suspension and insertion of an implant containing an RPE monolayer (Carr et al. 2013; Forest et al. 2015).

Recent reports on phase I/II clinical trials using hESc-RPE attest no significant adverse effects, including no abnormal cell proliferation or tumor formation, whether in suspension or monolayer implant (Schwartz et al. 2012; Carr et al. 2013). Furthermore, patients were monitored for improvement in visual acuity, with encouraging results, when comparing treated eyes with non-treated controls (Schwartz et al. 2015).

Still, because hES cells are derived from embryos, ethical questions and concerns related to allogeneic transplantation may arise. On the other hand, the use of iPS cells as starting material could surpass these disquiets, but entail other types of worries. Specifically, the first trial using iPSc-derived RPE revealed several mutations in the cells derived from one of the two patients included in the study, i.e. in the process of reprogramming the patients' somatic cells into hiPSc or during their differentiation towards RPE, the cells acquired random mutations, which precluded the continuance of the trial. For this reason, even though no evidence was found to indicate these mutations were problematic, these iPSc-RPE were not used, and the study was stopped, for precaution (Mandai et al. 2017). Still, despite being interrupted, this trial has since restarted, not without greatly contributing for the discussion on standardization of risk/benefit limits, defined to evaluate these particular therapies.

1.3.4 Using hPSc-RPE to model disease

While using hPSc-RPE for cell replacement is in the progress of being implemented, it is relevant to note that these therapies are very complex to apply in a broad way. There is, however, another approach to face the problem of AMD treatment: use this new readily accessible hPSc-RPE cells to study and model the molecular mechanisms of this disease. This methodology allows the development of efficient and more accessible remedies to prevent or to stop disease progression, in time.

While research using animal models of disease greatly contributes to our understanding of the cellular processes that drive these diseases, some argue there are serious limitations of these models. For instance, the most commonly used animal model (the mouse) does not have a fovea/macula. Furthermore, the surface area of the mouse retina is seventy times smaller than that of the human eye, precluding extrapolation of key findings, in some instances (Volland et al. 2015; Roska & Sahel 2018).

On the other hand, simpler RPE models, such as RPE primary cultures, allow researchers to easily manipulate human RPE. As mentioned, human RPE obtained from primary cultures, are relatively difficult to attain, when compared to hPSc-RPE. Not only hPSc-RPE is becoming widely used for *in vitro* studies concerning the molecular mechanisms underlying AMD, but it was also demonstrated that hiPSc-RPE derived from AMD patients recapitulate cardinal features of the disease. In fact, hiPSc-RPE models

display drusen biogenesis, with extracellular matrix (ECM) changes and importantly, the composition of the deposits found underneath these cells was shown to be different between controls and AMD patients-derived cells (Galloway et al. 2017). This study not only validates the use of iPS cell technology for the study of AMD, but also verifies the general reliability of stem cell-derived models of RPE for the study of macular degeneration. Eventually, our understanding of such a multifactorial disease as AMD greatly benefits from all the information that different models of disease may provide.

Together with the limitless proliferative capacity inherent of stem cells, the ability to reproduce cardinal features of disease ascertains the true potential and the ultimate promise of hPSc-RPE: find the molecular mechanisms of disease, test drugs and develop new therapies to tackle AMD and other retinal degenerative disorders.

1.4 Aging and Lysosome Dysfunction

While most chronic and age-related diseases are undisputedly multifactorial, it is becoming increasingly evident that many such diseases share common mechanisms due to the dysregulation of cellular homeostasis. Lysosomes have emerged in the past few years as critical players in the complex cellular network that comprises endo-lysosomal and autophagic pathways as well as metabolic sensing. Mounting evidence indicates that this network is prone to age and disease-related dysregulation.

Declining lysosomal function is postulated to cause and/or facilitate a number of chronic age-related disorders (Carmona-Gutierrez et al. 2016). In fact, dysfunction of the lysosomal network was shown to be associated with adult-onset forms of familial neurodegenerative diseases such as Alzheimer´s disease (AD) and Parkinson´s disease (PD), cancer, atherosclerosis, as well as a decline in lifespan (Wolfe et al. 2013; Zheng 2012; Bourdenx & Dehay 2016; Dehay et al. 2013). Specifically, in the visual system, dysfunction of the lysosomal network is a critical component in the pathogenesis of AMD, the most common blinding disease in the western world (Sinha et al. 2016). Lysosomal dysfunction in the RPE cells is thought to be at the center of a pathogenic hub contributing to proteotoxicity, mitochondrial dysfunction, redox imbalance and inflammation in AMD (Golestaneh et al. 2017; Ferrington et al. 2016).

The critical role of lysosomal pathobiology as causative of chronic, late-onset diseases affecting post-mitotic tissues represents a paradigm-shift from more traditional views (Appelqvist et al. 2013).

1.4.1 Main trafficking pathways to the lysosome

Inside the cell, trafficking routes closely interact and intertwine in a controlled and accurate fashion. In particular, there are mechanisms in place that allow for distinction of one specific organelle from another (Behnia & Munro 2005). The way a protein recognizes and associates to the correct organelle is by binding to specific lipids, such as phosphoinositides, or to activated forms of monomeric GTPases of the Rab and Arf

families (Schink et al. 2016; Segev 2011). Unique combinations of lipids and GTPases are distributed on a subset of intercellular membranes, hence providing each organelle with their identity and allowing for precise binding of proteins. Phosphoinositides are short-lived molecules and GTPases alternate between membrane-associated activated GTP-bound and cytosolic inactivated GDP-bound states, working as molecular switches. For this reason, whilst integral membrane proteins are subjected to complicated trafficking steps until they reach their destination, lipids can be synthesized or GTPases can be activated rapidly, only at the required site of action (Munro 2002). These are the tools with which the cell is able to segregate organelles in a defined way, while also allowing for interactions between them and maintaining a certain degree of plasticity within intracellular pathways (Behnia & Munro 2005).

There are three main pathways related to cargo processing inside the cells, namely endocytosis, phagocytosis and autophagy. Perturbations in the trafficking and processing of (un)digestible cargo through these pathways is of utmost importance to upkeep retinal health, particularly in the case of AMD (Gross & Bales 2015). Ultimately, all these different cargo-trafficking routes have in common their final destination: the lysosome. Lysosomes are the organelles responsible for maintaining the balance between production of new and degradation of old/damaged cellular components. For this reason, they are instrumental when it comes to prolonged retinal health and are definitely involved in the development of age-related dysfunction, particularly in the case of AMD.

Endocytosis

The endocytic pathway initiates with the incorporation of extracellular material by the cell, and comprises different trafficking events occurring inside the cell, until the endpoint, when cargo is targeted for degradation. Briefly, material is included into vesicles, at close proximity with the plasma membrane and interacts with other structures, by moving and fusing with other organelles and acquiring/exchanging specific molecular markers in a timely manner (Elkin et al. 2016).

During the first steps of the endocytic pathway, cargo is internalized in early endosomes (EE), through specific mechanisms, namely macropinocytosis, clathrin-mediated endocytosis, caveolin-mediated endocytosis and clathrin- and caveolin-independent endocytosis (Settembre, Fraldi, et al. 2013; Keeling et al. 2018). EE are typically identified by the presence of phosphoinositide-3-phosohate (Pi(3)P) and also a set of Rab GTPases, namely endocytic markers Rab4 and Rab5 and recycling endosome marker Rab11. These are responsible for sorting and targeting these EE to their destinations (Behnia & Munro 2005; Keeling et al. 2018; Ketel et al. 2016; Klumperman & Raposo 2014). From there, EE may enter retrograde trafficking either to have their content returned to the plasma membrane or to the trans-Golgi network, for re-use. Alternatively, EE can form intraluminal vesicles of multivesicular bodies (MVBs) and/or undergo maturation into late endosomes (LE) (Elkin et al. 2016). Maturation of EE into LE is typically described as the regulated exchange between EE marker Rab5 and LE's Rab7 and also Pi(3)P conversion

to Pi(3,5)P_2, as well as a gradual decrease of the vesicle's intraluminal pH (Huotari & Helenius 2011). Endosome pH is regulated by the large multimeric proton pump, vacuolar ATPase (vATPase), which associates with the endosomal membrane and drives protons into the lumen. While EE have a mildly acidic pH of 5.9-6.8, LE and lysosomes are highly acidic, with a pH of 3.8-5.0 (Keeling et al. 2018; Kissing et al. 2017) (Figure 1. 10).

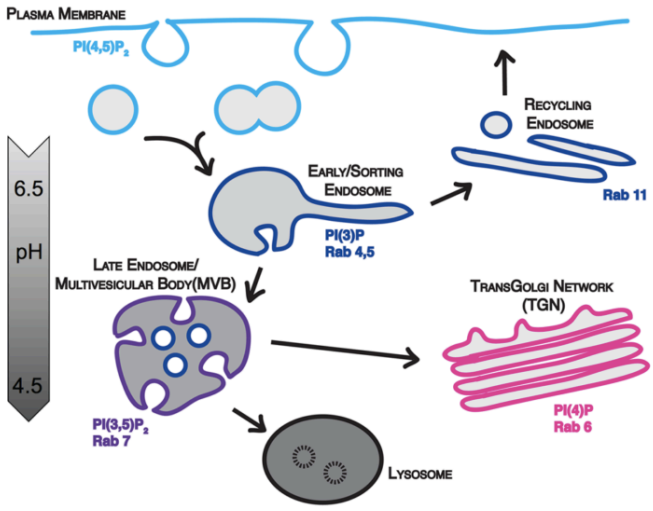

Figure 1. 10 - Schematic representation of the endocytic organelle identity (Elkin et al. 2016).

From the point of view of cargo processing, along the endosome maturation steps, hydrolytic enzymes are recruited to LE and lysosomes, and become active as the pH decreases. Regarding spatial localization within the cell, EE are usually located at the cell periphery and, as they mature, they are trafficked to the perinuclear area where degradative lysosomes reside (Cabukusta & Neefjes 2018).

Phagocytosis

Phagocytosis allows for internalization of particles of ≥1μm diameter (whilst endocytic cargo ranges between 200-500nm in diameter). Similarly to endocytosis, it occurs via a temporal sequence of events, which include recognition, binding to receptors, intracellular signaling, internalization and digestion (Kevany et al. 2010). It is primarily through phagocytosis that RPE cells incorporate POS, however this process has also been studied in detail in other professional phagocytes, such as macrophages or dendritic cells (Pauwels et al. 2017). Briefly, once internalized, phagosomes mature through a number of fusion events with EE, LE and lysosomes (Esteve-Rudd et al. 2014; Pauwels et al. 2017). In parallel to what was previously described for the endocytic pathway, phagosomes may also acquire Rab4, Rab10 or Rab11 and be recycled back to the plasma membrane, or go through the Rab5 to Rab7 conversion, as the phagosome matures (Kevany et al. 2010; Molino et al. 2016). Because RPE cells are polarized, POS are typically internalized at the apical side and transported toward the basal membrane for degradation (Figure 1. 11).

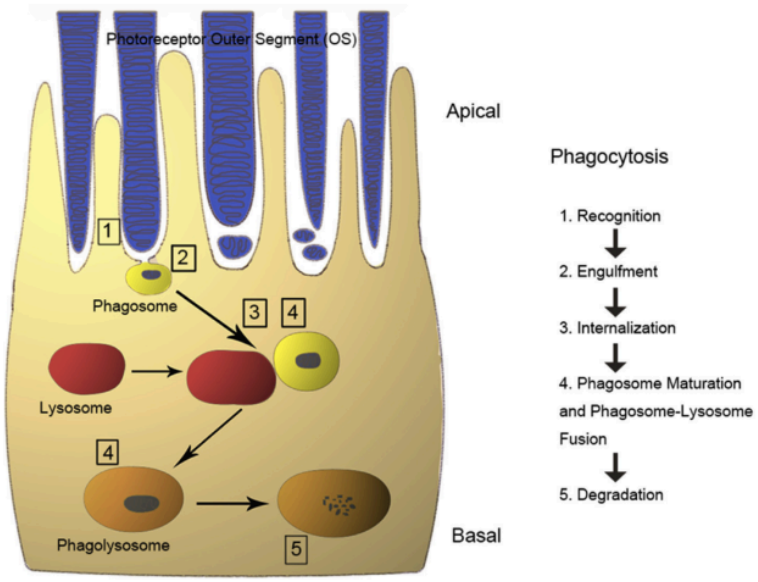

Figure 1. 11 - Schematic representation of the phagocytosis by RPE (Ferrington et al. 2016).

Finally, these structures become what is designated as phagolysosome, characterized by progressive acidification of the lumen and increased production of reactive oxygen species and proteolysis(Kevany et al. 2010; Keeling et al. 2018), not unlike typical endolysosomes. Taking into consideration that RPE cells are post-mitotic, it has been estimated that each RPE cell phagocytoses hundreds of thousands of POS discs over a human lifetime (Kevany et al. 2010; Keeling et al. 2018). Thus, RPE is considered one of the most active phagocytic cells in the human body, responsible for the efficient turnover of phagocytosed material on a daily basis, otherwise they suffer the damaging effects of undigested material build-up. In many eye pathologies this physiological function of the RPE is impaired (Ferrington et al. 2016).

Autophagy

Finally, the third main pathway through which cargo is degraded inside the cell is termed autophagy. Autophagy may work in a non-selective way, in response to nutrient or amino acid starvation, or it can be selective, to eliminate misfolded or aggregated proteins, oxidized lipids or damaged organelles (Galluzzi et al. 2017). In any case, it consists on a self-digestive mechanism (hence the term autophagy), in the sense that intracellular constituents are degraded so that their building blocks can be recycled. This is a crucial process, whether considering a stress situation, low energy stores or the effects of aging, particularly in post-mitotic cells, such as the RPE (Settembre, Fraldi, et al. 2013; Keeling et al. 2018; Frost et al. 2014).

Different types of autophagy have been described, namely microautophagy, chaperone-mediated autophagy and macroautophagy (Galluzzi et al. 2017). Microautophagy consists on direct engulfment of cytosolic proteins by the lysosome or by the endosomal membrane with consequent targeting for degradation in the lysosome; in chaperone-mediated

autophagy cytosolic proteins containing the KFERQ motif are preferentially captured by the lysosome through chaperone- and receptor- mediated internalization, directly via lysosome-associated membrane protein 2A (LAMP2A); macroautophagy can be selective, again through identification of the KFERQ motif, and requires the formation of double membrane-bound vesicles termed autophagosomes, which sequester cytoplasmic material, followed by fusion with EE, LE and finally, lysosomes (Keeling et al. 2018; Settembre, Fraldi, et al. 2013; Galluzzi et al. 2017).

Autophagy is tightly regulated by numerous autophagy-related proteins (Atg) and it is typically described as a sequence of initiation, nucleation, elongation and closure of autophagosomes, culminating with recycling of content or degradation in auto(phago)lysosomes (Frost et al. 2014) (Figure 1. 12).

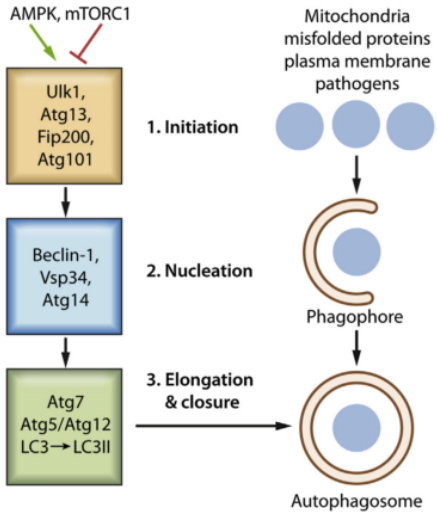

Figure 1. 12 - Schematic representation of the main molecular players involved in autophagy and respective stages (Frost et al. 2014).

It is relevant to mention that the proteasome too is responsible for degrading misfolded cytoplasmic proteins that have been ubiquitinated (Ferrington et al. 2016). However, whenever these proteins accumulate and aggregate, they are targeted by macroautophagy, through binding of autophagy receptors (Zhan et al. 2016). Because it plays such a remarkable role in the cell, including entire organelle sequestration, macroautophagy is the best characterized autophagic process so far and many times it is described simply as autophagy (Galluzzi et al. 2017).

The mammalian target of rapamycin complex 1 (mTORC1) plays the role of principal regulator of autophagy, metabolism and cell growth, through sensing and signaling mechanisms. Because this complex exerts its activity at the lysosomal surface, a tight co-regulation between cell growth or biosynthesis and cell catabolism has been suggested (Settembre, Fraldi, et al. 2013). Amino acids, glucose, growth factors, hormones, oxygen and stress have been shown to activate mTORC1 and trigger responses based on mRNA and protein regulation, lipid biosynthesis and ATP production (Settembre et al. 2013b; Settembre & Ballabio 2014; Ballabio 2016). Remarkably, when nutrients are available in

the cell, mTORC1 is activated and inhibits autophagy, through direct phosphorylation and thus repression of autophagy-initiating ULK1 complex, which comprises ULK1-ATG13-FIP200 (Settembre, De Cegli, et al. 2013). Conversely, inhibition of mTORC1 during nutrient depletion or low energy status leads to activation of this complex, consequently promoting autophagy initiation and triggering a cascade of events culminating in the degradation and recycling of cargo (Settembre, Fraldi, et al. 2013).

Autophagy has been proposed as a retinal protection mechanism against light-induced degeneration, particularly with a non-canonical form of autophagy being described to maintain the visual cycle (Kim et al. 2013; Ferguson & Green 2014; Frost et al. 2015). Specialized phagocytic cells have been reported to use a hybrid pathway, which combines the phagocytic and autophagic pathways, known as LAP: LC3 Associated Phagocytosis (Frost et al. 2014; Ferguson & Green 2014; Sanjuan et al. 2007; Galluzzi et al. 2017). LC3 recruitment to the phagosomal membrane, in this context, is Atg5-dependent and Ulk1 independent. Researchers looking at this process reported that the RPE circadian cycle of phagocytosis coincides with increase of LC3 lipidation, but not with autophagy initiation complex containing Ulk1 (Kim et al. 2013). Nevertheless, it is important to keep in mind that the majority of phagosomes do not associate with LC3, making LAP a secondary mechanism, possibly to compensate for an overload of the phagocytic pathway. LC3 association nonetheless has been shown to induce fusion of phagosomes to lysosomes, leading to rapid acidification and efficient degradation (Sanjuan et al. 2007). LAP is still not a consensual mechanism, but the reasoning behind these studies support the existence of overlap between autophagy and the phagocytic pathway.

Throughout these three main pathways, endosomes/phagosomes/autophagosomes at different stages of maturation co-exist and interact, according to their affinity or repulsion, driven by the cell's biological needs. For this reason, depending on their spatial subcellular localization or on the type of cargo they carry, hybrid organelles may form. These pathways play crucial roles within the cell, regulating entry and exit of molecules, finally converging at the lysosome (Figure 1. 13).

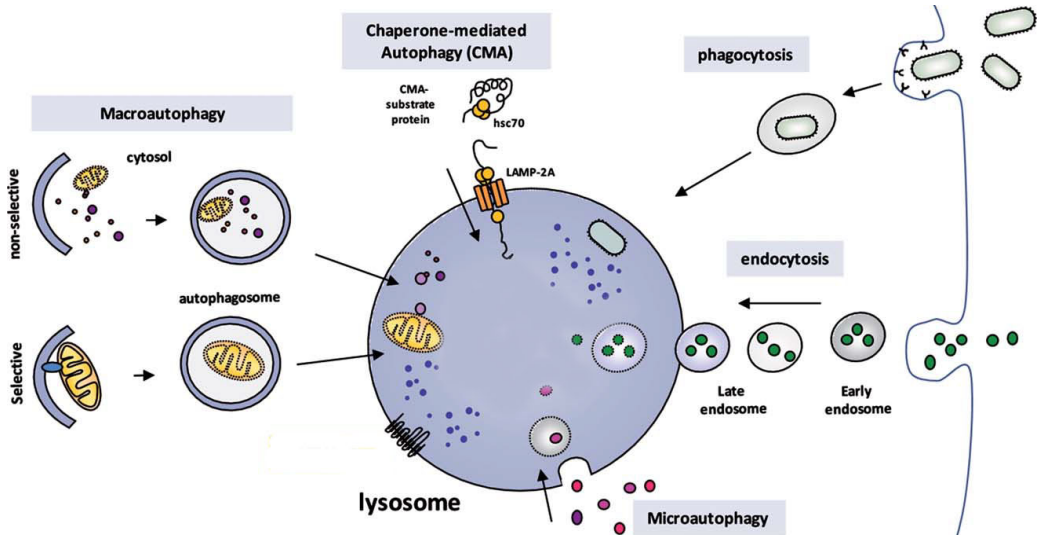

Figure 1. 13 - Representation of endocytic, phagocytic and autophagy pathways, all converging at the lysosome. Adapted from (Dehay et al. 2013).

1.4.2 Point of Convergence: The Lysosome

Lysosomes are found in all animal cell types, with the exception of erythrocytes, and represent the cell's principal catabolic organelle. They compose up to 5% of the volume content of animal cells and consist on vesicles, delimited by a single bilayer membrane, which can be heterogeneous in size and morphology, appearing as electron-dense or as multilamellar membrane structures, under an electron microscope (Klumperman & Raposo 2014; Settembre, Fraldi, et al. 2013).

The lysosomal membrane is decorated with proteins responsible for the transport of substances in and out of the lumen, for the maintenance of an acidic pH and also for the fusion of the lysosome with other structures (Saftig & Klumperman 2009). Among these, the Lysosomal-associated membrane proteins 1 and 2 (LAMP-1 and LAMP-2) together account for ~50% of the lysosomal membrane protein content (Wartosch et al. 2015). Enzymes within the lysosomal membrane are responsible for the degradation of a wide range of intracellular macromolecules, organelles, surface receptors and pathogens, among others (Luzio et al. 2007).

A mature lysosome is limited by a cholesterol-poor membrane, containing an inner glycocalyx-coating, in order to prevent the lysosomal membrane from being digested by luminal hydrolases and also to keep the highly acidic environment from contacting the rest of the cell (Settembre, Fraldi, et al. 2013). Specific lysosomal membrane proteins anchored at the membrane perform fundamental functions, serving as structural backbone, receptors or channels. Furthermore, the acidic environment is maintained by the proton-pumping V-type ATPase, also moored at the membrane, which pumps protons from the cytoplasm into the lysosome (Figure 1. 14).

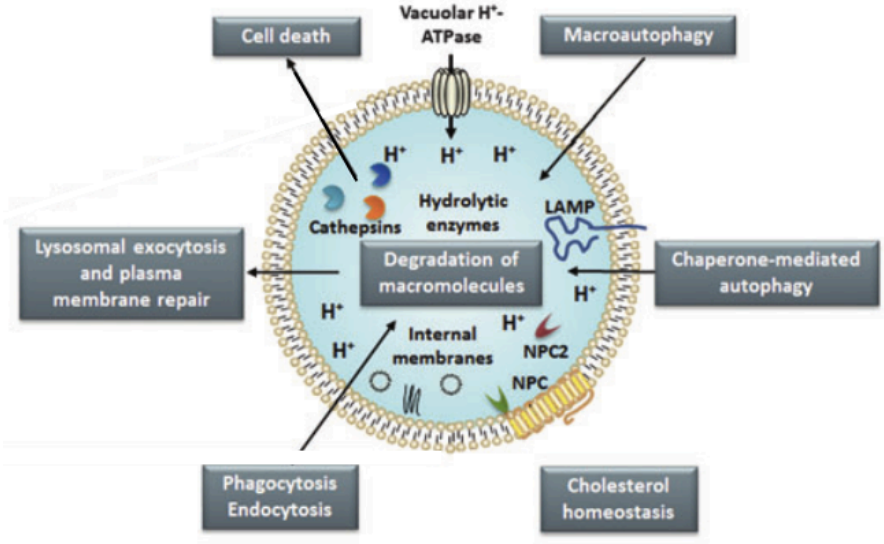

Figure 1. 14 – Main functions of Lysosomes, required for homeostasis maintenance (Appelqvist et al. 2013).

The V-ATPase also interacts with important protein complexes, such as the lysosomal nutrient sensing (LYNUS) machinery, in order to sense lysosomal nutrient content and signal information to the nucleus (Settembre, Fraldi, et al. 2013). Briefly, degradation

occurring at the lysosomal lumen is detected on the cytosolic face through amino-acid release and consequent activation of mTORC1 at the lysosomal surface. As such, the activity of specific proteins is directly affected by the lysosome and, conversely, lysosomal function is regulated by the proteins and protein complexes which interact at the lysosomal surface (Ballabio 2016).

A critical aspect which determines degradative function of a lysosome is its luminal pH (Kissing et al. 2015). In fact, the amount of available protons reflects the net charges of biological surfaces, impacting protein structure and function. Thus, acidification is a key feature which allows for protein sorting, receptor-ligand dissociation and recycling, post-translational modifications, and also membrane fusion and fission (Kissing et al. 2017). Additionally, although acidification and spatial distribution are typically thought of as coincidental events in endosome maturation steps, a causal effect has been demonstrated (Korolchuk & Rubinsztein 2011; Cabukusta & Neefjes 2018). In fact, when spatial localization of endocytic vesicles is altered, so is their intraluminal pH and, consequently perinuclear lysosomes are generally more acidic, while peripheral lysosomes are less acidic (Johnson et al. 2016). All of these aspects are thus required for efficient cargo processing within degradative pathways. In order to upkeep a low pH, the V-ATPase pumps protons into the endocytic vesicles, generating an electrochemical potential difference across the membrane. To that effect, the V-ATPase relies on a rotary mechanism composed by two sectors, acting together: sector V_1 is responsible for ATP hydrolysis and generation of the rotational force which drives proton transport through sector V_0, which manages the transport of protons through the membrane into the lumen (Maxson & Grinstein 2014).

Because the lumen of the organelle becomes positively charged, there is concomitant import of anions and/or export of cations, in order to neutralize the generated voltage. Chloride channels found in endosomes, phagosomes and lysosomes participate in this process, by regulating Cl^- intake, while transient receptor potential cation channel, mucolipin (TRPML) regulates cation export (Kissing et al. 2017). Another way to control organelle pH is by managing V-ATPase location and assembly of its two sectors, depending on isoform expression, tissue specificity or metabolic status, for instance. Lastly, lysosomes and phagosomes have been reported to exhibit proton leakage, with consequent increase of luminal pH, conveying acidification control with yet another layer of complexity (Kissing et al. 2017; Mindell 2012).

The acidic environment provides the lysosome with degradative ability by enabling the activity of several hydrolases, including proteases, lipases, nucleases, sulfatases, glycosidases and phosphatases, whose endeavor is optimal at pH 4.5-5 (Kissing et al. 2017). This vast collection of enzymes allows the processing of numerous biological substrates, such as sphingolipids, glycogen, glycosaminoglycans and proteins (Settembre, Fraldi, et al. 2013). Lysosomal hydrolases are trafficked from the Golgi into lysosomes (or targeted for secretion), mainly through mannose-6-phosphate receptors (M6PR)-mediated regulation. In fact, lysosomes can be distinguished from late endosomes by the absence M6PR (Brown et al. 1986; Bright et al. 1997). The lysosome itself is transported and fused

with other organelles, with Rab GTPases and SNAREs acting as mediators (Luzio et al. 2007). Particularly, several players involved in the fusion between (auto)phagosomes and endolysosomes also participate in their biogenesis (Settembre, Fraldi, et al. 2013; Wartosch et al. 2015). Cathepsins are the principal lysosomal proteolytic enzymes, and therefore, their activity is generally considered as a readout of lysosomal degradative ability. They are typically characterized as members of the lysosomal cysteine proteases family, even though there are also members of the serine protease (cathepsins A and G) and aspartic protease (cathepsins D and E) families (Laurent-Matha et al. 2006).

1.4.3 Lysosome biogenesis and regulation

Lysosome biogenesis is regulated mainly by the members of the Microphthalmia family of transcription factors. Together, Transcription Factor EB (TFEB), TFE3, TFEC and Microphthalmia-associated Transcription Factor (MITF) constitute the MiT/TFE family. Interestingly, the "microphthalmia" designation stands from the deficient eye development in MITF mutants, which also present abnormal pigmentation both in RPE and melanocytes (Fuhrmann 2010). This family has been shown crucial for nutrient sensing and maintenance of homeostasis, namely through regulation of lysosomal function and energy metabolism. Activity of this family of TFs has been shown important for different cell types, namely RPE, melanocytes, dendritic cells, osteoclasts, etc (Martina et al. 2015; Slade & Pulinilkunnil 2017; Napolitano & Ballabio 2016). Crucial functions related to cell survival, immunity, proliferation, tissue specification, pigmentation, all are regulated in some degree by this MiT family (Steingrímsson et al. 2004). It is not a coincidence that many of these functions rely on lysosomal or lysosome-related organelles' typical features.

The hypothesis by which lysosomal function is transcriptionally regulated was first tested by Ballabio's group (M Sardiello et al. 2009). Through the analysis of the promotor region of several lysosomal genes, one motif stood out for being able to recognize members of the MiT/TFE family. This motif was designated by Coordinated Lysosomal Expression and Regulation (CLEAR) element, and shown to drive the expression of lysosomal hydrolases and autophagy-related proteins (Keeling et al. 2018; Napolitano & Ballabio 2016; Platt et al. 2012).

Members of the MiT family have similar structures and are able to homodimerize or heterodimerize, a critical step for binding to DNA and consequently activate expression of target genes (Martina et al. 2015). TFEB, MITF and TFE3 also share a conserved activation domain, which is absent in TFEC (Zhao et al. 1993). Because these TFs regulate a similar set of genes and because they themselves are regulated in a similar way, studies concerning one member of the family generally can apply to all other members. Particularly TFEB has been described to regulate lysosomal genes that usually contain clusters of multiple CLEAR sequences: overexpression of TFEB causes increase in lysosomal gene expression, as well as added activity of hydrolytic enzymes, for instance Cathepsin D, and the opposite effect is observed upon its silencing (M Sardiello et al. 2009). Additionally, TFEB also induces lysosomal exocytosis and autophagy (Settembre, Fraldi, et al. 2013) (Figure 1. 15).

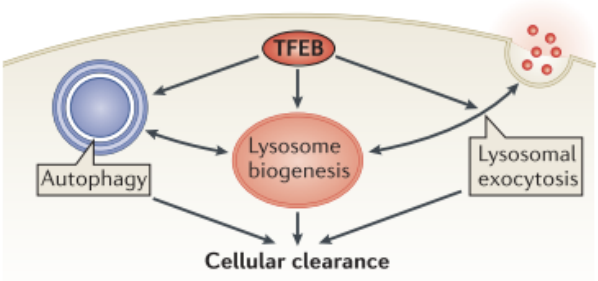

Figure 1. 15 - TFEB, and other MiT family members, control fundamental processes of cellular clearance. namely lysosomal biogenesis, autophagy and lysosomal exocytosis (Settembre, Fraldi, et al. 2013).

MiT/TFE transcription factors alternate between an inactive cytosolic form, when phosphorylated by mTORC1 or ERK2 (also known as MAPK1) and an active form, which upon de-phosphorilation translocates to the nucleus and drives gene expression (M Sardiello et al. 2009; Napolitano & Ballabio 2016). De-phosphorilation of TFEB occurs through mTORC1 inhibition and also activation of the phosphatase calcineurin. For example, during exercise, calcium release in muscle cells induces Calcineurin, which de-phosphorilates TFEB, causing it to translocate to the nucleus and drive mitochondrial biogenesis and also glucose uptake. AMP-activated protein kinase (AMPK), on the other hand, responds to reduced ATP levels, by inhibiting mTORC1 and by directly activating autophagy players ULK1 and BECN1(Galluzzi et al. 2017).

The physiological role of TFEB is highly context-specific, for instance while in the liver it plays a striking effect on lipid metabolism, in muscle tissue it has a strong influence on mitochondria biogenesis. For this reason, when studying the different processes driven by TFEB regulation, its role in cellular adaptation to challenges stands out: adaptation to starvation, adaptation to physical exercise, to infection, etc, with the lysosome at the center of these key processes. TFEB and TFE3 have also been reported in circadian rhythm regulation, with involvement in the rhythmic induction of lysosomal and autophagic genes, suggesting there is a direct link between light/day onset and nutrient management (Luo et al. 2016). Additionally, a recent study demonstrated mTORC1 activation subsequent to POS shedding-morning burst, and also after *in vitro* feeding of POS to RPE cells (Yu et al. 2018).

1.4.4 The dynamic nature of lysosomes

For a long time, lysosomes have been described as the degradative compartment of the cell and the endpoint of the endocytic and the autophagic pathways (de Duve 2005). More recently, lysosomes have been shown to be much more heterogeneous and dynamic than previously described, and our knowledge of functional interactions between all these pathways has significantly expanded (Settembre, Fraldi, et al. 2013; Luzio et al. 2017).

Lysosomes receive newly synthesized proteins from the trans-Golgi network and also cargo targeted for degradation, which is delivered by direct fusion of the lysosome with late endosomes, phagosomes or autophagosomes (Figure 1. 16).

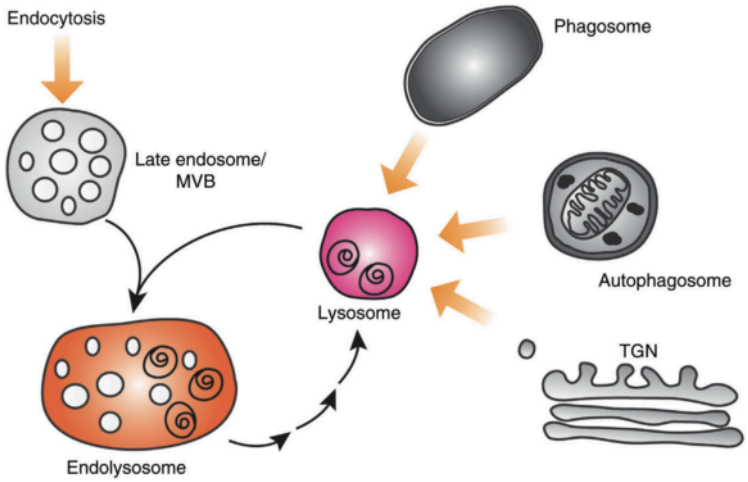

Figure 1. 16 - Lysosomes are very dynamic, continuously fusing with other organelles, to form hybrids, and reforming back into lysosomes, after cargo processing (Wartosch et al. 2015).

Lysosomes are thus in the center of the metabolic/catabolic balance of the cell. Nowadays, lysosomes are thought to have a crucial role in sensing nutrient availability and composition. Specifically, they are involved in signaling to the nucleus, mediating cellular responses to starvation and thus regulating energy metabolism, programmed cell death, plasma membrane repair, development, differentiation, immune response, among others (Settembre, Fraldi, et al. 2013; Luzio et al. 2017; Carmona-Gutierrez et al. 2016; Choy et al. 2018).

Some specific cell types evolved more permanent adaptation strategies, in order to provide specialized functions, in what are called collectively lysosome-related organelles (LROs) or secretory lysosomes. LROs are organelles that share many features with lysosomes, however LRO secretion has been shown to convey unique functions to specific cell types, such as bone resorption by osteoclasts, pigment transfer by melanocytes, degranulation of cytotoxic T lymphocytes, and hydrolase release by spermatozoa, during fertilization (Settembre, Fraldi, et al. 2013).

LROs and (conventional) lysosomes are thought to have similar origins and to use the same molecular machinery to move towards the plasma membrane and fuse. In fact, evidence suggests that virtually in all cell types lysosomes are able to undergo regulated exocytosis, in response to stimuli, such as an increase in intracellular calcium concentration (Reddy et al. 2001; Rodríguez et al. 1997; Andrews 2000; Luzio et al. 2014). This lysosome exocytosis mechanism was shown to be important in a variety of cellular processes, namely plasma membrane repair, microbial infection and ECM degradation (Appelqvist et al. 2013; Samie & Xu 2014). Importantly, lysosomal exocytosis, whether in the context of

LROs' or in stimulated conventional lysosomes, is thought to be regulated by TFEB (Medina et al. 2011).

The term "lysosome" occasionally acquires a broad denotation, when considering its different characteristics. As our understanding of the molecular mechanisms surrounding this organelle advances, new concepts emerge, in order to relay the full complexity of this compartment. Specifically, transient/kiss-and-run and complete fusion events between lysosomes and late endosomes or MVBs have been described as necessary for the delivery of macromolecules to acidic and hydrolase-active compartments inside the cell. From these fusion events, new hybrid organelles emerge, known as endolysosomes (or autolysosomes or phagolysosomes), which have a mixture of properties between late endosomes and lysosomes. After cargo processing, vesicles bud off from endolysosomal tubules and mature into dense lysosomes, completing the endocytic and autophagic cycles of degradation, by fission events and reformation of lysosomes (Platt et al. 2012; Bright et al. 2016). In this context, lysosomes can be regarded as storage compartments for acidic hydrolases that become active only upon fusion with endolysosomes, and return to an inactive state after this lysosome reformation, within what are designated terminal storage lysosomes (Figure 1. 17).

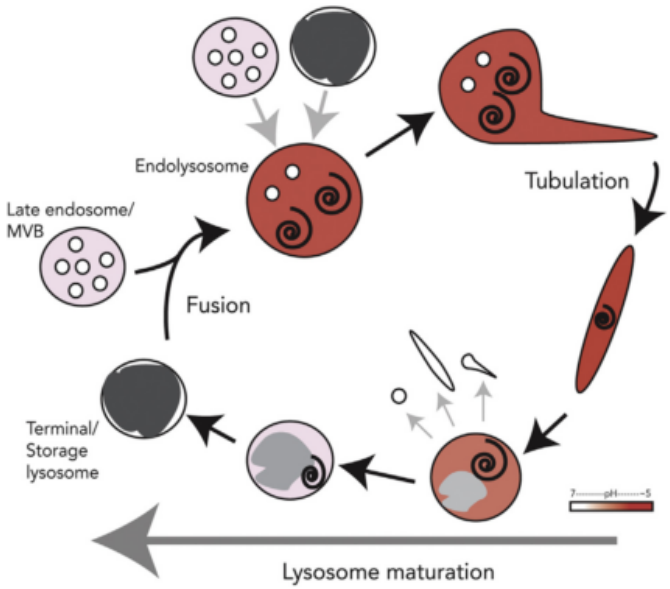

Figure 1. 17 - The lysosome cycles as it fuses to form hybrid catabolically active endolysosome and reforms back to a mature, terminal storage lysosome (Bright et al. 2016).

Likewise, luminal pH has been suggested to be highly acidic for endolysosomes, as it is required for hydrolytic events, while terminal storage lysosomes are proposed as a less acidic reservoir, which does not accumulate acidotropic probes (Bright et al. 2016). These relevant studies on lysosome biology are dissecting these intersections and shedding light on the true dynamic nature of the lysosome.

1.4.5 Lysosomal Dysfunction

At a molecular level, in lysosomal dysfunction settings, whether standing from genetic Lysosomal Storage Disorder (LSD) or from other contributory stressors such as aging, cells present excessive levels of undegraded macromolecules or catabolic products. Plus, increased numbers of endo/autolysosome are typically found in these cases. This accumulation arises from defects in intracellular clearance mechanisms (Li et al. 2016; Samie & Xu 2014). Undegraded material accumulated due to mutated lysosomal components will itself inhibit the activity of other lysosomal enzymes, leading to secondary substrate accumulation (Platt et al. 2012). Furthermore, TFEB signaling pathway was shown to be activated in several LSDs, suggesting this pathway to be abnormally stimulated, possibly as a coping mechanism (M Sardiello et al. 2009). Progressive accumulation of undegraded molecules triggers a cascade of events which impacts not only the above mentioned pathways, but also other organelles, such as mitochondria, the Endoplasmic Reticulum, Golgi, peroxisome and overall homeostasis (Platt et al. 2012). For this reason, there is a decrease of the autophagic flux and persistence of autophagosomes both without and with lysosomal markers (autolysosomes). Additionally, microautophagy and chaperone-mediated autophagy are also impaired in the lysosomal dysfunction context, as is lysosomal reformation, suggesting both fusion and fission problems (Platt et al. 2012; Valapala et al. 2014).

Altogether, genetic diseases characterized by lysosomal proteins' dysfunction and consequent accumulation of undigested cargo are collectively known as Lysosome Storage Disorders or LSDs (Platt et al. 2012). LSDs have an estimated incidence of 1 in every 5000 live births and comprise over 50 different disorders. Most LSDs stand from genetic mutations affecting hydrolytic enzymes, albeit some forms also result from defects in lysosomal membrane proteins or non-enzymatic soluble lysosomal proteins (Saftig & Klumperman 2009; Wartosch et al. 2015). LSDs usually present as infancy neurodegenerations, although adult-onset also occurs. A study in the UK revealed that lysosomal disorders are the most common cause of neurodegeneration diagnoses in children, accounting for 45% of cases (Verity et al. 2010; Platt et al. 2012). Central Nervous System (CNS) involvement in LSDs is fairly common, and associated neurodegeneration can occur in multiple brain regions. Neurons seem particularly susceptible to endo-lysosomal defects since mutations in lysosomal enzymes give rise to multiple neurodegenerative genetic diseases, in spite of the ubiquitous function of lysosomes.

LSDs are considered a group of rare diseases, however the same features related to impairment of cargo digestion and consequent effects namely for the endocytic and autophagy pathways, are thought to also underlie conditions such as Parkinson's disease (PD), Alzheimer's disease (AD) and Huntington's disease, among other neurodegenerative disorders (Keeling et al. 2018; Dehay et al. 2013; Carmona-Gutierrez et al. 2016). The mechanisms that drive mistrafficking and buildup of different substrates, in these cases (α-synuclein in PD, amyloidβ in AD or Huntingtin protein in the case of Huntington's), are

different in many aspects, but all culminate in lysosomal overburden and autophagy impairment (Keeling et al. 2018; Wartosch et al. 2015).

In general, disease manifestation may depend on the type of metabolite that becomes accumulated, on the type of response triggered (for instance local inflammation or apoptosis) and also on the susceptibility that different cell types present to lysosomal stress (Platt et al. 2012). Naturally, post-mitotic cells, such as neurons and the RPE, are vulnerable to lysosomal malfunction, yet other cell types may also be severely affected. For instance Type 1 Gaucher Disease is a relatively common LSD, caused by β-glucocerebrosidase deficiency, which manifests in macrophages (Platt et al. 2012).

In some forms of hereditary spastic paraplegias, in Chédiak-Higashi syndrome and also in the case of mucolipidosis, there is impairment of lysosome reformation from autolysosomes (Durchfort et al. 2012; Treusch et al. 2004; Chang et al. 2014). Studies where lysosome reformation was hampered using sucrose buildup in both late endosomes and endolysosomes showed they were able to fuse with lysosomes, depleting the cell of dense core (terminal storage) lysosomes. This implies there was no significant biogenesis in this case, but instead lysosomes reformed from endolysosomes, when sucrose digestion was resolved by uptake of exogenous invertase (Bright et al. 1997). A similar reformation defect was demonstrated by different approaches, including inhibition of PI3-kinase, PIKfyve and also of cathepsin activity (Olson et al. 1980; Kim et al. 2014; Bright et al. 1997; Yu et al. 2010; Choy et al. 2018). Niemann-Pick Type C (NPC) disease is an LSD which is characterized by mis-trafficking of cholesterol, and its accumulation at LE and lysosomes, among other lipids. Particularly in this case, lysosome reformation was shown to be hampered due to NPC1 or NPC2 protein deficiency, with cells presenting problems in LE/lysosomal fusion and fission, respectively (Goldman & Krise 2010). Interestingly, NPC1 and NPC2 are lysosomal proteins (membranar and soluble, respectively), with important roles related to ion-trapping mechanisms, in fact playing a role in amine accumulation and vacuolization of lysosomes. Accumulation of lysomotropic amines, for instance chloroquine, has been shown to stimulate LE/lysosome fusion events, as well as lysosome exocytosis, in an NPC1 dependent way (Goldman & Krise 2010; De Duve et al. 1974; Kaufmann & Krise 2008).

Even though some studies suggest a duality between lysosome biogenesis and reformation from pre-existing lysosomes, these concepts are tightly connected. However, the mechanisms that fail in lysosomal dysfunction settings are still unknown. In homeostatic conditions, upon degradation of cargo within the lysosome, the cell undergoes lysosome reformation mediated by mTOR reactivation. In this case, mTOR reactivation is thought to be triggered by amino acids leaving the lysosome to be recycled (Shang et al. 2017; Settembre, Fraldi, et al. 2013; Yu et al. 2018). Conversely, pharmacological inhibition of lysosomal proteases and general lysosomal impairment in LSDs settings, impair mTOR reactivation, thus impeding lysosomal reformation (Yu et al. 2010). On the other hand, upregulation of MiT family members, namely TFEB and TFE3, is crucial to clear accumulation of substrates resulting from defects in the lysosomal-autophagic

pathway in several models of disease (Ballabio 2016). In particular, TFEB overexpression was shown to reduce the buildup of substrates and ameliorate the damages in LSDs (Spampanato et al. 2013), in models of obesity (Settembre, De Cegli, et al. 2013) and in neurodegenerative disorders: Parkinson's (Decressac et al. 2013), Alzheimer's (Polito et al. 2014; Xiao et al. 2015) and Hungtington's (Tsunemi et al. 2012; M Sardiello et al. 2009), among others. What causes impairment in mTOR reactivation, whilst precluding sufficient activation of lysosomal biogenesis by MiT members remains the missing link. Nevertheless, it is not unreasonable to consider that a shift in the equilibrium of these processes reaches a chronic non-recoverable imbalance.

1.4.6 Lysosomes in Retinal Degeneration

In the eye, the RPE is responsible for maintaining photoreceptor health and to recycle the visual pigment, by daily digestion of POS. Each RPE cell contacts closely with 24-45 rod or cone photoreceptors and phagocytoses an estimated 10% of their volume every day (Keeling et al. 2018; Young 1971).

This lysosomal burden has been proposed as a key mechanism underlying AMD, Stargardt disease and Choroideremia (CHM) (Keeling et al. 2018; Guha et al. 2013; Anderson et al. 2017; Wavre-Shapton et al. 2013), among others. A common feature underlying these diseases is lysosomal dysfunction, typically characterized by increased lysosomal pH and accumulation of unprocessed cargo (Keeling et al. 2018; Sinha et al. 2016; Guha, Coffey, et al. 2014) (Figure 1. 18).

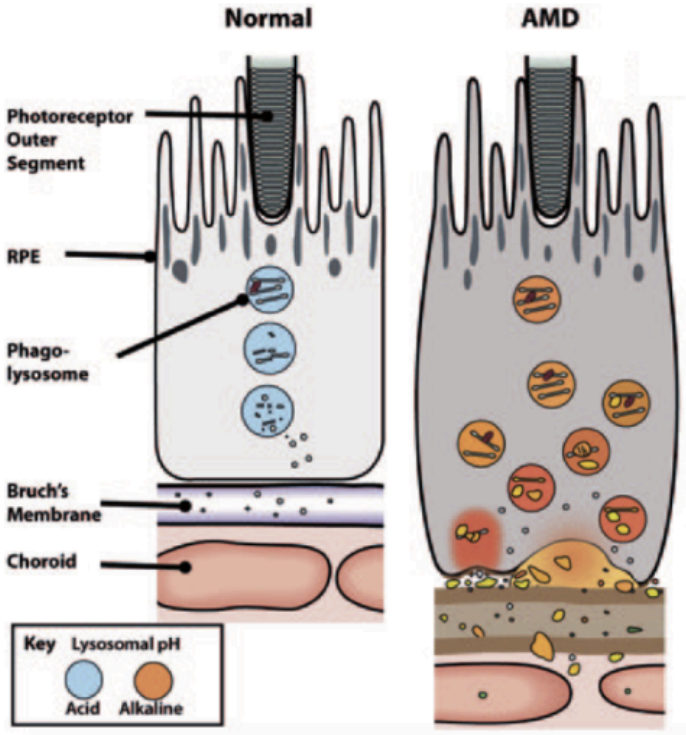

Figure 1. 18 - Normal/healthy RPE *versus* AMD settings: lysosomal pH is increased, and cargo accumulates both intra and extracellularly (Guha, Coffey, et al. 2014).

Additionally, pharmacological agents such as chloroquine have been shown to cause retinopathy, due to lysosomal impairment (Mahon et al. 2004; Guha, Coffey, et al. 2014).

These retinopathies are generally characterized by accumulation of undigested cargo, namely POS, as well as autophagy substrates, identified by typical markers such as LC3 and SQSTM1/p62. These components, together with oxidized lipids, are thought to originate lipofuscin granules. Lipofuscin occurs naturally and accumulates gradually with aging, but is exacerbated in disease settings. Such is the case of Stargadt disease, some LSDs, for instance Niemann-Pick C and neuronal ceroid lipofuscinosis, and also AMD (Anderson et al. 2017). Besides lipofuscin, appearance of complex granules such as melanolipofuscin and melanolysosomes have been proposed as trademarks of RPE damage and/or aging. Consistent with that model, researchers have found that while melanin content decreases with aging, lipofuscin and complex granules increase, together occupying up to 30% of RPE cytoplasmic area in aged eyes (Feeney-Burns et al. 1984).

Lipofuscin's molecular composition has not been fully characterized, however N-retinylidene-N-retinylethanolamine (A2E) is found in lipofuscin granules and has been extensively studied (Anderson et al. 2017). A2E was shown to be a cationic amphiphilic derivate of N-retinylidene phosphatidylethanolamine which builds up in RPE and interferes with phagolysosomal digestion of POS, by disturbing cholesterol metabolism, inhibiting the V-ATPase and irreversibly inhibiting protease activity up to 50% (Anderson et al. 2017; Kevany et al. 2010; Keeling et al. 2018). A2E can also cause damage to mitochondrial membranes and to DNA. Furthermore, it is photo-oxidized, generating free-radical species which modify lipids to form high molecular weight components that remain stable in the lysosome (Keeling et al. 2018; de Jong 2006).

Ultimately, lysosomal dysfunction is considered a central factor contributing to retinal degeneration. Accumulated cargo is thought to be in part retained by the RPE and in part exocytosed. Consequently, these aggregates are found both in the RPE and also in drusen deposits, underneath (Keeling et al. 2018; Guha, Coffey, et al. 2014). It has been proposed that in aged RPE, intracellular unwanted material can be released via exosomes (Wang et al. 2009). Still, it is possible that RPE lysosomes can fuse directly with the plasma membrane and release their contents to the extracellular milieu. In this case, lysosome exocytosis would function as an emergency safety valve for intracellular clearance. Indeed, the role of lysosome exocytosis in the maintenance of plasma membrane integrity has been extensively studied in tissues susceptible to mechanical or ischemic stress, such as skeletal and cardiac muscle and in epithelia (Appelqvist et al. 2013; Toops & Lakkaraju 2013). Additionally, abnormal lysosomal secretion in cardiac cells can promote changes in ECM turnover leading to inflammatory and apoptotic responses that contribute to the onset and progression of cardiovascular diseases. In cancer cells, on the other hand, the secretion of lysosomal hydrolytic enzymes was shown to promote ECM degradation, stimulating angiogenesis, tumor growth and invasion (Appelqvist et al. 2013; Machado et al. 2015).

Although lysosome exocytosis is an essential cellular process, the molecular machinery involved in the regulation of the different steps of this pathway is still not fully

characterized. Studies have shown that lysosomes can translocate from the perinuclear region to the cell periphery along microtubule tracks, independently of the intracellular calcium concentration, by a mechanism similar to that of lysosome-related organelles (Pu et al. 2015). In polarized cells, such as the RPE, lysosomes have been shown to fuse predominantly with the basolateral membrane in a process regulated by the actin cytoskeleton and membrane cholesterol (Xu et al. 2012).

1.5 Final Remarks

Vision impairment significantly alters quality of life of affected individuals and constitutes a large healthcare burden to society. In the developed countries, over 50% of blind patients suffer from retinal disorders caused by age-related, diabetic or genetic diseases. Current treatments focus mainly on symptom management, even though there are still large gaps in our knowledge of the eye homeostasis and its control mechanisms. Therapies aimed at the regeneration and repair of retinal cells, namely RPE, are of great interest, given the significant impact on patients' lives (Congdon 2004; Leach & Clegg 2015).

There are many advantages when it comes to studying the eye and developing therapies to improve vision. These are related to the fact that the eye is a relatively small organ, readily accessible for monitoring improvements or deficits non-invasively; moreover, it is separated from systemic circulation by the blood-retinal barrier and has potential immune privilege. Finally, it is convenient, for research purposes, to be able to compare progress in a treated eye, to its paired control (Bharti et al. 2010; Leach & Clegg 2015).

Nowadays, the concepts related to RPE differentiation from Pluripotent Stem cells are becoming familiar. Yet, part of the reason why there are few therapies targeting initial events of AMD is the scarcity of reliable human RPE *in vitro* models available before the advent of hPSc differentiation. Moreover, by studying differentiation of stem cells, as well as eye patterning, it is now possible to develop more complex systems, recapitulating not only the RPE monolayer, but other components of the visual unit, such as the Bruch's membrane and choroid (Leach & Clegg 2015; Song & Bharti 2016).

On the other hand, we know surprisingly little about lysosomes despite 60 years of research. The operational definition of a lysosome (pH 4.5-5, containing hydrolytic enzymes and specific membrane proteins such as LAMPs) is too simple to reflect the reality. By large, the biogenesis, ageing and degradation of lysosomes remain ill characterized. Therefore, it is not surprising that lysosome dysfunction is similarly ill characterized. Lysosomes are no longer considered merely the end-point of degradation in the cell. Instead, they are now regarded as hubs of nutrient sensing and cell signaling events, allowing for a tight control of degradation and recycling. Lysosomes can accumulate a variety of cargos and release them, depending on the cell's demand. This metabolism control implies harmony between the multiple pathways that reconcile at the lysosome, as well as interaction with transcription regulators, in order to keep the cellular energy balance.

Most common reports on degenerative diseases focus problems associated with the elimination of a single mutant protein, giving rise to accumulation of misfolded proteins aggregates. Conversely, age-related degenerations often stand from impaired turnover of long-lived proteins and organelles. Specifically, in the RPE, the lysosomal network is subjected to a heavy burden.

The working hypothesis in the basis of this work is that AMD degenerative process, occurring within the RPE, is caused by lysosome dysfunction. As an emergency mechanism, it is postulated that the RPE secrete the indigestible material by lysosomal exocytosis, which in turns initiates a series of characteristic extracellular events, such as drusen formation and inflammation. Eventually, RPE cells die and the associated photoreceptors die too, leading to retinal degeneration. In fact, many cardinal features of AMD are reminiscent of lysosomal dysfunction, including the intracellular accumulation of protein aggregates, gathering of lipofuscin and of extracellular, poorly digested deposits (drusen).

CHAPTER 2

Materials and Methods

2.1 Cell Culture and maintenance

All cells were maintained at humidified cabinet at 37ºC and 5% CO_2.

2.1.1 human Embryonic Stem cells (hESc)

Human embryonic stem cell line H9 (WiCell Research Institute, Madison, WI, http://wicell.org) was maintained in mTeSR1 medium or in Essential 8 Flex medium, on hESC-qualified matrigel-coated plates (BD Biosciences).

2.1.2 human RPE from Lonza (Lonza hRPE)

hRPE purchased fom Lonza were cultured in Retinal Pigment Epithelial Cell Growth Medium (Lonza) and, upon confluence, changed to Dubelcco's Modified Eagle Medium (DMEM) F12 (Biowest), supplemented with 1% FBS (Gibco/Invitrogen) and PenStrep (Gibco/Invitrogen). These cells are plated onto laminin-coated surfaces (BioLamina rhLaminin-521).

2.1.3 Porcine RPE primary cultures and maintenance (pRPE)

Porcine eyes were collected, pre-scalding, and eyes were kept on ice; RPE was collected and put in culture on the same day. Briefly, external tissue from the eye balls was removed and eyes were cleaned in an iodine surgical scrub solution, diluted 1:4 in water. Eyes were washed in a PenStrep/PBS solution for 5min. The eyes were opened, inside the tissue culture hood, using a scalpel, and kept in multiwell dishes, opening facing up. The eye cups were filled with PBS and the neural retinas were removed. PBS was replaced by trypsin and the eye cups were incubated for 30min, at 37ºC. RPE was ressuspended in DMEM 10% FBS, spun at 1000rpm at room temperature, 5min. The pelleted cells were ressuspended in fresh medium (containing 10% FBS) and seeded in 6-well plates. Medium

(DMEM F12 from Biowest) is changed once a week until cells reach confluency, at which point they are changed to reduced-serum medium (1% FBS). Primary cultures can be expanded and used for assays, by plating onto multiwell plates, maintained in DMEM F12 (Biowest), supplemented with fetal bovine serum (FBS) (Gibco/Invitrogen), 100U/mL Penicillin and 100µg/mL Streptomycin (PenStrep) (Gibco/Invitrogen). Whenever using glass coverslips or transwells, cells were seeded onto laminin-coated surfaces (BioLamina rhLaminin-521).

2.1.4 hESc-RPE differentiation and maintenance

Upon colony maturation, H9 cells were dissociated with Versene and passaged directly onto non-growth factor reduced Matrigel, in retinal differentiation medium (RDM): DMEM F12 with 1x B27, 1x N2 and 1x NEAA. For day 0, the following factors were added to the RDM: 10mM Nicotinamide, 50ng/mL noggin, 10ng/mL Dkk-1, 10ng/mL IGF-1. On day 1, medium is changed to remove cell debris, but composition is maintained. At day2, media composition is changed, as the following factors are added to the RDM, 10mM Nic, 10ng/mL noggin, 10ng/mL Dkk-1, 10ng/mL IGF-1 and 5ng/mL bFGF. At day 4, media is again changed, by adding to the RDM: 100ng/mL activin A, 10ng/mL Dkk-1, 10ng/mL IGF-1. At day 6, 100ng/mL activin A, 10µM SU5402 are added to the RDM. Finally, at days 8, 10 and 12, RDM is supplemented with 100ng/mL activin A, 10µM SU5402, 3µM Chir99021. At day 14, immature RPE is obtained, and cells are transferred to new wells (previously coated with growth factor reduced Matrigel), at $1x10^5$ cells/cm^2 density – P0. These new and small RPE cells are maintained with X-VIVO 10 medium (Lonza), changed twice a week, and left to mature for 30 days. At day 30 cell pigmentation is evident and cells are passaged again (P1) to further expand the culture. From this point on, cells are plated onto laminin-coated surfaces (BioLamina rhLaminin-521).

Table I: Retinal Differentiation Media Supplements and Reagents

Reagent	Supplier (Manufacturer)	Concentration
N2 Supplement	Thermo Fisher	1X
B27 Supplement	Thermo Fisher	1X
Nicotinamide	Sigma	1M
Recombinant mouse noggin	Fisher (R&D Systems)	10-50ng/mL
Recombinant human DKK-1	Fisher (R&D Systems)	10ng/mL
Recombinant human IGF-1	Fisher (R&D Systems)	10ng/mL
bFGF	Peprotech	5ng/mL
Recombinant h/m/r Activin A	Peprotech	100ng/mL
SU5402 FGF inhibitor	Santa Cruz Bio.	10µM
CHIR99021	Stemgent	3µM
Y27632	Fisher	10µM
Non-GFR Matrigel	Fisher	N/A

2.1.5 ARPE19

Human RPE cell line ARPE19 was obtained from American Type Culture Collection (ATCC). This cell line was cultured in DMEM/F12, containing 10% FBS and Pen Strep.

2.2 POS isolation from porcine eyes

Porcine eyes were collected and eyes were kept on ice. External tissue from the eye balls was removed and eyes were washed in a PenStrep/PBS solution for 5min. The eyes were opened, using a scalpel, and kept in multiwell dishes, opening facing up. The eye cups were filled with PBS and the neural retinas were removed and collected in a falcon containing homogenization solution (20% sucrose, 20mM tris acetate pH 7.2, 2mM $MgCl_2$, 10mM glucose, 5mM taurine). Retina homogenate was filtered through gauze and added to a continuous sucrose gradient (25-60%). POS are separated by centrifugation at 25.000 rpm (76,7g) for 120min, in a Beckman SW-32-Ti swing rotor. A single orange band in upper third of gradient, corresponding to POS, was aspirated with a P1000 tip and collected into a new falcon. After three washes, POS prep were stored in medium containing 10% FBS, 2.5% sucrose, azide 0.04% and PenStrep. Before Phagocytosis assays, POS preps were washed three times in PBS.

2.3 Phagocytosis Assays

RPE cells seeded onto polycarbonate Transwell® membrane inserts were challenged for 4 h at 37˚C with POS in basal medium with 10% FBS (50-200µg/mL), after POS were subjected to a 5-min sonication step in an ultrasonic bath. After the pulse, cells were washed three times with PBS to remove the unbound POS and chased for 24 h up to one week.

2.4 Chloroquine (CQ) treatments

All RPE cells tested were repeatedly subjected to the following treatments, on an everyday basis: a period of 4h pulse with medium containing 10% FBS, either without or with porcine POS (200µg/mL); this pulse was followed by an overnight treatment of either regular medium (reduced serum) or medium containing chloroquine with concentration ranging from 1µg/mL to 50µg/mL (corresponding to approximately 2-100µM, respectively). One round of this treatment is considered an acute CQ treatment; for three consecutive days it is considered a continued CQ treatment; seven consecutive rounds of this treatment are considered a chronic CQ treatment. At instances where Rapamycin and Bafilomycin were used as controls, they were acutely/continued/chronically added to the media, rather than CQ, in parallel wells.

2.5 Polarity assessment of RPE monolayers

Barrier function was assessed by monitoring TER with an epithelial volt/ohm meter using an electrode (STX2; World Precision Instruments, Sarasota, FL). The resistance values for individual monolayers at specific times (Ωcm^2) was determined from the average of three independent measurements, and corrected for background resistance produced by the blank filter and culture medium.

2.6 RNA isolation and Reverse Transcriptase (RT)-PCR

Total RNA was extracted using RNAse Mini kit (Qiagen) according to the manufacturer's instructions. One µg of RNA was converted into complementary DNA using random primers and SuperScript II reverse transcriptase (Life Technologies).

2.7 Viability assays - Lactate Dehydrogenase (LDH)

Conditioned media were collected after cells were appropriately treated. LDH activity was assessed, according to Kit instructions (Thermo Scientific Pierce LDH Cytotoxicity Assay Kit # 88953). Briefly, conditioned media were incubated with reaction mixture, for 30min at room temperature. Stop solution was added and absorbance was measured at 490 and 680nm.

2.8 Exosomes Isolation

Exosome isolation was performed by sequential centrifugation. Briefly, (exo-free) conditioned medium from hESc-RPE was collected and centrifuged at 300g, to remove cell debris. Medium was recovered into ultracentrifuge tubes and spun for 20min at 16500g, 4ºC. Medium was again recovered and filtered (200µm filter) into new ultracentrifuge tubes and centrifuged again for 1h10 at 120 000g, 4ºC. Medium was discarded and exosomes were ressuspended in PBS and re-centrifuged for 1h10 at 120 000g, 4ºC. PBS was discarded and exosomes were recovered in Ripa Buffer and prepared for Western Blot.

2.9 Flow Cytometry

Cells were washed with PBS, detached using trypsin and resuspended in FACS buffer (1% FBS and 2mM EDTA in PBS). Acquisition was performed in a FACS CANTO II (BD Biosciences) flow cytometer, and at least 20 000 cells were analyzed using FlowJo version 10.1r7 software.

2.10 ß-hexosaminidase (β-hex) release

β-hex release assay was performed as described elsewhere (Rodríguez et al., 1997; Kima et al., 2000). In brief, hESc-RPE cells were seeded transwells and incubated until confluency and formation of polarized epithelium (TER>150Ωcm^2) at 37°C, 5%CO_2.

Cells were treated with 200µg/mL POS for 4h from the apical side, following which medium of both chambers was changed to CQ-containing medium, for overnight incubation. This was repeated for three days, in the case of the continuous CQ treatment and for seven days, in the chronic treatment. Supernatant from the apical and basal chamber of the transwells were collected and kept on ice. Cells were also shifted to ice. In parallel, cells were lysed with 1% IGEPAL/dH_2O and diluted 1:5 in dH_2O. β-Hex activity was determined by incubating cell supernatant or lysate in a 96-well plate with 6 mM of the substrate 4-methyl-umbelliferyl-N-acetyl-β-d-glucosaminide (4-MU-β-D-GlcNAc; Glycosynth) resuspended in HBSS with 40 mM sodium citrate and 88 mM Na_2PO_4, pH 4.5, for 15 min at 37°C. Fluorescence was measured in a plate-spectrofluorimeter at excitation 365 nm/emission 450 nm. Protein content from cell supernatant and lysate was determined using the BCA protein assay kit (Thermo Fisher Scientific), as described by the manufacturer. HBSS-SLO-$CaCl_2$ and 1% IGEPAL 1%/dH2O were used as controls.

β-Hex activity is expressed as fluorescence (365 nm/450 nm) per milligram of cell protein. The total β-hex activity is the sum of apical and basal β-hex activity in the supernatants and 5 × (β-hex activity in the cell lysate). β-Hex released is expressed as the percentage of β-hex activity in the supernatant relative to the total β-hex activity.

2.11 Drugs and Dyes

Table II: Drugs and Dyes used for Lysosomal dysfunction studies

Drug/Dye	Action	Working dilution (Time)	Supplier
Bafilomycin	V-ATPase inhibitor	50-200nM	Sigma
Rapamycin	Autophagy inducer	100nM	Sigma
Chloroquine	Lysosome impairment	1-50µg/mL = 2-100µM	Sigma
DAPI	Nuclear staining	300nM	Thermo Fisher
Phalloidin	Actin staining	5µM	Thermo Fisher
DQ-BSA	Proteolisys read-out	10µg/mL (overnight)	Thermo Fisher
Magic Red	CatB/L activity read-out	1X (30min)	ImmunoChemistry
Bodipy CatD	CatD activity read-out	1µM (30min)	Invitrogen
Lysotracker	Acidic vesicle read-out	50nM (10min)	Thermo Fisher

2.12 Image Analysis and Statistics

Images were processed using ImageJ. Numerical data are presented as mean ± SD. Two-way analysis of variance significance analysis followed by Dunnett's test was used for comparison relative to control with GraphPad Prism software.

2.13 Antibodies used

Table III: List of Antibodies used

Antigen	Host Species	Working dilution (application)	Supplier	Catalog #
Bestrophin1	rabbit	1:50 (IF)/1:1000 (WB)	Alomone Labs	ABC-001
RPE65	mouse	1:50 (IF)/1:1000 (WB)	Abcam	ab13826
PMEL17	mouse	1:1000 (WB)/1:100 (EM)	Dako	HMB45 M0634
Rab27a	goat	1:500 (WB)	Sicgen	AB45-200
CANX	goat	1:1000 (WB)	Sicgen	AB41-200
CRALBP	mouse	1:50 (IF)	Abcam	ab15051
ZO-1	goat	1:50 (IF)/1:1000 (WB)	Sicgen	AB0054-200
TRP-1	mouse	1:50 (EM)	Abcam	ab3312
PEDF	rabbit	1:1000 (WB)	Milipore	ab07-280
VEGF	mouse	1:1000 (WB)	GeneTex	GTX23109
Flotillin-1	rabbit	1:1000 (WB)	Santa Cruz	sc-25506
CD63	goat	1:1000 (WB)	Sicgen	AB47-200
1D4	mouse	1:100 (IF);1:2000 (EM)	Abcam	ab5417
RET-P1	mouse	1:100 (IF);1:200 (EM)	Thermo Fisher	MA5-11741
TFEB	rabbit	1:50 (IF)	Werfen	1674240S
TFE3	rabbit	1:50 (IF)	Sigma	HPA023881
MitfA	mouse	1:50 (IF)	Abcam	ab12039
CatD	rabbit	1:1000 (WB)	GeneTex	GTX62063
p62	mouse	1:1000 (WB)	Santa Cruz	sc-28359
LC3	rabbit	1:1000 (WB)	Sigma	L8918
Actin	goat	1:1000 (WB)	Sicgen	AB0145-200
ApoE	goat	1:50 (IF)/1:1000 (WB)	Millipore	ab947
Lamp1	mouse	1:50 (IF)	Hybridoma bank	H4A3a

2.14 Protein Lysates and Western Blot

Whole cell lysates were collected in Ripa Buffer, quantified using the BCA kit and prepared together with Laemmli Sample Buffer. Total protein concentration of 25 µg/sample. Samples were denatured at 95°C for 10 min and then loaded in a 12% polyacrylamide gel. Proteins were transferred into a nitrocellulose membrane (Bio-Rad, USA) using the Trans-Blot® TurboTM Transfer System (Bio-Rad, Hercules, CA, USA), through a 7 min transfer. Membranes were then blocked with 5%Bovine Serum Albumin/Tris-buffered Saline – Tween 20 (5% BSA/TBS-T) (w/v) for 1 hour at room temperature and incubated overnight with the primary antibody diluted in PBS-T. The membranes were washed with PBS-T three times for 5 min each and incubated with the secondary antibody diluted in PBS-T for 1 hour at room temperature. After washing with PBS-T, the membranes were analyzed in the Chemidoc Touch (Bio-Rad, Hercules, CA,

USA) using the Pierce™ ECL Western Blotting Substrate (Thermo Fisher Scientific, Waltham, MA, USA).

In the case of VEGF and PEDF, media from 24 wells was collected from the apical and basal chambers of a set of transwells and pooled together. Protein was precipitated by incubating media in 5x vol. acetone overnight at -20ºC. The next day, media were spun 10min at 10.000rpm. Pellets were ressuspended in Ripa Buffer and prepared for western blot, as described above.

2.15 Immunofluorescence (IF)

Cells were seeded on glass coverslips (Menzel-Glaser), at $1x10^5$ cells/cm^2 density and left to mature for two weeks. Cells were washed with PBS and fixed with 4% paraformaldehyde (PFA) (Electron Microscopy Sciences) in PBS for 15min at room temperature. Cells were blocked and permeabilized with 1%BSA (Sigma) in PBS, with either 0.05% saponin (Sigma) or 0,02% Triton, for 1h at room temperature. Cells were incubated with primary antibodies, for 1h at 37ºC or overnight at 4ºC. After washing in PBS, cells were incubated with secondary antibodies for 30min at room temperature. Samples were mounted using ProLong Gold Antifade Mountant with DAPI (Thermo Fisher Scientific)

2.16 Light Microscopy

Coverslips were examined using a LSM 710 laser scanning confocal microscope (ZEISS) with a Plan-Apochromat 63× 1.4 NA oil-immersion objective; the 405, 488, 543, and 633nm laser lines; and spectral detection adjusted for the emission of DAPI fluorochromes. Digital images were analyzed by using LSM Image software or ImageJ.

For live-cell confocal imaging cells were seeded on glass-bottom eight-well (Labteks). After treatments, cells were incubated with the appropriate dyes, acording to table, washed three times with PBS and imaged.

2.17 Transmission Electron Microscopy (TEM/EM)

RPE cells were prepared and processed for conventional EM and for cryo-immuno EM.

2.17.1 Fixation and Embedding

For conventional EM of cells cultured on Transwell filters and glass coverslips: cells were fixed in 2% paraformaldehyde (PFA)/2% gluteraldehyde (GA) in 0.1M cacodylate buffer for 2 hours at room temperature, or overnight at 4°C. Post-fixation was performed with 1.5% osmium tetroxide/1.5% potassium ferrycyanite for 1 hour on ice before dehydrating with a series of ethanol solutions increasing from 70% to 100%. Cells on glass coverslips were further dehydrated with 100% propylene oxide. Transwell filters or coverslips were subsequently infiltrated with two 1 hour incubations in 100% Epon resin

and embedded in coffin moulds or Epon stubs, respectively, and polymerised overnight at 70°C.

For cryo-immuno EM, cells on Transwell filters were fixed in 4% PFA in 0.1M phosphate buffer (PB) overnight at 4°C. 0.1% GA was occasionally used in combination with PFA for enhanced structure preservation, although use of GA was limited by its masking of some epitopes. After removing the fixative, free aldehyde groups were quenched with 200mM glycine for 10 minutes before approximately 1mm x 1mm squares of filters were cut and infiltrated in 12% gelatine (Rousselot) for 1 hour at 37°C. The squares of filter were subsequently embedded in a thin layer of 12% gelatine between two glass slides, the gelatine allowed to solidify on ice for several minutes, and the embedded squares of filters were cut from the surrounding excess gelatine. Gelatine-embedded filters were sucrose-infused with a 2.3M sucrose solution overnight at 4°C for cryo-protection (Tokuyasu 1973) The specimens were mounted on pins and flash frozen and stored in liquid nitrogen.

2.17.2 Ultrathin Sectioning

For conventional EM, resin blocks were trimmed with a single-edged razor blade and the block face polished with a glass knife. 70-120nm ultrathin sections were cut on a Leica UM7 ultramicrotome using a diamond knife (Diatome), and placed on copper mesh grids or formvar-coated slot grids.

For cryo-immuno EM, trimming and polishing of frozen gelatine-embedded Transwell filters was performed using a diamond trimming tool (Diatome) in a liquid nitrogen-cooled chamber at -80°C, ultrathin sectioned at 90-120nm at -120°C, and ribbons of sections retrieved in a drop of a 1:1 mix of 2% methyl cellulose and 2.3M sucrose and placed on formvar-coated copper mesh grids.

2.17.3 Formvar Coating of Copper Grids

When single-slot grids were used, or for cryo-immuno EM, grids were coated with a thin layer of formvar to support sections. A solution of 1% formvar in chloroform was used to coat a clean glass slide, the formvar film floated upon distilled water, grids placed on top of the film and the film retrieved from the water using a parafilm-coated glass slide.

2.17.4 Immunogold labelling of ultrathin cryosections

Cryosections were labelled and thawed frozen sections were firstly placed section-side down in PBS at 37°C for 30 minutes to remove excess gelatine. All subsequent incubations were performed at room temperature. To reduce non-specific binding of antibodies, free aldehyde groups were quenched and proteins blocked using 200mM glycine and 1% BSA, respectively. Grids were incubated on a drop of diluted primary antibody in 1% BSA in PBS for 1 hour and washed several times with 0.1% BSA in PBS to remove unbound

antibodies. In the case of the primary antibodies being any species other than rabbit, the grids were incubated for 20 minutes with a bridging antibody (as protein A-gold).

2.17.5 Imaging

Specimens were observed with a JEOL 1010 transmission electron microscope and imaged with a Gatan Orius SC1000B charge-coupled device camera.

CHAPTER 3

Pluripotent Stem cell-derived Retinal Pigment Epithelium

Development and establishment of a disease model

The main goal of Chapter 3 is to describe the process through which a functional in vitro *model of human Retinal Pigment Epithelium, derived from Pluripotent Stem cells, was established in the lab. The ensuing direction of the work intends to use this newly obtained hPSc-RPE cells to address retinopathies' early events. In this section, the protocols used for differentiation are described in detail and the results obtained in each case as well as thorough characterization of newly obtained RPE cells are presented.*

3.1 RPE Differentiation Process

When human stem cells grow to confluence in the absence of basic fibroblast growth factor (bFGF) differentiation is triggered, giving rise to RPE pigmented foci, among other cell types. These pigmented cells can be excised and enriched, eventually forming RPE monolayers. This spontaneous differentiation of pluripotent stem cells into RPE began to be document thoroughly by 2002 when, after culturing monkey embryonic stem (ES) cells with a stromal cell line for 3 weeks, 8% of ES cell colonies were reported to contain polygonal pigmented cells, positive for Pax6 (Kawasaki et al. 2002). These cells were later characterized and shown to express typical RPE markers, as well as phagocytic capability (Haruta et al. 2004). Other authors invigorated this notion by demonstrating that ES cells alone can spontaneously differentiate into RPE-like cells, when cultured in the absence of FGF, for 4-6 weeks (Klimanskaya et al. 2004). The obtained cells were characterized and shown to more closely relate to human fetal RPE than to RPE cell lines, by gene expression profiling; moreover, these cells were capable of phagocytosing rod outer segments and even repair phagocytic function in the retinas of Royal College of Surgeons (RCS) rats, demonstrating their therapeutic ability in a widely used model of inherited retinal degeneration, *in vivo* (Vugler et al. 2008). Later in 2009, RPE was derived from induced

Plutipotent Stem cells (iPS cells) with similar characteristics, when compared to ESc-derived (David E. Buchholz 2009). These studies were crucial to determine that MERTK expression in these RPE cells was essential for outer segment phagocytosis (A.-J. Carr et al. 2009) and that RCS rats transplanted with human iPS cells-derived RPE have improved visual function (A. J. Carr et al. 2009), although studies have found the transplanted cells did not survive for long periods of time (Lu et al. 2009).

Even though the spontaneous differentiation method can yield high purity RPE cultures, it is lengthy and inefficient. Improvements to this technique have been developed, guided by our knowledge of the developmental biology of the eye. By relying on the effect of added exogenous factors to promote the neuro-ecotodermal lineage, followed by specification of RPE fate, it is now possible to efficiently obtain functional RPE from hPSc in as little as two weeks (Buchholz et al. 2013; Leach et al. 2015).

This process of directing differentiation towards RPE lineage has been perfected over the years. In 2008 and 2009, researchers started by using serum-free floating conditions in order to obtain neural precursors, preferably to mesodermal or endodermal lineages – this system was designated as serum-free embryoid body-like conditions, or SFEB (Hirami et al. 2009; Osakada et al. 2009; Osakada et al. 2008). Neural induction was further enhanced by adding Dkk1 and Lefty A to inhibit endogenous Wnt and Nodal signals, respectively. Cells were grown in suspension for approximately 20 days, and plated onto plates coated with poly-D-lysine, laminin or fibronectin (Hirami et al. 2009; Osakada et al. 2009). Other groups were also successful in obtaining RPE from collagen I (Kamao et al. 2014), laminin (Idelson et al. 2009), matrigel (Krohne et al. 2012) and fibronectin (Zhu et al. 2011)-coated plates.

Some researchers surpass the suspension culture step altogether and guide adherent pluripotent cells towards RPE fate, by changing medium conditions in a stepwise fashion (Brandl et al. 2014; Maruotti et al. 2013; Buchholz et al. 2013). In the end, most protocols converge in the idea that RPE specification is attained by sequentially adding neural differentiation factors followed by RPE promoting signals. One group in particular has reported over 97% efficiency (based on PMEL17 expression) of RPE differentiation, after only 14 days (Buchholz et al. 2013; Leach et al. 2015). They start by inducing neural retinal progenitors from ESc and iPSc using Noggin, Insulin Growth Factor 1 (IGF1), Dkk1 and bFGF; additional RPE-specification factors are also used, such as Nicotinamide (NIC), Activin A, Vasoactive Intestinal Peptide (VIP), SU5402 and CHIR99021(Buchholz et al. 2013; Leach et al. 2015).

The work presented herein was developed under the already validated hypothesis by which it is possible to derive hRPE cells from hPluripotent Stem cells (A. J. Carr et al. 2009; Singh, Shen, et al. 2013; Osakada et al. 2009; Maruotti et al. 2013; Buchholz et al. 2013; Eiraku & Sasai 2012; Zhu et al. 2013).

3.2 From Stem cells to RPE – Differentiation Protocol Implementation

In the course of this work, several differentiation protocols were put in place, in an effort to obtain RPE derived from Pluripotent Stem cells.

The scientific approach primarily applied to obtain a model of RPE was the follow-up of previous work, where pluripotent stem cells were reprogrammed from mouse embryonic fibroblasts (MEFs) (Pires 2014). Briefly, MEFs from a Choroideremia (CHM) mouse model were reprogrammed, either using the Yamanaka transcription factor cocktail to obtain iPS cells (Takahashi & Yamanaka 2006) or testing different combinations of eye-field transcription factors to directly reprogram MEFs into RPE, thus surpassing the pluripotent state. These particular cells had been engineered as a conditional knock-out of CHM (Pires et al. 2012; Pires 2014). During the course of the work presented herein, experiments were implemented in an effort to differentiate these previously obtained cells into functional mouse RPE, with the final goal of studying this model of retinal degeneration. Ultimately these attempts were not successful, as will be discussed in the following section.

Alternative approaches were undertaken, this time using human Embryonic Stem cells as base material, in order to obtain wild type human RPE. Differentiation protocols that had been used before for mouse iPS cells differentiation, were revisited, now for hES cells. For instance, starting from floating aggregates, protocols developed by Osakada and Zhu (Osakada et al. 2009; Zhu et al. 2013) were used; and, for adherent cell culture, protocols developed by Brandl, Maruotti and Buchholz were endeavored (Brandl et al. 2014; Maruotti et al. 2013; Buchholz et al. 2013). Among these different methodologies, application of the protocol developed by Buchholz et al. stood out with encouraging results, successfully giving rise to RPE-like cells.

Finally, all these previous experiments contributed to an enhanced stem cell- and RPE cell- handling know-how, with fruitful attainment of pure and fully mature human RPE cultures.

3.2.1 mouse RPE differentiation

As previously mentioned, differentiation protocols were first applied to mouse embryonic fibroblast cells which had been subjected to reprogramming. These earlier experiments were based on forced expression of TF-cocktails to induce changes in cell identity and ultimately originate RPE. A significant limitation of this strategy is the inability to guarantee reproducibility in the reprogramming process between experiments. To minimize this difficulty, a reporter system was developed, which was driven by Tyrosinase expression (Lenti-Tyr-GFP). Several sets of TFs were systematically tested, in particular MITF, OTX2, and PAX6 combinations, due to their relevance in RPE specification (Martínez-Morales et al. 2004). Hence, MEFs were first transduced with this lentiviral reporter system, driven by Tyrosinase expression. Subsequently, blasticidin-selected cells were further transduced with fresh combinations of TF-carrying lentiviral

vectors. Preliminary results (data not shown) were encouraging, with cells becoming pigmented and changing morphology after transduction (Pires et al. 2012).

Differentiation protocols applied were based on the premise that RPE originates from neural tissue, i. e. cells were firstly directed towards a neural fate and then to RPE, by adding chemical cues in the culture medium. With that in mind, cells were firstly exposed to neuro induction medium (Pires 2014). As expected, cells appeared to change morphology and Tyrosinase-driven GFP expression became evident. As cells grew to confluence, aggregates started growing upwards until they were released and begun floating in the cell culture medium, as live cell aggregates. Images of such cells are shown in Figure 3. 1.

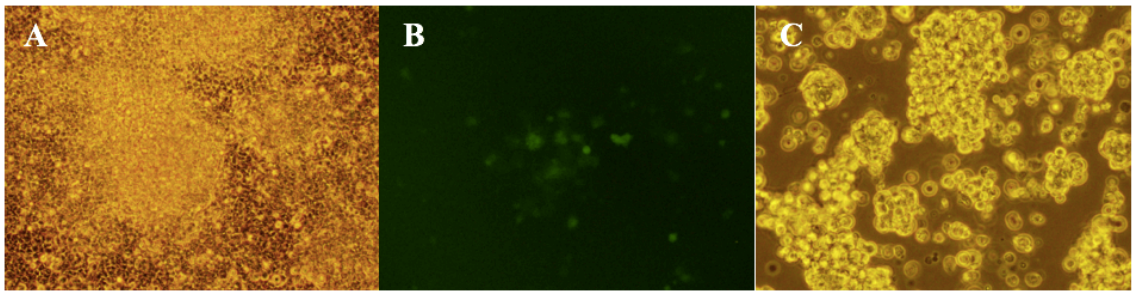

Figure 3. 1 - Cell morphology during early steps of differentiation, assessed by light microscopy. A: Differentiating cells grew to confluence, taken at 40x magnification. B: These cells express GFP fluorescence, driven by the Tyrosinase promoter, taken at 100x magnification. C: Live cell aggregates were released and floated in the culture medium, taken at 100x magnification.

As the differentiation proceeded, floating aggregated cells self-organized to an extent, seemingly to the whole embryoid bodies described by Gonzalez Cordero (Gonzalez-Cordero et al. 2013). Reorganization of cells inside these structures also resembled that described by these authors as a recapitulation of the optic vesicle and, later on, optic cup patterning. It was possible to observe the formation of protrusions in the extremities of the spheres, with GFP expression beginning to localize to the periphery, rather than the middle of the structure – Figure 3. 2.

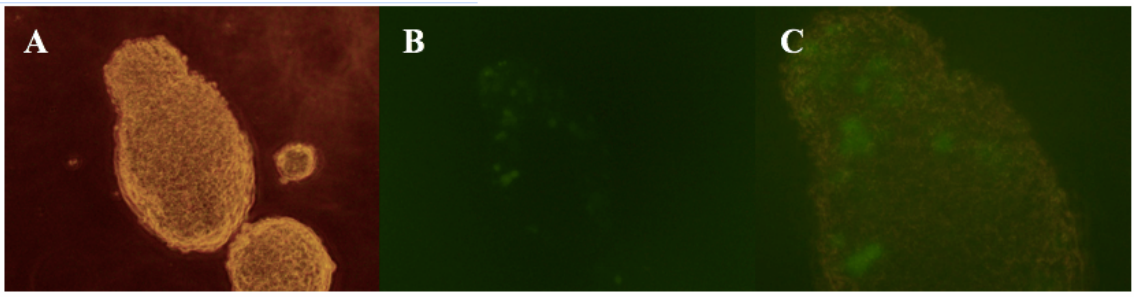

Figure 3. 2 - Differentiating cells self-organized, presenting protrusions in the extremities, assessed by light microscopy (A), taken at 40x magnification. Expression of GFP localized mainly to the extremities (B and C), taken at 100x magnification and zoomed (C) in for better visualization.

As time progressed, cell distribution and regional density in the aggregates changed. In some cases, aggregates resembled those described by Gonzalez Cordero (Gonzalez-Cordero et al. 2013) as optic cup precursors or whole embryoid bodies and in other cases,

the lumen of such aggregates appeared less dense alike neuroepithelium cysts described by Zhu (Zhu et al. 2013) (Figure 3. 3).

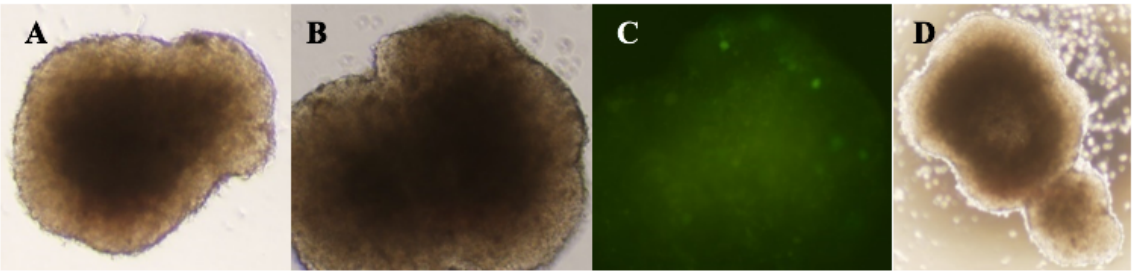

Figure 3. 3 - Differentiating cells produced optic cup-like configurations, assessed by light microscopy. A and B: Optic cup-like structures, similar to those described by (Gonzalez-Cordero et al. 2013) (taken at 40x and 100x magnification, respectively). C: Peripheral GFP expression (100x magnification). D: Neuroepithelium-like cysts, similar to those depicted by (Zhu et al. 2013) (40x magnification).

RPE differentiation protocols generally converge in a second step, corresponding to adherent culture conditions, using a medium supplemented with RPE specification factors.

After 30-45 days of adherent culture conditions, cells presented RPE-like morphology: polygonal shape, disposed as a monolayer of juxtaposed cells. However, cell populations were not homogeneous, with some clones presenting dissimilar features. In fact, even when considering a single clone, cell shape was not consistent throughout the well, with regions consistent of fusiform cells, amongst polygonal-shaped cells. A representation is shown in Figure 3. 4.

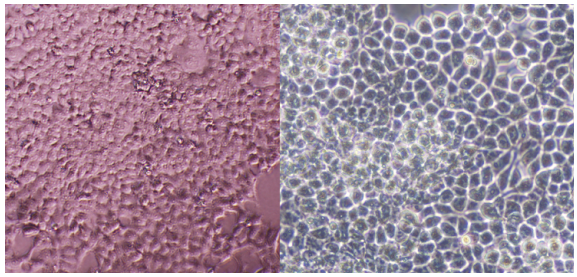

Figure 3. 4 - mouse cells gained RPE-like morphology, nevertheless with heterogeneous populations, 40x and 100x magnification, respectively.

When considering cell morphology, results were encouraging and in some cases, cells were starting to develop pigmentation. In some wells, there were lumps or protuberances, as if cells were forming domes, which has been reported as a characteristic feature of polarized maturing RPE, when cultured in non-porous supports (Maruotti et al. 2013; Singh, Shen, et al. 2013; Jin et al. 2012; Zhu et al. 2013).

Cells were transferred to transwells, to further stimulate a fully polarized and mature RPE. Shortly after seeding, cells regained an RPE-like morphology, with packed polygonal-shaped juxtaposed cells. In some cases, cells appeared to have become pigmented, as can be observed in Figure 3. 5.

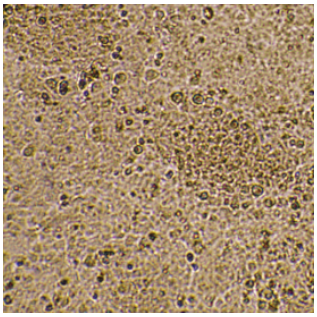

Figure 3. 5 - mouse cells display RPE-like morphology and pigmentation, when cultured in transwells. Illustrative light microscopy image, taken at 40x magnification.

In order to assess polarization, TER was measured. Usually, RPE is considered to be efficiently polarized when cells reach a TER value over 150Ωcm^2 (Song & Bharti 2016; Bharti et al. 2006; Brandl et al. 2014; Zhu et al. 2013). TER values were inconsistent and ultimately inconclusive. There was no increase of TER with time and measurements were significantly under what would be expected for polarized RPE, with values < 30 Ωcm^2. Additionally, expression of relevant RPE-specific markers was negative (data not shown). Ultimately, cells were not properly differentiated into polarized and mature RPE and these protocols were discontinued.

3.2.2 human RPE differentiation process

H9 human Embryonic Stem (hES) cells constitute a standard commercially available cell line, commonly used for differentiation protocols as well as other applications. In particular, these cells have been used before to obtain RPE (Zhu et al. 2013; Leach et al. 2015; Buchholz et al. 2013), and thus were selected as the starting material. H9 cells are depicted in Figure 3. 6.

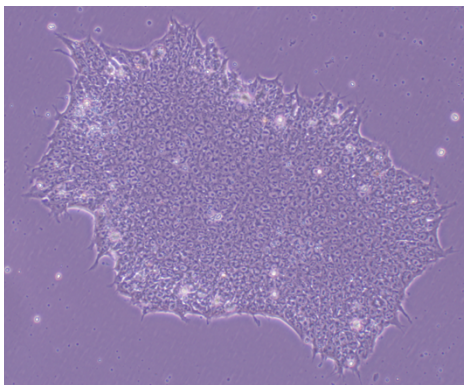

Figure 3. 6 - Undifferentiated H9 embryonic stem cell colony. hES cells typically grow as compact, multicellular colonies, with distinct borders, as depicted. High nucleus-to-cytoplasm ratio and prominent nucleoli are also characteristic of these cells. Phase contrast illustrative light microscopy image, taken at 100x magnification.

Empirically determined aspects such as initial cell confluency and the maturation state of stem cell colonies are of utmost importance for the differentiation process to run according to a timeline. Visual interpretation of the differentiation progress is key, as the protocol can be adjusted in terms of time. For these reasons, the protocols described in the

papers do not always reference initial cell confluency or plating densities. Each researcher must adjust the method, according to pluripotent stem cell line, for instance, as they can have specific characteristics/timing demands.

The following sections depict the results obtained from the two most promising differentiation approaches used throughout the course of this work.

Spontaneous differentiation method

Spontaneous differentiation requires long waiting periods and relies on technical skill, in order to manually pick out the pigmented foci that arise, to enrich the final RPE culture. The spontaneous differentiation method is fairly simple, as depicted in Figure 3. 7.

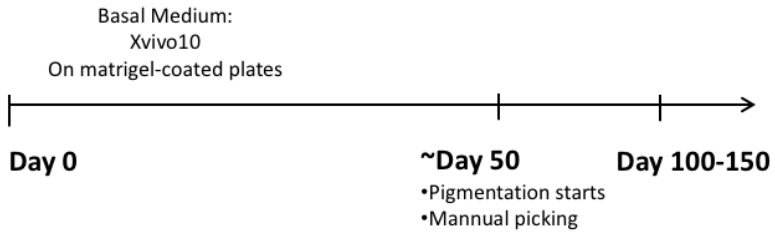

Figure 3. 7 - Schematic representation of the spontaneous differentiation method timeline. Stem cells are plated at high confluency, in X-VIVO10 medium, and allowed to differentiate for >50 days until pigmented foci become evident.

Several different media have been used as basal medium, for being compatible with stem cell unprompted differentiation into RPE (Pennington et al. 2015). X-VIVO 10 is one of such media and, because it was reported to yield highly pure RPE cultures (Leach et al. 2015), it was selected as the basal medium for these experiments. hES cells were plated at high confluency and left to spontaneously differentiate, for >50 days, until pigmented foci started to appear; those pigmented foci are to be picked out to continuously enrich the culture, in order to yield homogeneous RPE. Spontaneously differentiated RPE is depicted in Figure 3. 8.

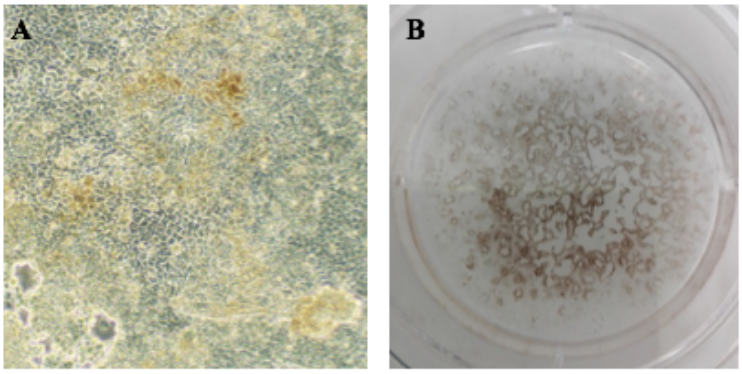

Figure 3. 8 - RPE typical morphology and pigmentation. A: RPE-like cells, at differentiation day 45. Cells are heterogeneous with pigmented and non-pigmented patches. Phase contrast light microscopy illustrative image, taken at 100x magnification. B: Pigmented foci are visible to the naked eye, typically after 3-4 months, as pigmented cells are organized in ridges and circles of darker color; photograph of a well from a multiwell plate.

After 120 days of differentiation, pigmented and polygonal-shaped cells were picked out, and went through an enrichment phase. Scraping off undifferentiated colonies or selecting and picking out pigmented cells to re-plate require proficient handling skills and deep knowledge of these cells behavior. Ultimately, not all the cells that were selected were pre-RPE. Additionally, the cells were plated at lower confluency than would be ideal, causing this fragile presumed-to-be pre-RPE to transdifferentiate. In the end, this protocol was discontinued, as it was possible to obtain high yield of RPE cultures and in a shorter time-frame, using the directed differentiation method.

Nevertheless, and despite their lower efficiency, spontaneous differentiation protocols continue to be used by several research groups, as they are effective and yield high purity RPE cultures.

Directed differentiation method

After first attempts to differentiate RPE, the protocol shown to be most promising was the one developed by Buchholz and colleagues at the Clegg Lab, University of California, Santa Barbara (Buchholz et al. 2013). Buchholz's protocol requires several different factors to be added sequentially to the basal medium. Further contributions to the protocol made it more expensive, but significantly improved differentiation efficiency and efficacy (Leach et al. 2015) (Figure 3. 9).

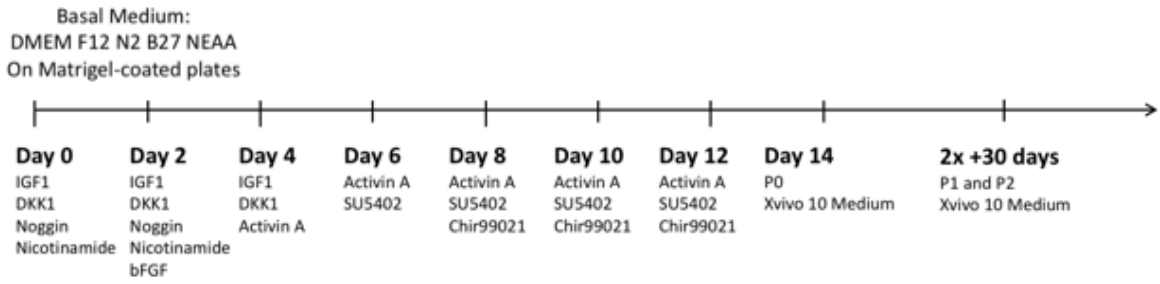

Figure 3. 9 - Schematic representation of the directed differentiation method timeline. Cells are given different differentiation factors every other day, in a specific order, to induce differentiation to RPE.

As described in the papers, not all factors are absolutely required, for instance Nicotinamide and SU5402 are not essential, but were shown to improve differentiation (Leach et al. 2015). Likewise, on first attempts to reproduce the protocol, not all the factors were used, as not all were available in the lab. Pre-RPE colonies were obtained, with small groups of cells showing a polygonal shape. However, the wells were not completely homogeneous and not all cells were pigmented (data not shown).

After encouraging preliminary results, the directed differentiation protocol was adjusted, based on the conclusions drawn from both articles (Buchholz et al. 2013; Leach et al. 2015). In the end, the factors used to induce differentiation were Nicotinamide, Noggin, Dkk-1, IGF-1, bFGF, Activin A, SU5402 and Chir99021, sequentially added, as depicted in Figure 3. 9.

Following the initial period of protocol adjustments, the guided differentiation process was successful and efficiently gave rise to mature RPE, with full wells containing pure populations (Figure 3. 10).

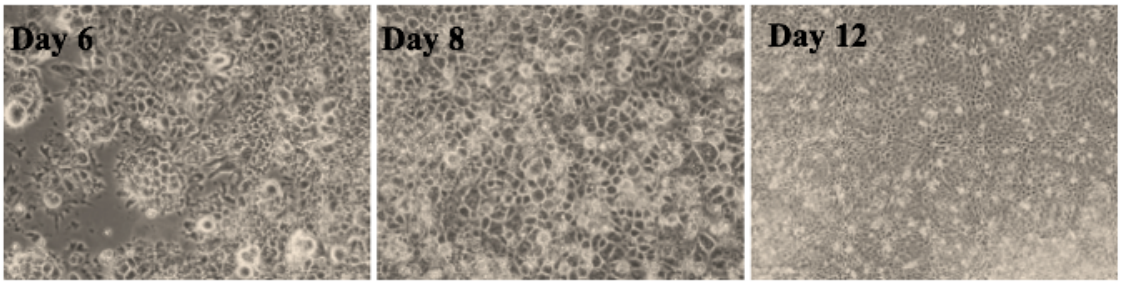

Figure 3. 10 - hES cells differentiation stages, until defining an RPE fate. Images were taken at differentiation days 6, 8 and 12, respectively. Morphological changes are observed, as the differentiation process develops, giving rise to a monolayer of homogeneous polygonal cells. Phase contrast light microscopy illustrative images, taken at 100x magnification.

During the first days, cells start to spread out from the compact stem cell colonies and become "spiky", as neural projections start to come off the edges. Later on, when the bottom of the wells becomes full (days 4-6), cells adhere to each other, become more polygonal and even-out their cell size, relative to one another. At the end of the 14-days period, the wells are consistent, with a monolayer of small uniform cells, which can then be passaged to new plates (Passage 0), in order to expand and further mature. Approximately 1 month after P0, typical features of maturing RPE are readily visible, such as dome formation and pigmentation (Figure 3. 11).

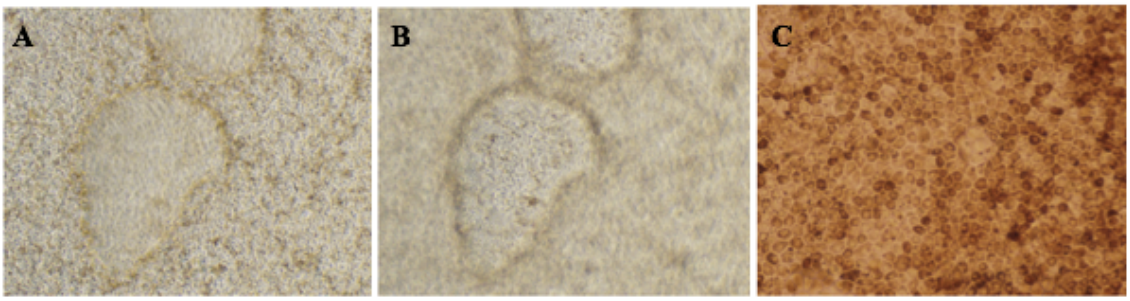

Figure 3. 11 - Typical features of mature RPE: dome formation (A and B), pigmentation and polygonal shape (C). Phase contrast light microscopy illustrative images (A and B), taken at 100x magnification, at day 35. The bright field image (C) was taken at day 135 and zoomed in for better visualization of fully mature RPE.

Dome formation occurs due to polarized fluid secretion towards the basolateral side, and is characteristic of newly differentiated RPE plated on impermeable plastic plates (Leach et al. 2015; Maruotti et al. 2013; Zhu et al. 2013). This effect works as a visual indicator of polarized cells and together with distinct hexagonal shape and readily visible pigmentation imply mature and functional RPE. At this point, cells are ready to be passaged again, to be expanded or used for experiments.

Prior to further investigations, however, a comprehensive characterization of these cells is required, in other to assure correct RPE establishment.

3.3 hESc-RPE characterization

Human Pluripotent Stem Cell derived-RPE cells (hPSC-RPE) have been shown to share many characteristics with native human RPE, including morphological similarities, gene expression, protein expression electrophysiologic properties and fluid transport (Klimanskaya et al. 2004; A.-J. Carr et al. 2009; Idelson et al. 2009; Leach et al. 2015; Vugler et al. 2008; Singh, Phillips, et al. 2013; Meyer et al. 2009; Zhu et al. 2013; Kamao et al. 2014). Typical features may vary depending on the differentiation or culture method and even maturation stage of seemingly analogous hPSC-RPE. Nevertheless, comparative studies suggest hPSC-RPE resemble human fetal RPE more closely than adult RPE (Klimanskaya et al. 2004; Lu et al. 2009), with the exception of one study (Kamao et al. 2014). In an effort to standardize RPE characterization, a systematic approach has been suggested, in which a panel of characteristics would be evaluated and considered as a minimum requirement to validate RPE fate. This panel includes gene and protein analysis, a phagocytosis assay, TER evaluation, growth factor secretion and retinoid metabolism assays (David E. Buchholz 2009).

To thoroughly characterize the newly-produced hESc-RPE, different types of assays were preformed, to assess specific RPE features and compare these newly established cells to other commonly used RPE cell lines.

3.3.1 RPE Morphology and Polarization

RPE cells organize as a polarized epithelium, in a single monolayer, by establishing close connections with their neighboring cells. This is visible by light microscopy, with the cells presenting characteristic polygonal shape (Figure 3. 12).

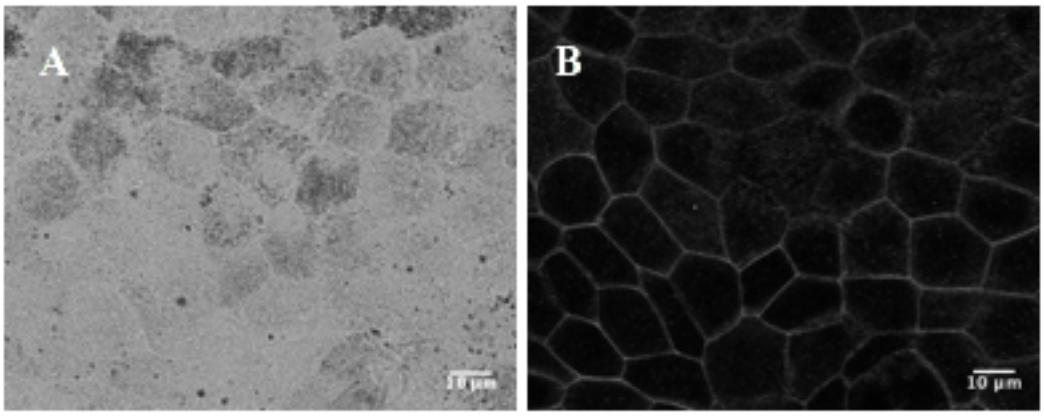

Figure 3. 12 - hESc-RPE organizes as a monolayer of pigmented polygonal-shaped cells, as evidenced by A: bright field confocal image and correspondent B: Phalloidin fluorescence staining. Scale bar 10µm.

The use of Phalloidin allows the clear visualization of the defined polygonal shape. On the other hand, the bright field image allows for the assessment of typical pigmentation, also characteristic of these cells. The pigment covers the cells, allowing the distinction of the nuclear area, devoid of it.

Formation of tight junctions is necessary in order to guarantee the epithelium properties regarding barrier function. Polarized epithelia forms, as cells grow to confluence, and this is verifiable by regarding their structure and distribution with great detail. Electron Microscopy (EM) images allow a very thorough analysis of these cells. In particular, they permit observations referring to monolayer organization and polarized structure. In particular, it is possible to confirm that 1) cells do organize side-to-side, as a monolayer, rather than superimposed, and 2) cells arrange their intracellular components in a polarized manner: basal nucleus (N), apical processes (AP) and basal infoldings (BI); also visible within the cell are mitochondria and melanosomes. Melanosomes are readily identified as very dark electron dense structures, widely distributed throughout the cells (Figure 3. 13).

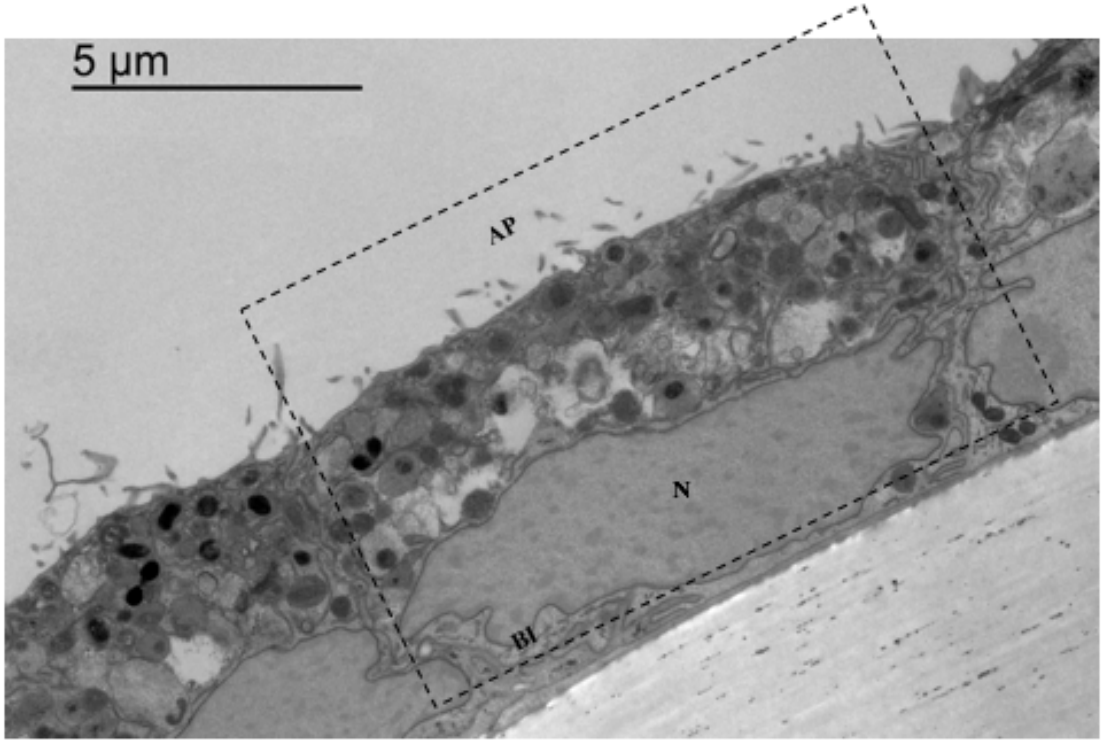

Figure 3. 13 - hESc-RPE monolayer observed by Transmission Electron Microscopy. Image shows an RPE cell (dashed line) plated onto a filter, flanked by two other RPE cells. Notice the apical processes (AP) and basal infoldings (BI), typical of polarized RPE; also visible are the nucleus (N), melanosomes and mitochondria.

When comparing the newly established hESc-RPE to other RPEs, their morphological similarities become evident. Specifically, hESc-RPE were compared side by side with RPE lines derived from primary cultures, namely porcine RPE (pRPE) and a commercially available human RPE line, from now on designated as Lonza hRPE (Figure 3. 14).

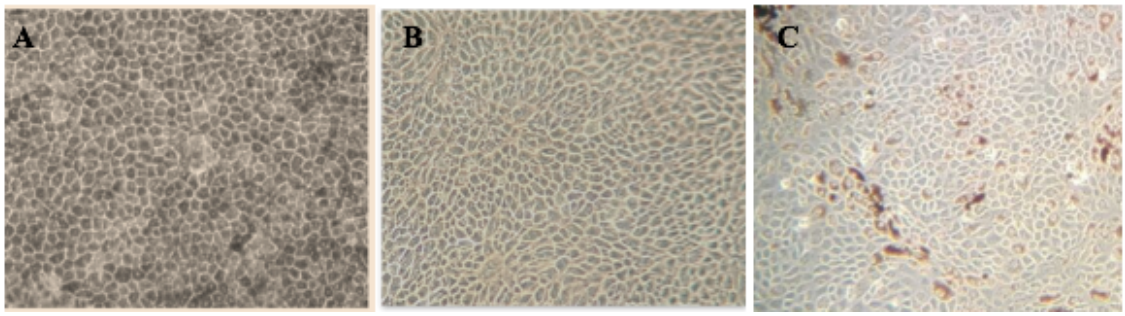

Figure 3. 14 - hESc-RPE cells (A) have similar morphology to Lonza hRPE (B) and also to pRPE (C), as evidenced by the monolayer appearance of polygonal shaped cells. Phase contrast images taken using a wide field light microscope, taken at 100x magnification.

A closer look, by EM, allows us to exhaustively compare the hESc-RPE to pRPE. As such, it is possible to confirm similar cell size and polarization features (such as apical processes and basal infoldings), as well as the presence of mitochondria and pigment-loaded melanosomes. pRPE melanosomes are much bigger and generally darker than hESc-RPEs' (Figure 3. 15).

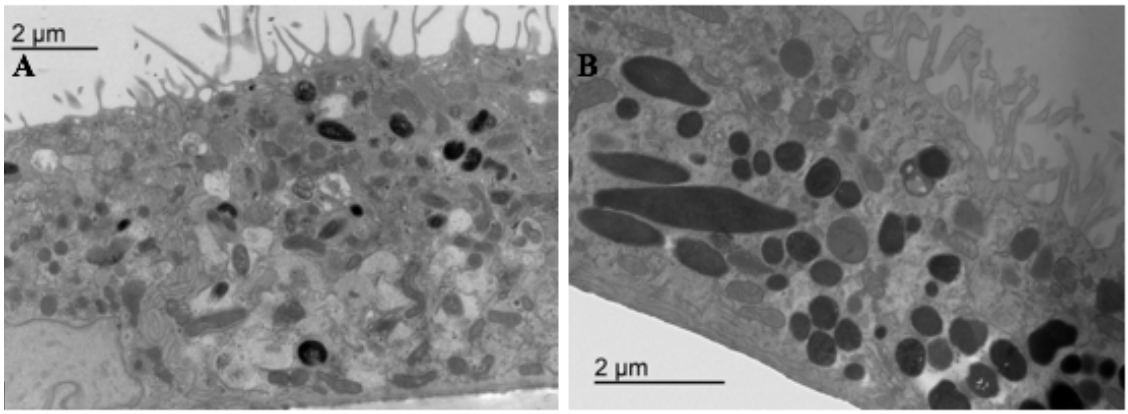

Figure 3. 15 - Transmission Electron Microscopy images of hESc-RPE and pRPE. hESc-RPE cells (A) have similar morphology to pRPE (B): prolonged apical processes, basal infoldings, melanosomes, similar size and intracellular organization.

As mentioned, when plated at high confluency, RPE cells connect to each other via tight junctions, which dynamically interact with numerous other proteins to regulate permeability, polar orientation of membrane proteins and trafficking within the cell. Epithelial cell polarity is usually measured by assessing the TER. While RPE cell lines, such as ARPE19, typically have low (<50 Ωcm^2) TER, other types of RPE, such as primary porcine RPE (pRPE), human fetal RPE (hfRPE) or hESc-RPE have been shown to develop tight monolayers, with TER above 200 Ωcm^2 (Rizzolo 2014; Lehmann et al. 2014; Sonoda et al. 2009).

TER is routinely measured, to guarantee a certain standardization of assays; i. e. because barrier function is characteristic of mature RPE, TER indicates if cells are mature and thus ready for experiments, when they reach a certain threshold, above 150 Ωcm^2. As part of the characterization of the newly obtained hESc-RPE, TER was measured regularly (Figure 3. 16).

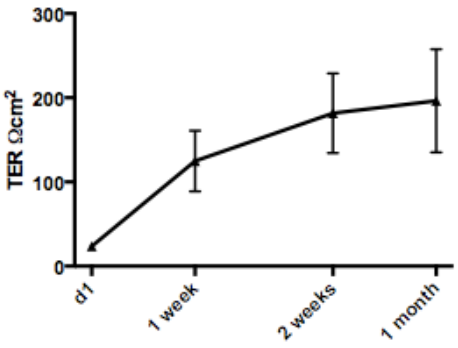

Figure 3. 16 - hESc-RPE become polarized, approximately after two weeks, with a Transepithelial Electrical Resistance value above 500Ω, which translates to a Unit Area Resistance reaching 200Ω.cm^2. n>40.

As the cultures reach confluency and form a monolayer, there is an increase of TER. This increase is consistent throughout the experiments and highly dependent on the initial cell confluency.

3.3.2 RPE Gene Expression and Molecular Markers

In order to assess gene expression, undifferentiated hES cells were collected, as well as hESc-RPE, during the differentiation process (day 9) and fully matured at day 136 of differentiation (Figure 3. 17 A). Additionally, protein levels of relevant RPE markers were evaluated by western blot and compared to Lonza hRPE, pRPE and commonly used human RPE cell line ARPE19 (Figure 3. 17 B).

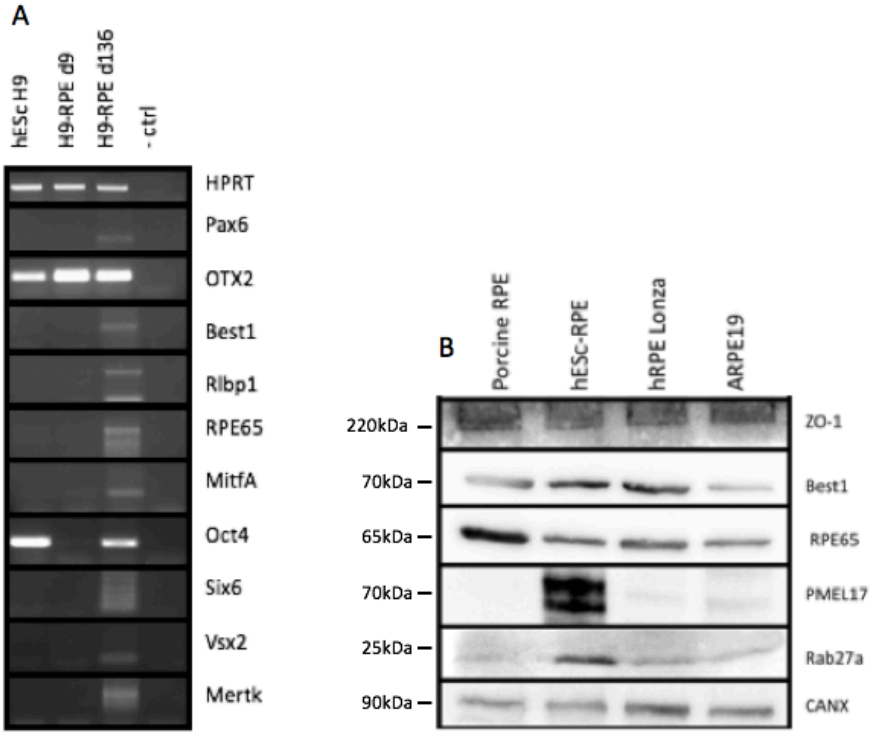

Figure 3. 17 - hESc-RPE express markers characteristic of mature RPE. A: PCR relative expression of relevant RPE markers was compared between undifferenciated hESc and differentiated hESc-RPE. HPRT was used as loading control B: protein levels of RPE markers were evaluated by western blot, by comparison between the RPE lines: porcine RPE, hESc-RPE, Lonza hRPE and ARPE19; CANX was used as loading control.

Contrary to undifferentiated stem cells, mature RPE expresses specific functional markers, such as Rlbp1 and Best1. Otx2 is expressed by undifferentiated H9 cells, but is even more expressed in differentiated RPE. Oct4 on the other hand is expressed in H9 cells and in hESc-RPE, but expression appears to be downregulated as the RPE matures, comes up again in differentiated hESc-RPE, though at relatively lower levels (Figure 3. 17 A). This evaluation is merely preliminary, and should be confirmed by further testing.

Protein levels of relevant markers of mature RPE were further confirmed by western blot. To this end, human ESc-RPE cells lysates were run side-to-side with pRPE, hRPE from Lonza and the human RPE cell line ARPE19 and analyzed for expression of typical RPE markers (Figure 3. 17 B). hESc-RPE were shown to express RPE65 and Best1, as did the other RPE lines evaluated. RPE65 is a retinoid isomerohydrolase responsible for the conversion of all-trans to 11-cis retinal, during the visual cycle. Best1, on the other hand, is a calcium-activated anion channel. Expression of these markers is typical of mature RPE and suggests these cells to be readily functional.

PMEL17 composes melanosome internal matrix fibers, playing an essential role for melanin deposition. As expected, its expression is higher in hESc-RPE than other cell lines, corroborating the observation that these cells are actively undergoing melanogenesis. While usually pRPE is heavily pigmented, the absence of a distinct band could mean that the cells used here were in fact less pigmented or that PMEL fibers are masked by melanin (Figure 3. 17 B).

Regarding Rab27a, it is highly expressed in hESc-RPE, with lower levels being detected for hRPE from Lonza and ARPE19. Rab27a is not RPE specific, but it is involved in vesicular transport, namely trafficking of melanosomes and exosome release and therefore it was expected to be present.

Immunofluorescence (IF) stainings were produced, using antibodies specific for mature RPE markers (Figure 3. 18).

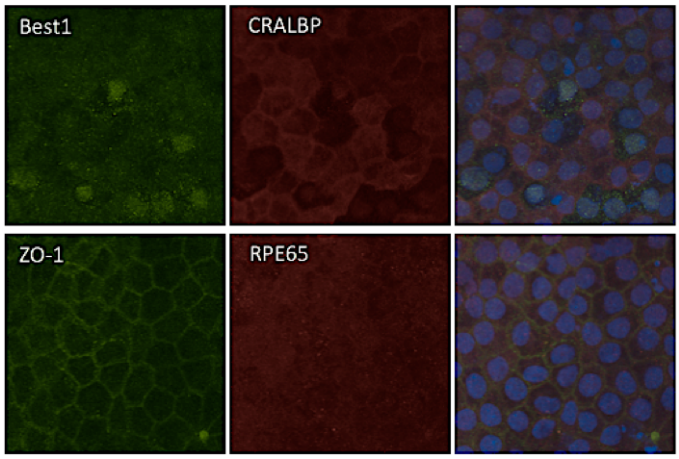

Figure 3. 18 - IF images show hESc-RPE express characteristic RPE markers, evaluated by light microscopy, such as Best1, CRALBP, ZO-1 and RPE65. Taken at 100x magnification.

hESc-RPE presented relevant markers, as detected by IF. In particular, there is expression of Zonula Occludens (ZO-1) which attests for the monolayer tightness, and of components involved in the visual cycle, such as cellular retinaldehyde-binding protein (CRALBP) and RPE-65. Furthermore, expression of Best-1 was also assessed by IF and its presence suggests that the RPE is functionally able to regulate essential processes, such as maintenance of cellular volume and Ca^{2+} signaling.

3.3.3 Functional characterization of hESc-RPE

As discussed in section 1.1.2, the RPE is responsible for a broad range of functions, critical to ensure vision. In order to assure hES cells differentiated properly, it is necessary to confirm these hESc-RPE cells are capable of essential functions, characteristic (though not exclusive) of the RPE. To this effect, these cells were evaluated regarding their ability to pigment, to secrete important growth factors (namely VEGF and PEDF) and exososomes, and finally, their ability to phagocytose POS.

Melanogenesis

Melanosomes are specialized organelles which contain melanin, providing color and photoprotection to pigmented structures. Specifically, in the RPE, melanosomes are thought to be retained within the cell, to capture scattered stray light and protect from oxidative attack (Raposo & Marks 2007; Lopes, Wasmeier, et al. 2007).

During melanosome maturation, protein fibers of amyloid nature are formed, to a great extent by polymerization of Pmel17. Later on, the enzymes involved in melanin synthesis (such as Tyrosinase and Tyrp1) are carried to premelanosomes, to provide for the actual pigment (Delevoye et al. 2011; Raposo & Marks 2007). To assess melanogenesis in hESc-RPE, the cells were prepared for cryo-immuno EM and gold-labeled for representative markers (Figure 3. 19).

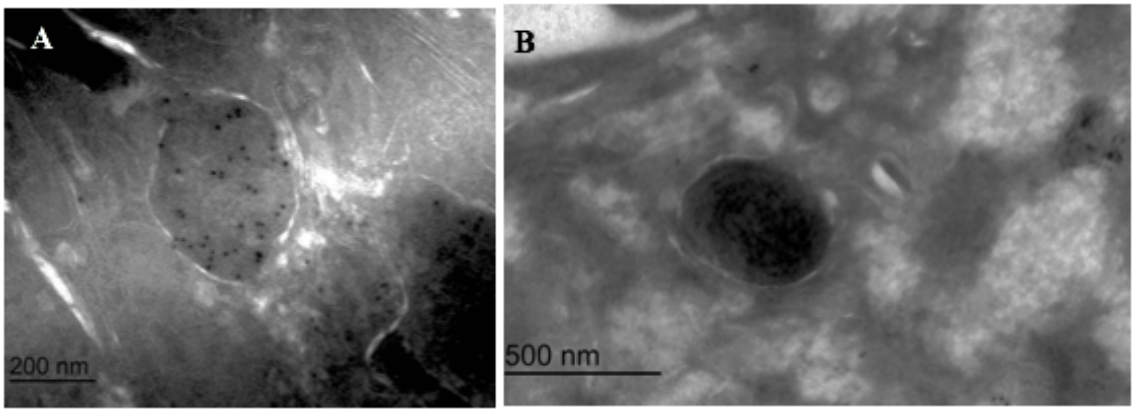

Figure 3. 19 - immuno-EM staining showing specific labeling of melanosomes, analyzed by TEM. A: PMEL17-labeled premelanosome and B: TRP1-labeled late melanosome. 10nm gold.

Melanosomes mature through four defined stages, based on their morphology, as observed by EM. During this process, an immature non-pigmented premelanosome begins

to form (stage I) and progressively acquires matrix fibers (completed by stage II), as well as an ellipsoid conformation. Starting from stage II, melanin is synthesized and deposited onto the protein fibrils, thickening and blackening stage III melanosomes, until all internal structure is concealed in a homogeneous stage IV mature melanosome (Figure 3. 20).

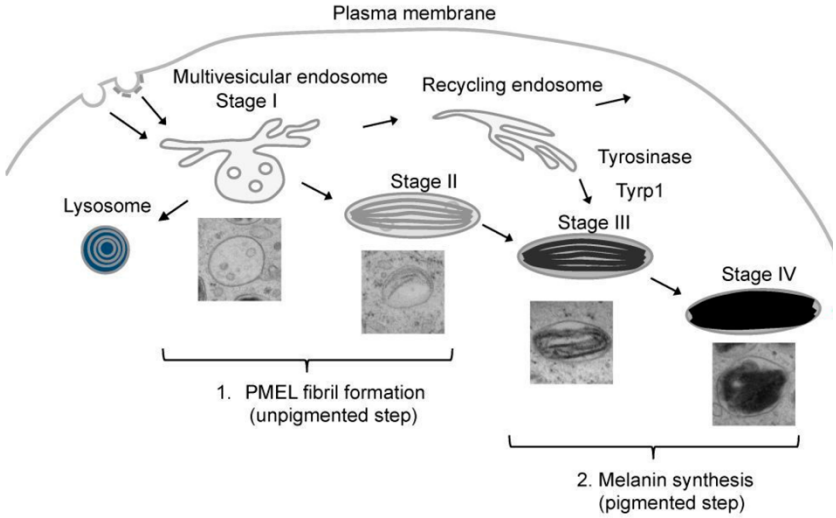

Figure 3. 20 - Schematic representation of the four stages of melanosome maturation, from stage I premelanosome to heavily pigmented stage IV. Adapted from (Bissig et al. 2016).

Melanogenesis occurs during a short window of embryogenesis, in mammals. In humans, melanin granules are observed up to 30 days of fetal development and by the 14th week, melanosomes at all stages of maturation are present (Rózanowska 2011). Within a few weeks melanogenesis stops and the RPE cells keep roughly the same melanin content throughout life. Commonly used cell culture protocols for human RPE usually lead to the loss of pigment granules through their repeated dilution in daughter cells. This is true for established cell lines and primary cultures of adult donor RPE. However, in some RPE lines, such as fetal RPE and pluripotent stem cell-derived RPE, melanogenesis is observed. In fact, hESc-RPE obtained through the course of the present work do continuously produce melanosomes (Figure 3. 21).

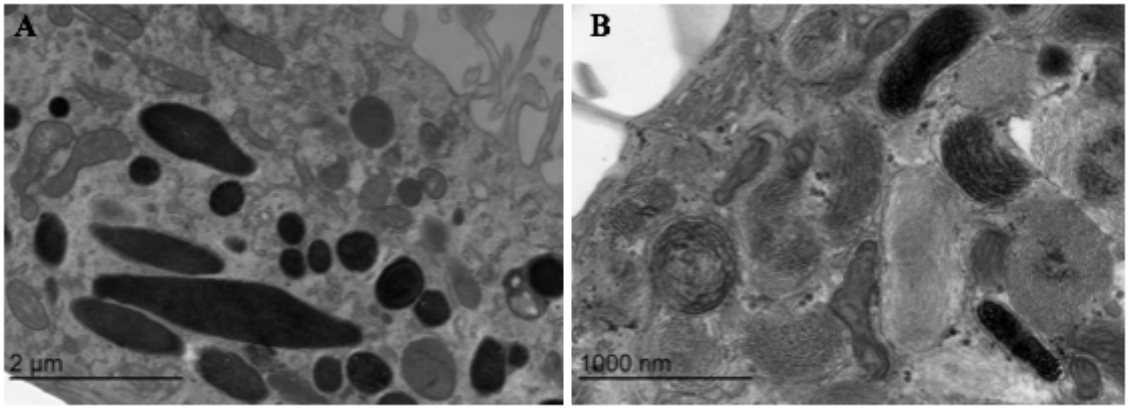

Figure 3. 21 - Melanosomes are fully matured in porcine RPE, but at different stages of maturation in hESc-RPE, assessed by TEM. A: porcine RPE with heavily pigmented melanosomes; B: hESc-RPE's melanosomes at different stages of melanogenesis.

Because postnatal RPE cultures do not readily produce melanosomes, melanogenesis has been studied to a greater extent in skin melanocytes, but not in the RPE. hESc-RPE have now emerged as a key tool to study molecular mechanisms of RPE pigmentation, both in healthy conditions and in ocular disorders, which frequently manifest with pigmentation anomalies, as previously discussed.

Secretion

Another important aspect, which indicates the RPE is mature and polarized, is secretion of essential factors, such as VEGF and PEDF: polarized RPE secretes PEDF predominantly from the apical side, and VEGF primarily through the basolateral side. For this reason, polarized secretion of these factors has been suggested as functional criteria to evaluate hESc-RPE newly established lines.

In order to evaluate this feature, medium was collected from upper and bottom chambers of transwells containing hESc-RPE and processed according to the description in Materials and Methods. A western blot obtained from the precipitation of conditioned medium proteins, from apical and basal chambers of the transwells, showing PEDF and VEGF content in the respective media (Figure 3. 22).

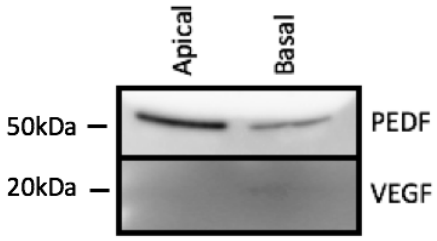

Figure 3. 22 - hESc-RPE cells secrete VEGF and PEDF into the medium, in a polarized manner, as assessed by western blot. Medium was collected from apical and basal chambers of transwells and precipitated, as described in Materials and Methods.

Even though these are preliminary data, and VEGF is hard to visualize in the presented image, the result for PEDF suggests cells are in fact secreting this factor in a polarized manner.

Additionally, though not RPE-specific, exosome release was evaluated in hESc-RPE cells and shown occur, under standard culture conditions (Figure 3. 23).

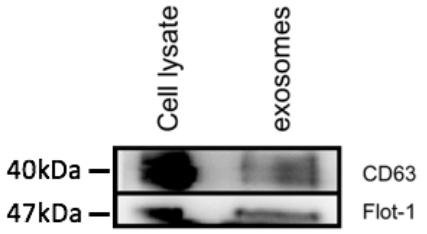

Figure 3. 23 - hESc-RPE release exosomes into the medium, detected by western blot. Exosome markers CD63 and Flotillin-1 were evaluated in whole cell lysate and correspondent exosome fraction, isolated from the medium, according to Materials and Methods.

In order to evaluate exosome production by these cells, conditioned medium was collected and exosomes were isolated by sequential centrifugations, as described in Materials and Methods. These exosomes were run side-to-side with whole cell lysates and blotted using anti-CD63 and anti-Flotillin1 antibodies, typical markers of exosomes. Results suggest hESc-RPE produce and release exosomes (Figure 3. 23).

Phagocytic Ability

Phagocytosis consists on capturing extracellular material, typically utilizing specific ligand-receptor interactions. Some of the most fundamental roles of the RPE, necessary to our visual process, include phagocytosis of POS and subsequent recycling of visual pigment, through the retinoid cycle.

POS are specialized light sensing organelles contained within photoreceptor cells. They are composed by stacked disc membranes, containing rhodopsin, as described in Chapter 1. Two different rhodopsin antibodies were used to stain POS: RET-P1 and 1D4. These two antibodies have been shown to recognize different epitopes of rhodopsin, thus identifying distinct stages of phagosomal maturation (Wavre-Shapton et al. 2014). On the one hand, RET-P1 recognizes an epitope at the N-terminus (extracellular) intradiscal domain of the rhodopsin molecule and labels both rhodopsin monomers and aggregates. 1D4, on the other hand, recognizes the C-terminal amino acids (cytoplasmic domain) of rhodopsin. For this reason, early phagosomes located at the apical region contain both epitopes and are thus 1D4- and RET-P1- positive. As the phagosome matures, RET-P1 staining continues visible, but 1D4 is gradually lost, indicating a progression from double-labelled to single labelled phagosomes in a time-dependent manner (Wavre-Shapton et al. 2014).

To determine whether hESc-RPE were able to phagocytose POS, it was first necessary to establish a POS-isolation protocol in the lab. Upon optimization, it was possible to obtain pure preparations of porcine POS, using a sucrose gradient, as described in Materials and Methods. The obtained POS were analyzed by EM (Figure 3. 24).

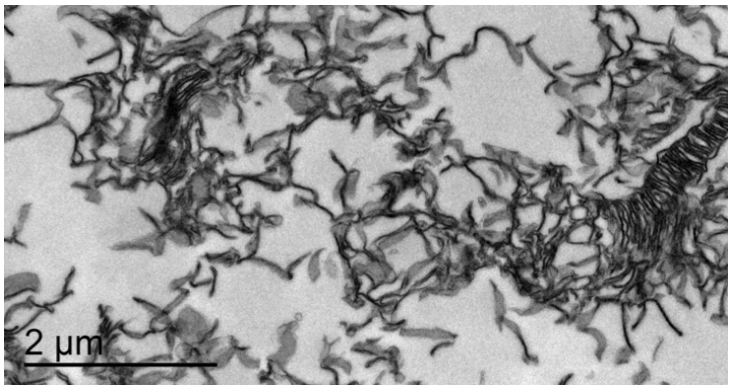

Figure 3. 24 - Isolated porcine POS consist on multi-membrane discs, as evaluated by TEM. The sucrose gradient method produces pure preparations of POS membranes.

EM images depict pure preparations of POS, without other organelle contamination (Figure 3. 24).

hESc-RPE cells were fed with porcine-POS, and IF staining anti-rhodopsin (1D4) was performed, in order to establish whether these cells indeed phagocytose (Figure 3. 25).

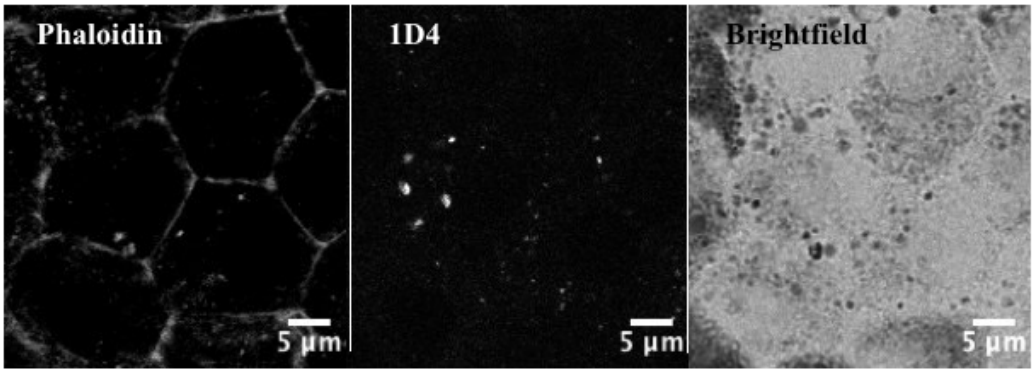

Figure 3. 25 - hESc-RPE are able to phagocytose porcine POS, as evidenced by IF rhodopsin staining (1D4). Phaloidin fluorescence evidences the cell limits.

hESc-RPE were also observed by EM (both conventional EM and cryo-immuno EM, as described in Materials and Methods), after being fed with porcine POS (Figure 3. 26).

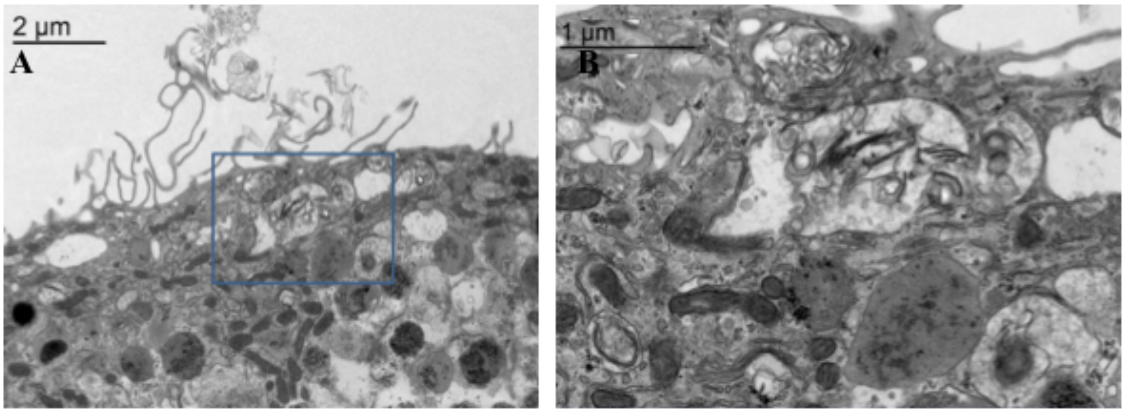

Figure 3. 26 - Conventional EM images show hESc-RPE are able to phagocytose porcine POS. A: apical processes extend to touch POS membranes and cells are able to engulf and create intracellular compartments containing POS membranes, as depicted. B: further magnification of the section highlighted in image A.

It is possible to identify phagosomes containing POS membranes, which typically get degraded after an overnight chase. Gold-labeling using different rhodopsin antibodies confirmed that these vesicles are indeed consistent with POS-containing phagosomes (Figure 3. 27).

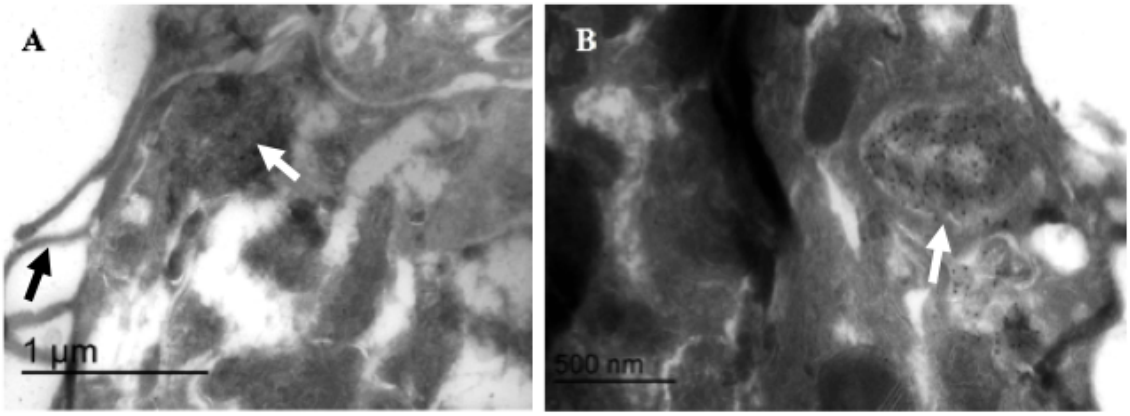

Figure 3. 27 - cryo-immuno EM images show hESc-RPE are able to phagocytose porcine POS, using rhodopsin antibodies (white arrows). A: 1D4 staining and B: RET-P1 staining, both specifically labeling POS-containing phagosomes inside the RPE cell. Black arrow indicates RPE apical processes. 10nm gold.

While 1D4 staining is found at the apical region of the cell, near the apical processes, RET-P1 staining is generally found more to the interior of the RPE cell. Specific labeling of these structures by rhodopsin antibodies confirms their phagosomal origin. Therefore, hESc-RPE were shown to uptake POS and to store them within (Figure 3. 27). Phagosome processing by RPE cells is characterized by progressive maturation and ultimate degradation of this cargo at the lysosome, as discussed in Chapter 1.

3.4 hESc-RPE Processing of Phagocytic Cargo

hESc-RPE cells were fed with porcine POS, to load the lysosomes with digestible cargo, and then analyzed regarding different aspects. Initially, POS presence was directly measured, using anti-Rhodopsin antibodies, as previously.

3.4.1 hESc-RPE Phagocytic ability

Degradation kinetics may be variable depending on the situation, namely considering *in vivo* situation versus *in vitro* and also from cell line to cell line. Therefore, first, in order to assess the normal time frame of POS degradation by the newly established model of hESc-RPE, cells were fed with a single pulse of POS (at 200µg/mL) for a 4h period, followed by chronological chase periods, as described in the schematic representation of Figure 3. 28.

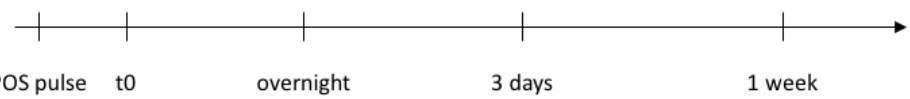

Figure 3. 28 - Schematic representation of the experimental layout. hESc-RPE were pulsed with a single POS feeding and chased at time 0 after pulse, overnight, 3 days and 1 week.

At each of the time points, cells were fixed for IF, and stained using rhodopsin RET-P1 antibody, in order to follow POS degradation through time (Figure 3. 29).

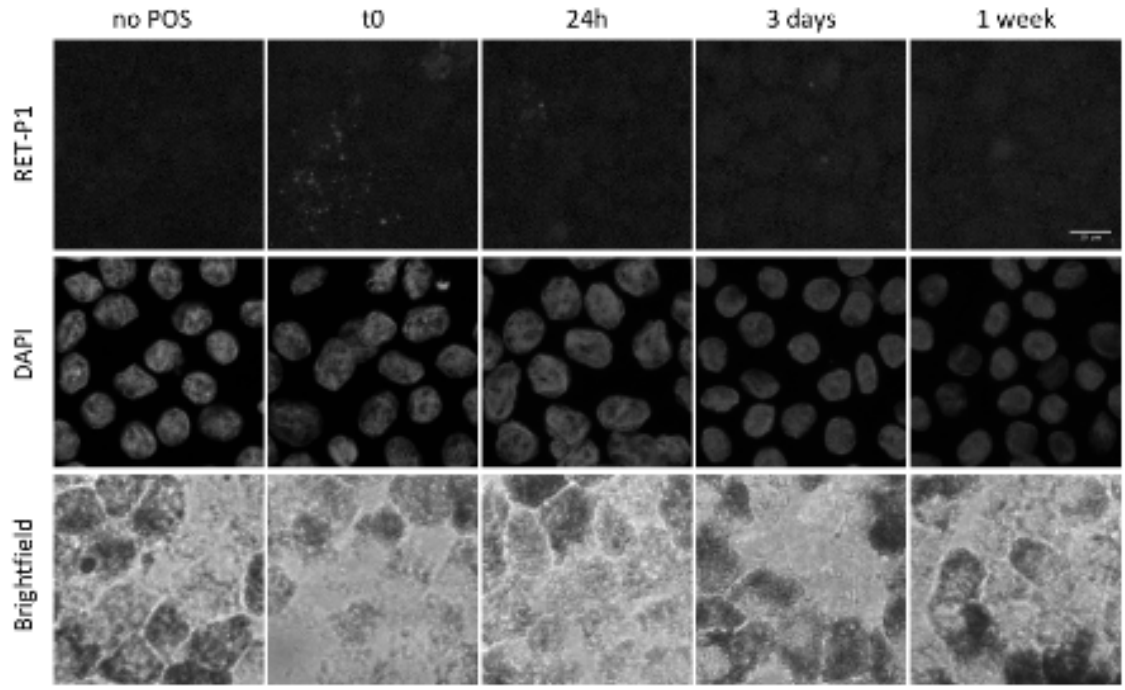

Figure 3. 29 - Time course of POS processing by hESc-RPE, assessed by light microscopy. Before POS feeding RET-P1 staining is missing, suggesting specific labeling of rhodopsin. hESc-RPE were able to uptake POS, as evidenced by staining at time 0, and were successful in digesting them, as shown by little rhodopsin staining after overnight chase and at day 3, and none at all after 1 week. Scale bar 10µm.

These experiments regarding POS uptake and normal digestion allowed for a setup of the experimental time frame: hESc-RPE are able to uptake POS, as can be observed by the IF images obtained for time 0 (Figure 3. 29). RET-P1 staining at early time points consists of dispersed small dots, consistent with several early phagosomes, at the cell periphery. An overnight chase is sufficient to allow most of the POS to be degraded, with few RET-P1 positive vesicles being detected at this time. Notably, after the third day of chase, RET-P1 staining seems to become fainter and no staining was detected after 1 week (Figure 3. 29).

3.4.2 Lonza hRPE and pRPE Phagocytic ability

The same experiment was performed using Lonza hRPE: a single 4h POS (200µg/mL) pulse was chased from time 0 after POS washout up until one week. While in hESc-RPE, POS digestion was only followed through rhodopsin staining, in Lonza hRPE another readout was observed: POS-induced autofluorescence. Therefore, POS digestion was followed by observing POS-derived autofluorescence and RET-P1 staining (Figure 3. 30).

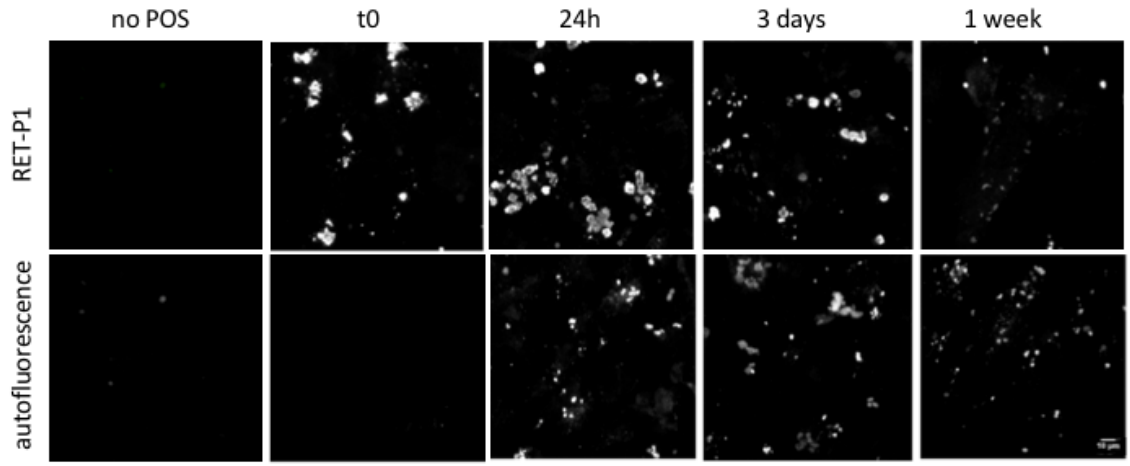

Figure 3. 30 - RET-P1 IF staining and POS-derived autofluorescence in Lonza hRPE, detected by light microscopy. Cells were able to uptake POS, as evidenced by rhodopsin RET-P1 staining from time 0 and up to 3 days after pulse. After one week, the staining is fainter, suggesting degradation. Autofluorescence starts to appear 24h after POS pulse and remains after 1 week. Scale bar 10µm.

It is important to mention that autofluorescence is observed whether or not cells are stained, meaning that it is not bleed through from another channel, but instead derived from POS.

Not unlike hESc-RPE, Lonza hRPE cells are able to uptake and process rhodopsin, as evidenced by RET-P1 IF staining and by POS-derived autofluorescence. Prior to POS feeding there is no rhodopsin staining and few auto fluorescent dots. After POS feeding, RET-P1 staining is detected immediately at time 0, and remains until one week, although it starts to become fainter. Conversely, autofluorescence starts to develop later, it is only visible 24h after feeding and remains even after digestion of the majority of rhodopsin at one week.

Finally, single POS pulse (200µg/mL) and chase was also tested in porcine RPE, considering rhodopsin staining with RET-P1 antibody and autofluorescence (Figure 3. 31).

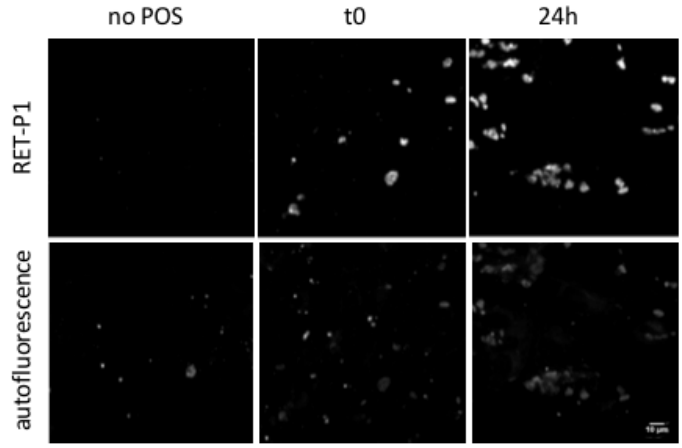

Figure 3. 31 - RET-P1 IF staining and POS-derived autofluorescence in pRPE, detected by light microscopy. Cells were able to uptake POS, as evidenced by RET-P1 rhodopsin staining from time 0 and 24h after pulse. pRPE presents autofluorescent dots even before POS feeding. Autofluorescence increases 24h after POS pulse and remains 24h post-pulse. Scale bar 10µm.

Porcine RPE cells were able to uptake POS, as evidenced by the staining at time 0 after washout, and continue phagosome processing for over 24h, shown by the abundant presence of RET-P1 positive aggregates at this time point. Regarding autofluorescence, pRPE cells already contained autofluorescent particles, before POS feeding (Figure 3. 31). The number of autofluorescent specks increases after POS feeding, in some cases in close proximity to RET-P1 staining, although not necessarily co-localizing.

3.4.3 POS-derived Autofluorescence

In order to further confirm this autofluorescence is in fact POS-derived and establish a correlation with increase of POS, two different concentrations of POS preparation were used: 50µg/mL and 200µg/mL. POS-derived autofluorescence was detected by flow cytometry analysis, in this case of Lonza hRPE (Figure 3. 32).

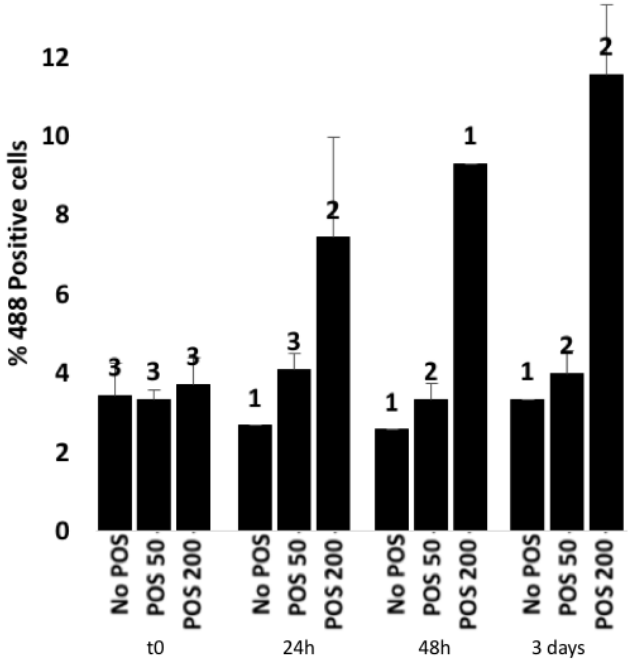

Figure 3. 32 - POS-derived autofluorescence in Lonza hRPE detected by flow cytometry, in unstained cells. Autofluorescence appears after 24h, in a dose-dependent manner. The number of autofluorescent cells increases with time, for the higher concentration of POS. n= 20.000 cells acquired for each condition and experiment represented; Results are expressed as mean ± s.d.; the numbers over the bars indicate repeats of the same condition.

At time 0 post-pulse, autofluorescence is at the same levels as in control unfed cells. This is consistent with the microscope images (Figure 3. 30) and therefore, since Lonza hRPE were found not to be autofluorescent before POS feeding, this is considered a baseline. As the phagocytic cargo is processed, autofluorescent cells appear, again coherent with microscopy findings (Figure 3. 30). Comparing "No POS" situation with POS at 50µg/mL, a modest difference is detected, with higher numbers of autofluorescent cells in the POS 50 situation than in control (No POS) situation, at the same time point (Figure 3. 32). Regarding POS at 200µg/mL, a regular increase of autofluorescent cells is verified at each time point. In spite of the seemingly modest differences (less than 10%), when analyzing these data, it is important to keep in mind the method of detection: while

microscopy images allow the detailed visualization of particles within cells, flow cytometry detects whole cell fluorescence; i.e. establishing the threshold of detection relies on sufficient autofluorescent particles per cell which confer this property to the cell. For this reason, flow cytometry is regarded as a less sensitive technique than microscopy. Still, considering reproducibility between assays and a high number of cells per experiment, a direct correlation can be found between POS processing by RPE cells and the appearance of autofluorescent particles/cells.

In accordance with the previous experiments, RPE cells fed with different concentrations of POS produce different amounts of autofluorescent particles. POS-derived autofluorescence in parallel with RET-P1 IF staining within the same cells, both in Lonza hRPE and in pRPE, using POS at 50µg/mL or 200µg/mL, is represented in Figure 3. 33.

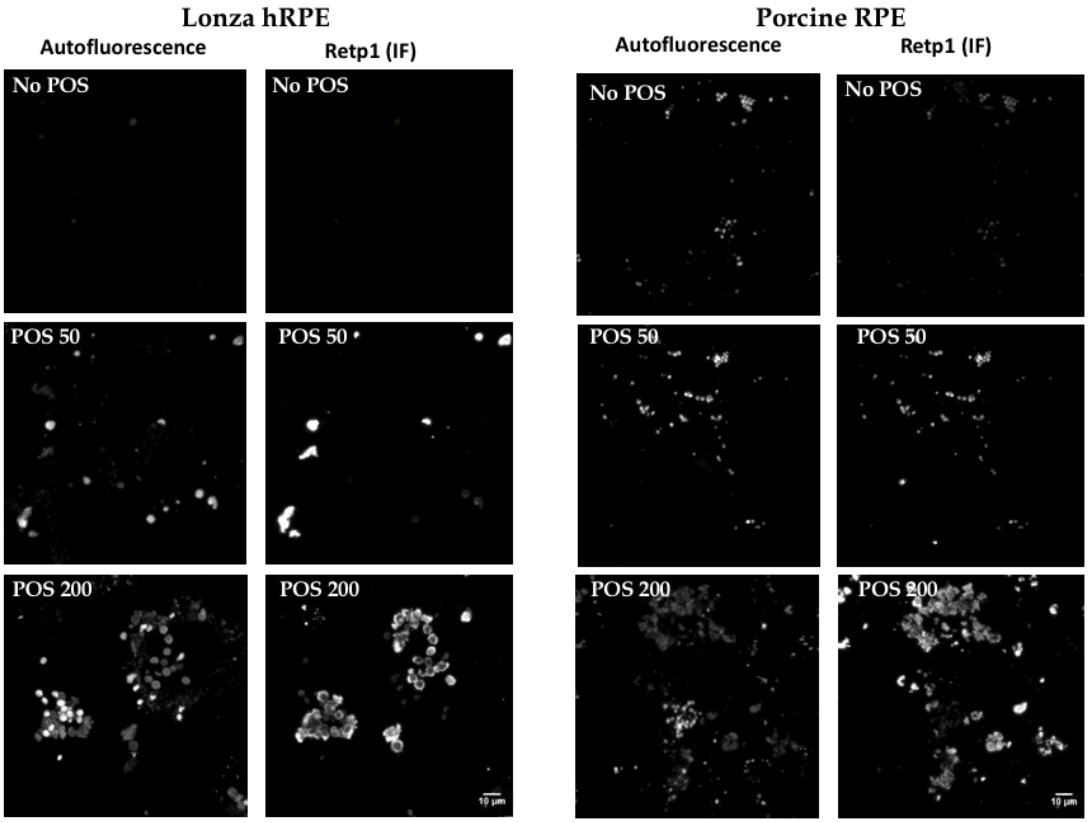

Figure 3. 33 - Lonza hRPE and pRPE develop POS-derived autofluorescence in a dose dependent manner, as indicated by RET-P1 IF staining, after single pulse and overnight chase; assessed by light microscopy. Both rhodopsin staining and autofluorescence increase in a dose-dependent manner. Scale bar 10µm.

First of all, by comparing Lonza hRPE to porcine RPE, it is possible to observe that pRPE cells already contained POS, labeled by RET-P1 antibody, as well as specks of autofluorescence, before feeding (No POS situation) (Figure 3. 33). Lonza hRPE is a fetal RPE cell line, and for this reason, should be fairly naïve in terms of photoreceptor phagocytosis. On the contrary, pRPE is derived from adult porcine eyes, which means that the RPE has been digesting POS on a daily basis throughout the pig's whole life. This could be one explanation for the remaining rhodopsin staining in the porcine cells, although the

staining is faint, consistent with partial degradation of POS by these cells. For the same reason, autofluorescence is evident in pRPE while absent in Lonza hRPE: pRPE are adult cells, with a lifetime accumulation of mis-processed material and possibly with presence of autofluorescent lipofuscin and complex granules (Figure 3. 33).

A 4h POS pulse (either using 50µg/mL or 200µg/mL POS) followed by overnight chase resulted in evident increase of both RET-P1 staining and autofluorescence, in both cell types. The concentration of POS cells were fed with directly impacts the area of RET-P1 staining and also of autofluorescence (Figure 3. 33).

Finally, although RET-P1 staining co-localizes with autofluorescence, many times autofluorescence seems to come from the inside of RET-P1 stained vesicles. On the other hand, despite RET-P1 IF staining almost always co-localize with autofluorescence, autofluorescence does not always co-localize with RET-P1 IF staining (Figure 3. 33). Importantly, for these experiments, autofluorescence was detected using the 405 nm channel whereas RET-P1 IF staining was acquired in the 488 nm channel. So, efforts were made to prevent bleed-through from one channel to the other. RET-P1 labeling has been described to be lost upon fusion of the phagosome with the lysosome (Wavre-Shapton et al. 2014), and autofluorescence may in fact be derived from POS processing within the lysosome. This would be consistent with the absence of autofluorescence in unfed Lonza hRPE and also with the appearance of RET-P1 around autofluorescent particles, which may represent phagolysosomes actively digesting POS.

In an effort to quantify this POS-derived autofluorescence and establish dose-dependency, Lonza hRPE and pRPE were again incubated with increasing concentrations of POS, from 50µg/mL to 600 or 400µg/mL, respectively, and analyzed by flow cytometry (Figure 3. 34).

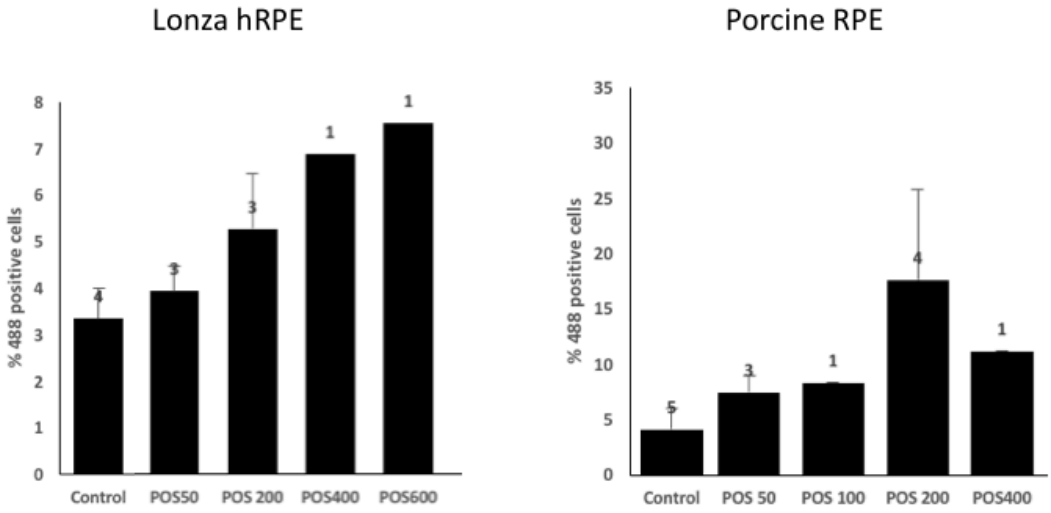

Figure 3. 34 - Lonza hRPE and pRPE develop POS-derived autofluorescence, dependent on initial POS concentration (50-600 and 50-400 µg/mL, respectively), after single pulse overnight chase, assessed by flow cytometry. n= 20.000 cells acquired for each condition represented; Results are expressed as mean ± s.d.; the numbers over the bars indicate repeats of the same condition.

Consistent with previous findings, there is an increase of the autofluorescent cell numbers, in direct proportion to initial POS concentration, for Lonza hRPE. As for pRPE, there is also an increase, dependent on POS concentration, but this increase seems to plateau/decrease at the highest concentration (400 µg/mL) (Figure 3. 34). There is some variability between assays, as represented by the error bars. Similar to Figure 3. 32, there is a modest but consistent increase of the autofluorescent cell numbers and it is interesting to find the increase is more significant in porcine than in human cells (Figure 3. 34). It is not possible to draw conclusions from the baseline differences in both cases, as these can be attributed to intrinsic differences, but also to settings adjustment for each experiment. Still, comparing to the control situation in each case, POS-derived autofluorescence increases more in pRPE than in Lonza hRPE (Figure 3. 34). It could be that pRPE are able to uptake higher amounts of POS (for instance more rapidly). It can also mean that pRPE take more time to process autofluorescent granules derived from POS degradation. As for the apparent reduction in autofluorescent pRPE cell numbers from 200 to 400 µg/mL, it would be necessary to repeat the experiment, in order to obtain statistical significance. However, it is reasonable to consider the existence of a limit of the RPE's phagocytic ability, at which point there wouldn't be further increase.

3.5 Model of POS-induced Lysosomal Dysfunction

The timeframe of phagocytosis of POS, by *in vivo* RPE cells has been documented by other researchers. Based on such reports, early phagosomes are typically detected at the apical region and stained with both 1D4 and RET-P1 rhodopsin antibodies, from time 0 after POS feeding pulse and until 2 hours after washout; 4 to 6 hours after pulse, both phagosomes and phagolysosomes containing POS at different stages of degradation can be found; between 12 and 24 hours post-pulse POS are found within lysosomes at the perinuclear region (Wavre-Shapton et al. 2014). Additionally, other reports state that LC3 positive phagosomes are present 12 hours up until 48 hours after pulse (Keeling et al. 2018).

RPE cells are able to phagocytose porcine POS also *in vitro*. The three RPE lines tested (hESc-RPE, Lonza hRPE and pRPE) were shown able to internalize POS and process them (Figure 3. 29 Figure 3. 30 and Figure 3. 31, respectively). Whilst studies concerning POS renewal in animal models suggest a circadian burst of POS digestion by the RPE (Young 1971; Strauss 2005a; Wavre-Shapton et al. 2014), the experiments presented previously suggest that RPE cells take more than 24h to process POS, with rhodopsin staining present one week after initial pulse. Furthermore, porcine RPE primary culture cells also exhibit remaining rhodopsin staining, after being in culture for over two weeks, as depicted in Figure 3. 33. This suggests that either RPE cells take more time to fully digest POS than previously thought, or that RPE cultured *in vitro* is not as efficient at processing POS. This means the delay could in fact be an artifact caused by culture conditions, comparing to the *in situ* situation.

On the one hand, the circadian rhythm control of the MiT transcription factors together with POS-derived activation of mTORC1 (Luo et al. 2016; Yu et al. 2018) would agree

with a daily cycle of POS degradation. On the other hand, a morning boost of lysosomal function doesn't necessarily mean that all rhodopsin is processed and some might remain in the RPE. In theory, as the RPE ages and lysosomal function decays, more rhodopsin would accumulate each day, undegraded, disturbing RPE function in the long-run. Curiously, hESc-RPE were able to process rhodopsin faster than Lonza hRPE and pRPE. Specifically, hESc-RPE rhodopsin staining is almost negligible after 24h, while in Lonza hRPE it starts to become fainter after 1 week and in pRPE remains even after excising the RPE from the pigs' eyes and leaving them in culture, without additional POS feeding. These "degradation efficiency" differences may be related to intrinsic characteristics of the cells and culture conditions (medium composition, etc), but they could also result from the fact that porcine cells are adult RPE, which were already subjected to a lifetime of POS digestive burden. On the other hand, not all porcine RPE cultures present RET-P1 IF staining before POS feeding, as evidenced by Figure 3. 31, which argues for variability among pools of cells in primary cultures.

Regarding POS-derived autofluorescence, microscope images and flow cytometry analysis of autofluorescent cells suggest a correlation between POS feeding and manifestation of autofluorescent structures, in a dose and time-dependent manner (Figure 3. 33 and Figure 3. 34). Opposed to rhodopsin IF staining, which is readily visible at time 0, autofluorescence appears only hours after POS feeding (Figure 3. 33). This is consistent with autofluorescence occurring as the result of POS processing by lysosomal digestion. In fact, analysis of rhodopsin staining and autofluorescence in the same cells suggests that autofluorescence emmerges from RET-P1-surrounded vesicles, i.e. phagosomes/ phagolysosomes labeled for rhodopsin exhibit autofluorescent material in their center. POS preparations contain lipids and proteins other than rhodopsin, which can also account for the autofluorescent granules.

Autofluorescence detection in hESc-RPE has proven difficult to observe, possibly because these cells are heavily pigmented. Pigmentation in this case may be masking the subtle effect of autofluorescence resultant from POS accumulation, as assessed in the other RPE lines. One way to circumvent this would be to avoid pigmentation in hESc-RPE, for instance by using Tyrosinase inhibitors. Still, a consistent increase of POS autofluorescence was detected, whether in Lonza hRPE or pRPE, following POS pulse. This suggests autofluorescence as a byproduct of POS processing, but further characterization of the autofluorescent granules is necessary, to confirm their origin.

CHAPTER 4

Chloroquine-induced hESc-RPE Model of Lysosomal Dysfunction

Chapter 4 focuses on the establishment and characterization of a lysosomal dysfunction model, as a way of reproducing RPE degenerative features, particularly in the case of AMD. This model of disease was attained by treating human Stem Cell-derived Retinal Pigment Epithelium cells, previously characterized, using Chloroquine as the lysosome dysfunction-inducing agent.

4.1 Significance of Lysosomal pH

Regulation of lysosomal pH has been extensively studied and its importance for different cellular functions definitely proven (Kissing et al. 2015; Hughes & Gottschling 2012; Miao et al. 2015; Davidson & Vander Heiden 2017; Appelqvist et al. 2013). In fact, lysosomal re-acidification strategies have been proposed to contribute to solving a number of chronic pathologies (Bourdenx et al. 2016; Folts et al. 2016; Trudeau et al. 2016; Lööv et al. 2015). On the other hand, it is important to keep in mind that overly acidic pH may also have detrimental effects. This has been proposed to be the case of chronic inflammatory disorders, such as Systemic Lupus Erythematosus (SLE) and Rheumatoid Arthritis (RA) (Al-Bari 2015). Still, the mechanisms involved in lysosome pH maintenance and the consequences of a pH imbalance on overall lysosomal function and cellular homeostasis are poorly characterized. Keeping in mind specific cellular functions, a tight pH regulation, dependent on cell type and on cellular needs/states is essential.

Inhibitors of the V-ATPase, such as Bafilomycin A_1 (Baf) or Concanamycin A (ConcA), are commonly used to block lysosomal degradative function. They work as specific and strong inhibitors of the V-ATPase V_0 subunit, virtually stopping the pump's activity (Huss & Wieczorek 2009). An analogous effect can be obtained using weak base lysosomotropic agents, such as Chloroquine (CQ) or NH_4Cl, and also ionophores, such as Monensin or Nigericin (Florey et al. 2015; Guha, Coffey, et al. 2014; Huotari & Helenius 2011). Specifically, weak bases diffuse into the lysosome and become trapped upon

protonation, accumulating and thereby dissipating the pH, whereas ionophores pump ions, in this case against the H^+ gradient, dispersing it (De Duve et al. 1974; Guha et al. 2013).

CQ is widely used as a therapeutic agent, for instance for malaria prevention, cancer treatments and to manage auto-immune disorders (Kissing et al. 2017; Wozniacka et al. 2002). In these cases, CQ's beneficial effects are thought to come from the increase of lysosomal pH and respective downstream effects on antigen processing and Toll-like receptor signaling. Particularly, CQ is thought to facilitate a decrease of auto-antigenic peptide loading and also to downgrade Cathepsins B and D activity, thus reducing MHC class II processing (Al-Bari 2015). However, despite its therapeutic potential, CQ was found to induce retinopathy as a side-effect of prolonged administration (Tanga et al. 2011; Bergstrom & Garcia-Valenzuela 2009; Korah & Kuriakose 2008; Biccas Neto & Mesquita 2009; Fung et al. 2007; Kellner et al. 2008). Currently, other CQ-based pharmaceutical formulations are prescribed, namely hydroxychloroquine (HCQ). HCQ is thought to work in a similar manner as CQ, but with reduced toxicity (Al-Bari 2015; Sundelin & Terman 2002).

4.1.1 Understanding Chloroquine-induced Retinopathy

From a research perspective it is interesting to note that CQ-induced retinopathy shares clinical features with other retinal degeneration disorders, particularly AMD. These features include: retinal thinning (Bergstrom & Garcia-Valenzuela 2009; Korah & Kuriakose 2008; Kellner et al. 2008), multilamellar structures within the RPE (Tanga et al. 2011), RPE atrophy (Biccas Neto & Mesquita 2009; Fung et al. 2007), photoreceptor loss (Bergstrom & Garcia-Valenzuela 2009; Kellner et al. 2008; Korah & Kuriakose 2008) and lipofuscin-derived autofluorescence (Kellner et al. 2008). Moreover, studies using animal models corroborate this parallel between CQ-induced retinopathy and AMD. In fact, prolonged administration of CQ (from one week up to four months) causes mice, rats and cats to develop deposits in the Bruch's membrane and photoreceptor loss (Peters et al. 2006; Ivanina et al. 1983; Lezmi et al. 2013). Furthermore, rhesus monkeys develop CQ-induced retinopathy, with macular degeneration, similar to human patients (Rosenthal et al. 1978).

The mechanism by which CQ exerts its effect is not completely understood. The highest concentrations of CQ ensue in melanin-containing cells and reportedly the RPE from the macula region concentrates a peak of melanin density (Rimpelä et al. 2017). Thus it is within reason to consider RPE degeneration as a primary event, leading to secondary loss of neural retina and consequent visual impairment (Rimpelä et al. 2016). Findings from RPE cell models seem to agree on the increased toxicity caused by pigment-affinity and consequent accumulation of CQ (Guha, Coffey, et al. 2014; Mannerström et al. 2002). Typically, studies of primary RPE cultures and RPE cell lines treated with CQ report intracellular vacuolization (Chen et al. 2011; Kaufmann & Krise 2008), increased pH (Coffey et al. 2014; Lu et al. 2017; Guha et al. 2013), autophagy substrates accumulation (p62/ and LC3 II) (Wu et al. 2017; Song et al. 2016; Sanjuan et al. 2007; Coffey et al. 2014;

Lu et al. 2017; Szatmári-Tóth et al. 2016; Zhan et al. 2016), inhibited phagocytic and endocytic degradative function (Song et al. 2016; Liu et al. 2008; Guha, Coffey, et al. 2014; Chen et al. 2011; Guha et al. 2012), increased autofluorescence (Lei et al. 2017; Guha et al. 2013; Guha et al. 2012), lysosomal exocytosis and increase in membrane permeability (Beckel et al. 2018; Korthagen et al. 2015). Additionally, few studies regarding RPE CQ-exposure report increase of Cathepsin activity, followed by the expected decrease, upon dosage escalation (Toimela et al. 1995).

4.1.2 Modeling CQ-induced Lysosomal Dysfunction

Cellular responses may vary dramatically with different drug concentrations, exposure times and also with the cells' own features and states. In this chapter experiments undertaken considering relative low dosages of CQ are reported, and at three extensive time points, comparing to most *in vitro* studies (Mahon et al. 2004; Sundelin & Terman 2002; Yu et al. 2018; Wu et al. 2017; Lu et al. 2017; Liu et al. 2008; Guha et al. 2012; Szatmári-Tóth et al. 2016; Chen et al. 2011; Zhan et al. 2016; Beckel et al. 2018; Rimpelä et al. 2016; Korthagen et al. 2015; Mannerström et al. 2002).

A strong hypothesis for the mechanism behind early CQ-induced retinopathy events is lysosomal dysfunction (Mahon et al. 2004; Coffey et al. 2014). Still, lysosomal dysfunction is generally considered as a broad concept, difficult to underpin and modulate. Lysosomes provide essential functions from phagocytic turnover of POS to recycling of intracellular components and even ECM maintenance. All these tasks require macromolecules to travel through the endocytic pathway, trafficking from endosomes to late endosomes, followed by transient or complete fusions between late endosomes and lysosomes. These processes are generally accompanied by a decrease of pH, necessary for acid hydrolase activity and consequent degradation of their substrates. To add complexity to the system, lysosomes tightly associate to transcriptional regulation of cellular metabolism, as described in Chapter 1.

The work developed herein aims to clarify critical aspects of RPE cell biology and of lysosomal activity, and in particular establish hESc-RPE as a reliable model to study retinal degenerative disease. To this effect, cells were subjected to CQ for prolonged periods of time and a detailed characterization of this models' lysosomal functions is presented. In particular, this chapter reports how hESc-RPE cells respond to acute (overnight), continued (three days) and chronic (one week) CQ insults.

For the experiments presented herein, Rapamycin (Rap) and Bafilomycin (Baf) were used as controls. On the one hand, Rap is an mTORC1 inhibitor, therefore promoting autophagy and lysosomal biogenesis; on the other hand, Baf is a V-ATPase inhibitor, thus preventing lysosomal degradation. As such, Rap is considered a positive control and Baf is the negative control, regarding active lysosomal function.

4.2 Chloroquine titration - LDH viability assays

Newly established hESc-RPE lines were first tested for viability, when treated with different concentrations of CQ. Porcine RPE (pRPE), obtained from primary cultures, as well as the Lonza hRPE were tested in parallel and compared to hESc-RPE.

Measurement of lactate dehydrogenase (LDH) enzyme released into the media was used as a read-out of damaged cells and cytolysis. CQ's cytotoxicity corresponds to higher absorbance readings and, in this case, analysis was always carried out considering values relative to the mean of control non-treated (NT) cells.

The first approach taken consists on assessing viability for an acute overnight treatment, as described in the Materials and Methods (Chapter 2). Briefly, cells were fed with porcine POS for 4h, in order to load the lysosomes, followed by an overnight incubation with CQ-containing medium at different concentrations; medium was collected the following day and secreted LDH activity was quantified (Figure 4. 1).

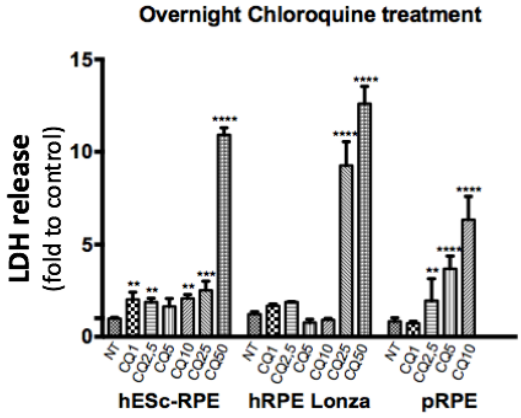

Figure 4. 1 - Chloroquine toxicity evaluation for the three RPE lines indicated, upon an overnight drug treatment, assessed by LDH activity determination. The three cell lines exhibited different sensitivities to the overall concentrations used (1-50 µg/mL). Absorbance values are considered as relative to NT control mean value, for each of the cell lines used and thus presented as fold change, relative to NT (1x fold). Results are expressed as mean ± s.d. and n≥3 (**p<0.01; ***p<0.001; ****p<0.0001).

The three different RPE lines were incubated with CQ concentrations ranging from 1 to 10µg/mL, in the case of pRPE, and 1 to 50µg/mL, in the case of human RPE. Lower concentrations of CQ induced reduced cytotoxicity (approximately a 2x fold increase of LDH release); CQ at 5µg/mL (CQ5) induced a significant increase of LDH release to the medium (4x fold increase) in pRPE cells, while in hRPE it did not have a significant increase, but instead caused a slight decrease in the case of Lonza hRPE. CQ at 10µg/mL (CQ10) led to significant pRPE cell death (6x fold LDH increase), whereas hRPE lines were able to withstand it, similarly to CQ5. For both human RPE lines, the threshold was higher, resisting up to CQ25, in the case of Lonza hRPE (9x fold), and CQ50, for hESc-RPE (11x fold). It is relevant to note that even at CQ50, a mean 11x fold increase (Figure 4. 1) does not mean that all hESc-RPE cells died as a result of the overnight treatment. In fact, in some cases cells were able to survive for three days with no apparent changes in morphology or adherence (as assessed by observation under light microscopy).

Observations on the microscope corroborated the LDH results (data not shown): pRPE cells were visibly affected by 10µg/mL of CQ overnight, dissociating the monolayer and detaching from the wells. On the other hand, hRPE cells seemed visibly affected as a result of the overnight treatment only when CQ was given at 50µg/mL; in particular, they became darker and ultimately detached, disrupting the monolayer. In any case, the overall goal of this titration was to understand the range of concentrations which would be useful for treatment of cells in a more chronic way, i.e. continuing treatment of the cells with CQ for several days, using under-lethal concentrations.

In order to recapitulate a continued insult and maintenance of the dysfunctional lysosome, cells were treated repeatedly with daily POS feedings followed by overnight incubations with CQ, for a three-day period. After the third overnight incubation of CQ, the medium was recovered and analyzed for LDH activity (Figure 4. 2).

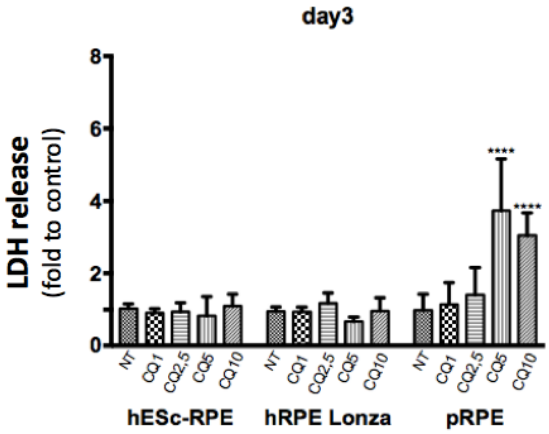

Figure 4. 2 - hESc-RPE, Lonza-hRPE and pRPE viability, following 3 days of CQ treatment, assessed by LDH activity determination. CQ was considered to have cytotoxic effects for porcine cells at 5 and 10µg/mL. Absorbance values are considered as relative to NT control mean value, and thus representing fold change, relative to NT (1x fold). Results are expressed as mean ± s.d. and n≥3 (****p<0.0001).

All three cell lines displayed similar LDH absorbance levels relative to control (NT) cells, for the lower concentrations of CQ (CQ1, CQ2.5) at the third day of CQ stimulus (Figure 4. 2). When CQ5 and CQ10 were used, a similar result was obtained for both human RPE lines: LDH levels stabilized to match controls; however, these concentrations were too high for pRPE, with significant cell death at day 3 (4x fold) (Figure 4. 2).

The main objective of this experiment was to assess if the cytotoxicity would become more severe after continued incubations. For this reason, it is worth mentioning that the medium was collected on a daily basis, meaning that the results displayed represent LDH released during the third day of treatment only and not the accumulated LDH over a three-day period.

In an effort to recapitulate the effects of chronic lysosome dysfunction, cells were subjected to a week-long treatment of CQ. A cumulative burden of CQ is expected to increase cytotoxicity over time. On the other hand, it is important to verify whether cells

are able to adapt to the first days of insult, i.e. if there is selection of the cell population, resistant to the hostile environment. In any case, experimental conditions were pondered based on viability studies, as described before. Briefly, cells were subjected to an everyday feeding of POS, for 4h, followed by replacement of the culture medium to that containing the different concentrations of CQ. Again, medium was collected every day, for seven consecutive days, and LDH secretion was evaluated for each day (not cumulatively), for all of the RPE lines used. Results are shown separately for each RPE line, for better visualization (Figure 4. 3, Figure 4. 4 and Figure 4. 5).

The results obtained for LDH release by hESc-RPE cells treated with CQ, repeatedly, for a week, are presented in Figure 4. 3.

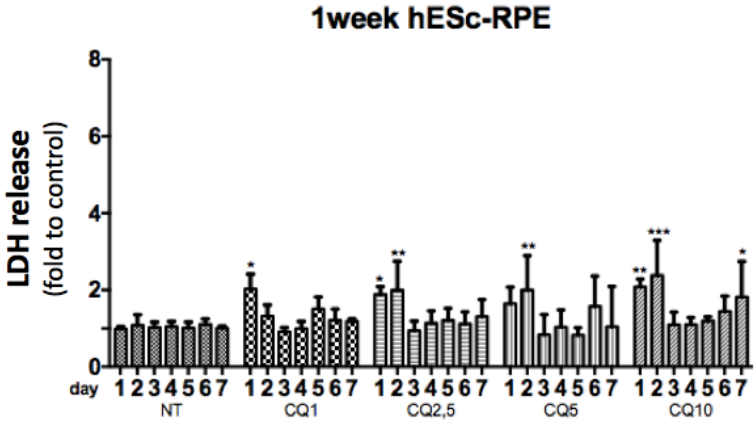

Figure 4. 3 - hESc-RPE viability, after being submitted to a week-long CQ treatment, assessed by LDH activity determination. During days 1 and 2, there was modest increase of LDH release to the medium (2x fold) for the whole range of CQ concentrations used. Absorbance values are considered as relative to NT control mean value, and thus presented as fold change, relative to NT (1x fold), for each day. Results are expressed as mean ± s.d. and n≥3 (*p<0.05; **p<0.01; ***p<0.001).

hESc-RPE was able to withstand CQ for the whole one-week period, without showing evidence of cytotoxicity with the tested concentrations. There was an increase (2x fold) of LDH release in the first two days of the experiment, with no observable changes to cell morphology or adherence. These LDH secretion values returned to matching NT controls, with minimal oscillations thereafter (Figure 4. 3).

A tentative pattern seems to emerge, where the first day of insult results in a modest increase of LDH release, followed by a period of stabilization and return to control values, more obvious when looking at 10µg/mL (CQ10). This can be interpreted as a two-phased response to CQ: on the first two days, the LDH in the medium may increase due to death of more sensitive or damaged cells; the majority of cells, however, survives this first selective phase and thus LDH release is kept at control levels for the remaining days; this was confirmed by light microscopy observations, which revealed cells did not lose their monolayer configuration. If the experiment were to be prolonged for more time, one could speculate that the chronic stressor would ultimately cause the cells to succumb (there is a slight increase of LDH release at day 7, although too modest to consider relevant cytotoxicity). However, the purpose of the experiment was precisely to cause a chronic

non-lethal environment, thus CQ concentrations were kept at relatively low levels and these experiments were not followed further.

Ultimately, LDH release by hESc-RPE is not significantly altered throughout the week-long CQ treatment, meaning cells are able to survive and manage the insult.

LDH release after a week-long CQ treatment of Lonza hRPE (Figure 4. 4).

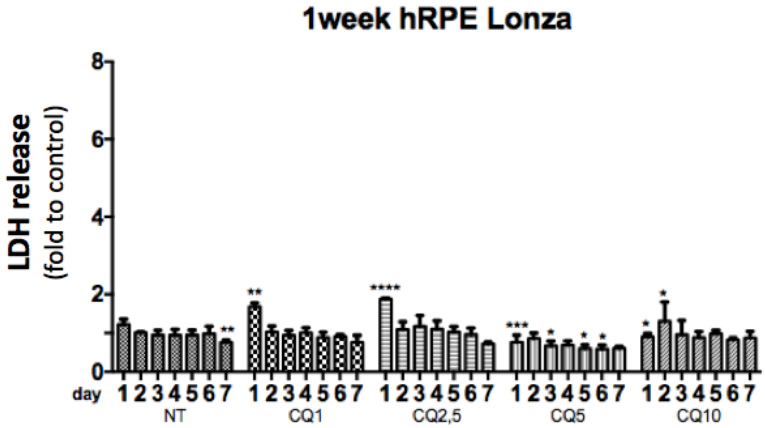

Figure 4. 4 - Lonza hRPE viability, after being submitted to a week-long CQ treatment, assessed by LDH activity determination. There was a modest increase of LDH in the medium for cells treated with lower CQ concentrations (1.7x fold for CQ1, 1.9x fold for CQ2.5). Absorbance values are considered as relative to NT control mean value, and thus presented as fold change, relative to NT (1x fold). A significant difference was found between the NT cells, at day 7 (**); nevertheless, the medium collected each day was compared to its respective NT condition, for the statistical analysis. Results are expressed as mean ± s.d. and n≥3 (*p<0.05; **p<0.01; ***p<0.001; ****p<0.0001).

LDH release, in the case of Lonza hRPE, is not expressively altered throughout the range of CQ concentrations and for the whole experiment. There were slight oscillations in the absorbance values obtained, but always less than a 2x fold change (Figure 4. 4). For this reason, these concentrations of CQ were considered not to exert acute toxic effects on Lonza hRPE cells. Again, after the first days, LDH levels returned to control (NT) levels, or even lower (0.6x fold) (Figure 4. 4).

Finally, medium from pRPE submitted to the same CQ regimen was also collected and LDH secretion was evaluated during the parallel experiment (Figure 4. 5).

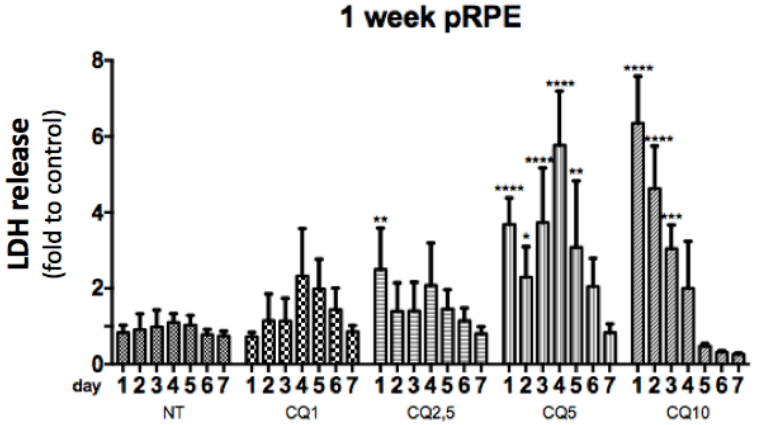

Figure 4. 5 - pRPE viability, upon week-long CQ treatment, assessed by LDH activity determination. Cytotoxicity was verified for higher concentrations of CQ (4x to 6x fold increase of LDH). Absorbance values are considered as relative to NT control mean value, and thus presented as fold change, relative to NT (1x fold), for each day. Results are expressed as mean ± s.d. and n≥3 (*p<0.05; **p<0.01; ***p<0.001; ****p<0.0001).

pRPE cells are more sensitive to CQ, comparing to both human cell lines (Figure 4. 3, Figure 4. 4 and Figure 4. 5). Hence, porcine cells exposed to higher concentrations of 5µg/mL (CQ5) or 10µg/mL (CQ10) died during the experiment. This is readily visible by the increase of LDH found in the medium: CQ5 caused the cells to release 4x fold more LDH than control cells (NT) on the first day, while CQ10 caused a 6x fold increase. While for CQ5 LDH release remained relatively high until day 4 and decayed thereafter, for CQ 10 LDH values continuously declined from the first day, until the end of the experiment (Figure 4. 5). This decline of LDH values can be attributed to cell death: as the experiment continues, and cells under higher CQ burden perish, there are less and less cells in the well and therefore fewer LDH secretion each day. This is consistent with observations by light microscopy (data not shown), which revealed cells detaching from the wells with disruption of the monolayer, interpreted as evidence of damage and death, when using higher concentrations of CQ.

Considering lower concentrations (CQ1 and CQ2.5), there is a first increase in LDH release to the medium, comparing to NT controls, whereas LDH levels remained steady (similarly to hRPE). This relatively minor increase (2x fold) in LDH release was not accompanied by evident cell death, and for this reason these relatively soft fluctuations were attributed to more sensitive/ already damaged cells. Again, alike in hRPE cells, the first LDH increases gave rise to a stabilization to control levels (Figure 4. 5).

Ideally, measurement of LDH secreted to the medium would be accompanied by measurement of intracellular LDH, in order to assess the proportion and extrapolate the values to "dead cells" *versus* "living cells" remaining in the well. However, this would require the use of a significantly higher amount of cells, to be collected on a daily basis. Nevertheless, based on these preliminary experiments, the aim of the experiment was achieved and it was possible to assess the range of under-lethal concentrations to be used in the following sections.

4.2.1 Chloroquine-induced Pigmentation Modifications

A curious finding of these CQ early experiments was the pigmentation change that cells underwent. Specifically, as time progressed, pigmentation became evident to the naked eye, and in accordance to CQ concentration: the higher the concentration, the darker the well. This effect was not always detected in Lonza hRPE nor in pRPE, but readily visible in hESc-RPE (Figure 4. 6).

A feature of the newly established hESc-RPE is the fact that these cells continue to produce pigment, developing an obvious dark tone, after a month of maturation. Here, however, cells were left to mature for only two weeks before the tests, which means cells were pigmented, but not very dark, at the beginning of the experiment. hESc-RPE cells treated with the highest concentrations of CQ (25µg/mL and 50µg/mL) experienced pigmentation changes more promptly and displayed a darker shade (Figure 4. 6).

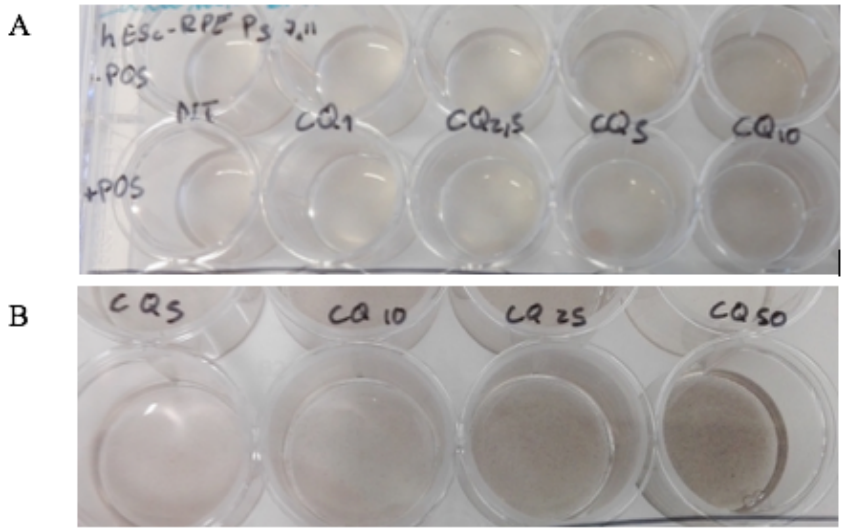

Figure 4. 6 - hESc-RPE exhibit pigmentation changes, when treated with CQ for 1 week (A) or 3 days (B). Cells exhibit apparent color intensification, proportional to the CQ concentrations, as indicated on the multiwell plate, and duration of treatment. Photograph depicts observation of a multiwell plate, by the naked eye.

Although pigmentation was not objectively measured and quantified, this visual effect does not necessarily mean that cells are producing more pigment. In fact, another explanation for this result could be the aggregation/accumulation of pigment, causing it to become more readily visible. Furthermore, this color change is also observed when cells are treated with Baf (data not shown), indicating a direct correlation between pigmentation and lysosomal pH. This relationship has already been studied by other researchers, in different contexts, substantiating the relevance of such effects namely in hESc-derived RPE (Juuti-Uusitalo et al. 2017).

These findings were not further explored at this time, despite the apparent correlation between retinal degenerative disorders and pigmentation anomalies in the RPE. Particularly, pigmentation is thought to have a protective role and the risk of AMD development and progression correlates inversely with macular pigment optical density (Arunkumar et al. 2018). On the other hand, the MiT family of TFs actively regulates pigmentation, with MITF being at the heart of many RPE specification and pigmentation studies (Steingrímsson et al. 2004; Bharti et al. 2012; Fuhrmann et al. 2014). Consequently, it is not surprising that there is a correlation between lysosomal dysfunction and pigment changes in the RPE and, despite this being outside the scope of the present work, it opens interesting avenues for future work.

Considering previous results regarding detection of autofluorescence, either by microscopy or flow cytometry (Figure 3.33 and Figure 3.34), together with the pigmentation-related data (Figure 4.6), some reflections are due. Specifically, in hESc-RPE, autofluorescence was found to be inherently high, compared to Lonza hRPE or pRPE. This feature was attributed precisely to pigmentation because, contrary to the others, when hESc-RPE are dissociated and collected as a cell pellet, it is dark to the naked eye (not shown). For this reason, when cells were analyzed by flow cytometry, detection threshold did not allow visualization of CQ- or POS-derived autofluorescence (Figure 4. 7).

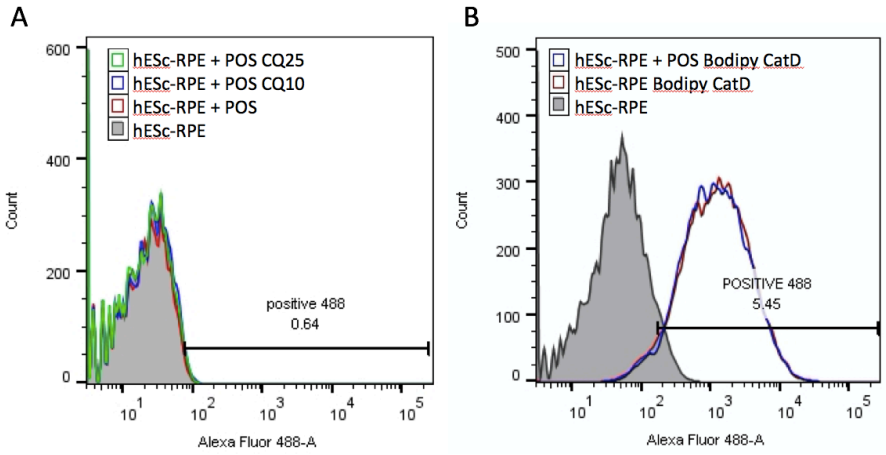

Figure 4. 7 - (Auto)fluorescence detection in hESc-RPE, by flow cytometry. A: autofluorescence histogram overlap between non-treated hESc-RPE, POS-fed hESc-RPE, CQ10- and CQ25-treated cells; autofluorescence detection ≤1% of cells per condition. B: Bodipy CatD fluorescence histogram showing non-treated hESc-RPE unstained, non-treated hESc-RPE stained with Bodipy CatD and POS-fed hESc-RPE stained with Bodipy CatD; fluorescence detection ≥99% of cells per conditions. n=20.000 cells acquired for each condition represented.

CQ autofluorescence or POS autofluorescence alone were not present at detectable levels. In particular, only 1% of cells were found autofluorescent over the detection limit (Figure 4. 7 A). In comparison, acquisition of fluorescent dyes (presented in the following sections) was easily detected. In fact, Bodipy CatD fluorescence, in the same 488nm channel, is represented by a completely different peak in the respective histogram (Figure 4. 7 B). Based on these preliminary results, a possible interfering effect of either CQ or POS on background fluorescence was disregarded in following experiments. In fact, Bodipy CatD fluorescence was much more intense and over 99% of cells were brightly labeled (Figure 4. 7). When considering the remaining dyes (DQ-BSA, Magic Red or Lysotracker), fluorescence was detected in both the 568nm and 647nm channels, showing similar profiles (data not shown). In the end, the data were analyzed in the 647nm, to avoid bleed through from visible light spectrum. Therefore, although CQ or POS autofluorescence may interfere with the results, it is expected that the error found is similar for all samples analyzed and small, relatively to the bright fluorescence detected when using these dyes.

Finally, an experimental layout was established by setting a timeline and a range of non-lethal concentrations, and by considering experimental limitations. Cellular responses to an acute, continued and chronic lysosomal dysfunction was recapitulated and the overall features of this disturbance were thoroughly characterized, and are discussed in the following sections.

4.3 Chloroquine-induced MiT TFs Nuclear Translocation

The MiT family of TFs are major players in control of lysosomal function. These TFs are responsible for the regulation of lysosomal hydrolases necessary for substrate degradation, of membrane proteins which mediate lysosome fusion, and of components of the V-ATPase complex, responsible for lysosomal acidification. In particular, TFEB

regulates response to starvation, by targeting autophagy-related genes and regulating autophagosome formation and its fusion with the lysosome, as discussed in Chapter 1.

As described previously, the mammalian target of rapamycin (mTOR), which is part of mTOR complex 1 (mTORC1), interacts with TFEB at the lysosomal membrane. This interaction occurs when the cell is in homeostatic conditions and leads to phosphorylation of TFEB and thus to its cytosolic retention. On the other hand, upon starvation or other types of cellular stress, TFEB is no longer phosphorylated and is able to translocate to the nucleus and activate autophagy and lysosomal genes.

Based on these premises, the subcellular localization of TFEB, TFE3 and MITF was assessed by immunofluorescence (IF), both in homeostatic conditions and upon challenge with CQ.

In a preliminary experiment, TFEB subcellular localization was evaluated, upon overnight treatment of hESc-RPE with 5µg/mL of CQ. The result of this experiment demonstrated a clear effect regarding nuclear translocation (Figure 4. 8).

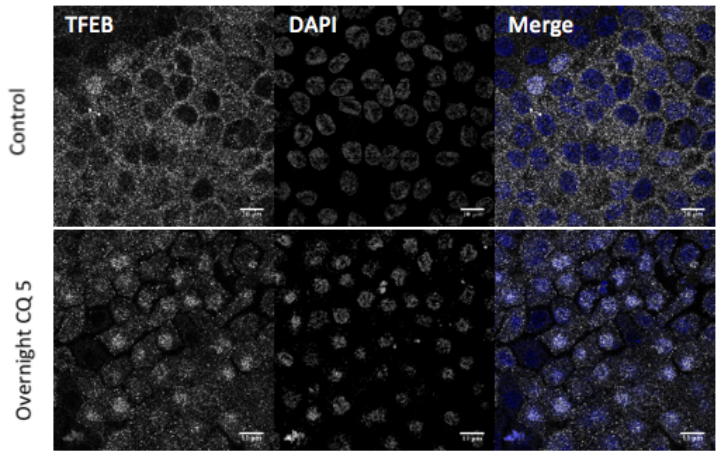

Figure 4. 8 - Acute CQ treatment of hESc-RPE induced TFEB translocation to the nucleus, as evidenced by co-localization with DAPI nuclear staining, assessed by IF. Scale bar: 10µm.

As depicted, in homeostatic conditions TFEB localizes mostly to the cytoplasm of the cell, almost avoiding nuclear localization (Control). On the other hand, under the effect of CQ (Overnight CQ5) it translocates to the nucleus, co-localizing notably with DAPI. In order to further evaluate this effect, TFEB translocation to the nucleus was quantified, by assessing the integrated intensity inside the nuclear area defined by DAPI (Figure 4. 9).

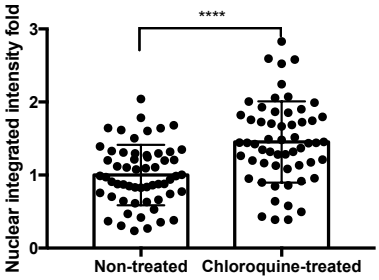

Figure 4. 9 - Acute CQ treatment induced TFEB translocation to the nucleus in hESc-RPE, as determined by selecting the nuclear area of random cells (stained with DAPI) and analyzing intensity of TFEB staining within that area, within three representative IF images. ****p<0.0001, n=57 and n=58, respectively.

A significant difference between non-treated and CQ-treated cells was found; specifically, the difference between integrated intensity means was determined as approximately 1.5x-fold increase, relative to non-treated cells. For this quantification, a set of three representative images was selected for each condition and a total of n=57, n=58 cells were considered, respectively (Figure 4. 9).

In subsequent experiments, evaluation of the subcellular localization of TFEB, TFE3 and MITF was undertaken, in parallel in hESc-RPE incubated with either regular medium or medium containing 5µg/mL CQ, overnight (Figure 4. 10).

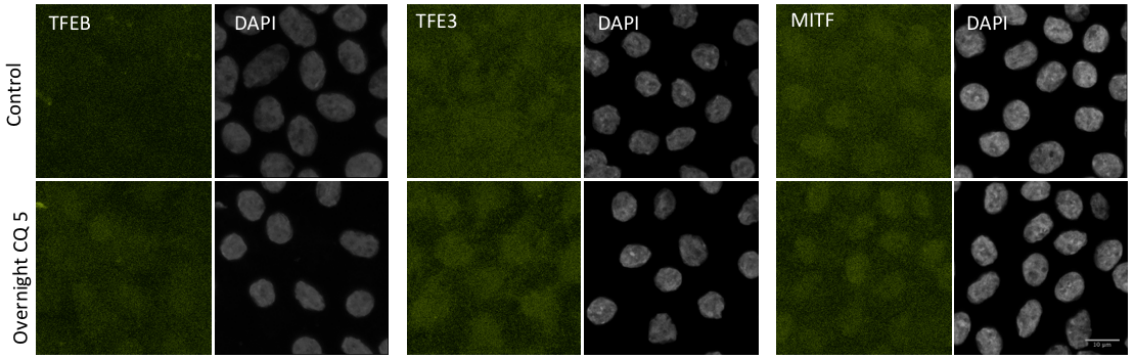

Figure 4. 10 - TFEB, TFE3 and MITF translocate and concentrate at the nucleus, upon acute CQ treatment, as evidenced by co-localization with DAPI, assessed by IF. Scale bar 10µm.

Although TFEB staining of hESc-RPE is generally faint, it is possible to observe that it becomes more distinct at the nuclear area, upon CQ treatment. This difference is more noticeable in TFE3 staining, which is dispersed in control cells and concentrated at the nuclear region in CQ-treated cells. As for MITF staining, it is found in the nuclear region both in control and in CQ-treated cells, but again, becomes more concentrated in the nuclear area (Figure 4. 10).

After 3 days of CQ treatment of hESc-RPE cells, TFEB, TFE3 and MITF subcellular localization was evaluated again, by IF. Medium was changed every day: control cells with fresh regular medium, CQ-treated with medium containing 5µg/mL CQ (Figure 4. 11).

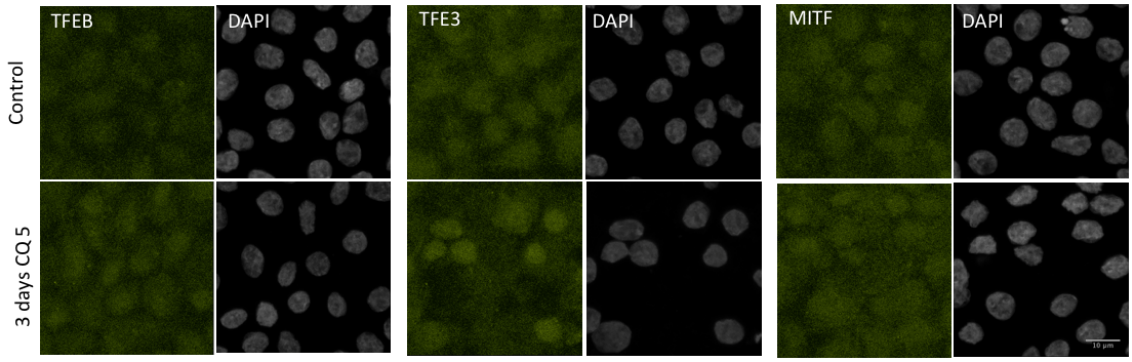

Figure 4. 11 - TFEB, TFE3 and MITF translocate to the nucleus upon treatment with 5µg/mL CQ, for three consecutive days, as evidenced by co-localization with DAPI, assessed by IF. Scale bar 10µm.

After three consecutive days of treatment, it is possible to notice an intensification of the staining at the nuclear area, for TFEB and TFE3. As for MITF, the difference between non-treated and CQ-treated cells is less evident (Figure 4. 11).

The consecutive treatments continued, as formerly described, and intracellular localization of the three TFs was evaluated after seven days of treatment (Figure 4. 12).

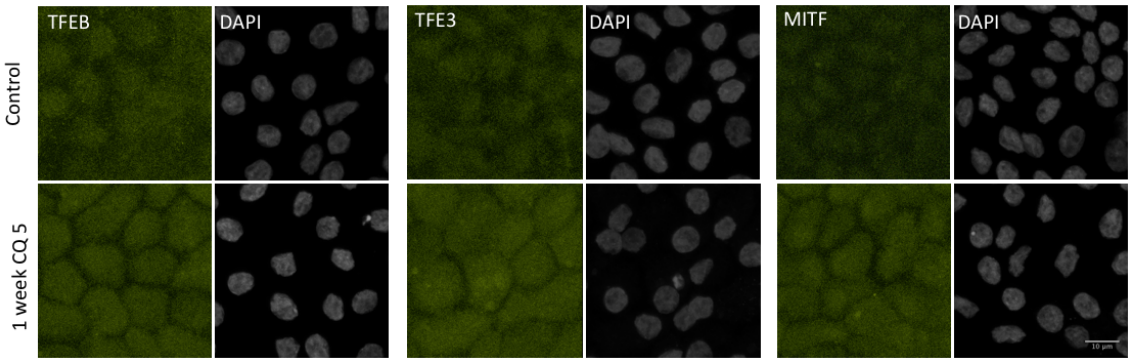

Figure 4. 12 - TFEB, TFE3 and MITF subcellular localization is severely changed upon treatment with 5µg/mL CQ, for seven consecutive days (1 week), as evidenced by co-localization with DAPI, assessed by IF. Scale bar 10µm.

Strikingly, after one week of 5µg/mL CQ treatment, TFEB, TFE3 and MITF stainings are spread throughout the whole cell (cytoplasm and nuclei). Only the cell membrane is left unstained, emphasizing the typical RPE monolayer polygonal shape Figure 4. 12.

Interestingly, regarding the control cells and comparing overnight (Figure 4. 10) to the third day (Figure 4. 11), translocation of the three TFs to the nucleus seems to be induced merely by the change of regular fresh medium, without CQ. One week of media change every day, in the control situation (Figure 4. 12), also induces nuclear translocation of the TFs, when compared to the overnight-treated control cells (Figure 4. 10), but apparently not more than the three-day control cells (Figure 4. 11). A recent study identified that HEPES, a buffering compound commonly used in cell culture media, induces lysosomal biogenesis (Tol et al. 2018). For this reason, it is important to reflect carefully on the conclusions drawn from these results and to consider potential confounding effects. On the other hand, it is not surprising to find MITF in the nuclear area (even in cells that were not treated with CQ) because this TF is involved in pigmentation. MITF regulates expression of Tyrosinase and TRP1, for instance, which are required for pigmentation. As described in Chapter 3, hESc-RPE are continuously pigmenting, possibly even more so when subjected to CQ treatment (Figure 4. 6).

Regardless, the addition of CQ to the media seems to increase the nuclear area intensity of the stainings, comparing to the control for the same time points, in the overnight and the third day situations. After one week, the staining pattern is completely altered, occupying the whole cell (Figure 4. 12). A chronic CQ insult possibly causes upregulation of these TFs, suggesting a cellular stress-response. Additionally, the fact that these TFs localize both to the cytoplasm and to the nucleus suggests inactivation of mTOR, pointing to defects in lysosome reformation, as discussed in Chapter 1.

Together, these IF results suggest there is potential induction of lysosomal biogenesis, more pronounced at the third day of insult than in the overnight treatment, followed by lysosomal dysfunction induced by chronic CQ burden.

4.4 CQ-induced Impairment of Phagocytic Cargo Digestion

When treated with CQ, cells are expected to have impairment of their degradative ability. This damage is anticipated to become more severe for extended periods of drug regimen. The degradative function of lysosomes was evaluated in the same conditions of CQ treatment as in the previous experiments. Specifically, in order to verify lysosomal dysfunction and consequent degradative deficiency, POS digestion was followed again, for the different time points, in hESc-RPE cells treated with CQ.

Unless otherwise indicated, POS feedings were ensued using 200µg/mL working concentration. This concentration was chosen based on the ability of hESc-RPE to digest them within the timeframe evaluated in previous experiments (Chapter 3). POS degradation was directly measured, using anti-Rhodopsin antibodies, as previously.

Control cells (without CQ) present RET-P1 positive particles, similar to those found in previous experiments, and almost no 1D4 staining, consistent with the fact that 1D4 epitope is lost during early phagosome maturation, as assessed by IF staining of rhodopsin, after overnight incubation of hESc-RPE with CQ. CQ-treated cells also present RET-P1 staining and, interestingly, seem to exhibit more 1D4 staining than control cells, indicating presence of early phagosomes even after overnight chase (Figure 4. 13).

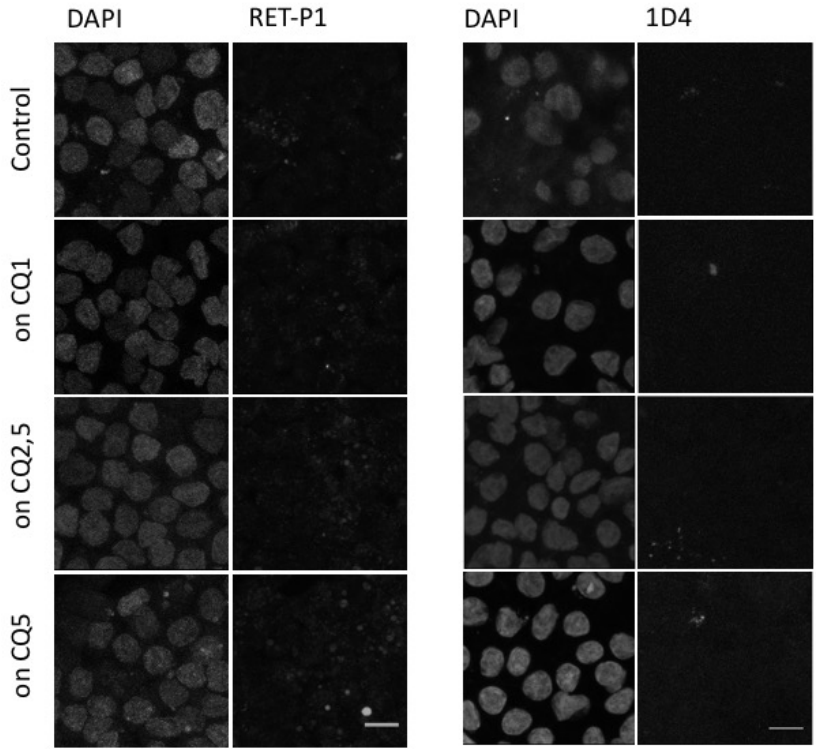

Figure 4. 13 - POS accumulation, when hESc-RPE are treated with CQ overnight and depending on drug concentration (1-5µg/mL). Rhodopsin IF staining, using anti-RET-P1 and 1D4 antibodies and DAPI for nuclei labeling. Scale bar 10µm.

Accumulation of POS by hESc-RPE cells is aggravated when cells are subjected to higher CQ concentrations, namely when treated with 10 and 25µg/mL CQ overnight (Figure 4. 14).

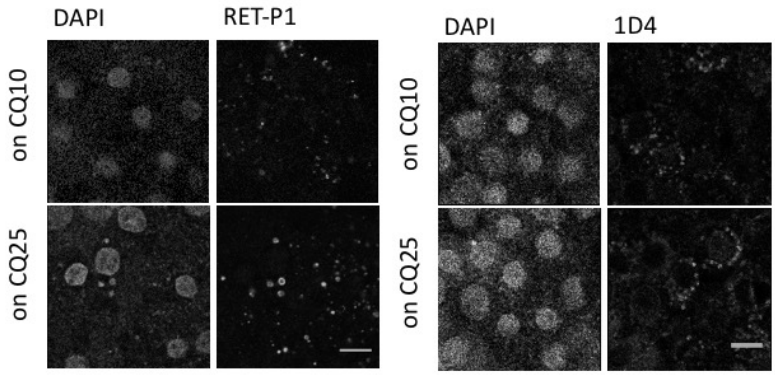

Figure 4. 14 - POS accumulation becomes more evident upon treatment with higher CQ concentrations. Rhodopsin IF staining, using anti-RET-P1 and 1D4 rhodopsin antibodies and DAPI for nuclei labeling, after treatment with CQ at 10 and 25µg/mL. Scale bar 10µm.

At higher CQ concentrations, not only 1D4 epitope remains readily visible after overnight chase, but also RET-P1 accumulation is easily detected (Figure 4. 14). Interestingly, the pattern of rhodopsin staining (using both antibodies) seems different. In particular, RET-P1 stains donut-shaped enlarged compartments, resembling those found in Lonza hRPE (Figure 3.33); alike previously discusses, this could be indicative of an active degradative compartment consisting of an autofluorescent granule within RET-P1-labeled vesicle. In fact, autofluorescence bleed-through to the DAPI channel is visible, in this particular case (Figure 4. 14). Regarding 1D4 rhodopsin staining, it is focused within perinuclear early phagosomes. Still, in experiments with higher concentrations of CQ there is generally increase in background autofluorescence, precluding a more detailed analysis (Figure 4. 14).

Furthermore, images acquired in these conditions were evaluated for rhodopsin staining intensity (Figure 4. 15).

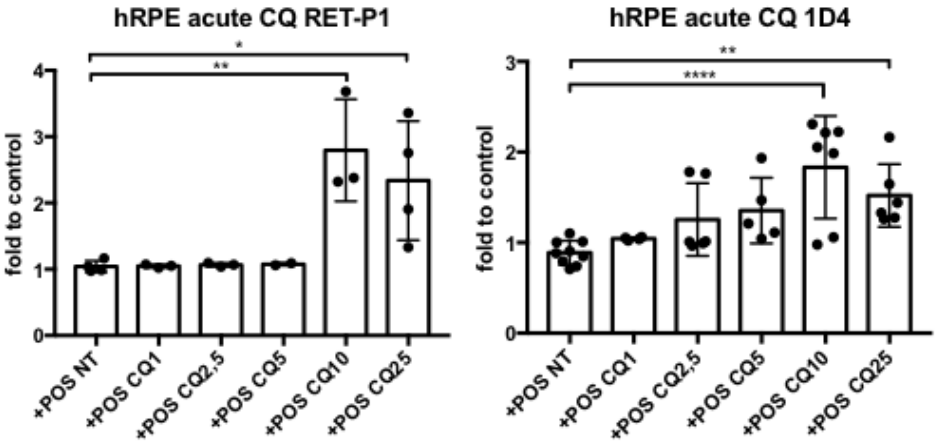

Figure 4. 15 - Quantification of POS accumulation, with increasing CQ concentrations, upon hESc-RPE acute treatment. Fluorescence was quantified for each condition, with each dot representing a different IF image's mean fluorescent integrated intensity as fold increase, compared to control (NT) cells using anti-RET-P1 and anti-1D4 antibodies. Results are expressed as mean ± s.d. from independent images, n≥2 (* $p<0.05$, **$p<0.01$; ****$p<0.0001$).

By analyzing image quantification, it becomes obvious that RET-P1 epitope is retained after overnight chase, in cells treated with high CQ concentrations 10 and 25µg/mL, as previously shown in representative images (Figure 4. 14). Regarding 1D4 epitope, it is also retained in the cells, when treated with CQ. In some images of cells treated with lower CQ dosages (2.5 or 5µg/mL), the staining's mean integrated intensity is higher than in control cells. However, different image fields and images obtained from different experiments using these same concentrations present similar intensity to that of control cells. For this reason, statistical significance was only found when looking at higher CQ concentrations, 10 and 25µg/mL (Figure 4. 15).

Next, hESc-RPE were treated with CQ in a continued manner, and analyzed again for their ability to process phagocytic cargo. In order to continuously load the lysosome, cells were fed POS on a daily basis, for 4h, followed by overnight incubation in CQ-containing medium, during 3 consecutive days. Representative IF images of RET-P1 and 1D4 stainings are presented in Figure 4. 16.

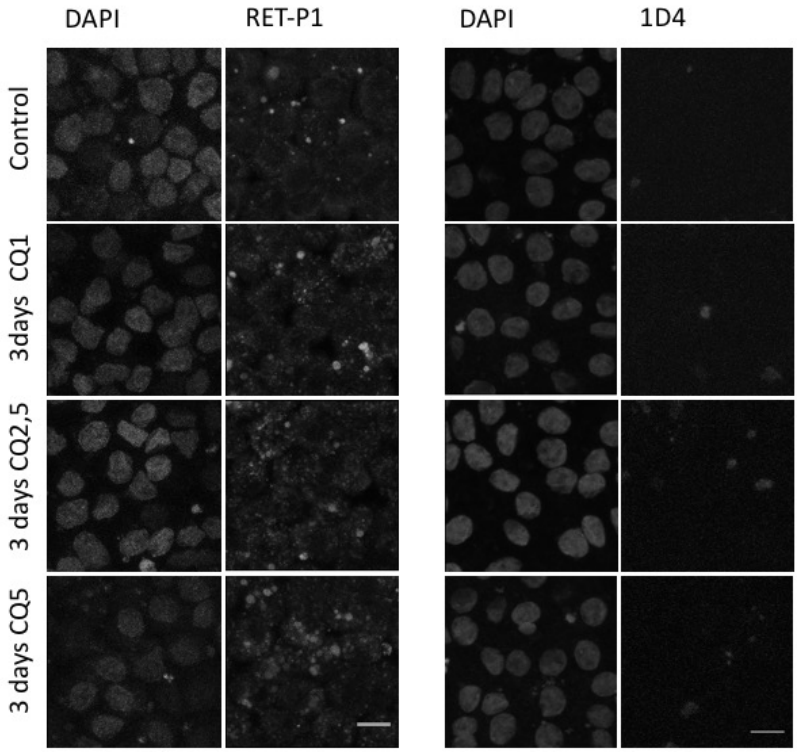

Figure 4. 16 - hESc-RPE treated with CQ for three consecutive days accumulate more rhodopsin than control cells. hESc-RPE rhodopsin IF staining, using anti-RET-P1 and 1D4 antibodies and DAPI for nuclei labeling, after continued CQ treatment. Scale bar 10µm.

After three days of POS feeding and overnight incubation with regular medium (control situation), hESc-RPE accumulate more RET-P1-positive vesicles than control cells which were fed only once (Figure 4. 14). 1D4 epitope continues to be readily processed by control cells and, therefore its staining is inconspicuous. Upon CQ treatment, RET-P1 positive vesicles become more evident and 1D4 staining remains visible in the cells (Figure 4. 16).

Quantification of representative images was performed and is depicted in Figure 4. 17.

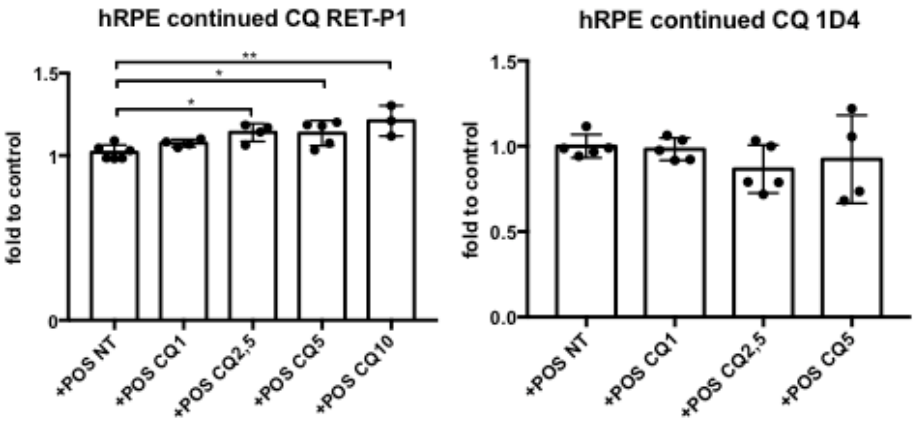

Figure 4. 17 - Quantification of POS accumulation, with increasing CQ concentrations, upon hESc-RPE continued treatment with CQ at 1-10 µg/mL. Each dot represents a different IF image's mean fluorescent integrated intensity as fold increase, compared to control (NT) cells using anti-RET-P1 and 1D4 antibodies. Results are expressed as mean ± s.d. from independent images n≥3 (* $p<0.05$, ** $p<0.01$).

Accumulation of rhodopsin in CQ-treated cells occurs in a concentration-dependent manner, as assessed by RET-P1 staining. However, 1D4 staining is not altered upon treatment. One explanation could be that at low concentrations, CQ does not interfere with early phagosomes (1D4), but only affects phagolysosome processing, as RET-P1 labels early to late phagosomes (Figure 4. 17).

hESc-RPE were also subjected to a week-long treatment of CQ, similarly to previous experiments. Rhodopsin staining with RET-P1 and 1D4 antibodies were performed (Figure 4. 18).

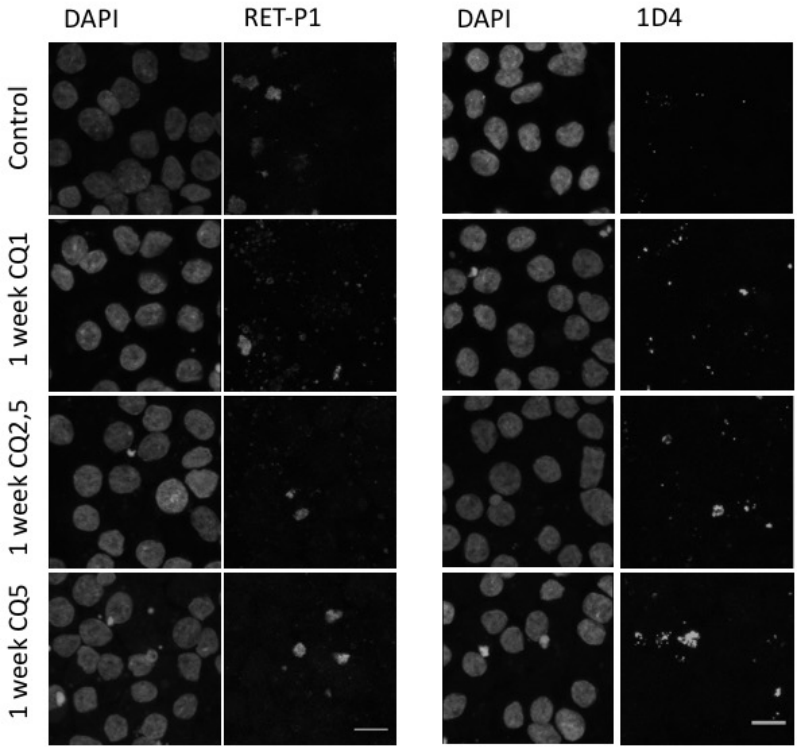

Figure 4. 18 - POS accumulate as the result of chronic treatment with CQ (1-5µg/mL) for seven consecutive days, when comparing to control. hESc-RPE rhodopsin IF staining, using anti-RET-P1 and 1D4 antibodies and DAPI for nuclei labeling. Scale bar 10µm.

Cells fed with POS and treated with CQ for one week render accumulation of rhodopsin-positive vesicles, whether stained with RET-P1 or 1D4 antibodies. Comparing Figure 4. *16* to Figure 4. 18, there seem to be fewer phagosomes in the cells, after a week of treatment, but those that are present are larger in size and have brighter intensity. Regarding 1D4 staining, it is almost unnoticeable in control cells, but readily visible in CQ-treated cells, indicating impairment of early phagosome processing.

Quantification of images obtained using the same conditions is shown in Figure 4. 19.

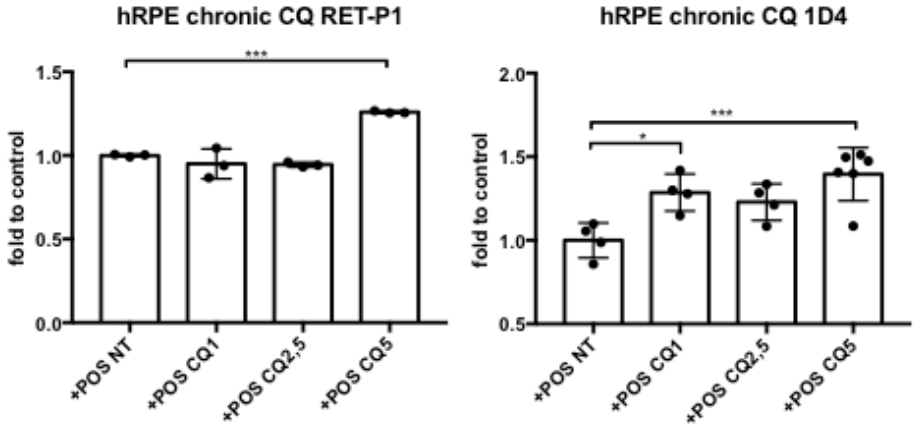

Figure 4. 19 - POS accumulate, in hESc-RPE cells, upon chronic treatment with CQ 5µg/mL. Each dot represents a different IF image's mean fluorescent integrated intensity as fold increase, compared to control (NT) cells, using anti-RET-P1 and 1D4 antibodies. Results are expressed as mean ± s.d. from independent images n≥3 (* $p<0.05$, ***$p<0.001$).

One week of CQ treatment leads to accumulation of RET-P1 and 1D4-labeled structures in hESc-RPE cells. In the case of RET-P1 staining, it also accumulates in control cells (Figure 4. 18), suggesting not all rhodopsin is processed over a 24h period, which is consistent with Figure 3.30. However, when comparing intensity of the staining, it is at similar levels to those of CQ-treated cells, for concentrations 1 and 2.5µg/mL. At 5µg/mL of CQ, however, RET-P1 staining is more intense than that found in control cells, for the same time point. Regarding 1D4 staining, results indicate that there is significantly more labeled rhodopsin, when cells are treated with CQ at 1µg/mL and at 5µg/mL. This means CQ hinders processing of early phagosomes, which remain in the cell for longer, comparing to control (NT) cells (Figure 4. 19).

Altogether, evidence obtained here suggests that rhodopsin-containing phagosomes remain within the hESc-RPE cells, rather than being promptly digested. This is true for control cells, which were not treated with CQ, indicating that POS are not completely digested overnight, accumulating as the result of repeated feedings. It could be the case that 200µg/mL of POS is a high concentration, by itself sufficient to elicit a certain degree of lysosomal dysfunction, which could worsen over time. When cells are subjected to CQ treatment, POS processing is further impaired. High doses of CQ (10 and 25µg/mL) cause rhodopsin to accumulate significantly, even in the case of an acute treatment. Although there are indications that continued CQ burden may induce lysosome biogenesis (section 4.3), it is not sufficient to clear rhodopsin-positive structures. This is substantiated by RET-

P1 staining increase, dependent on CQ concentration, at the third day of treatment (Figure 4. 16). Finally, after one week of chronic CQ burden, rhodopsin-labeled vesicles are still observed in the cells and accumulate significantly, compared to the control cells at the same time point. At this point, there is accumulation not only or RET-P1-positive vesicles, but also of 1D4-positive ones (Figure 4. 18). This suggests disturbance in early phagosome processing, which points to a more severe dysfunction.

4.5 CQ-induced Impairment of Degradative Ability

In order to convincingly assess the degradative ability of hESc-RPE cells when subjected to CQ burden, cells were given DQ Red BSA™ (DQ-BSA). This tool consists on a derivate of bovine serum albumin (BSA), labeled with a Bodipy™ dye, which is strongly self-quenched, but becomes dequenched upon breakdown by proteases. For this reason, detection of fluorescence, originating from digestion of the BSA conjugates, is commonly used to easily monitor intracellular proteolytic activity.

Degradative ability of hESc-RPE cells was assessed by incubating the cells with medium with or without POS, for 4h, followed by overnight incubation in CQ-containing medium, at increasing concentrations, to which DQ-BSA red was added. The next day, cells were collected and processed for flow cytometry (Figure 4. 20).

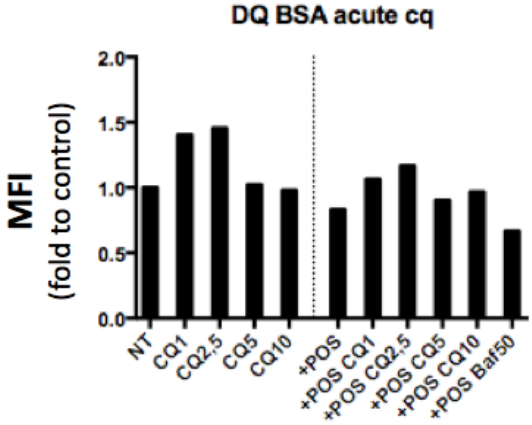

Figure 4. 20 - hESc-RPE cells proteolytic ability is not severely altered upon overnight treatment with CQ, assessed by DQ-BSA fluorescence evaluated by flow cytometry. The dashed line separates non-fed from POS-fed cells (+POS). Each column represents the Mean Fluorescence Intensity fold change, relative to NT cells. Baf at 50nM was used as a negative control. N=20.000 cells acquired for each condition represented.

Cells treated overnight with low doses of CQ alone (1µg/mL and 2.5µg/mL) produce more DQ-BSA-fluorescence than control non-treated cells. Relative mean fluorescence intensity returned to control levels at higher CQ concentrations (5 and 10µg/mL). When cells were fed POS (to the right of the dashed line), a similar effect was recorded: modest increase of DQ-BSA fluorescence for lower CQ concentrations and return to control values for higher CQ dosages. Baf was used as negative control, as it directly inhibits V-ATPase activity and effectively prevents DQ-BSA processing; for this reason, Baf-treated cells'

DQ-BSA fluorescence consists the baseline signal, below control NT cells (0.6x fold), as expected.

Overall differences whether or not cells were fed with POS were not substantial, suggesting that POS by themselves do not interfere with the cell's ability to degrade substrates (Figure 4. 20).

A closer look at the DQ-BSA distribution within the cell, by confocal microscopy, and the quantification of integrated fluorescence detected in these images allowed for a deeper analysis of this readout (Figure 4. 21).

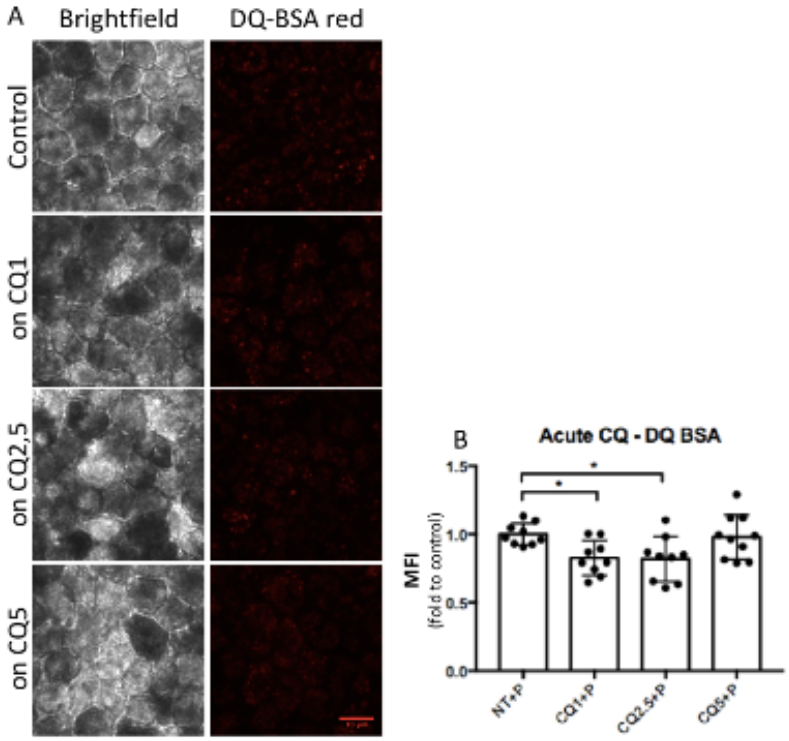

Figure 4. 21 - hESc-RPE degradative ability is not severely impaired by acute CQ treatment, assessed by DQ-BSA fluorescence evaluated by light microscopy. A: DQ-BSA distribution in a vesicular pattern, consistent with lysosomes. Scale bar 10µm. B: Quantification of representative images; each dot represents a different image's mean fluorescent integrated intensity, as compared to control (NT) cells. Results are expressed as mean ± s.d. from independent images $n \geq 9$ (*$p<0.05$).

Typical vesicular-like DQ-BSA fluorescence distribution in the cell was found, upon incubation of hESc-RPE cells, whether with or without CQ. A significant difference was found between NT and CQ-treated cells: hESc-RPE cells treated with CQ exhibit lower fluorescence intensity (Figure 4. 21).

This, however, is inconsistent with the flow cytometry analysis (Figure 4. 20). Still, in the flow cytometer, 20.000 cells were analyzed per conditions, and individually. In comparison, dozens of cells were observed together by microscopy, and the images' mean intensities were compared to the control situation. If, on the one hand, confocal images allow for the detailed visualization of size and distribution of the DQ-BSA-labeled vesicles within cells, flow cytometry should be a more reliable way of quantifying mean

fluorescence per cell. Still, CQ-induced differences were, in this case, relatively subtle, and the cells were generally able to cope.

Following the same experimental mindset as before, DQ-BSA fluorescence was also evaluated at the third day of CQ continued stimulus. Briefly, hESc-RPE cells were fed with POS for 4h and incubated overnight in CQ-containing medium, for three consecutive days. In this case of repeated CQ incubations, DQ-BSA red was added to the medium only the day before analysis, therefore representing degradative ability at that specific time point. DQ-BSA fluorescence on the third day of CQ treatment was evaluated by flow cytometry (Figure 4. 22).

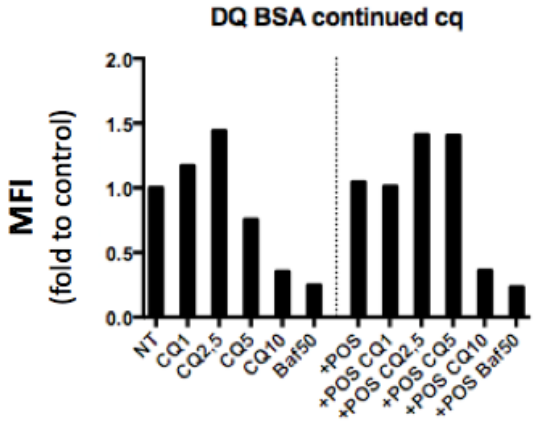

Figure 4. 22 - hESc-RPE degradative ability is compromised after continued CQ treatment, assessed by DQ-BSA fluorescence evaluated by flow cytometry. The dashed line separates non-fed from POS-fed cells (+POS). Each column represents the Mean Fluorescence Intensity fold change, relative to NT cells. Baf at 50nM was used as a control. N=20.000 cells acquired for each condition represented.

Not unlike overnight treatment, continued CQ treatment causes an increase of the mean DQ-BSA fluorescence intensity, when considering low CQ concentrations (1 and 2.5µg/mL), followed by decrease of fluorescence for higher CQ concentrations (particularly 10µg/mL), relative to NT control cells.

When cells are fed with POS, the fluorescence increase appears only when using CQ at 2.5 and 5µg/mL, decreasing drastically in the case of CQ 10µg/mL. In fact, after the third day, cells treated with CQ10 have similar fluorescence to that of Baf-treated cells, i.e. baseline values. This indicates CQ-induced substantial impairment of DQ-BSA-reported degradative ability.

Again, in order to visualize intracellular distribution of DQ-BSA, representative confocal images were acquired and quantified (Figure 4. 23).

Upon viewing the cells, it becomes obvious that DQ-BSA red fluorescence is condensed when cells are exposed to CQ. This manifests through brighter focused fluorescence found in fewer vesicles, within a cell, rather than equally distributed throughout the cell, as in the control (NT) situation (Figure 4. 23).

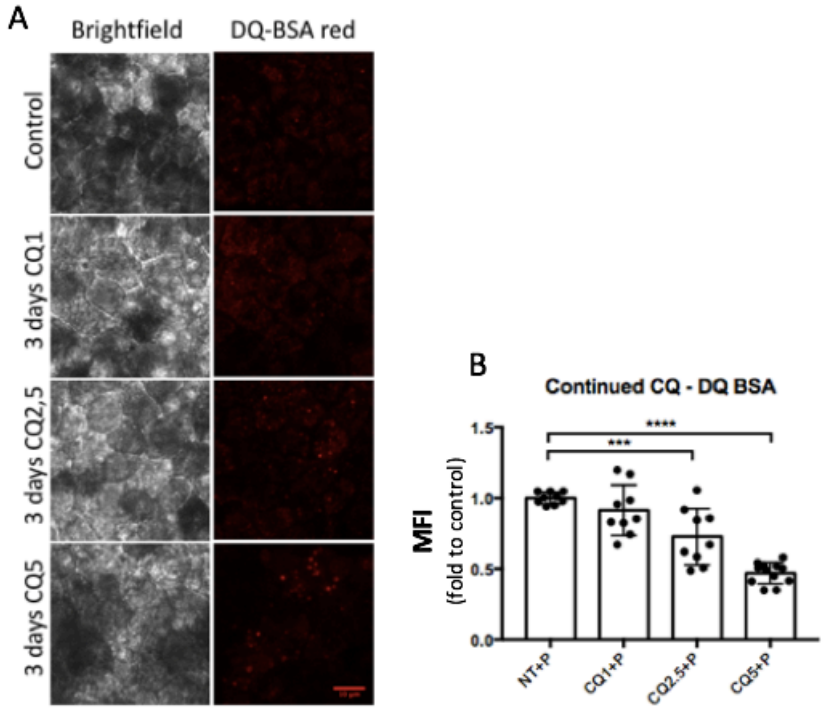

Figure 4. 23 - Continued CQ treatment impairs degradative ability of hESc-RPE cells, evaluated by light microscopy. A: DQ-BSA fluorescence distribution and accumulation upon CQ treatment. Scale bar 10µm. B: DQ-BSA fluorescence quantification for each condition, with each dot representing a different image's mean fluorescent integrated intensity, and compared to control (NT) cells. Results are expressed as mean ± s.d. from independent images n≥9 (***p<0.001; ****p<0.0001).

Confocal images illustrate the general decrease of fluorescence, inversely proportional to the CQ concentration increase. A significant difference in mean fluorescence intensity was obtained for cells treated with 2.5 and 5µg/mL CQ for three days (Figure 4. 23).

Once more, hESc-RPE were subjected to a week-long treatment of CQ at the different concentrations through overnight incubation, for seven consecutive days. DQ-BSA fluorescence was evaluated at the seventh day of CQ chronic stimulus by flow cytometry (Figure 4. 24).

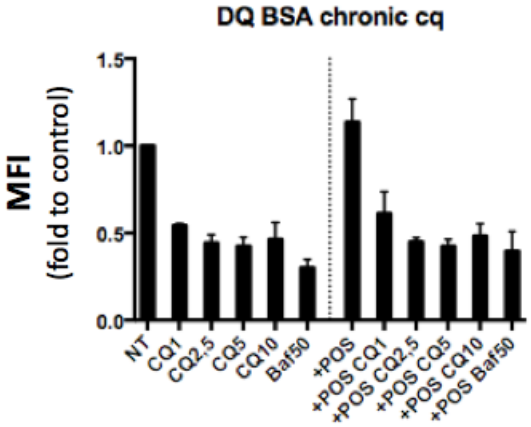

Figure 4. 24 - Chronic CQ treatment impairs degradative ability of hESc-RPE cells, assessed by DQ-BSA fluorescence evaluated by flow cytometry. The dashed line separates non-fed from POS-fed cells (+POS). Each column represents the Mean Fluorescence Intensity fold change, relative to NT cells. Baf at 50nM was used as a control. n=20.000 cells acquired for each condition. Results are expressed as mean ± s.d. from two independent experiments. All drug treatments show significant differences, compared to control p<0.0001.

Chronic exposure to CQ disturbs the degradative ability of hESc-RPE cells, as evaluated by DQ-BSA fluorescence. In accordance with what was expected, given the POS degradation assays, the cells' ability to process cargo through lysosomal degradation is impaired after one week of CQ treatment. As such, all CQ-treated cells show a significantly lower mean fluorescence intensity ($p<0.0001$), as compared to control NT cells. Fluorescence levels found in CQ-treated cells were similar to those of negative control cells which were treated with Baf (Figure 4. 24).

Fluorescence microscopy images of hESc-RPE cells treated chronically with CQ are represented in Figure 4. 25.

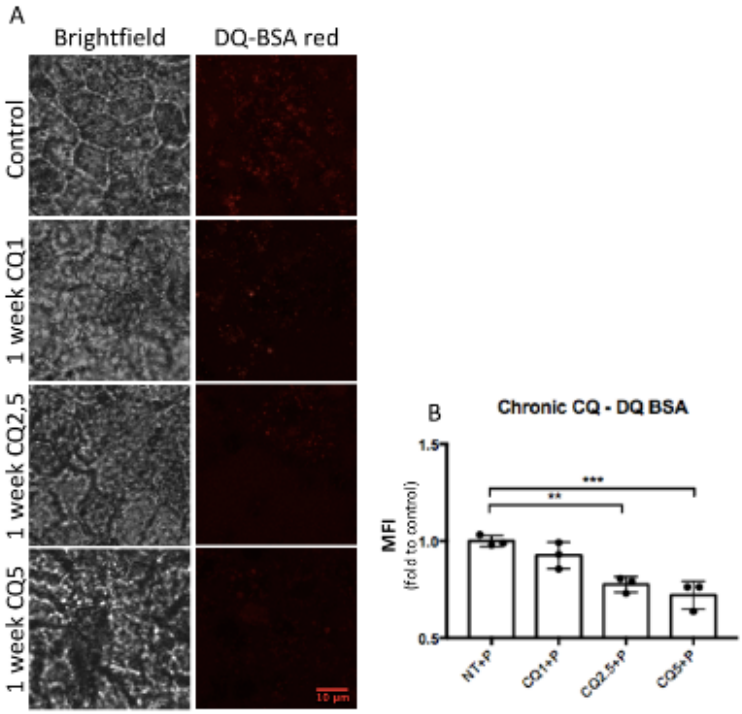

Figure 4. 25 - Chronic CQ treatment severely impairs degradative ability of hESc-RPE, evaluated by light microscopy. A: DQ-BSA fluorescence distribution and accumulation upon CQ treatment, shown in representative images. Scale bar 10µm. B: Fluorescence quantification indicates decrease of proteolytic activity. Each dot represents a different image's mean fluorescent integrated intensity, compared to control (NT) cells. Results are expressed as mean ± s.d. from independent images n≥3 (**p<0.01; ***p<0.001).

Quantification of the images is consistent with findings from flow cytometry: a reduction of DQ-BSA red fluorescence suggests impaired degradative ability of hESc-RPEs' lysosomes upon chronic CQ treatment.

Overnight treatment with CQ did not induce substantial differences in total DQ-BSA fluorescence found in the cells (Figure 4. 20, Figure 4. 21). This suggests that uptake is not impaired by CQ treatment and that the overnight DQ-BSA pulse allows for a bright detection, without significant fluorescence loss over time. Nevertheless, when pondering these results, it is important to keep an open mind and contemplate all the experimental variables and limitations.

It is conceivable that chronic lysosomal dysfunction may disturb cellular functions at a deeper level and end up unsettling overall endocytic function. For this reason, the possibility of lower detection levels as the result of fewer uptake of the dye should not be excluded. Still, considering all evidence from these experiments, taken together with previous results regarding POS accumulation, it is reasonable to assume there is in fact a cargo degradation impairment rather than intake deficiency.

As for the negative control, Baf is very efficient, though the concentration used was relatively low. In fact, 200nM were shown to effectively block lysosome activity, assessed through DQ-BSA fluorescence, Magic Red™ and Lysotracker® signals (data not shown). However, in this case, Baf was used at 50nM, and for this reason, complete ablation of the signal was not achieved in the acute treatment. When similar experiments were performed, using higher concentrations, hESc-RPE cells died, after the third day of Baf 200nM incubation. As such, in an effort to maintain similar conditions at the three time points chosen, a lower dose was used.

A potential limitation of using fluorescently-labeled dyes is related to the fact these cells are pigmented. Melanin may quench the fluorescence, meaning heavily pigmented cells may present weaker signal. As previously discussed, CQ-treated cells and Baf-treated cells become darker. This may be the result of MiT TFs regulation, which also manage melanosome biogenesis and processing (Bharti et al. 2006; Napolitano & Ballabio 2016). To circumvent this aspect, an effort was made to depict cells presenting similar pigmentation levels. This, however is a subjective assessment, as pigmentation levels were not effectively quantified. Still, and consistent with previous rhodopsin stainings increase (rather than pigment-quenching), DQ-BSA findings were found to support lysosomal dysfunction settings.

In an effort to clarify how the hESc-RPE's proteolytic activity is affected, the function of lysosomal Cathepsins was evaluated next.

4.6 CQ stimulates Cathepsin B and L proteolytic activity

A straightforward way of detecting Cathepsin activity is to use Magic Red™ reagent, which consists on a membrane permeable non-toxic substrate that emits red fluorescence upon cleavage by active Cathepsins. The substrate concerned, in this case, comprises two Cathepsin target peptide sequences and, when coupled to cresyl violet, it precludes its fluorescence. This substrate may be directly added to the cell culture medium and freely permeates membranes (plasma membrane and organelles). Upon enzymatic cleavage at one or both peptides, mono or non-substituted cresyl violet fluorophores produce fluorescence when excited at 550-590nm. Because Cathepsins are active within acidic organelles, Magic Red™ is expected to fluoresce at the lysosomes. And since the peptides coupled to the fluorophore are tailored, in this case, for Cathepsin B or Cathepsin L preferential targeting, fluorescence is expected to reflect these enzymes' activity directly.

Cells were treated with medium either without or with POS, for 4h, followed by overnight incubation in medium containing increasing concentrations of CQ, from 1-10µg/mL. The V-ATPase inhibitor Baf was used as negative control. As before, fluorescence was measured by flow cytometry and fluorescence microscopy images were obtained, in order to assess cellular distribution pattern of the dyes (Figure 4. 26, Figure 4. 27).

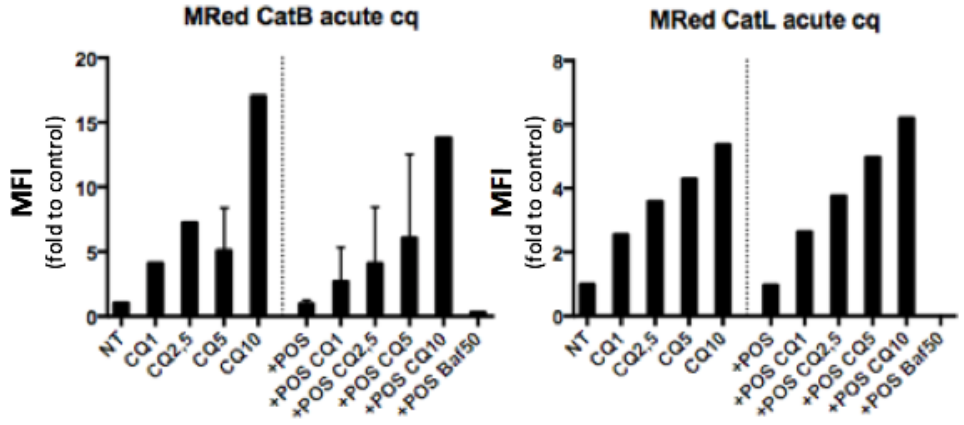

Figure 4. 26 - Acute CQ treatment causes increase of Cat B and L activity, assessed by Magic Red™ fluorescence evaluated by flow cytometry. The dashed line separates non-fed from POS-fed (+POS) cells. Each column represents the Mean Fluorescence Intensity fold change, relative to NT cells. Baf at 50nM was used as negative control. n=20.000 cells acquired for each condition Results are expressed as mean ± s.d. from independent experiments (two for CatB, one for CatL).

Both graphs depict a direct correlation between increase of CQ concentration and Magic Red™ fluorescence fold increase, relative to control NT cells. Addition of POS alone does not have a significant effect on Cathepsins B or L activities. Instead, the fluorescence gain seems to be a direct result from CQ treatment. Surprisingly, rather than impairing Cathepsin activity, CQ appears to boost it, upon acute overnight treatment. Baf, on the contrary, completely extinguished Magic Red™ signal, in both cases, effectively serving as negative control (Figure 4. 26).

Representative images showing CatB substrate-derived fluorescence is shown in Figure 4. 27.

hESc-RPE cells display Magic Red™ fluorescence with a vesicular pattern, assumedly representing the active lysosomal population. The cellular active lysosomal content is increased, upon CQ treatment, observed as more fluorescent vesicles, distributed inside the cells. The nuclear area is spared from the dye, suggesting specific localization to the endocytic compartments. Alike the flow cytometry results, cells show increased Magic Red™ fluorescence, in proportion to CQ concentration rise (Figure 4. 27).

Image quantification further confirms results obtained by flow cytometry: Cathepsin B activity produces fluorescence in proportion to CQ concentration, suggesting increased proteolytic activity (Figure 4. 26 and Figure 4. 27).

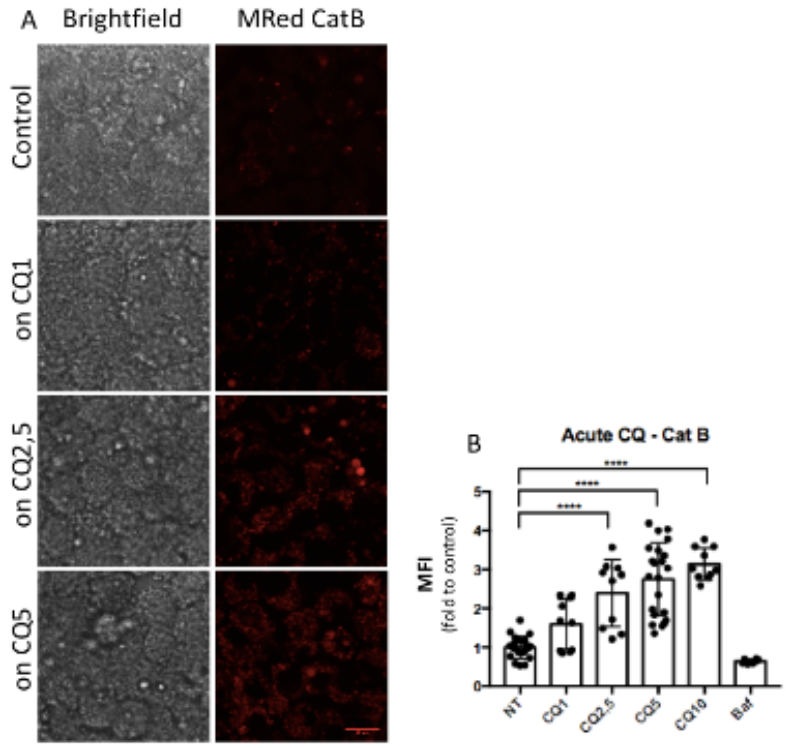

Figure 4. 27 - CatB activity increases upon acute CQ treatment of hESc-RPE cells, evaluated by Magic Red™ fluorescence, assessed by light microscopy. A: Representative images showing the dye's distribution in a vesicular pattern, consistent with lysosomes. Scale bar 10µm. B: Quantification of fluorescence mean integrated intensity of representative images. Each dot represents a different image's mean fluorescent integrated intensity, compared to control (NT) cells. Results are expressed as mean ± s.d. from independent experiments, n≥6 (****p<0.0001).

Following the protocol previously described for continued CQ treatment, cells were fed POS and treated with CQ overnight, for three consecutive days. Flow cytometry results report Cathepsins B and L activity, measured as Magic Red™ fluorescence (Figure 4. 28).

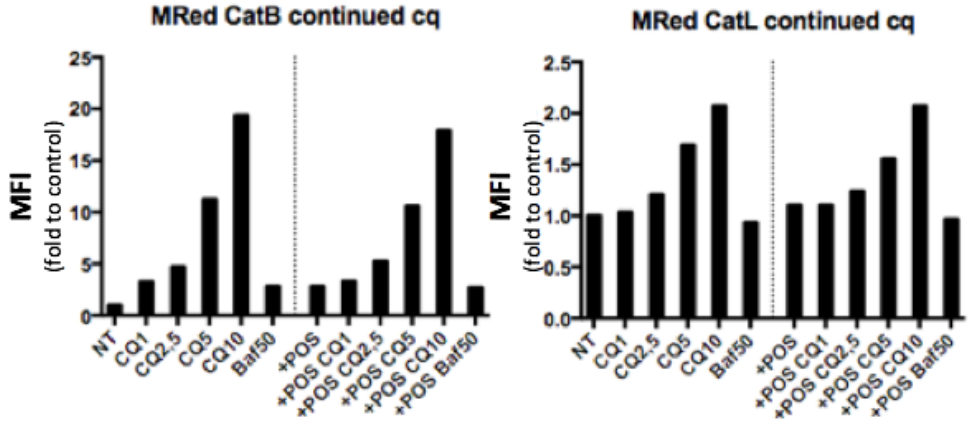

Figure 4. 28 - Continued CQ treatment induces CatB and CatL activity, assessed by Magic Red™ fluorescence evaluated by flow cytometry. The dashed line separates non-fed from POS-fed cells. Each column represents the Mean Fluorescence Intensity fold change, relative to NT cells. Baf at 50nM was used as negative control. n=20.000 cells acquired for each condition represented.

Continuous CQ-treatment leads to consistent increase of Cathepsins' B and L activity, compared to control non-treated cells. Again, this effect is independent of POS feeding,

occurring whether or not the cells were fed. Interestingly, in the case of Cathepsin L, Baf treatment does not produce the expected reduction of activity to baseline levels (Figure 4. 28). The systematic increase of Cathepsin activity resulting from CQ burden is unexpected, but could mean these enzymes are pH permissive or that their expression is stimulated.

Cellular distribution pattern of the Magic Red™ fluorescence was assessed by microscopy images and quantified (Figure 4. 29).

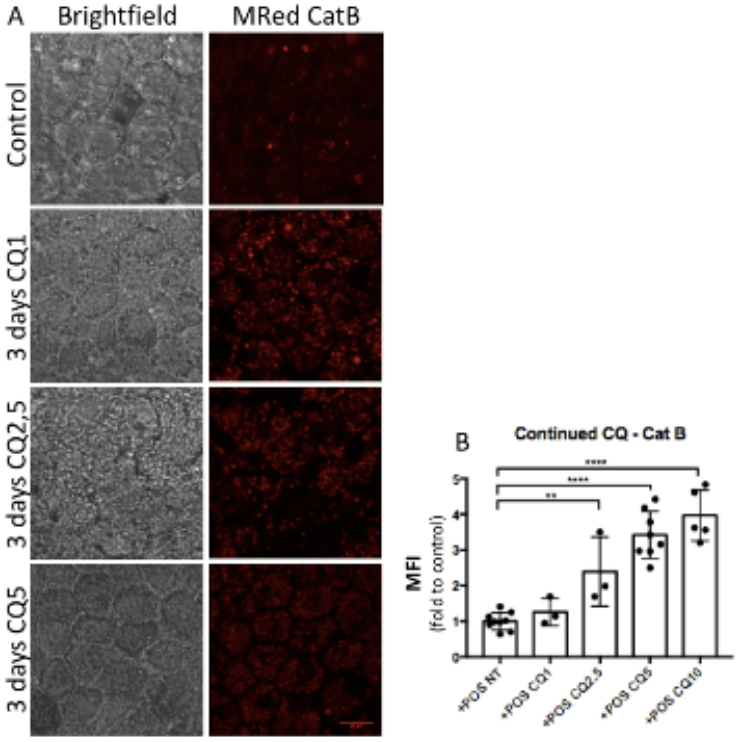

Figure 4. 29 - Continued CQ treatment alters cellular distribution of CatB activity in hESc-RPE cells, evaluated by Magic Red™ fluorescence microscopy. A: Distribution of the dye, spreading throughout the cell, upon CQ treatment. Scale bar 10µm. B: Fluorescence quantification for each condition, with each dot representing a different image's mean fluorescent integrated intensity, and compared to control (NT) cells. Results are expressed as mean ± s.d. from independent images n≥3 (**p<0.01; ****p<0.0001).

Cathepsin B and L effectively degraded their respective substrates, thus giving rise to fluorescence. Cathepsin B-related fluorescence appears in a vesicular pattern, consistent with lysosomes and other acidic endocytic vesicles. This fluorescence increases upon CQ treatment, in a dose-dependent manner. Image quantification is consistent with flow cytometry findings, conveying a consistent intensification, in proportion to the rise in CQ concentration (Figure 4. 28 and Figure 4. 29).

In order to evaluate the chronic effects of CQ burden in hESc-RPE's Cathepsin activity, the same experimental approach used before was put in place: cells were fed POS for 4h, followed by overnight incubation with increasing CQ concentrations, for seven consecutive days. Following the seventh day's overnight incubation, cells were given Magic Red™ Cathepsin B or L and prepared for flow cytometry analysis (Figure 4. 30).

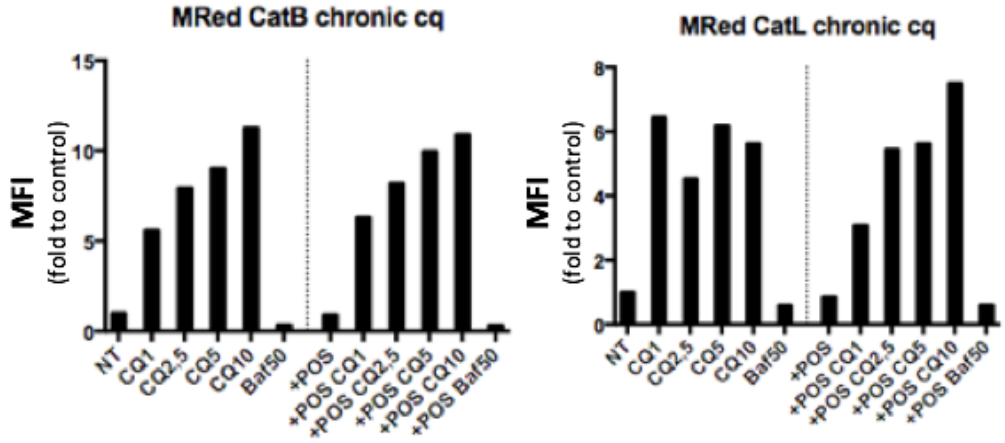

Figure 4. 30 - Chronic CQ burden induces CatB and CatL activity in hESc-RPE cells, assessed by Magic Red™ fluorescence evaluated by flow cytometry. The dashed line separates non-fed from POS-fed cells. Each column represents the Mean Fluorescence Intensity fold change, relative to NT cells. Baf at 50nM was used as negative control. n=20.000 cells acquired for each condition represented.

Similarly to the acute and continuous treatments, chronic CQ burden produces increased Magic Red™ fluorescence, compared to control situation, suggesting increased activity both of Cathepsin B and L. On the contrary, long-term treatment of these cells with Baf returns very low levels of fluorescence, indicating few Cathepsin-active compartments, as would be expected (Figure 4. 30).

Surprisingly, Magic Red™ fluorescence implies an increase of Cathepsins' B and L activities, rather than the expected decrease, upon CQ treatment. This constant surge in fluorescence, proportionally to CQ concentration rise is rather puzzling. It may be interpreted as a compensatory mechanism, which partially allows the cell to process cargo (POS or DQ-BSA), despite CQ. In addition, Cathepsins B and L have been described to be active within a relatively high range of pH (Turk et al. 1997). For this reason, it is possible that CQ-induced pH increase is not sufficient to inhibit these Cathepsins activity. On the other hand, overnight treatment with CQ was shown sufficient to induce TFEB, TFE3 and MITF nuclear translocation, which potentiates lysosomal biogenesis, as discussed previously. Therefore, there might be a stimulation of Cathepsin B and L expression and hence activity.

Another potential caveat of using Magic Red™ reagents is that the red fluorophore accumulates overtime and may accumulate not only in lysosomes, but also in other areas of low pH, such as mitochondria (ImmunoChemistryTechnologies 2002). Nevertheless, a substantial degree of specificity is expected from this assay, thus Magic Red™ fluorescence was considered as an appropriate read-out to measure lysosomal cysteine protease activity, though results should always be kept in context.

4.7 CQ-induced disturbance of Cathepsin D activity and expression

Cathepsin D (CatD) is the only aspartic-type protease ubiquitously expressed in all the cells of the human body, and it is present at high level in the retina and brain (Rakoczy et

al. 1997). CatD is a soluble lysosomal enzyme, which is synthesized in the rough endoplasmic reticulum as preproCathepsin D. PreproCathepsin D is processed into the proCathepsin D form (52 kDa) and targeted to endosomes, phagosomes and lysosomes. ProCathepsin is cleaved, when in the acidic lysosomal lumen. This cleavage gives rise to a 48 kDa intermediate form and further proteolytic processing originates the final mature form: the globular structure of CatD, composed of a heavy (34 kDa) and a light (14 kDa) chains non-covalently linked(Benes et al. 2008; Laurent-Matha et al. 2006) (Figure 4. 31).

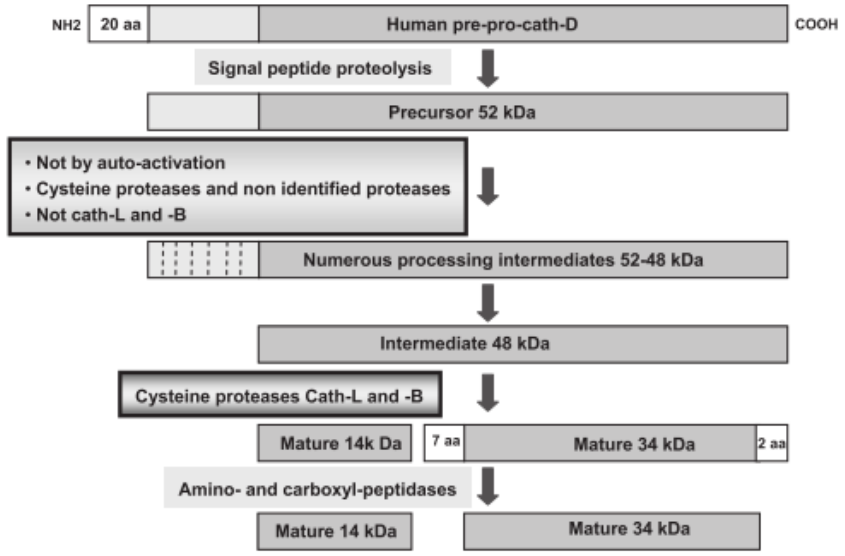

Figure 4. 31 - Representation of the human CatD processing steps, from pre-pro-enzyme up to the mature active form. Image from (Laurent-Matha et al. 2006).

CatD is responsible for the degradation of unfolded or oxidized protein aggregates, delivered to lysosomes via autophagy or endocytosis. In addition, it is an important player in rhodopsin proteolysis (Rakoczy et al. 1997). For this reason, its activity and levels of expression were evaluated in the proposed experimental settings. In particular, Pepstatin A, Bodipy™ FL reagent was used to evaluate CatD activity. To obtain this reporter, pepstatin A was covalently conjugated with Bodipy™ fluorophore. The resulting commercially available product is able to selectively bind to the protease at low pH and thus stains CatD active lysosomes (Chen et al. 2000). This probe competes with other CatD substrates and therefore inhibits this enzyme's activity. Still, since the tool was used immediately before acquiring the signal, rather that exposing the cells to a continued treatment, consequently it is considered here as a reliable readout of that moment's active enzyme.

Additionally, CatD protein levels were evaluated by Western Blot, in the different experimental conditions tested, as before. Using this technique, it is possible to compare total amount of CatD in the cell lysates obtained in each of the settings and also to study the ratio of mature (lower molecular weight) and proCathepsin forms (higher molecular weight).

hESc-RPE were fed with POS for 4h, after which cells were incubated overnight in CQ-containing medium, with concentrations ranging from 1 to 10 µg/mL. The next day, Bodipy™ FL was added to the medium and cells were prepared for flow cytometry analysis, as described in the Materials and Methods section (Figure 4. 32).

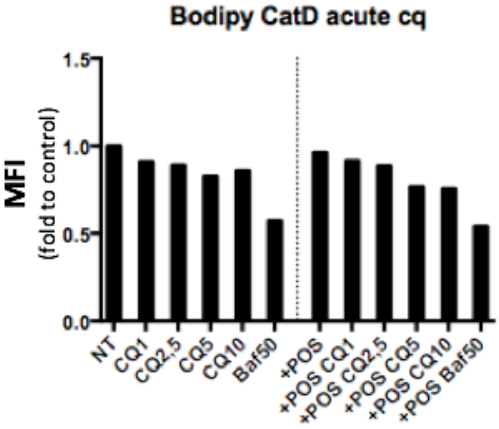

Figure 4. 32 - Acute CQ treatment leads to decreased CatD activity in hESc-RPE cells, assessed by Bodipy™ fluorescence evaluated by flow cytometry. The dashed line separates non-fed from POS-fed cells. Each column represents the Mean Fluorescence Intensity fold change, relative to NT cells. Baf at 50nM was used as negative control. n=20.000 cells acquired for each condition.

Active CatD, adjudicated as Bodipy™ fluorescence, is decreased upon CQ treatment. In particular, the reduction of active CatD, varies opposed to CQ concentration. Baf was used as negative control, decreasing CatD activity to half, relative to control non-treated cells, considered as baseline. Feeding the cells with POS does not produce significant changes in cat D activity patterns, comparing to the non-fed situation (Figure 4. 32).

Moreover, CatD protein levels were evaluated resorting to Western Blot, using the same conditions as previously described (Figure 4. 33).

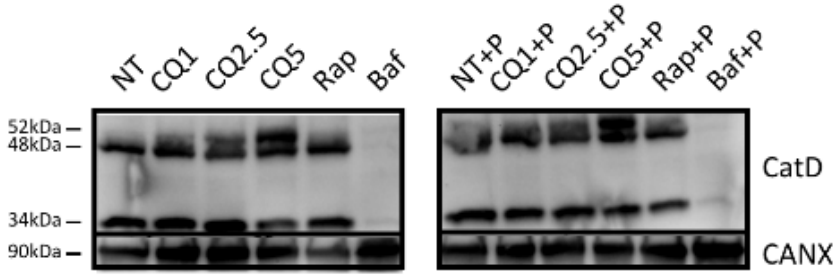

Figure 4. 33 - CatD protein profile is altered by CQ acute treatment of hESc-RPE. Western Blot using anti-CatD antibody shows immature (52 and 48kDa, upper bands) and mature (34kDa, bottom bands) forms of this Cathepsin. Rap and Baf were used as positive and negative controls, respectively. +P: POS-fed cells. Calnexin was used as loading control. A representative result is shown from three independent experiments.

The first thing to notice is the strong effect Baf has over this enzyme, effectively depleting the cells of proCathepsin and leaving trace amounts of mature CatD. Secondly, comparing non-fed with POS-fed cells (+P), the blots are very similar, thus the lysosomal cargo itself does not seem to produce an effect. Strikingly, as CQ concentrations increase, a band becomes visible at approximately 52 kDa, corresponding to the proCathepsin form.

The mature (34kDa) form, on the other hand, seems slightly reduced at CQ5, compared to the control (Figure 4. 33).

In order to assess total CatD, bands were quantified and the respective graph is represented in Figure 4. 34.

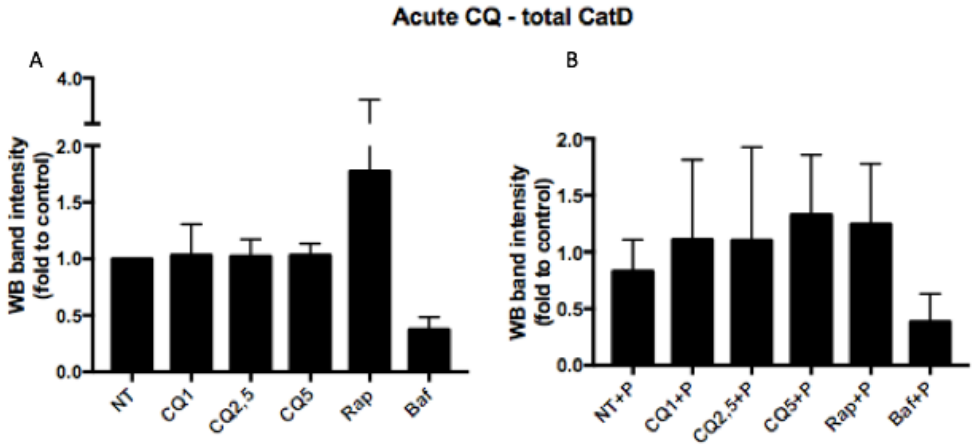

Figure 4. 34 - CatD total amounts are not altered upon acute CQ treatment of hESc-RPE. Western Blot relative quantification of bands represents total CatD, per condition. A: cells treated with CQ alone. B: CQ treatment after POS feeding (+P). Rap and Baf were used as positive and negative controls, respectively. Band intensity was normalized according to the loading control. Results are expressed as mean ± s.d. from independent experiments, n=3.

By observing the quantification of total CatD, as evaluated by Western Blot, it is possible to confirm that Rap induced CatD expression, while Baf effectively inhibited it, as predicted. CQ does not produce a significant effect on Cathepsin total amounts, in unfed cells. POS-fed cells, however, when treated with CQ, exhibit a slight increase of CatD total amounts (Figure 4. 34). Next, the ratio between mature and immature CatD forms was pondered and the graph the obtained data is presented in Figure 4. 35.

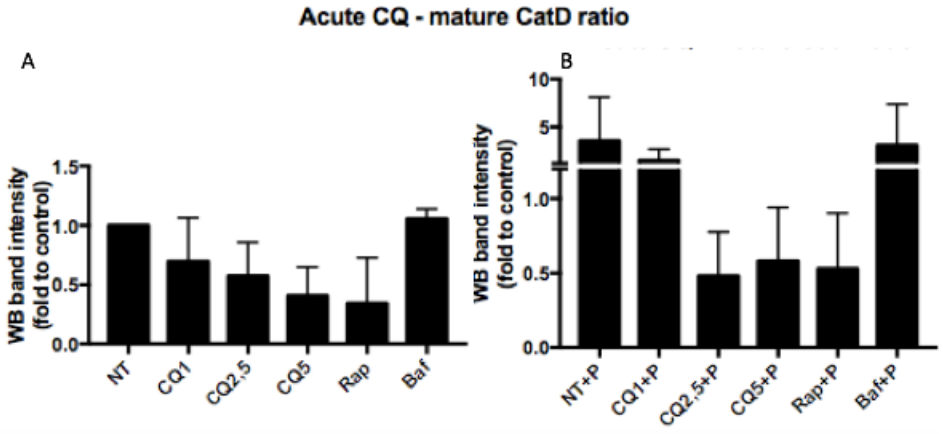

Figure 4. 35 - The ratio of mature/immature CatD is altered upon acute CQ treatment of hESc-RPE. Ratio between mature (34kDa) and immature forms (48 and 52kDa) of CatD was obtained from Western Blot relative quantification. A: cells treated with CQ alone. B: CQ treatment after POS feeding (+P). Rap and Baf were used as positive and negative controls, respectively. Band intensity was normalized according to the loading control. Results are expressed as mean ± s.d. from independent experiments, n=3.

A decrease of the mature form, relative to immature forms of CatD, directly correlated with an increase of CQ concentration is observed. This is true for cells that were not POS-

fed. Regarding POS-fed cells, there is relatively more mature catD in the POS-fed control (NT+P) and CQ1+P cells, relative to non-treated, unfed cells (NT) (Figure 4. 35). Considering the previous graph, this increase in mature CatD form occurs at the expense of the immature forms, as total levels remain unchanged (Figure 4. 34). As CQ concentration increases, the mature form of Cathepsin is reduced, while immature forms increase. As depicted in Figure 4. 33, Baf causes the immature forms to vanish and the mature forms to fade away, and for this reason, the ratio seems so elevated. As for Rap, considering the total amount increase in this case (Figure 4. 34), the low value for mature/immature CatD means there is more immature CatD than mature (Figure 4. 35). Therefore, it is possible to conclude: Baf causes a strong reduction of both forms of CatD; Rap leads to an increase of the total amount and especially the immature form, indicating biogenesis; CQ causes an increase of the immature forms, at the expense of mature CatD. Since, in the case of unfed cells there is no increase in the total amount, it means proCathepsin is not being processed into the mature form (up to 0.5x fold difference, relative to control) (Figure 4. 35); in the case of POS-fed cells, there can also be biogenesis, but still there is reduction of functional enzyme (up to 10x fold, relative to POS-fed control) (Figure 4. 35).

For the continued treatment, hESc-RPE were fed with POS and subsequently incubated overnight in CQ-containing medium, for three consecutive days. After the third day, Bodipy™ FL was added to the medium and cells were prepared for flow cytometry analysis (Figure 4. 36).

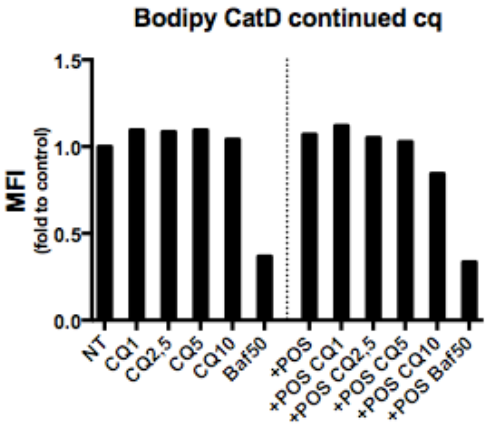

Figure 4. 36 - Continued CQ treatment does not alter CatD activity in hESc-RPE cells, assessed by Bodipy™ fluorescence evaluated by flow cytometry. The dashed line separates non-fed from POS-fed cells. Each column represents the Mean Fluorescence Intensity fold change, relative to NT cells. Baf at 50nM was used as negative control. n=20.000 cells acquired for each condition.

Again, Baf is able to abolish Bodipy^{TM} fluorescence, meaning it blocks CatD activity, as expected. CQ does not produce a strong apparent effect on CatD activity, in the case of unfed cells. In POS-fed cells there is a 15% reduction in CatD-derived fluorescence, at 10µg/mL CQ (Figure 4. 36).

Western Blot permitted the evaluation of relative protein amounts (Figure 4. 37).

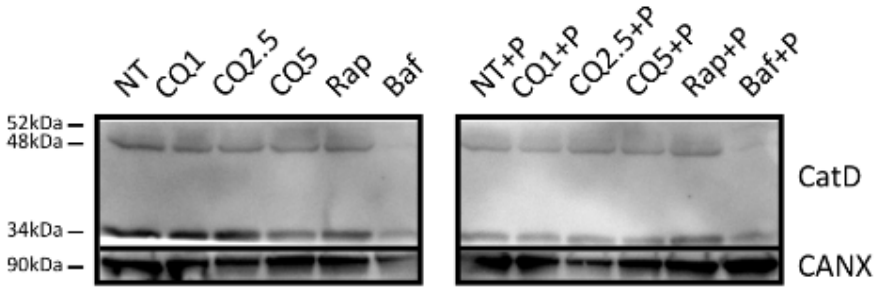

Figure 4. 37 - Continued CQ treatment does not change CatD protein profile in hESc-RPE cells. Western Blot using anti-CatD antibody shows mature (34kDa) and immature (48 and 52kDa) forms of this Cathepsin. Rap and Baf were used as positive and negative controls, respectively. +P: POS-fed cells. Calnexin was used as loading control. A representative result is shown from at least two independent experiments.

Similarly to the previous experimental setup Figure 4. 33, there seems to be a slight reduction of the mature form of CatD in CQ5-treatment, compared to control NT cells. Baf effectively reduced both immature and mature forms of CatD and Rap caused a slight increase of the immature proCathepsin (more readily visible in the POS-fed situation) (Figure 4. 37). Relative quantification of the bands was ensued, and the respective graphic representation is presented in Figure 4. 38.

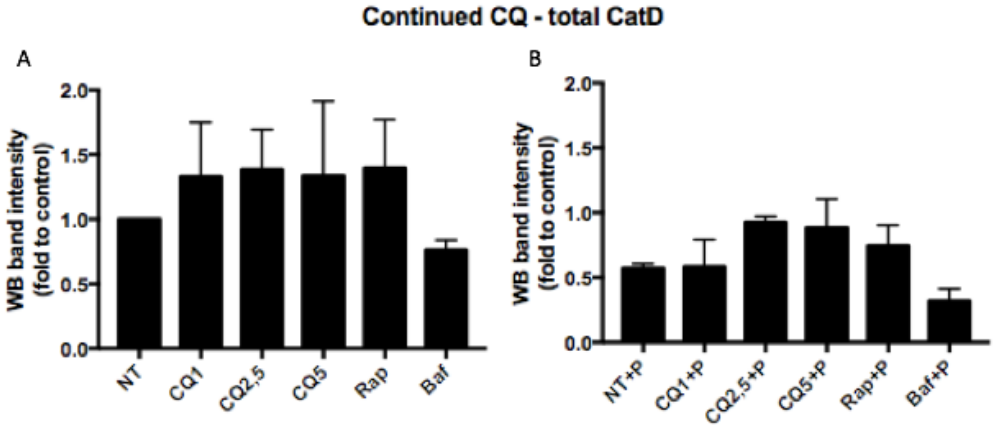

Figure 4. 38 - Continued CQ treatment causes a slight increase of total CatD in hESc-RPE cells. Western Blot relative quantification of bands represents total CatD, per condition. A: cells treated with CQ alone. B: CQ treatment after POS feeding (+P). Rap and Baf were used as positive and negative controls, respectively. Band intensity was normalized according to the loading control. +P: POS-fed cells. Results are expressed as mean ± s.d. from independent experiments, n=2.

Quantification of Western Blot bands suggests a general increase of the total CatD amount, induced by CQ treatment (except in the POS-fed CQ1 condition) and Rap. Baf causes a reduction of total CatD (Figure 4. 38). The ratio between mature and proCathepsin forms is presented in Figure 4. 39.

Taking into account the Western Blot image and quantification of the total CatD (Figure 4. 37 and Figure 4. 38), it is possible to verify that despite increase of the total CatD, the proCathepsin is more abundant than the mature form.

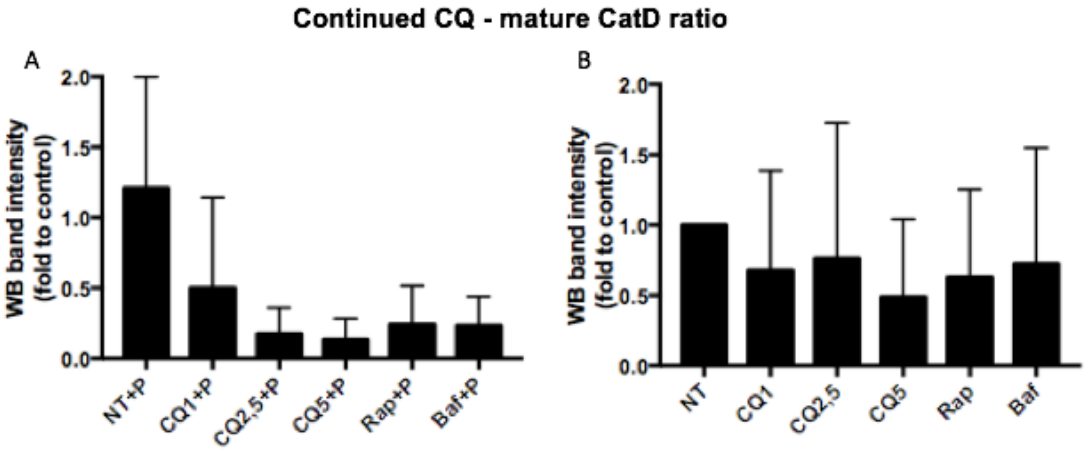

Figure 4. 39 - CatD ratio is altered upon CQ continued treatment of hESc-RPE cells. Ratio between mature (34kDa) and immature forms (48 and 52kDa) of CatD was obtained from Western Blot relative quantification. A: cells treated with CQ alone. B: CQ treatment after POS feeding (+P). Rap and Baf were used as positive and negative controls, respectively. Band intensity was normalized according to the loading control. Results are expressed as mean ± s.d. from independent experiments, n=2.

This is shown by the relative decrease of the ratio (34 kDa/ 48 and 52 kDa forms), compared to control NT cells (Figure 4. 39). In POS-fed cells, this effect is stronger, in fact, although there is more total CatD, CQ5-treated cells have lower levels of the mature CatD form than Baf-treated cells (Figure 4. 38 and Figure 4. 39). Together these data suggest that CQ leads to biogenesis of Cathepsin (total CatD increase), but failed processing and maturation into the active form.

The same treatment was repeated for seven consecutive days, as described in previous sections, in an effort to recapitulate the chronic CQ-burden situation. In some of these experiments, hESc-RPE were analyzed in parallel to Lonza hRPE cells. After the seventh day of POS feeding and overnight CQ treatment, Bodipy™ FL was added to the medium and cells were prepared for flow cytometry analysis (Figure 4. 40).

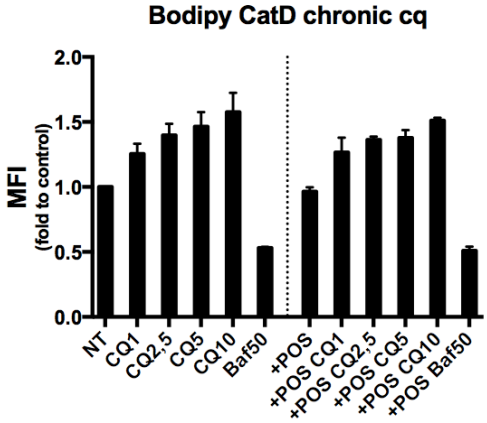

Figure 4. 40 - CatD's activity is increased by chronic CQ treatment of hESc-RPE cells, assessed by Bodipy™ fluorescence evaluated by flow cytometry. The dashed line separates non-fed from POS-fed cells. Each column represents the Mean Fluorescence Intensity fold change, relative to NT cells. Baf at 50nM was used as a control. n=20.000 cells acquired for each condition. Results are expressed as mean ± s.d. from two independent experiments.

Following seven consecutive days of treatment with CQ, hESc-RPE cells react by increasing CatD activity. This increase occurs whether or not cells were fed with POS, indicating a direct correlation with CQ, rather than POS feedings (Figure 4. 40). In addition, the active CatD seems to increase in proportion to CQ concentration. Baf establishes the baseline, corresponding to inactive CatD. Using the anti-CatD antibody, Western Blots were produced, in order to visualize the forms of CatD being expressed (Figure 4. 41).

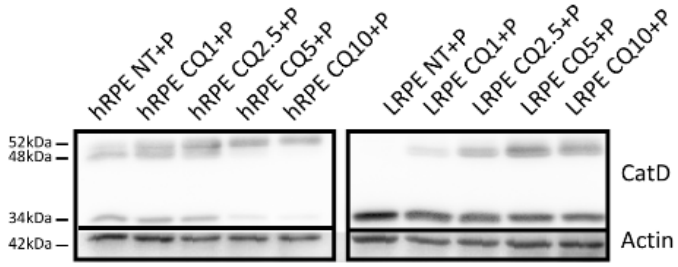

Figure 4. 41 - Chronic CQ treatment alters CatD protein profile in both hESc-RPE (hRPE) and Lonza hRPE (LRPE). Western Blot using anti-CatD antibody shows mature (34kDa) and immature (48 and 52kDa) forms of this Cathepsin. Actin was used as loading control. +P: POS-fed cells. A representative result is shown from at least two independent experiments.

Results show a striking increase of the proCathepsin immature forms is striking in the images above: as CQ concentration increases, so does the higher molecular weight forms of CatD. In the case of hESc-RPE, on the left, this increase is of the 52 kDa forms, with decrease of both the 48 kDa forms and the mature 34 kDa forms. In the case of Lonza hRPE, on the right, there is also a reduction of the mature form of CatD, compared to non-treated NT cells. However, in this case, the mature form remains at sufficient amounts to produce a clearly visible band, as opposed to the hESc-RPE case, in which the mature form almost vanishes (Figure 4. 41). This might indicate an extended half-life of this protein in Lonza hRPE. An alternative would be to consider there is still significant cleavage of proCathepsin into mature CatD form. In order to confirm these observations, quantification of representative blots was preformed (Figure 4. 42).

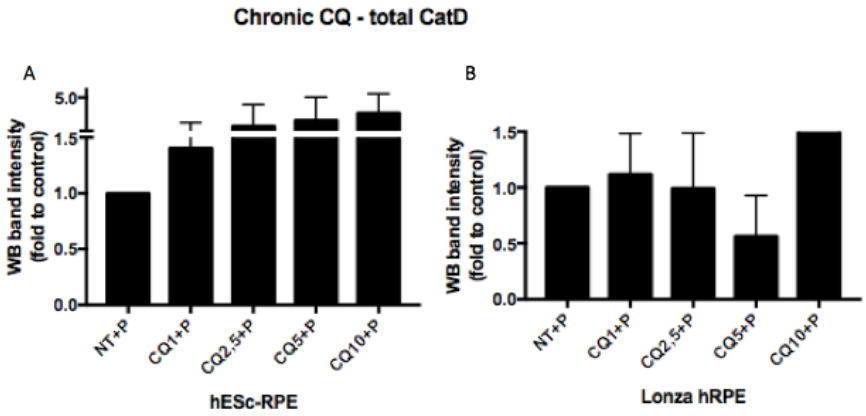

Figure 4. 42 - Total CatD is increased by CQ chronic treatment. hESc-RPE cells (A) and Lonza hRPE (B) total Cat D was quantified based on Western Blot images. Band intensity was normalized according to the loading control. +P: POS-fed cells. Results are expressed as mean ± s.d. from independent experiments, n≥3, except CQ10 (n=2).

Western Blot quantification suggests increase of total CatD after chronic CQ treatment. In the case of hESc-RPE, this increase is in proportion to CQ concentration increase. In the case of Lonza hRPE cells, the total CatD was only found to be increased when using CQ at 10µg/mL and in fact might be reduced, in the case of CQ 5µg/mL (Figure 4. 42). This suggests the reason why the mature form was kept visible in the blot is related to an extended CatD half-life, and not to proCathepsin turnover (Figure 4. 41). This is, however, a preliminary observation, which should be confirmed by repeated experiments and statistical analysis, to confirm significance. Next, the ratio between mature and immature CatD forms was evaluated (Figure 4. 43).

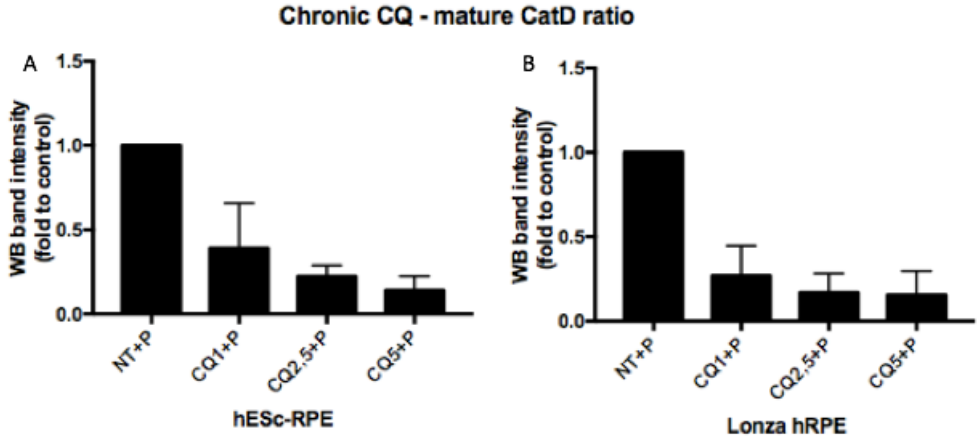

Figure 4. 43 - CatD ratio is severely altered by chronic CQ treatment, of hESc-RPE cells (A) and Lonza hRPE (B). Ratio between mature (34kDa) and immature forms (48 and 52kDa) of CatD was obtained from Western Blot relative quantification. Band intensity was normalized according to the loading control. +P: POS-fed cells. Results are expressed as mean ± s.d. from independent experiments, n≥3.

Considering the previous graph indicated increase of total CatD (Figure 4. 42), the relative decrease of the mature form, at the expenses of the proCathepsin form is implied here, by this graph (Figure 4. 43). In fact, in both hESc-RPE and Lonza hRPE there is a dramatic reduction of the ratio between mature and immature forms of CatD, according to the increase in CQ concentration (Figure 4. 43).

Together the presented data suggest that although activity is increased slightly (according to Bodipy™ FL flow cytometry analysis - Figure 4. 40), the CatD maturation step is hindered. A chronic CQ burden instigates CatD biogenesis, with increase of total CatD, readily noticeable in hESc-RPE, although not so clear in Lonza hRPE (Figure 4. 42). CatD biogenesis could account for the increased activity detected by flow cytometry. Still, because CatD maturation is impaired, there is more proCathepsin than mature Cathepsin, compared to controls (Figure 4. 43).

There seems to be a time-frame dependent response. An acute overnight CQ treatment causes reduction of the activity, possibly by hampering CatD maturation (Figure 4. 32). Immediately the cell responds with new proCathepsin (Figure 4. 33). After the third day of insult, the cells are able to return to the levels of activity found in control non-treated cells, except for the highest CQ concentration, in POS-fed situation (Figure 4. 36). This is achieved in spite of an unbalanced mature/immature CatD ratio, which possibly means that

the active CatD is overcompensating for the lower amounts (Figure 4. 39). On the other hand, since there is overall increase of total CatD, it could mean that the same amount of mature Cathepsin is active (thus similar activity levels), and there is only more proCathepsin, rather than the mature form (Figure 4. 38). A week of chronic treatment partially depletes the cells of the mature form of Cathepsin (Figure 4. 41). This suggests a turnover imbalance, i.e. the previously existing mature CatD surpassed its half-life, whilst there was no compensatory processing of new proCathepsin into the mature form, effectively reducing its levels (Figure 4. 43). And this occurs despite the substantial increase of proCathepsin, which means it is not being cleaved (Figure 4. 41).

4.8 CQ-induced Alteration of Lysosomal Acidity

LysoTracker® (LT) consists of a weakly basic amine linked to a fluorophore. This acidotropic probe permeates cell membranes and concentrates at low pH organelles (pH < 6.5). Its retention mechanism in the membranes of these organelles is not yet fully understood. Yet LT probes have been shown to be selective for endocytic vesicles, most notably lysosomes and, for this reason, they are commonly used as lysosomal markers. In this case, LT was used as a reporter for the presence of acidic vesicles, in an effort to evaluate the actual acidity of lysosomes, when the cells are subjected to CQ treatment. In this context, considering a selective affinity for acidic vesicles, more fluorescence of LT would correspond to higher numbers/bigger acidic vesicles.

hESc-RPE cells were treated with medium either without or with POS (+POS), for 4h, followed by overnight incubation in medium containing increasing concentrations of CQ, from 1-10µg/mL. Baf was used as negative control. The next day, cells were incubated with LT and prepared, as described in Materials and Methods. Fluorescence was measured by flow cytometry and fluorescence microscopy images were obtained, in order to assess cellular distribution pattern of the dye (Figure 4. 44 and Figure 4. 45).

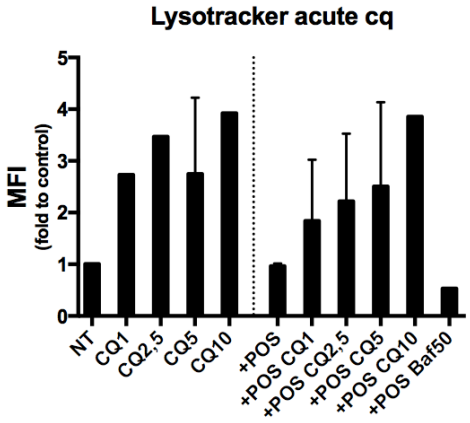

Figure 4. 44 - Acute CQ treatment causes increase of LT fluorescence in hESc-RPE cells, evaluated by flow cytometry. The dashed line separates non-fed from POS-fed (+POS) cells. Each column represents the Mean Fluorescence Intensity fold change, relative to NT cells. Baf at 50nM was used as negative control. n=20.000 cells acquired for each condition Results are expressed as mean ± s.d. from two independent experiments.

Flow cytometry results depict an increase of LT fluorescence intensity, with CQ concentration, relative to control NT cells. Again, addition of POS alone does not seem to produce an effect on LT fluorescence, with the fluorescence gain appearing as a direct result from CQ treatment. Surprisingly, rather than reducing lysosome activity, CQ appears to boost it, upon acute overnight treatment. Baf, on the contrary, extinguished the signal to baseline levels, effectively working as negative control (Figure 4. 44).

Representative images showing LT fluorescence intracellular distribution in hESc-RPE cells is shown in Figure 4. 45.

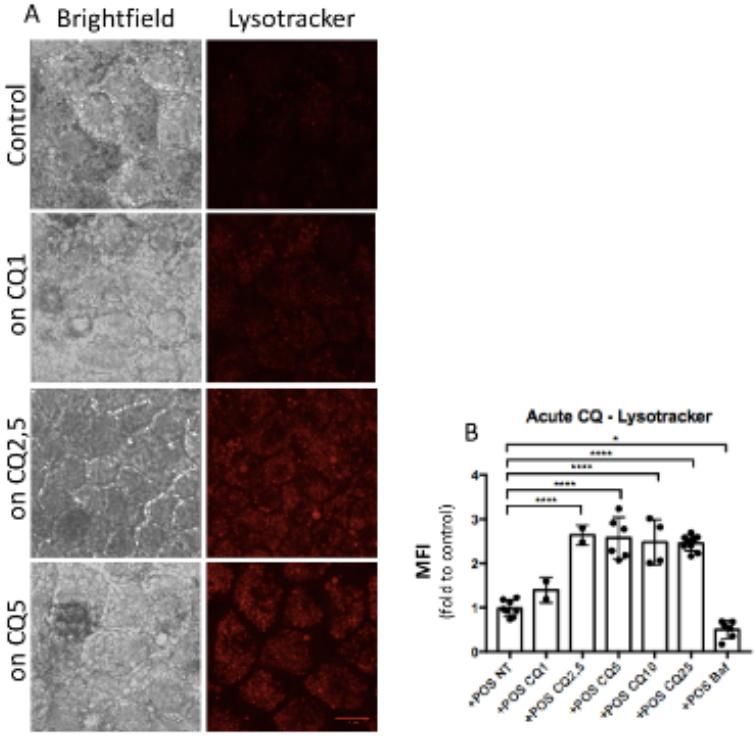

Figure 4. 45 - Acute CQ treatment causes increase of LT fluorescence in hESc-RPE cells, assessed by light microscopy. A: Representative images displaying LT distribution in cells treated with 1-5µg/mL CQ. Scale bar 10µm. B: Quantification of fluorescence mean integrated intensity of representative images. Results are expressed as mean ± s.d. from independent images n≥2 (*p<0.05; ****p<0.0001).

hESc-RPE cells display LT fluorescence with a vesicular pattern, consistent with acidic endocytic vesicles. The number and intensity of the acidic vesicles upturns and expands within the cell area, upon CQ treatment, directly correlated to CQ concentration. Alike the flow cytometry results, cells show significant increase of fluorescence ($p<0.0001$), proportional to CQ concentration rise, as confirmed through image intensity quantification (Figure 4. 44 and Figure 4. 45).

Following the protocol previously described for continued CQ treatment, cells were fed POS and treated with CQ overnight, for three consecutive days. LT fluorescence was evaluated by flow cytometry (Figure 4. 46).

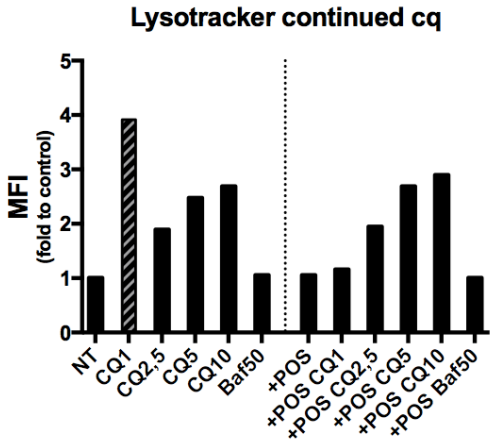

Figure 4. 46 - Continued CQ treatment causes increase of LT fluorescence in hESc-RPE cells, evaluated by flow cytometry. The dashed line separates non-fed from POS-fed (+POS) cells. Each column represents the Mean Fluorescence Intensity fold change, relative to NT cells. Baf at 50nM was used as negative control. n=20.000 cells acquired for each condition represented.

Three days of CQ-treatment causes a consistent increase of LT fluorescence, and thus acidic vesicles, compared to control non-treated cells. Again, this effect is independent of POS feeding, occurring whether or not the cells were fed. Baf-treated cells' fluorescence levels are not very different from the control situation, indicating that, un-stimulated, cells normally have baseline acidity (Figure 4. 46). However, it is important to take into account the threshold of detection this technique offers and look at the images before reaching such conclusions. In non-fed CQ1 condition, emphasized in the graph, there is abnormally high fluorescence; this, however, may be considered as an outlier, because the cells from the well in question were unusually depigmented (data not shown). Although treatment conditions were not changed throughout the experiments, this well in particular had less apparent pigmentation (evaluated by eye). When analyzing fluorescence intensity, it is of utmost importance to regard this feature, as pigment may quench the signal and interfere with the results. Nonetheless, the cells were processed and analyzed, and are depicted merely to demonstrate potential confounding factors and caveats to this type of analysis (Figure 4. 46).

The systematic increase of acidic vesicles resulting from CQ burden is unexpected, but could be indicative of lysosomal biogenesis or abnormal distribution within the cells. To evaluate that, cellular distribution pattern and microscopy images LT fluorescence quantification were ensued (Figure 4. 47).

LT fluorescence increases, due to a wider distribution of acidic vesicles detected: while in the control image, lysosomes are spread apart, with a few more prominent at the perinuclear region of cells, in cells treated with CQ, the fluorescent vesicles occupy the whole cytoplasmic area, excluding only the membrane and the nucleus (Figure 4. 47). In fact, the cell's profile becomes readily visible, with typical polygonal shape, because fluorescent vesicles extend from nucleus to the membrane periphery (Figure 4. 47).

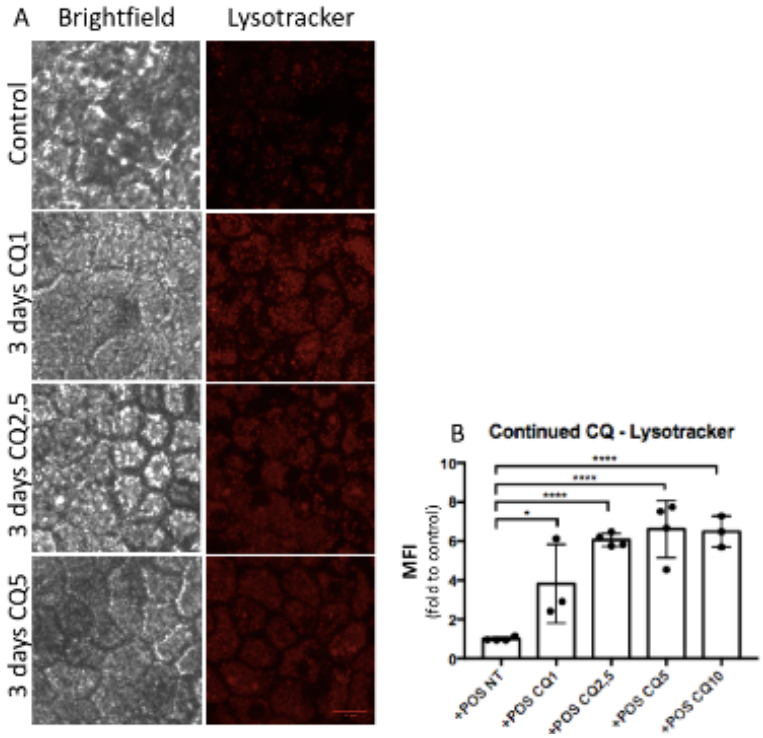

Figure 4. 47 - Continued CQ treatment causes increase of LT fluorescence and wider distribution in hESc-RPE cells, assessed by light microscopy. A: Representative images show the distribution of the dye, spreading throughout the cell, upon CQ treatment (1-5µg/mL). Scale bar 10µm. B: Fluorescence quantification for each condition, with each dot representing a different image's mean fluorescent integrated intensity, and compared to control (NT) cells. Results are expressed as mean ± s.d. from independent images n≥3 (*p<0.05; ****p<0.0001).

The fluorescence increases upon CQ treatment, in a dose-dependent manner, for the lowest concentration, but rapidly reaches a plateau. Image quantification is consistent with flow cytometry findings, conveying a consistent intensification, in proportion to the rise in CQ concentration (Figure 4. 46 and Figure 4. 47).

CQ chronic effect on hESc-RPE's lysosomal acidity was evaluated, by feeding cells with POS for 4h, to load lysosomes, followed by overnight incubation with increasing CQ concentrations, for seven consecutive days. Following the seventh day's overnight incubation, cells were exposed to LT and prepared for flow cytometry (Figure 4. 48).

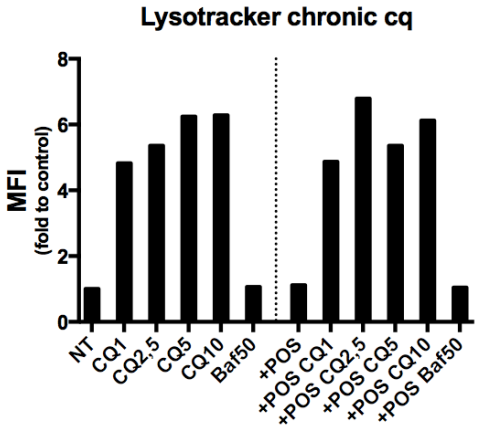

Figure 4. 48 - Chronic CQ burden causes increase of LT fluorescence, as measured by flow cytometry. The dashed line separates non-fed from POS-fed cells. Each column represents the Mean Fluorescence Intensity fold change, relative to NT cells. Baf at 50nM was used as control. n=20.000 cells acquired for each condition represented.

Chronic CQ burden yields more LT fluorescence, compared to the control situation, possibly indicating lysosome biogenesis. Curiously, long-term treatment of these cells with Baf results in fluorescence equivalent to those of control cells. This is puzzling because Baf is a potent V-ATPase inhibitor, and because images depicting LT in Baf-treated cells show absence of fluorescence (data not shown). Therefore, flow cytometry might not be the most sensitive technique to analyze LT fluorescence, since it reflects only whole cell fluorescence, not the distribution within the cell, which in this case is invaluable. Nevertheless, cells treated with CQ are highly fluorescent, which does indicate LT accumulation. Based on this data, and taking together the three time points and corresponding images for acute and continued treatments, CQ produces a higher number and wider distribution of acidic vesicles in the cells (Figure 4. 45 and Figure 4. 47).

4.9 Endocytic pathway and Autophagy impairment

As discussed in Chapter 1, CQ is known to disturb the endocytic and autophagic pathways, in particular by disrupting lysosomal cargo processing, thus causing it to accumulate in the cells. In an effort to evaluate this dysfunction and characterize the proposed CQ-induced hESc-RPE model of lysosomal dysfunction, a set of experiments was performed. Specifically, cells were imaged for the presence/distribution of Apolipoprotein E (ApoE), a protein found in endocytic membranes and known to accumulate in AMD settings (Golestaneh et al. 2017; Hamdi & Kenney 2003). Additionally, whole cell lysates were collected and probed for ApoE, as well as autophagy-related proteins p62 and LC3, by Western Blot.

hESc-RPE cells were treated with medium either without or with POS (+POS), for 4h, followed by overnight incubation in medium containing increasing concentrations of CQ, from 1-5µg/mL. IF images were obtained using an anti-ApoE antibody, and quantified (Figure 4. 49).

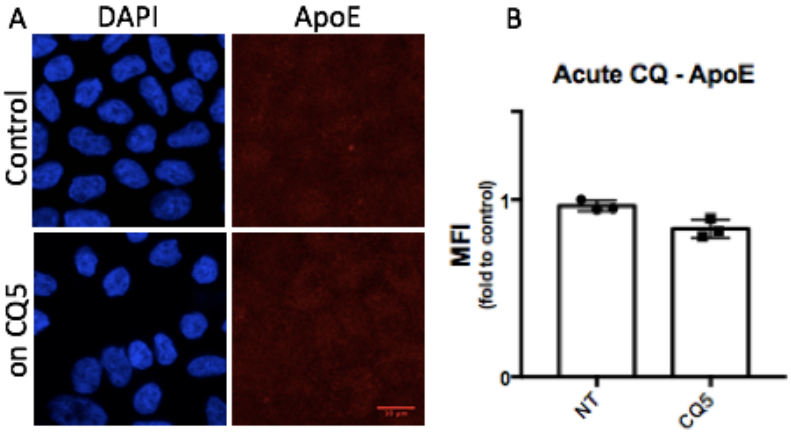

Figure 4. 49 - ApoE protein levels and intracellular distribution are not altered upon acute CQ treatment of hESc-RPE. A: Representative IF images of the anti-ApoE staining, in control non-treated cells and in cells treated with CQ. Scale bar 10µm. B: Quantification of fluorescence mean integrated intensity of representative IF images. Each dot represents a different image's mean fluorescent integrated intensity, compared to control (NT) cells. Results are expressed as mean ± s.d. from independent images, n=3.

ApoE staining was shown to be faint, precluding detailed analysis of its subcellular localization in hESc-RPE. Quantification of representative images reveal similar mean fluorescence intensity whether cells were treated with CQ or not (Figure 4. 49 B). Nevertheless, in order to further evaluate how the level of ApoE is affected in hESc-RPE when treated with CQ, whole cell lysates obtained in this experiment were analyzed by Western Blot (Figure 4. 50).

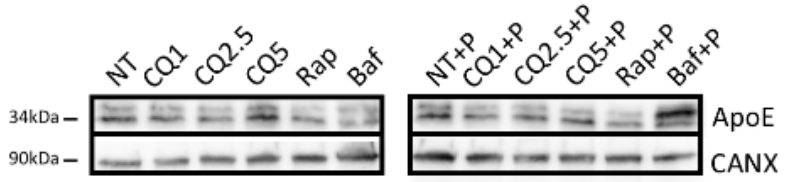

Figure 4. 50 - ApoE protein levels are not altered upon acute CQ treatment of hESc-RPE. Western Blot using anti-ApoE antibody shows two adjoining bands in each condition, representing the native 34 kDa protein and the higher molecular weight sialylated isoprotein (Xu et al. 1999). +P: POS-fed cells. Rap and Baf were used as positive and negative controls, respectively. Calnexin was used as loading control. A representative result is shown from four independent experiments.

In this experiment, acute CQ does not seem to produce modifications in cellular ApoE quantities. Rap was used here as an autophagy/lysosomal inducer, and for this reason, a slight decrease of ApoE is to be expected. On the contrary, Baf was used to inhibit lysosomal degradation leading to ApoE accumulation in the cell (readily visible in the Baf+P condition) (Figure 4. 50). However, in order to draw conclusions, quantification of bands was ensued, taking into consideration results obtained in four independent experiments (Figure 4. 51).

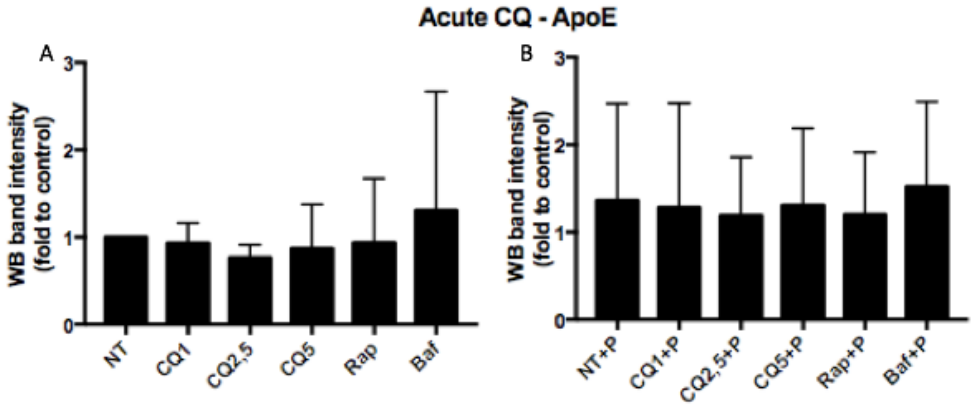

Figure 4. 51 - ApoE total amounts are not altered upon acute CQ treatment. Western Blot relative quantification of bands represents total ApoE, per condition. A: cells treated with CQ alone. B: CQ treatment after POS feeding (+P). Rap and Baf were used as controls. Band intensity was normalized according to the loading control. Results are expressed as mean ± s.d. from independent experiments, n=4.

Upon quantification of representative blots, no substantial difference was found regarding ApoE protein content. There seem to be slightly higher amounts in cells which were fed with POS, which could indicate ApoE expression induction or slower degradation, but most likely reflects ApoE coming from the POS prep. Still, taking into account the large error bars, this observation might be misleading, and more experiments would be necessary to confirm (Figure 4. 51).

Next, the levels of important autophagy players p62/SQSTM1 (p62) and LC3 levels were evaluated in the conditions tested, by Western Blot. In NT conditions, hESc-RPE are express low detectable levels of p62 (Figure 4. 52).

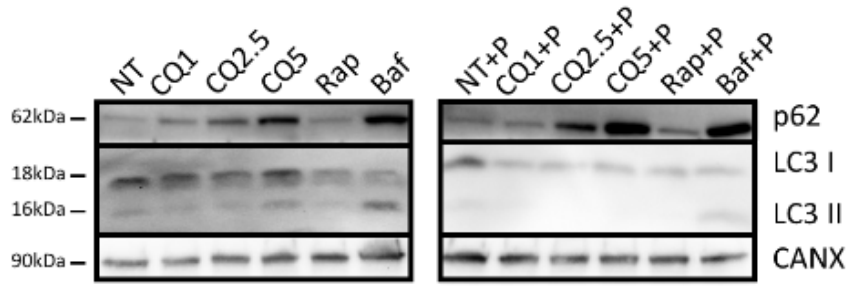

Figure 4. 52 - Acute CQ treatment alters p62 and LC3 protein levels in hESc-RPE cells, detected by Western Blot. Rap and Baf were used as positive and negative controls, respectively. +P: POS-fed cells. Calnexin was used as loading control. A representative result is shown from three independent experiments.

When cells are treated with CQ they seem to gradually accumulate p62, according to increasing CQ concentrations. In cells treated with CQ at the highest concentration (5μg/mL), p62 is found at similar levels as in Baf-treated cells, suggesting there is impairment of its clearance (Figure 4. 52).

Regarding LC3, its lipidated form LC3 II is visible in Baf-treated cells and in NT cells in both POS-fed and unfed cells. In the case of Rap, there is decrease of both LC3 I and II forms, which suggests induction of autophagy, as predicted. On the contrary, in Baf-treated cells, the decrease of LC3 I compared to NT cells seems to be at the expense of LC3 II, which increases significantly (Figure 4. 52).

This indicates autophagy blockade, with accumulation of autophagosomes. In comparison to these control situations, CQ seems to cause accumulation of the LC3 I form, at similar levels to those of control NT cells in the case of POS-deprived cells. LC3 II also seems to accumulate, in proportion to CQ increase, in cells without POS. In POS-fed cells, however, there seems to be a decrease of both LC3 I and II in CQ-treated cells, compared to control. In fact, in this image, CQ-treated cells' bands resemble that of Rap-treatment, which suggests induction of autophagy (Figure 4. 52).

Quantification of representative images for p62 is depicted next (Figure 4. 53).

Quantification of p62 bands suggests a slight reduction, in POS-deprived cells treated with CQ or with Rap and return to control levels upon Baf-treatment. To the right of the dashed line, in POS-fed conditions, hESc-RPE cells display generally lower p62 levels than NT cells (that were not POS-fed). Nonetheless, regarding POS-fed cells alone, and comparing NT+POS to CQ-treated cells, there is a slight increase in p62, dependent on CQ concentration (Figure 4. 53).

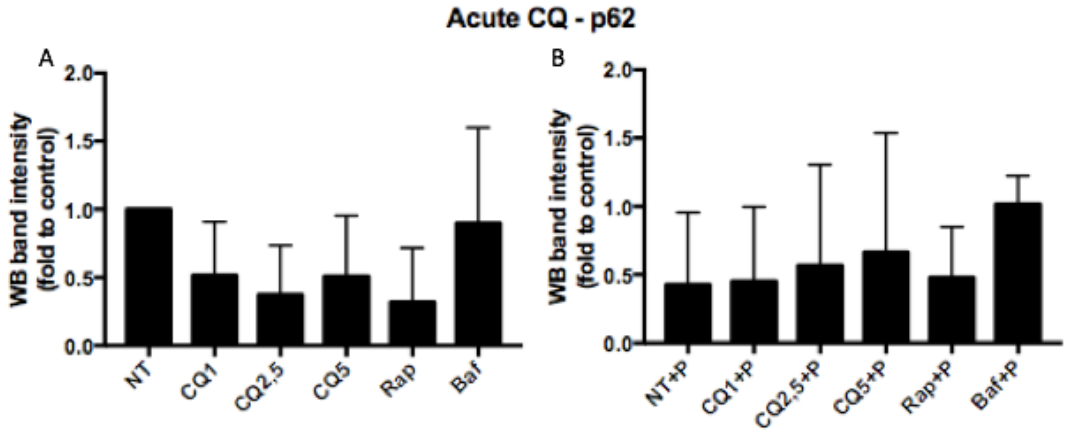

Figure 4. 53 - p62 protein levels are slightly increased in POS-fed hESc-RPE cells. Rap and Baf were used as controls. Western Blot band intensity was normalized according to the loading control. A: cells treated with CQ alone. B: CQ treatment after POS feeding (+P). Results are expressed as mean ± s.d. from independent experiments, n=3.

This increase is more noticeable in Baf-treated cells. Together this suggests some impairment of p62 clearance, in POS-fed cells, caused by CQ (and, as expected, Baf). Still, to confirm these findings, more experiments would be needed, as the error here is considerable (Figure 4. 53).

LC3 bands were also quantified from representative images and the ratio between lipidated and non-lipidated LC3 forms was calculated, to illustrate autophagy flux, as compared to Rap or Baf treated cells (Mizushima & Yoshimori 2007) (Figure 4. 54).

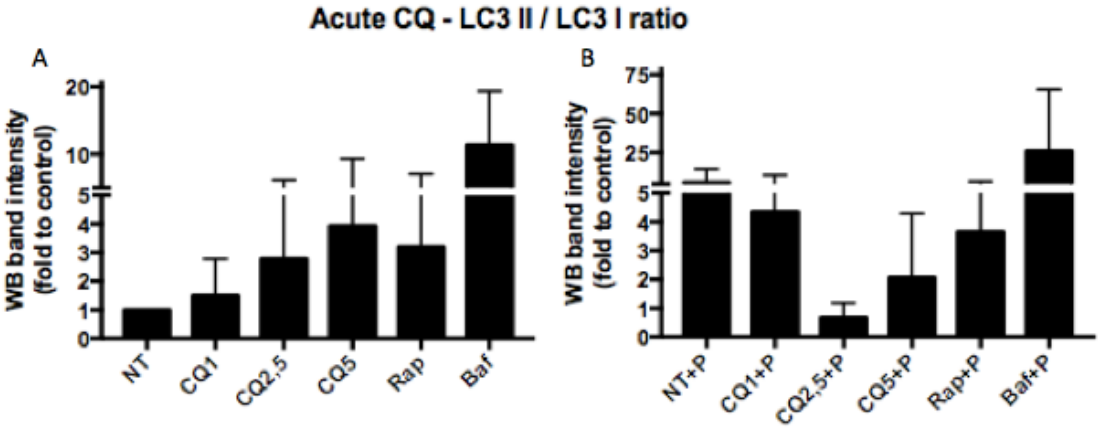

Figure 4. 54 - Ratio LC3 II/LC3 I is altered upon acute CQ treatment of hESc-RPE cells. Western Blot relative quantification of bands represents the ratio between LC3 II and LC3 I, per condition. A: cells treated with CQ alone. B: CQ treatment after POS feeding (+P). Rap and Baf were used as controls. Band intensity was normalized according to the loading control. Results are expressed as mean ± s.d. from independent experiments, n=3.

Quantification reflects the increase in LC3 II, in the case of Baf-treated cells, revealed by increased LC3 II/LC3 I ratio (Figure 4. 54). In CQ-treated cells there is also a gradual increase of the ratio, in the non-fed conditions. This increase is proportional to CQ concentration, yet upon visualization of the blots the cause for this effect is not always obvious (Figure 4. 52).

For the continued CQ treatment, hESc-RPE cells were treated with medium either without or with POS (+POS), for 4h, followed by overnight incubation in medium containing increasing concentrations of CQ, from 1-5µg/mL, for three consecutive days. IF images obtained by probing cells with an anti-ApoE antibody, and the respective quantification are depicted in Figure 4. 55.

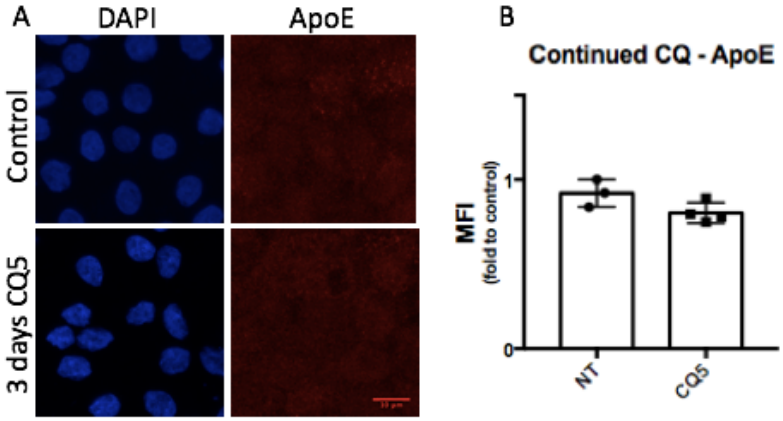

Figure 4. 55 - ApoE protein levels and intracellular distribution are not altered upon continued CQ treatment. A: Representative images of anti-ApoE IF staining, in control non-treated cells and in cells treated with CQ. Scale bar 10µm. B: Quantification of fluorescence mean integrated intensity of representative IF images. Each dot represents a different image's mean fluorescent integrated intensity, compared to control (NT) cells. Results are expressed as mean ± s.d. from independent images, n≥3.

Again, no significant difference is observed in the IF staining with ApoE antibody. In some cells, a vesicular pattern is apparent, but no differences were found in the staining intensity of treated *versus* non-treated cells (Figure 4. 55). Western Blot of cells treated in a similar manner as before, for three days (Figure 4. 56).

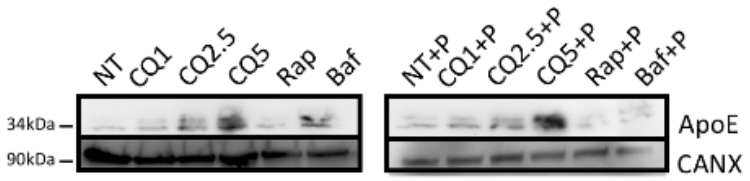

Figure 4. 56 - ApoE accumulates upon continued CQ treatment of hESc-RPE cells, assessed by Western Blot. Anti-ApoE antibody shows two adjoining bands in each condition, representing the native 34 kDa protein and the higher molecular weight sialylated isoprotein (Xu et al. 1999). Rap and Baf were used as positive and negative controls, respectively. +P: POS-fed cells. Calnexin was used as loading control. A representative result is shown from three independent experiments.

A continued CQ treatment, for three days, causes accumulation of ApoE in the cells extracts, as shown by increasingly intense bands, in proportion to CQ's concentration increase (Figure 4. 56). Rap treatment causes ApoE clearance, while Baf-treated cells accumulate ApoE (in the case of non-POS-fed cells). Quantification of representative images was ensued (Figure 4. 57).

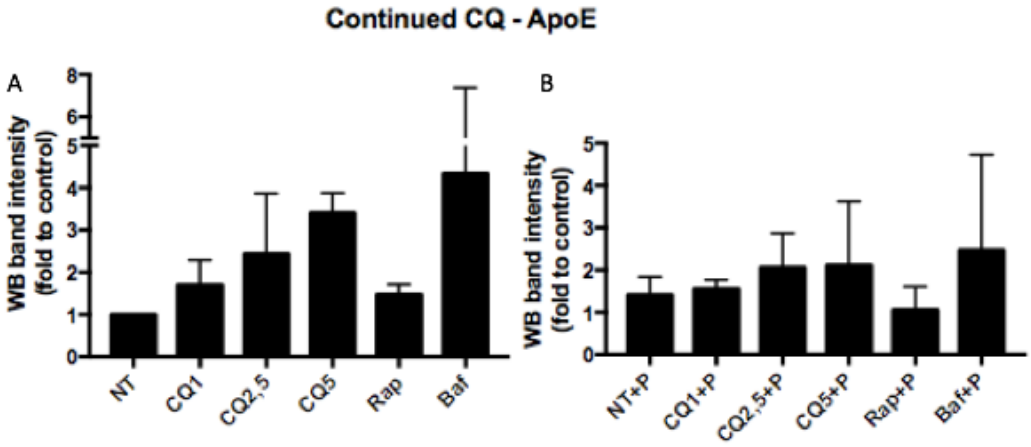

Figure 4. 57 - ApoE accumulates in hESc-RPE upon continued CQ treatment. Western Blot relative quantification of bands represents total ApoE, per condition. A: cells treated with CQ alone. B: CQ treatment after POS feeding (+P). Rap and Baf were used as controls. Band intensity was normalized according to the loading control. Results are expressed as mean ± s.d. from independent experiments, n=3.

Quantification of bands from three different experiments show similar results to those observed in Figure 4. 56: consistent increase of ApoE in CQ treated cells, depending on the increase in CQ's concentration; there is a decrease in the case of Rap treatment, to NT control levels or lower, and increase of ApoE in the case of Baf-treated cells (Figure 4. 57). This indicates that lysosomal function is necessary for ApoE turnover in the cell and it is impaired by both CQ and Baf, after three days of treatment.

A Western Blot image showing p62 and LC3 levels is presented next, depicting cells treated in the same manner (Figure 4. 58).

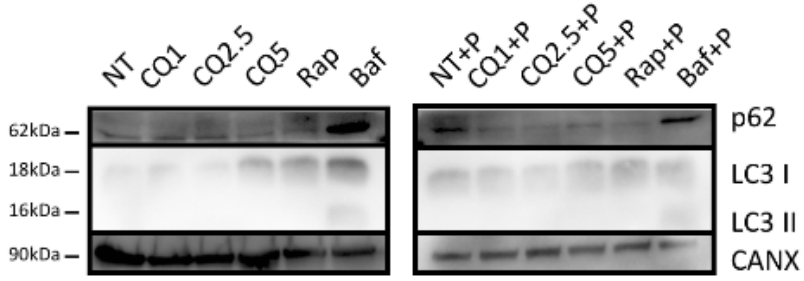

Figure 4. 58 - p62 and LC3 protein levels show autophagy clearance after continued CQ treatment, in hESc-RPE cells. Rap and Baf were used as positive and negative controls, respectively. +P: POS-fed cells. Calnexin was used as loading control. A representative result is shown from at least two independent experiments.

Western Blot results shows low levels of both p62 and of LC3. In fact, it is not easy to observe p62 in these conditions, as the expression is fairly low, compared to Baf-treated cells. Still, a continuous treatment seems not to cause increase of p62, relative to control, suggesting that cells are able to adapt. As for LC3, it is difficult to visualize the LC3 II form, except in Baf-treated cells (Figure 4. 58). This also indicates there is a general clearance, possibly due to lysosome biogenesis triggered by MiT TFs. Quantification is shown in Figure 4. 59 and Figure 4. 60.

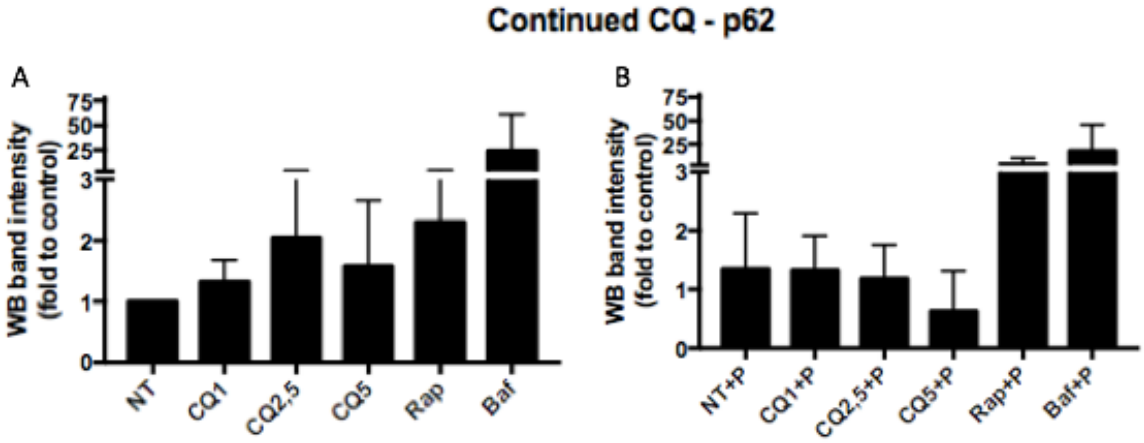

Figure 4. 59 - p62 levels do not increase in hESc-RPE continuously treated with CQ. A: cells treated with CQ alone. B: CQ treatment after POS feeding (+P). Rap and Baf were used as controls. Band intensity was normalized according to the loading control. Results are expressed as mean ± s.d. from independent experiments, n=3.

Results obtained confirm low levels of p62, comparable to those found in the NT control situation and also lower than those found for Rap-treated cells. On the contrary, Baf-treated cells accumulate substantial doses of p62 (Figure 4. 59). This suggests that at this time-point there is no significant lysosomal dysfunction, caused by CQ treatments.

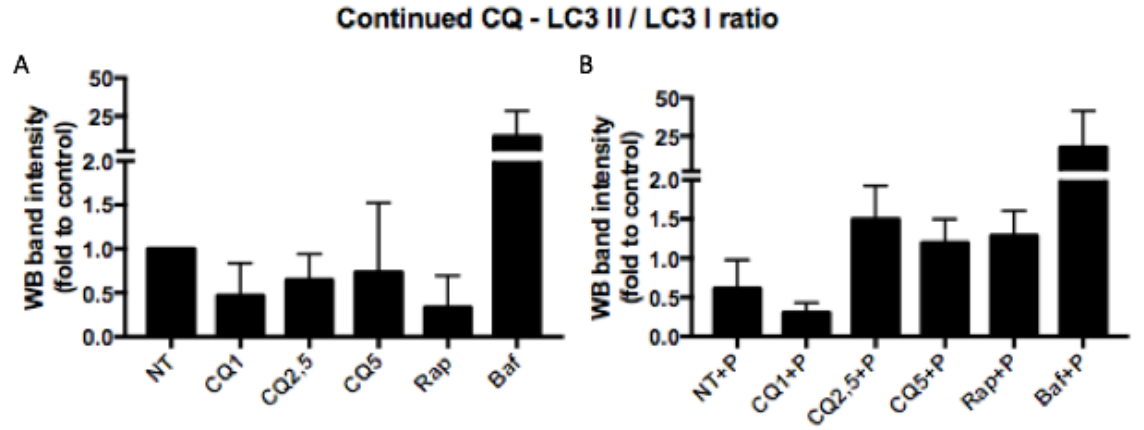

Figure 4. 60 - LC3 ratio does not suggest autophagy impairment in hESc-RPE treated continuously with CQ. A: cells treated with CQ alone. B: CQ treatment after POS feeding (+P). Rap and Baf were used as controls. Band intensity was normalized according to the loading control. Results are expressed as mean ± s.d. from independent experiments, n=2.

The ratio between LC3 II and LC3 I was evaluated (Figure 4. 60). Based on its interpretation and on visualization of a representative western blot image (Figure 4. 58), it is possible to determine that only in Baf-treated conditions there is substantial accumulation of LC3 II, indicating autophagy flux impairment. In CQ-treated cells, although in some cases it might look increased, relative to NT cells, LC3 ratio is not very different from Rap-treated cells, thus precluding further conclusions (Figure 4. 60).

In order to assess the consequences of chronic CQ burden, hESc-RPE cells were treated with medium with POS (+POS), followed by overnight incubation in medium containing increasing concentrations of CQ, from 1-5µg/mL, for seven consecutive days. In addition, whenever possible, Lonza hRPE and pRPE were also tested, in order to confirm findings

in the different cell models available. IF images were obtained by probing hESc-RPE cells with an anti-ApoE antibody, and the respective fluorescence was quantified (Figure 4. 61).

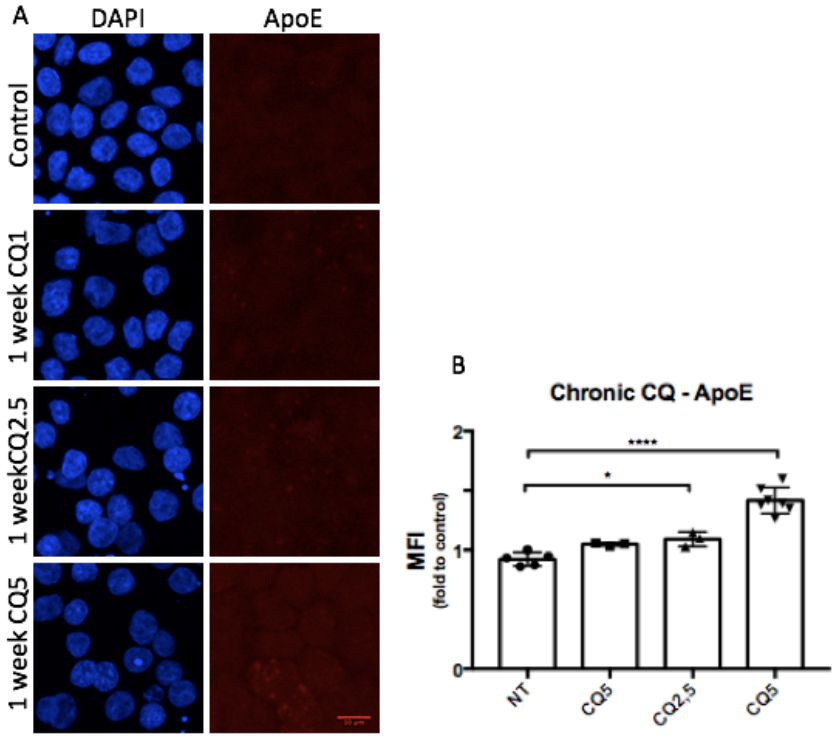

Figure 4. 61 - ApoE gets accumulated in hESc-RPE cells treated chronically with CQ. A: Representative IF images represent the anti-ApoE staining, in control non-treated cells and in cells treated with CQ. Scale bar 10µm. B: Quantification of fluorescence mean integrated intensity of representative IF images. Each dot represents a different image's mean fluorescent integrated intensity, compared to control (NT) cells. Results are expressed as mean ± s.d. from independent images, n≥3 (*p<0.05; ****p>0.0001).

After a seven-day treatment, ApoE staining starts to become more noticeable, with a vesicular pattern. Additionally, the cell's profile become more evident, possibly indicating cytosolic ApoE. Image quantification regarding cells treated with mounting concentrations of CQ confirms an increase of ApoE detected by IF, upon chronic treatment with higher concentrations (up to 1.5x fold) (Figure 4. 61). To confirm these result, Western Blot analysis was performed, this time comparing hESc-RPE (hRPE) in parallel with Lonza hRPE (LRPE) (Figure 4. 62).

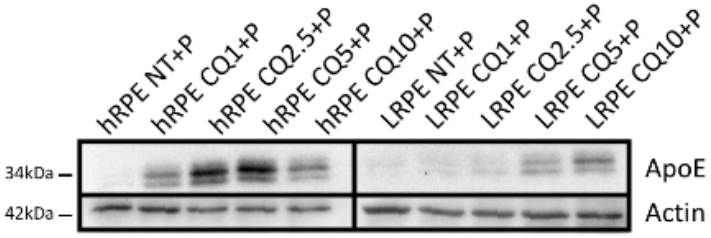

Figure 4. 62 - ApoE accumulates upon chronic CQ treatment of hESc-RPE (hRPE) and Lonza hRPE (LRPE). +P: POS-fed cells. anti-ApoE antibody shows two adjoining bands in each condition, representing the native 34 kDa protein and the higher molecular weight sialylated isoprotein (Xu et al. 1999).Actin was used as loading control. A representative result is shown from three independent experiments.

Western Blot results clearly show a consistent increase in cellular ApoE, in both hESc-RPE and in Lonza hRPE cells, depending on CQ concentration. This suggests that a week-long treatment with relatively low doses of CQ is sufficient to impair ApoE turnover, causing it to accumulate (Figure 4. 62). Although this antibody was also tested in pRPE, it did not recognize the porcine protein (data not shown). Representative image quantification is shown next (Figure 4. 63).

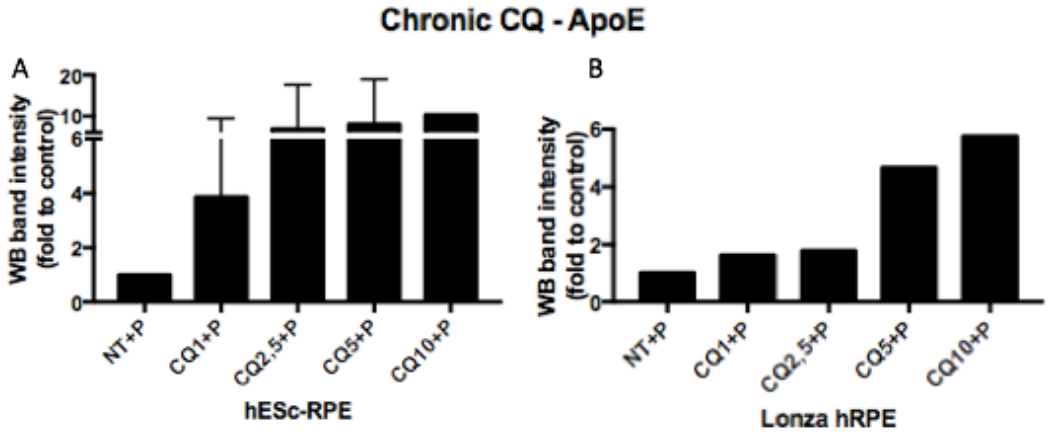

Figure 4. 63 - ApoE accumulates severely with CQ chronic treatment of hESc-RPE cells (A) and Lonza hRPE (B).. Western Blot relative quantification of bands represents total ApoE, per condition. Band intensity was normalized according to the loading control. Results are expressed as mean ± s.d. from independent experiments, n=3 for hESc-RPE, n=1 for Lonza hRPE.

Quantification performed for several independent experiments confirms the increase in ApoE content of cells treated with the higher concentrations of CQ, for a period of one week. This was found to be true for both human RPE lines tested (Figure 4. 63). This result suggests impairment of ApoE degradation, since it is expected that CQ would impair endocytic trafficking. However, at this point, ApoE expression induction should not be ruled out.

As before, Western Blot analysis was performed, in order to convey p62 and LC3 levels in cells treated chronically with CQ. Again, the p62 antibody used worked only in human cells. LC3, on the other hand, worked for the three RPE lines tested (Figure 4. 64).

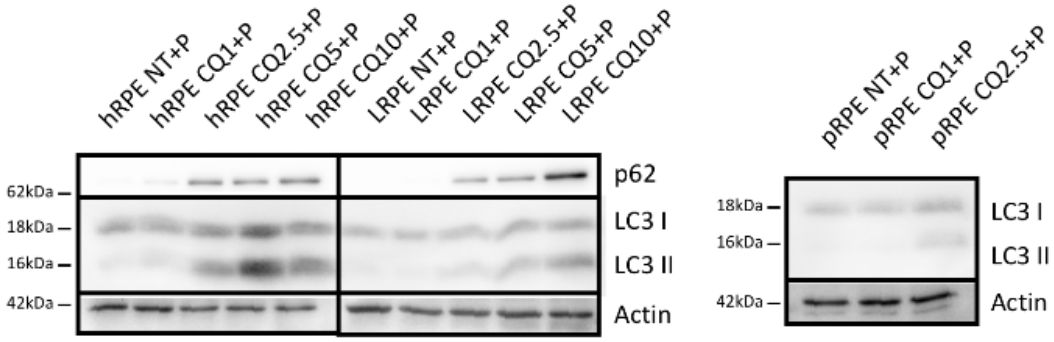

Figure 4. 64 - p62 (in human cells) and LC3 II accumulate after a chronic CQ treatment, in hESc-RPE (hRPE), Lonza hRPE (LRPE) and porcine RPE (pRPE). +P: POS-fed cells. Actin was used as loading control. A representative result is shown from at least two independent experiments.

Results obtained show that there is a concomitant increase of p62 in cells treated with CQ, proportional to the increase in concentrations used and for both hESc-RPE and Lonza hRPE. Regarding LC3, there seems to be induction of LC3 II form, with general maintenance of the LC3 I form, for the three RPE lines tested (Figure 4. 64). This strongly suggests impairment of the autophagy pathway and, considering possible LC3-associated phagocytosis, impairment of LAP-mediated phagocytic processing.

In the next step, quantification of the obtained blots was performed (Figure 4. 65 and Figure 4. 66).

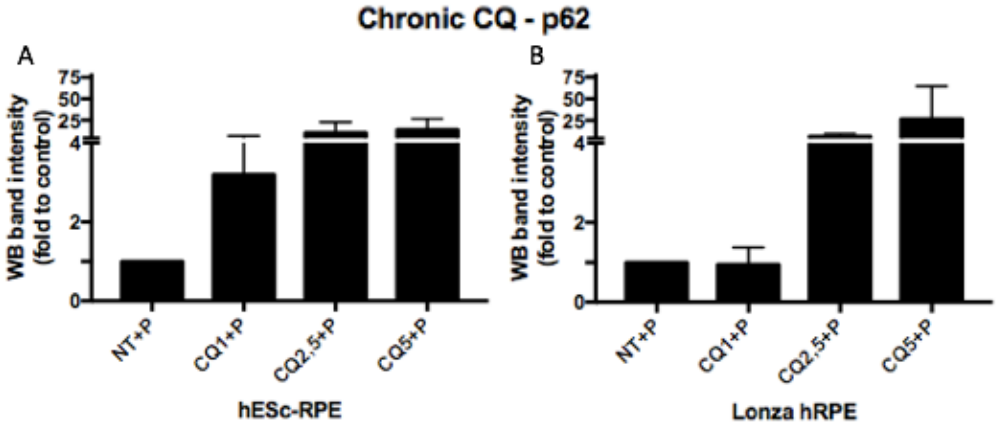

Figure 4. 65 - p62 accumulates upon chronic CQ treatment of hESc-RPE cells (A) and Lonza hRPE (B). Band intensity was normalized according to the loading control. The dashed line separates hESc-RPE from Lonza hRPE. Results are expressed as mean ± s.d. from independent experiments, n≥4.

Quantification results of the blot images is consistent with the initial observation: p62 accumulates regularly, depending on CQ concentration (Figure 4. 66).

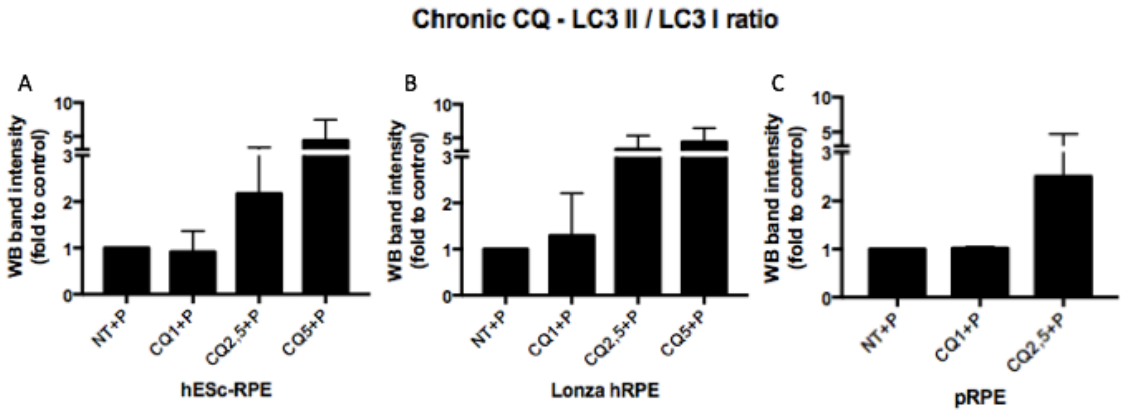

Figure 4. 66 - Chronic CQ treatment causes LC3 II to accumulate, relative to LC3 I, in hESc-RPE (A), Lonza hRPE (B) and pRPE (C) cells. Western Blot relative quantification of bands represents the ratio of LC3 II/LC3 I, per condition. Band intensity was normalized according to the loading control. Results are expressed as mean ± s.d. from independent experiments, n=6 for hESc-RPE; n=4 for Lonza hRPE; n=2 for pRPE.

Regarding LC3 ratio and the representative image shown in Figure 4. 64, the previous observation is reinforced: LC3 II accumulates, relative to LC3 I, in the three RPE lines

tested. This indicates impairment of (auto)phagosome clearance by the RPE cells, upon chronic CQ treatment.

Altogether, these results suggest that CQ is indeed impairing the endocytic and autophagic pathways, thus causing accumulation of substrates, which would otherwise be degraded by the lysosome. As undegraded material builds up in the cell, in association with increased pH and wide distribution of lysosomes, the cell may meet the conditions for lysosomal exocytosis (Blott & Griffiths 2002; Carmona-Gutierrez et al. 2016; Settembre, Fraldi, et al. 2013). This was evaluated in the next section.

4.10 CQ-induced Lysosomal exocytosis

Lysosomal exocytosis may be used as a membrane repair mechanism, and it has also been proposed to be a cellular stress-defense mechanism, transcriptionally regulated by TFEB (Medina et al. 2011).

hESc-RPE cells, plated onto transwells, were fed with POS for 4h, followed by overnight incubation in medium containing increasing concentrations of CQ, from 1-5µg/mL. The next day, medium was collected from the apical and the basal chambers of the transwells and analyzed for ß-hexosaminidade (b-hex) release, according to the procedure described in Materials and Methods. b-hex is a lysosomal enzyme and its detection is based on the enzymatic hydrolysis of its fluorescent substrate, normalized for the respective protein content (Figure 4. 67).

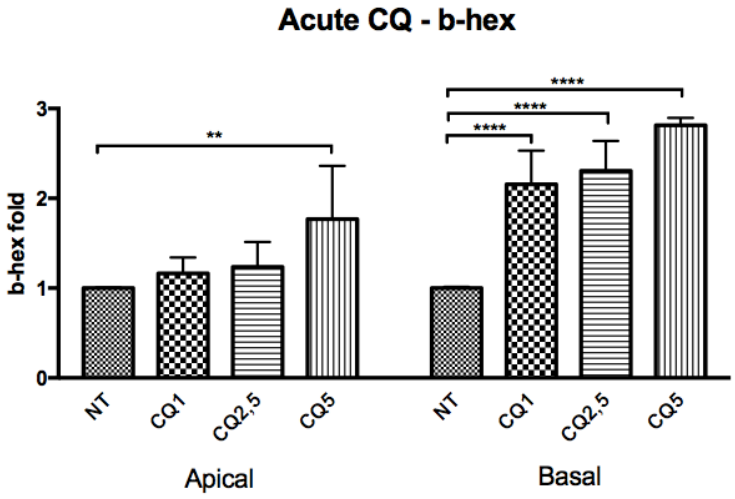

Figure 4. 67 - Acute CQ treatment leads to basal release of b-hex by hESc-RPE cells. The graph shows fold increase of β-hex release in the supernatant from CQ-treated cells, compared to control NT cells, from the apical side and from the basal side of the cells. Results are expressed as mean ± s.d. from independent experiments, n = 4 (**p<0.01; ****p<0.0001).

Upon acute overnight treatment with CQ, hESc-RPE cells partially exocytose their lysosomal content, as evidenced by b-hex increase in the collected medium. As a polarized epithelium, the RPE secreted its lysosomal content mostly via the basalolateral side, with

CQ causing up to a 2.8x fold increase, compared to NT control. Regarding the apical secretion, there is also increase in the CQ 5µg/mL condition (Figure 4. 67).

hESc-RPE cells, plated onto transwells, were subjected to the same treatment as previously described; treatment was repeated for three consecutive days and after the third day, medium was collected from the apical and the basal chambers of the transwells and analyzed for ß-hexosaminidade (b-hex) release. This means that the b-hex release analyzed corresponds only to the third day of stimulus, and not the cumulative release over those three days (Figure 4. 68).

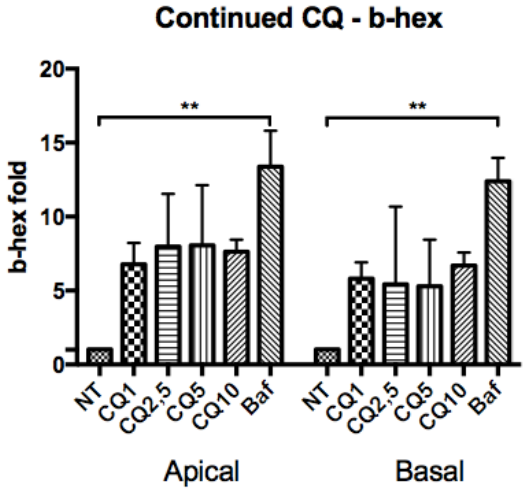

Figure 4. 68 - Continued CQ treatments leads to apical and basal release of b-hex by hESc-RPE. Baf was used as positive control. The graph shows fold increase of β-hex release in the supernatant from CQ-treated cells, compared to control NT cells, from the apical side and from the basal side of the cells. Results are expressed as mean ± s.d. from independent experiments, n = 2 (**p<0.01).

hESc-RPE subjected to continued CQ burden release significant more b-hex than control non-treated cells, both apically and basally. Baf was used as a positive control and indeed resulted in higher b-hex release. In this case, comparing CQ-induced apical to basal release, the differences seem modest: up to 6.7x fold difference for the basal side and up to 8x fold for the apical side, relative to their respective NT controls (Figure 4. 68). As to the CQ concentrations used, no significant difference was found, with all causing similar levels of b-hex release.

hESc-RPE cells, polarized on transwells, were again fed with POS for 4h, followed by overnight incubation in medium containing increasing concentrations of CQ, for seven consecutive days. After stimulus, medium was collected from the apical and the basal chambers of the transwells and analyzed for b-hex release. Thus b-hex release from the seventh day of stimulus, not week-long cumulative release (Figure 4. 69).

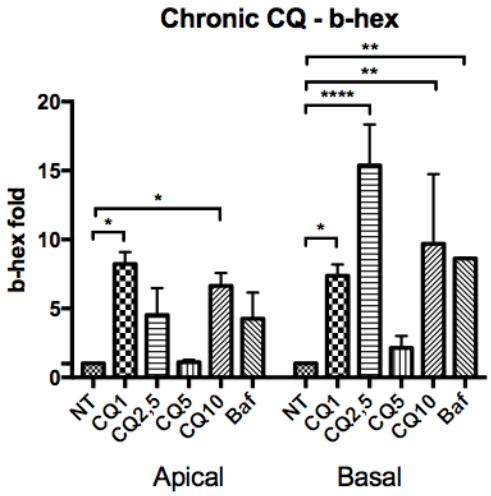

Figure 4. 69 - Chronic CQ burden leads to both apical and basal release of b-hex by hESc-RPE. Baf used uses as positive control. The graph shows fold difference of β-hex release in the supernatant from CQ-treated cells, compared to control NT cells, from the apical side and from the basal side of the cells. Results are expressed as mean ± s.d. from independent experiments, n = 2 (*p<0.05; **p<0.01; ****p<0.0001).

hESc-RPE were able to endure a chronic CQ burden, with no noticeable cell detachment or monolayer apparent disturbance (data not shown), but again, released significant amounts of b-hex. Baf was used as a positive control, only this time causing b-hex release at similar levels to those of CQ-treated cells, suggesting maximization of the effect (Figure 4. 69). The steep rise of basal b-hex release indicates a dose-dependent effect, from NT to CQ at 2.5 µg/mL. This is accompanied by increased release through the apical side. In both apical and basal chambers, the CQ-induced release grows higher than that of Baf-treated cells. In both apical and basal chambers, the b-hex found when using CQ at 5µg/mL was at much lower levels. This possibly indicates an outlier caused by, for instance, an experimental error regarding the preparation of that particular CQ-medium solution. These experiments should be repeated, in order to confirm these findings. Nevertheless, a strong CQ-induced lysosomal exocytosis effect was shown and moreover, the outcome aggravates with time of stimulation.

3.11 Final Conclusion: Model of CQ-induced Lysosomal Dysfunction in RPE

Altogether, the previous results indicate that hESc-RPE lysosomal exocytosis emerges as a CQ stress-induced adaptation the cell resorts to, when overburden by lysosomal dysfunction.

In the acute stimulus, there is impairment of rhodopsin processing (Figure 4. 15) and, to a small extent, of DQ-BSA fluorescence (Figure 4. 21), possibly due to CatD impairment (Figure 4. 32), and correspondent modest accumulation of autophagy substrates (Figure 4. 52); this impairment leads to b-hex secretion mostly though the cells' basolateral side (Figure 4. 67). This is accompanied by translocation of MiT TFs to the cells' nuclei (Figure 4. 10), which may account for increase of CatB and CatL activity (Figure 4. 26)

Upon continued CQ burden, rhodopsin remains after three days (Figure 4. 16), as well as DQ-BSA (Figure 4. 23); although CatB and CatL activity continue elevated (Figure 4. 28), CatD activity is partially impaired (Figure 4. 36), possibly due to imbalance of its processing mechanism into the mature form (Figure 4. 37 and Figure 4. 39); LT is elevated, indicating presence of acidic vesicles (Figure 4. 47), possibly due to induction of lysosomal biogenesis (Figure 4. 11); still, ApoE moderately accumulates (Figure 4. 56); on the other hand, p62 and LC3 recover from initial insult (Figure 4. 58); b-hex release at this time point occurs through both apical and basal sides (Figure 4. 68), at maximum levels, based on Baf-treated cells.

Upon chronic CQ treatment, hESc-RPE cells seem to be overwhelmed: MiT TFs appear widely distributed in the cell (Figure 4. 12), which may account for the CatB and L increased activity (Figure 4. 30), as well as for LT increase (Figure 4. 48); still, there is severe impairment of POS and DQ-BSA processing (Figure 4. 19 and Figure 4. 25, respectively), as well as accumulation of ApoE (Figure 4. 62), and p62 and LC3 II (Figure 4. 64), which could be the result of CatD misprocessing (Figure 4. 41). At times, these effects were verified for Lonza hRPE and pRPE as well, reaffirming the significance of these results concerning RPE cell biology. Ultimately, hESc-RPE resort to lysosomal exocytosis (Figure 4. 69), both through apical and basal sides.

b-hex release through apical and basal regions might indicate over-stressed cells that are overflown with cargo, therefore releasing to both sides, but may also reflect an effect of CQ in RPE polarization and on the epithelial barrier structure itself (Korthagen et al. 2015; Beckel et al. 2018). Cellular stress and loss of epithelial integrity are fundamental steps in that process. This is supported by ZO1 and Lamp1 IF images obtained upon acute CQ treatment of these cells where stronger intensity and wider distribution of Lamp1 stained lysosomes is observed, upon overnight CQ treatment. Moreover, tight junctions labeled by ZO-1 are disturbed, and it is possible to visualize cells separating from each other upon CQ treatment (Figure 4. 70).

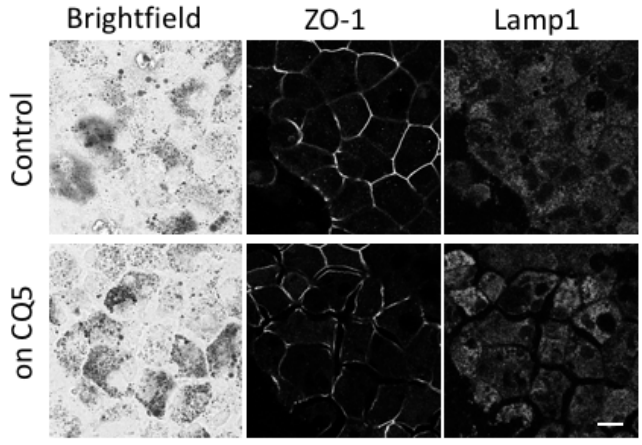

Figure 4. 70 - hESc-RPE lose their epithelial integrity, upon CQ treatment. IF images using anti-ZO1 and anti-Lamp1 antibodies demonstrate cellular tight junctions and lysosomal distribution, respectively. Scale bar 10µm.

Still, considering the parallel between CQ-induced retinopathy and other retinal degenerations, namely AMD, it is reasonable to consider this mechanism as a possible explanation for the origins of RPE basal deposits, occurring as an emergent mechanism, of cells that survive the burden and bear with it. In fact, drusen-like deposits are found in both pathologies, CQ-induced retinopathy and AMD, and have been proposed to stem from RPE stress (Peters et al. 2006; Ivanina et al. 1983; Luthert 2011; Galloway et al. 2017).

Taken together, the data presented throughout this Chapter support the reasoning behind this proposition of lysosomal dysfunction being the basis of age-related retinal degeneration in AMD. To further confirm morphology of aggregates caused by CQ-induced lysosomal dysfunction, hESc-RPE and pRPE cells were imaged by Electron Microscopy. Briefly, hESc-RPE and pRPE cells, plated onto transwells, fed with POS for 4h, followed by overnight incubation in medium containing 25 and 10 µg/mL CQ, respectively. Cells were fixed and prepared for Electron Microscopy imaging, according to the protocols described in Materials and Methods (Figure 4. *71*).

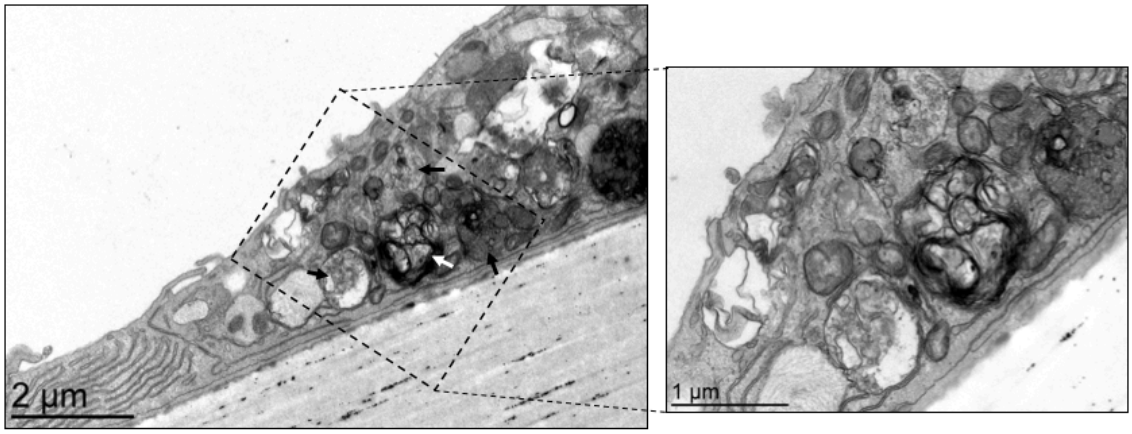

Figure 4. 71 - hESc-RPE treated with CQ accumulate large aggregates. Electron micrograph image shows a flattened cell, filled with multilamellar structures (white arrow) and multivesicular structures (black arrows). Boxed area shows a higher magnification of these structures, resembling a misprocessed phagosome, near the basal region.

EM images of hESc-RPE after CQ acute treatment show the presence of large aggregates, with multivesicular structures and multilamellar bodies (Figure 4. *71*). These could be reminiscent phagosomes, which were not fully processed and accumulate within the cell. pRPE subjected to an acute CQ burden of 10 µg/mL also display severely altered morphology (Figure 4. *72*).

pRPE treated overnight with CQ displayed multivesicular structures, at times containing a mixture of phagosomal reminiscent membranes together with melanosomes (Figure 4. *72*). These are consistent with the complex granules found in AMD patients' RPE and in age-related degeneration models of disease, which could be at the source of melanolipofuscin (Feeney-Burns et al. 1984; Boulton 2014; Ramkumar et al. 2010; Boulton et al. 1994; Song & Dunaief 2013; Holz et al. 2014; Wavre-Shapton et al. 2013).

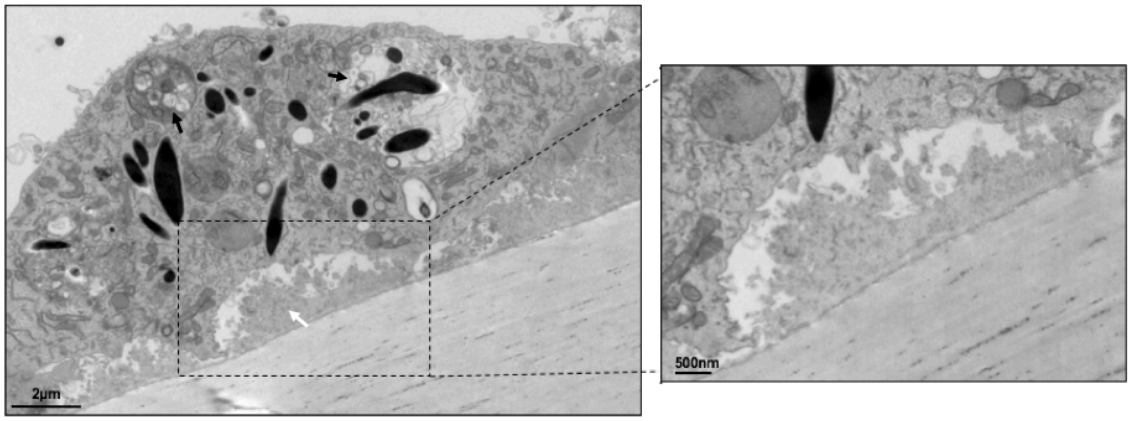

Figure 4. 72 - pRPE cells treated overnight with CQ present complex granules and subcellular deposits. Electron micrograph images show a stressed cell, filled with multivesicular structures some of which containing melanosomes (black arrows). Underneath the cell, there are extracellular drusen-like deposits Boxed area shows a higher magnification of one such structure.

Ultimately, both hRPE and pRPE cells present multivesicular and multilamellar structures, consistent with reminiscent phagosomes and dysfunctional lysosomes (Figure 4. *71* and Figure 4. *72*). Furthermore, in pRPE, acute CQ stimulus was enough to for the cells to form basal extracellular deposits, similar to drusen from AMD RPE cells. The RPE morphology and ultrastructure seen in EM images is overall consistent with CQ-induced retinopathy (Mahon et al. 2004) and notably with several models of aging RPE and general AMD-models (Ferrington et al. 2016; Yoshida et al. 2005; Yang et al. 2014; Cano et al. 2010; Golestaneh et al. 2017; Sinha et al. 2016; Zhao et al. 2011; Rakoczy et al. 2002; Shang et al. 2017). Moreover, hPSc-RPE developed from AMD patients iPS cells were shown to recapitulate similar features *in vitro*, namely drusen formation and ECM remodeling (Galloway et al. 2017).

Taken together, evidence supports the use of the proposed hESc-RPE cells as a reliable model to study lysosomal dysfunction, as key initiation event underlying age-related retinal degenerative disorders.

CHAPTER 5

Conclusion and Future Perspectives

The molecular underpinning of age-related disorders is very complex and ill defined. Mechanisms common to these diseases have been proposed as the hallmarks of aging. Specifically, aging leads to genomic instability, with telomere abrasion and epigenetic modifications, to loss of proteostasis and nutrient-sensing defects, to mitochondrial defects and cell senescence (López-Otín et al. 2013) (Figure 5.1).

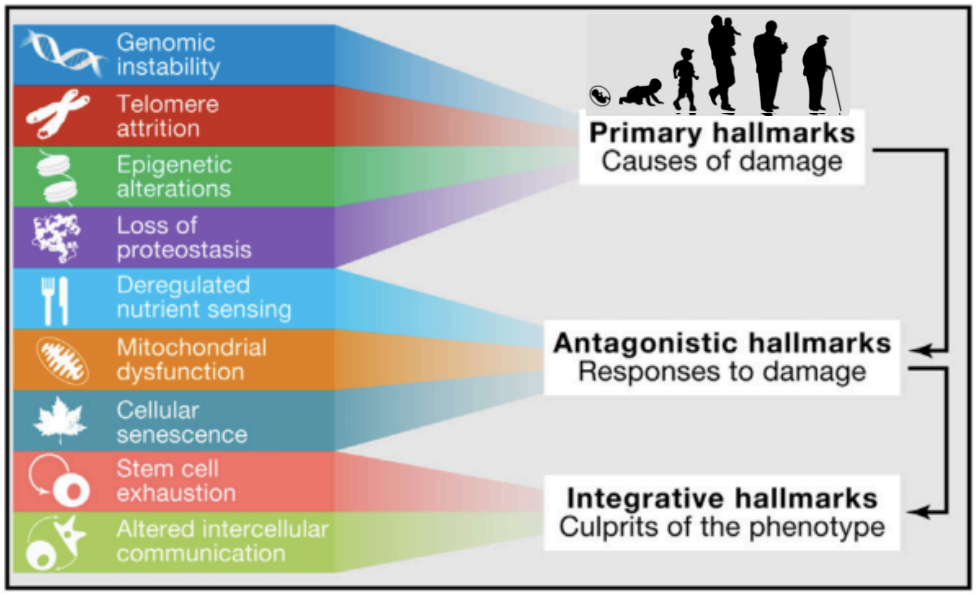

Figure 5. 1 - The hallmarks of aging functional interconnections. Adapted from (López-Otín et al. 2013).

Notably, most of these processes are in some degree dependent on lysosomal function, and on the efficient continuous recycling and replacing of cellular constituents. When this turnover is defective or loses its efficiency, for instance in the case of long-lived postmitotic cells, accumulation of "cellular waste" occurs.

The goal of the present work was to obtain an RPE model of retinal degeneration which closely recapitulates features of age-related degeneration, particularly focused on those that are common to Choroideremia and AMD.

The full complexity of the ocular unit is only recapitulated in the animal model system and genetically modified animals, such as the Chm conditional knockout mouse (Chm^{FLOX}, Tyr-Cre+), permit the manipulation of the whole visual system and an in-depth study of the whole retinal degenerative process (Wavre-Shapton et al. 2013). With this in mind, the initial experiments were aimed at establishing a cell-based model from this genetically modified mouse. However, mouse RPE precursor cells were shown to be much harder to manipulate than their human counterpart. This might have been a consequence of the improved technical skills and manipulation dexterity, but it can also reflect on intrinsic characteristics of species differentiation aspects. Also, it could be related to the fact that mouse cells went through several rounds of additional manipulation: culture of MEFs, reprogramming by viral transduction and clone selection, transduction with reporters and re-selection, continuous passaging and expansion for characterization. Throughout these processes, many things might influence the differentiation potential of the cells.

Ultimately, the use of cell-based strategies rather than animals permits a critical simplification of the system, while maintaining the cellular features which, in the case of RPE, recapitulate the *in situ* situation. In particular, cell models of disease allow a higher degree of control over experimental variables and also higher throughput. Furthermore, in this particular case, since the retinal degeneration disorders under study affect primarily the macula region, the mouse model might not be the better option.

On the other hand, whilst first experiments contemplated an already modified cell line which would recapitulate Chm features, in the case of the human ESc, after differentiation, the disease features have to be induced. This plan-adjustment allows the ultimate goal to remain the same, whereas the process is simplified, more standardized and with a higher degree of control over variables. Nevertheless, the study of specific mechanisms involved in Chm disease development were not discarded, and in fact, future projects surfaced, which foresee using human iPS cells from Chm patients and differentiate them into RPE.

For the present work, spontaneous and directed differentiation approaches of hES cells, were undertaken. While spontaneous differentiation takes around 120 days before starting the enrichment phase, this step is almost surpassed with the guided differentiation method. This happens because guided differentiation triggers all cells virtually at the same time, step by step, and thus renders higher purity at the end of the 14-day period. Consequently, the guided differentiation method takes approximately 90 days to achieve mature, pure RPE. After first passage, these cells can already be plated onto the appropriate wells destined for a certain assay; from that point on, cells take approximately two weeks to 30 days to fully regain polarization and pigmentation, typical of mature RPE, and thus to be ready for experiments.

Following differentiation experiments, characterization assays were performed, in order to demonstrate the reliability of hESc-RPE as a model of RPE. Morphologically, these cells resemble both primary RPE lines evaluated (pRPE and Lonza hRPE). hESc-RPE are able to polarize properly and develop into a monolayer, secured by tight junctions and with substantial TER, resembling other RPE lines tested, or found in literature.

Moreover, these cells express critical markers, typical of RPE, which suggest they are readily functional, at least to the same extent as primary RPE and other RPE cell lines are. In some regards, both hESc-RPE and primary RPE (pRPE and Lonza hRPE) surpass standard RPE cell lines in their RPE-likeness.

hESc-RPE actively pigment and, when passaged, suffer pigmentation dilution (as other RPE lines do), but regain their heavy dark color again, whereas most RPE lines do not re-pigment. This is a factor that should be taken into account when analyzing the outcomes of subsequent experiments. While porcine cells are moderately pigmented with fully matured melanosomes, Lonza hRPE cells are only slightly pigmented (but can be stimulated to pigment) and hESc-RPE become heavily pigmented over time. This might be because both human lines (hESc-RPE and Lonza-RPE) are more similar to fetal RPE than adult, as is the case of porcine cells.

Furthermore, hESc-RPE were evaluated for their secretion ability. While the results are preliminary and VEGF should be re-evaluated by finer techniques (such as ELISA), there is a strong indication that the cells are in fact secreting PEDF and VEGF in a polarized manner.

Under homeostatic conditions, RPE cells work as professional phagocytes, taking part in the daily visual cycle by engulfing and digesting POS. RPE cells are post-mitotic, meaning they endure proteolytic processing of an estimated billion photoreceptor disks over a 70-year lifetime(Kevany et al. 2010; Mazzoni et al. 2014; Keeling et al. 2018). For this reason, lysosomal burden and dysregulation of endocytic and autophagic cargo handling are considered crucial for retinal degeneration disorders. Age-related accumulation of POS-derived products has been proposed to occur as the result of a slower rate of POS processing, stemming from lysosomal dysfunction. In this context, the ability of RPE cells to digest POS was evaluated thoroughly. Although hESc-RPE were able to promptly process their phagocytic cargo, single-pulse experiments using primary culture RPE (porcine and human) revealed that POS may take more than one week to be fully processed. Moreover, upon continuous feedings of hESc-RPE, reminiscent rhodopsin was found to increase, suggesting accumulation of unprocessed material from one feeding to the next. Building on this notion, autofluorescence granules derived from POS lysosomal processing were found to appear following POS feedings and remain within cells for long periods of time. Emergence of autofluorescent granules is typically found in the human eye, from adulthood, and aggravated with aging and notably in retinal disease settings.

Another important feature is pigmentation. Specifically, contrary to other more established RPE cell lines such as ARPE19, D407 or hTERT-RPE01, hESc-RPE actively produce and retain their pigment. Pigmentation is another critical aspect, particularly when studying lysosomal function. This is due to the fact that melanosomes are lysosome-related, meaning the same molecular players involved in fundamental aspects of melanosome biology are shared with typical degradative lysosomes. And more importantly, pigmentary changes are often observed in disease settings (Rakoczy et al. 2002; Rimpelä et al. 2016; Juuti-Uusitalo et al. 2017; Arunkumar et al. 2018).

These two properties (autofluorescence and pigmentation) establish these RPE lines as promising models that recapitulate important clinical features, therefore useful to dissect the molecular mechanisms underlying these diseases. The fact that autofluorescence is easily detected in models of RPE, opens new avenues of research, namely using the chemically defined byproduct of POS degradation which is thought to be responsible for the autofluorescence granules, A2E. As discussed in Chapter 1, A2E is the main component of lipofuscin and it is found heavily accumulated in Stargardt's patients RPE cells (Luthert 2011; Moreno-García et al. 2018). A2E is uptaken by RPE cells and causes ill-characterized lysosomal dysfunction (Keeling et al. 2018). Because of similarities between Stargardt's early onset macular degeneration and late-onset AMD, the study of lysosomal dysfunction triggered by A2E accumulation appears as an interesting research avenue. A2E autofluorescence can be readily identified (either by microscopy or flow cytometry), namely using the herein established RPE models (data not shown). This potentiates the use of the newly established hESc-RPE cells to underpin the molecular mechanisms underlying A2E-derived lysosomal dysfunction and the importance of these processes for retinal degenerative disorders' early events.

In comparison to primary cultures, whether from human or from porcine origin, hESc-RPE offer virtually endless clonality. And, because of this potentially endless dividing-capacity of stem cells, hESc-RPE pave the way for high throughput drug screenings, aiming at restoring RPE function, particularly lysosomal function. This is imperative, taking into account the scarce sources for human RPE, but also to ensure standardization of experimental variables, by using practically the same cells from one experiment to the next. Furthermore, induced Pluripotent Stem cell-derived RPE cells from macular dystrophies' patients were recently shown to recapitulate critical features of the diseases. Such is the case of drusen formation and also the ability of these cells to modulate their extracellular matrix (ECM) constitution and turnover (Galloway et al. 2017). Still, the molecular mechanisms underlying these events have not been fully elucidated.

In an effort to explain the initial events which trigger AMD-hallmark drusen formation, CQ-based model of lysosomal dysfunction was proposed and characterized thoroughly.

Initially, viability studies and comparison between the three RPE cell lines were important to establish the range of CQ concentrations used in the following studies. Although the three RPE lines displayed different thresholds of cytotoxicity, a pattern of response was inferred: when subjected to low CQ concentrations, there was a modest cytotoxicity (increase of LDH secretion), followed by a return to normal (non-treated control) values. This first increase may be attributed to the early death of more fragile cells, which are not able to endure the insult, releasing LDH into the medium. The remaining cells, however, were shown able to withstand a low-dose CQ burden for a week.

Regarding the differences between the three RPE lines, it became obvious that pRPE is more sensitive to CQ than human RPE. This characteristic may be attributed to species inherent differences, but also to the fact that these porcine cells are adult cells, while both human RPE lines are more closely related to embryonic RPE. In fact, human RPE lines

were obtained from fetal RPE primary cultures (Lonza hRPE) and from human Embryonic Stem cells differentiation (hESc-RPE). As previously discussed, RPE cells are kept virtually unchanged throughout life, meaning that porcine cells endured a pig's lifetime of challenges, which can result from a wide range of factors, from typical light-induced oxidative stress to abnormal life-style related variables. For instance, prior to collection, porcine RPE cells exerted their phagocytic function of POS, necessary for the pig's visual function. In theory, because Lonza hRPE was collected at embryonic stage, this RPE virtually never participated in the visual process, as it was retrieved before birth. As for hESc-RPE, since it was derived through a directed differentiation approach, these cells effectively never came into contact with POS before experiments. On the one hand, the "age-related" differences of the three RPE lines add an extra level of complexity to the subsequent studies, with many new variables to consider. On the other hand, the fact that we have these three different lines allows for a deeper understanding of the general RPE biology. Specifically, our RPE systems range from a completely naïve hESc-RPE to an adult pRPE, essentially allowing us to deeply ponder every inference and more confidently extrapolate conclusions from the results.

Following the establishment of CQ dosages and stimulus timeline, experimental conditions were set. Specifically, the experimental layout consisted on daily 4h POS pulse, followed by overnight CQ treatment. At this point it is important to mention that during the course of the daily POS feeding, cells were kept in medium supplemented with 10%FBS and without CQ. This experimental setup was implemented for two reasons: 1) RPE cells' phagocytic ability relies on stimulated receptor engagement (possibly from serum-contained ligands) and also on high energy levels; for this reason, low serum/serum free RPE cultures run out of energy and cease phagocytosis and digestion; 2) in order to avoid confounding factors, such as a possible CQ-induced effect on POS uptake by the cells, CQ was added to the medium only after the 4h POS pulse; this was a way to assure the phagocytic cargo reached the lysosome and that tentatively only the degradation step was hindered. When setting up a new experimental protocol, there are many parameters that should be taken into account. On this regard, the fact that CQ regimen is stopped every day, for the duration of the POS pulse, could mean that the cells have a short time-window to partially recover from the insult. Nevertheless, this potential experimental bias was always taken into account during the discussion of results. Furthermore, CQ-induced effects were significantly different throughout time, suggesting that cells are not able recover completely, thus experiencing a chronic dysfunction.

These time-dependent responses were characterized in depth, beginning with MiT TF subcellular characterization. Overall, the results obtained in this regard indicate that CQ burden, over time, induces observable changes in MiT TFs subcellular localizations. CQ remains in the cells for long periods, even after treatment discontinuation, which may account for a cumulative effect over time. An acute overnight treatment with CQ at 5µg/mL is sufficient to cause translocation of TFEB, TFE3 and MITF to the nuclear area of the cells (Figure 4.9). After three consecutive days of continued treatment, the nuclear

localization of the TFs is even more obvious (Figure 4.10). After a week of chronic stimulation, the whole cell area is stained with these TFs (Figure 4.11). These results suggest there is potential induction of lysosomal biogenesis and of the TFs themselves, which must be confirmed, for instance through qPCR to evaluate expression of MiT-driven lysosomal genes.

Finally, crucial lysosomal functions were evaluated, in an effort to describe the lysosomal disturbance produced by CQ burden.

Impairment of phagocytic cargo processing was demonstrated by the presence of reminiscent rhodopsin granules which accumulate intracellularly, depending on CQ concentration and becoming more and more severely accumulated over time. Deficiency of cargo processing was further demonstrated, through the decline of DQ-BSA proteolytic breakdown, and consequent fluorescence decrease. The damage is not very pronounced with the acute treatment, but explicit in the continued situation, using higher CQ concentrations, and in the chronic CQ-treatment, for all concentrations used. This indicates that although the effects using low CQ dosages are less pronounced, it is a question of time until they accumulate sufficiently to cause damage. Finally, ApoE, p62 and LC3 protein levels were evaluated and shown to be disturbed upon chronic CQ treatments, in hESc-RPE and in Lonza hRPE and, in the case of LC3, in pRPE as well.

ApoE can be found in endocytic membranes and, in fact, it has been described to be involved in sorting of endocytic amyloids, within pigmented cells, to melanosomes and to exosomes (van Niel et al. 2015). In the proposed model of CQ-induced hESc-RPE degeneration, ApoE was shown to accumulate concomitantly with the increase in CQ concentration the cells were subjected to. This accumulation is rapidly induced using Baf, as shown by the acute treatments. After continued CQ treatment, ApoE accumulation is already at similar levels than those found in Baf-treated cells. And this buildup is more severe after a week-long treatment. ApoE accumulation was evaluated here only considering whole cell lysates, or imaging cells in glass coverslips. Because of the way lysates were collected, directly from the well, there is no distinction between intracellular and extracellular ApoE content, i.e. drusen-like deposits. And, in fact, the extracellular matrix content of this protein might not be enough for a prompt detection. In any case, accumulation of ApoE in this model agrees with the parallel with AMD-related retinal degeneration, where ApoE builds up in drusen deposits (Hageman et al. 2001; Wang & Neufeld 2010; Klaver et al. 1998).

p62 was found to accumulate consistently, when cells were treated with CQ for long periods of time. It is interesting to notice that, alike in the case of CatD, there seem to be different time-dependent adaptations. Specifically, there is initial accumulation of the protein, in the acute treatment, followed by partial resolution, after three days of continued treatment and, finally, the cells can no longer cope with the insult and, in the chronic situation, there is strong accumulation again. It is worth mentioning that it is not easy to probe p62 in non-treated cells, by western blot, as basal levels are low; in fact, in some cases, the only readily visible band is that of Baf-treated cells. When processing images to

quantify, this should be taken into account, to avoid over interpretation of results. Still, in CQ-chronically-treated cells, p62 is readily visible, with a progressive increase, depending on CQ concentration.

Furthermore, in order to determine LC3 and thus (auto)phagosome turnover, the ratio of lipidated to non-lipidated forms was evaluated. According to established guidelines, the total amount of LC3 II is directly correlated to the number of autophagosomes that will fuse with the lysosome for degradation. Still, to evaluate autophagic flux at a given point, each of the control situations should be considered and established as boundaries (Mizushima & Yoshimori 2007). In the acute situation, the blots suggest that CQ causes an impairment of autophagy clearance, with increase of LC3 II. In the case of POS-fed cells, even though there is also, perhaps, LC3-associated phagocytosis-cargo, it seems to be readily processed instead of accumulating as LC3 II (auto)phagosomes. In accordance to p62 findings, at the third-day time point of CQ-treatment, LC3 II levels are lower, at times hard to detect. At the continued time point, fewer membranes were measured precisely because detection was difficult. This indicates that the levels are low, but also stresses the need to optimize the protocol and repeat the experiments. Still, at the seventh-day time point, there is a clear accumulation of LC3 II, suggesting autophagy blockade, consistent with p62 findings.

Accumulation of all these different types of cargo may be attributed to proteases malfunction and, regarding this aspect, CatD proteolytic activity and protein levels were assessed. CatD was shown to be affected by the acute CQ treatment and, despite a compensatory response of overexpression, was shown not to be fully processed. When CatD is synthesized, it undergoes numerous proteolytic cleavages. The 52 kDa procathepsin is the result of the initial removal of a signal peptide. This procathepsin is targeted to lysosomes where it is cleaved into the 48 kDa single-chain molecule and then cleaved again into the mature two-chain (Laurent-Matha et al. 2006). CQ could, therefore, be impairing correct trafficking of procathepsin and delivery into the lysosome or it could inhibit proteolytic activity of enzymes responsible for procathepsin processing, within the lysosome. Both the 48 kDa procathepsin and the mature 34 kDa forms are reduced after one week of CQ treatment, suggesting not only impairment of single-chain molecule cleavage to produce the mature form, but also disruption of the previous step where the 52 kDa form is cleaved into the 48 kDa form. Regarding the role of CatB and CatL in the later steps of CatD processing, these two cysteine proteases are not involved in the first steps of precursor processing (Laurent-Matha et al. 2006). Furthermore, CatD processing has been described to be independent of its own catalytic function, which indicates CQ is effectively disrupting the activity of other proteases, responsible for initial CatD processing events. It is interesting to note that CatD mutations are sufficient to cause retinal degeneration (Zhang et al. 2005). Specifically, CatD mutant animal models accumulate undigested material, most notably, POS, and develop degeneration of the RPE, similarly to AMD, presenting drusen-like deposits (Rakoczy et al. 1996; Rakoczy et al. 2002; Myllykangas et al. 2005). Because CQ produced an effect regarding CatD maturation, it would be interesting to

modulate this protease alone and verify whether the other CQ-induced could be traced back to the inactive CatD. Because the present work demonstrated the possibility of studying CatD maturation impairment in the cell-based RPE models, there are now plans being put in place, in that regard. Specifically, CatD dominant negative mutants are now being developed, in an effort to deepen our understanding of the molecular mechanisms behind this specific trigger for RPE degeneration (data not shown).

Coming back to the present study, CatB and CatL proteolytic activity assessment results may sound counter-intuitive considering the rhodopsin and DQ-BSA proteolytic processing results. However, these cathepsins might not be the main players in these substrates degradation. Furthermore, it is worth mentioning that cathepsins can be permissive in their target amino acid sequence and recognize substrates of other proteases. CQ causes a raise of lysosomal pH, sufficient to disrupt some proteases' activity (for instance CatD), but this was shown not to be the case of CatB nor CatL. In addition, the dogma in the field is that LT's fluorescence is reduced in the presence of lysosomotropic compounds (such as CQ), but in fact the present study shows contradictory results to that statement. This was also the case of a recent study (using RPE cells), which reports that upon prolonged CQ burden there is actually increase of LT and of Magic Red fluorescence. In fact, this study includes results showing lower LT fluorescence levels upon short (30min-1h) treatments with lysosomotropic drugs (including CQ) and subsequent increase of LT fluorescence detected in cells treated for longer periods of time (4h-24h) (Lu et al. 2017). These are consistent with the results presented herein, obtained using hESc-RPE. The difference is that, in the present study, 24h incubation is considered as an acute rather than chronic stimulation, in which case cells were burdened for one week.

Contrary to what was expected, LT fluorescence increases upon CQ treatment, which lowers lysosomal pH. This is perplexing because in fact, both LT and CQ work by accumulating within acidic organelles. However, LT's retention mechanism in the membranes of these organelles is not yet fully understood and although this dye is widely used to label generic acidic vesicles, the manufacturer reports that it exhibits fluorescence "largely independent of pH" (Invitrogen 2007).

Lysosomal pH is a difficult property to measure because lysosomes are intrinsically dynamic and, for the V-ATPase to pump protons into the lysosomal lumen, a gradient is required, which can be rapidly dissipated in dying cells (Guha, Coffey, et al. 2014). For this reason, lysosomal pH should be assessed in living cells. Still, reliable pH reporters are hard to come by and more complex techniques are difficult to implement in a standardized manner. For instance, it is possible to assess pH through ratiometric measurements of pH sensitive to pH insensitive fluorophores. Fluorescein, Oregon Green and rhodamine derivates, for instance, can be used to this effect. Yet, these techniques require extensive calibration procedures, which may not always be straightforward (Kissing et al. 2017). Other methods, such as the DAMP assay, which consists on labeling acidic organelles with DAMP (3-(2,4-dini- troanilino)-30-amino-N-methyldipropylamine) and fixing samples for

electron microscopy, could be used but still pose drawbacks similar to those of LT (Kissing et al. 2017).

The use of LT is sometimes controversial; thus analysis of the results should always be subjected to a detailed critique for proper clarification. Firstly, detection of LT's fluorescence conveys either an increase/decrease of pH or a change in the number or area of labeled structures that occupy the cells. This includes smaller to swollen lysosomes and also few lysosomes to cytoplasm-filled cells variations (Guha, Coffey, et al. 2014). For this reason, LT is not considered the most sensitive probe and, particularly in flow cytometry experiments, data are harder to interpret. Whenever using LT, it is important to keep in mind that it is sensitive to a relatively high range of pH. In addition, it accumulates with time within those vesicles and can itself raise the organelle's pH. For this reason, low concentrations and short pulse periods should be implemented, to prevent unwanted effects. Specifically regarding the presented experiments, LT was added only before signal acquisition, thus should represent relatively low pH compartments (not exclusively lysosomes) at that time.

A crucial aspect of the analysis is the pigmentation confounding factor. Although it is expected that cells treated in the same manner will behave the same, this is not always the case. In fact, as shown prior, hESc-RPE are continuously pigmenting, even more so when they are subjected to CQ or Baf treatments. This is to be expected, given the role of MiT TFs in pigmentation and also the role of the V-ATPase and lysosomal pH in their regulation and *vice-versa* (Napolitano & Ballabio 2016). For this reason, in order to confirm the results obtained, these experiments must be repeated. Nevertheless, in this case, pigmentation would, in theory, quench the fluorescence signal. Even if there is more pigmentation in cells treated with CQ, LT fluorescence still increases. This excludes fluorescence-quenching as a confounding factor in this case, and reaffirms a CQ-mediated upsurge (and wider distribution) of labeled vesicles.

Finally, lysosomes are known to fuse with the plasma membrane, thereby releasing their content through a processed termed lysosomal exocytosis. This property was initially attributed to professional secretory cells with specialized lysosome-related organelles. However, unspecialized cells are also able to secrete their lysosomal contents, upon stimulation. The molecular machinery required for lysosomal exocytosis includes SNAREs, Ca^{2+} sensors and Rab proteins, among others (Blott & Griffiths 2002). Additionally, autophagy-related proteins have been associated with polarized secretion of lysosomes (DeSelm et al. 2011). Because lysosomal positioning is tightly regulated and relative to their intraluminal pH, lysosomal exocytosis was evaluated here. The reasoning behind these experiments lies with the idea of different lysosomal pools exerting specific functions within the cell, dependent on both their position and luminal pH (Cabukusta & Neefjes 2018; Korolchuk et al. 2011; Johnson et al. 2016). As such, less acidic lysosomes would stay at the cell membrane periphery, possibly secreting their content, and overall regulating extracellular exchange of material, important namely for ECM remodeling. The experiments presented herein support that idea. In fact lysosomal exocytosis was found to

occur, towards the basal side, after acute CQ insult of hESc-RPE cells. Furthermore, consistent with this line of thought, extracellular basal deposits were found in pRPE cells, upon acute CQ treatment.

Overall, throughout this work, several aspects of lysosomal biology were shown perturbed by overburden (Table IV).

Table IV: Summary of findings regarding the hESc-RPE CQ-induced lysosomal dysfunction model.

	Summary of Findings		
	Acute CQ Overnight	Continued CQ three days	Chronic CQ a week
MiT TFs	partial nuclear translocation	evident nuclear translocation	nucleus + cytoplasm
Pigmentation	darker after Baf or high [CQ]	darker after Baf or high [CQ]	darker according to [CQ]
Rhodopsin Processing	no change except for high [CQ]	late phagosome accumulation	early and late phagosome accumulation
Degradative Ability (DQ-BSA)	no significant change	proteolytic impairment	severe degradative impairment
CatB/CatL activity	increase/wider distribution with [CQ]	increase/wider distribution with [CQ]	increase with [CQ]
CatD activity/protein levels	decreased activity; procathepsin upregulation	partial recovery	increased activity; CatD maturation impairment
Lysosomal Acidity (LysoTracker)	increase/wider distribution with [CQ]	increase/wider distribution with [CQ]	increase with [CQ]
Endocytic Turnover (ApoE)	no significant change	accumulation with [CQ]	accumulation with [CQ]
Autophagy Impairment (p62/LC3)	accumulation of p62 and LC3 II	partial recovery	severe accumulation of p62 and LC3 II
Lysosome Exocytosis	mostly basal exocytosis	apical and basal exocytosis	apical and basal exocytosis over Baf-treatment

More importantly, clinically relevant features of AMD, namely autofluorescence, pigmentation differences and drusen-like deposits were found in the presented cell-based models of RPE (Figure 5.2).

Concerning the CQ model specifically, seemingly conflicting results arose. If, on the one hand, lysosomal dysfunction was shown by the accumulation of undegraded cargo and CatD misprocessing, on the other hand, MiT TFs nuclear translocation also occurred, as a result of CQ treatments. TFEB in particular is a well-known modulator of lysosomal function and stimulation of its function has been proposed to resolve lysosomal storage diseases (Spampanato et al. 2013; Decressac et al. 2013; Polito et al. 2014; Tsunemi et al. 2012), as discussed in Chapter 1. Therefore, MiT subcellular localization dysregulation after prolonged CQ treatments is puzzling. Nevertheless, TFEB was shown to become abnormally activated in the context of LSDs (Marco Sardiello et al. 2009), which may conflict with the idea of using it as a therapeutic agent.

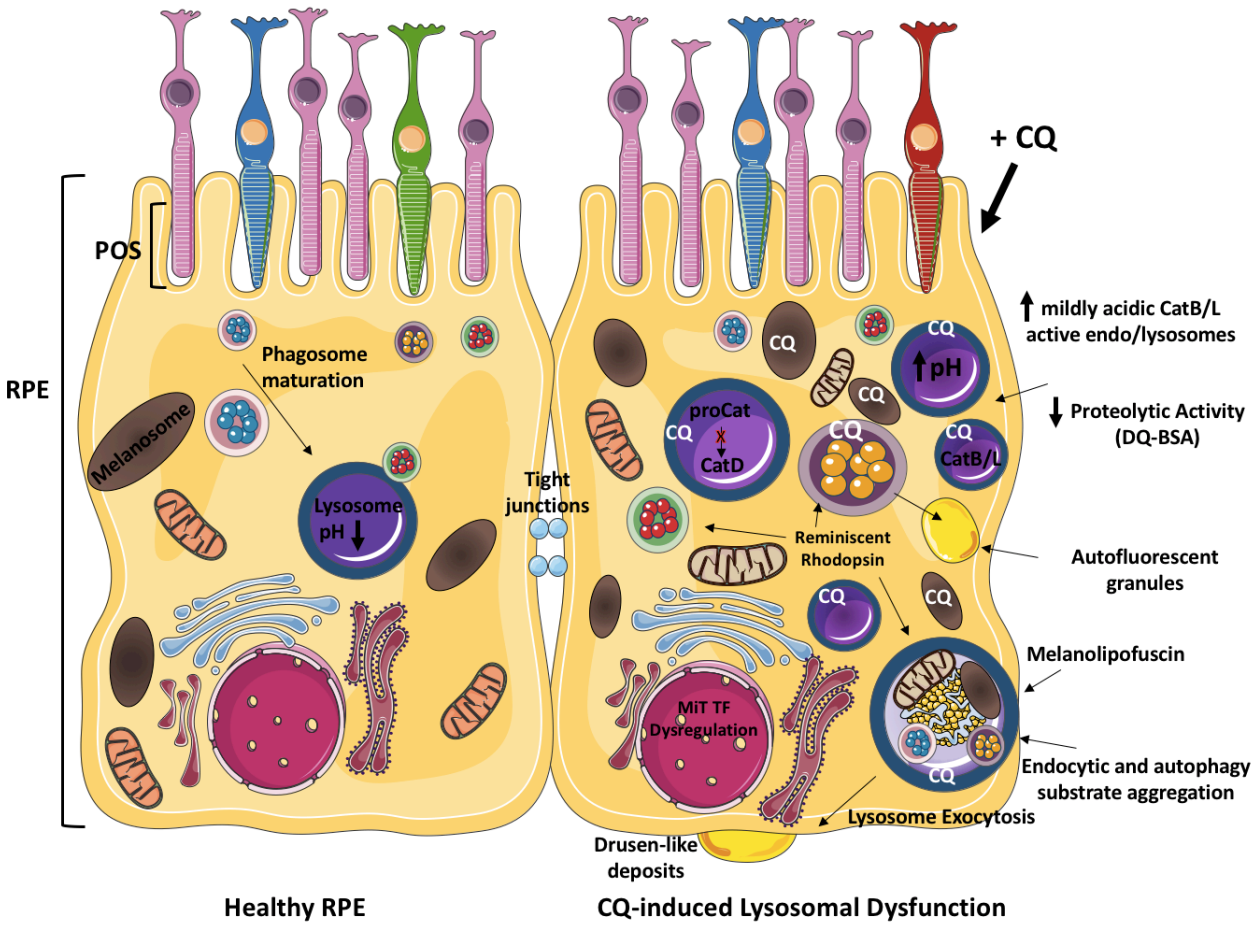

Figure 5. 2 - RPE model of chloroquine-induced lysosomal dysfunction. Chloroquine accumulates in mildly acidic compartments; MiT transcription factors translocate to the nucleus; Phagocytic, endocytic and autophagy-cargo accumulate; Lysotracker-labeled CatB and CatL-active lysosomes accumulate; CatD processing is impaired; Lysosomal exocytosis occurs and basal extracellular deposits are formed.

Ultimately, the present work confirmed the complex regulation of lysosome biology, and highlighted some undetermined mechanisms, now under study.

Perhaps in the CQ model the lysosomal dysfunction is too complex to easily dissect. Still, from these assays, it was possible to find isolated targets, altered as a consequence of CQ treatment, which by themselves are interesting to dissect. From this point on, a more targeted approach may be undertaken, specifically to dissect the roles of MiT TFs and CatD in phagosomal processing, using the novel now established cell-based models of RPE.

Looking back to the very beginning of the PhD, a significant amount of effort was adjudicated to construct a pathway from RPE studies done in mice and in mouse iPS cells up to studies in reliable human RPE cells, namely those derived from stem cells, but also in the Lonza hRPE. In particular, state of the art research projects came out from these first experiments and are paving the way into industry and pre-clinical settings. Specifically, there are projects underway, aiming at developing a complex *in vitro* system recapitulating not only the RPE, but also the Bruch's membrane and the choroidal vascular network and also collaborations based on the use of these cell-based models to test pharmaceutical

components to reverse and/or prevent AMD. Overall, the present work opened up a whole new perspective concerning the work currently being developed in the lab. In particular, several new lines of research came out of it, with promising targets of study and with reliable new models with which to dissect them.

CHAPTER 6

References

Ablonczy, Z. & Crosson, C.E., 2007. VEGF modulation of retinal pigment epithelium resistance. *Experimental Eye Research*, 85(6), pp.762–771.

Ablonczy, Z., Dahrouj, M. & Marneros, A.G., 2014. Progressive dysfunction of the retinal pigment epithelium and retina due to increased VEGF-A levels. *FASEB Journal*, 28(5), pp.2369–2379.

Aboul Naga, S.H. et al., 2015. Intracellular pathways following uptake of bevacizumab in RPE cells. *Experimental Eye Research*, 131, pp.29–41.

Al-Bari, A.A., 2015. Chloroquine analogues in drug discovery: new directions of uses, mechanisms of actions and toxic manifestations from malaria to multifarious diseases. *J Antimicrob Chemother*, 70(February 2015), pp.1608–1621.

Al-Zamil, W. & Yassin, S., 2017. Recent developments in age-related macular degeneration: a review. *Clinical Interventions in Aging*, Volume 12, pp.1313–1330.

Anderson, D.M.G. et al., 2017. Bis(monoacylglycero)phosphate lipids in the retinal pigment epithelium implicate lysosomal/endosomal dysfunction in a model of Stargardt disease and human retinas. *Scientific Reports*, 7(1), p.17352.

Andrews, N.W., 2000. Regulated secretion of conventional lysosomes. *Trends in Cell Biology*, 10(8), pp.316–321.

aoa.org, 2017. Qué es la DMAE | Asociación Mácula Retina. Available at: https://www.macula-retina.es/que-es-la-dmae/.

Appelqvist, H. et al., 2013. The lysosome: From waste bag to potential therapeutic target. *Journal of Molecular Cell Biology*, 5(4), pp.214–226.

Arunkumar, R. et al., 2018. What do we know about the macular pigment in AMD: the past, the present, and the future. *Eye (Basingstoke)*.

Astrid Limb, The eye and stem cells: the path to treating blindness | Eurostemcell. Available at: https://www.eurostemcell.org/eye-and-stem-cells-path-treating-blindness.

Ballabio, A., 2016. The awesome lysosome. *EMBO Molecular Medicine*, 8(2), pp.73–76.

Basagiannis, D. & Christoforidis, S., 2016. Constitutive endocytosis of VEGFR2 protects the receptor against shedding. *Journal of Biological Chemistry*, 291(32), pp.16892–16903.

Beckel, J.M. et al., 2018. Stimulation of TLR3 triggers release of lysosomal ATP in astrocytes and epithelial cells that requires TRPML1 channels. *Scientific Reports*, 8(1), pp.1–14.

Behnia, R. & Munro, S., 2005. Organelle identity and the signposts for membrane traffic. *Nature*, 438(7068), pp.597–604.

Benes, P., Vetvicka, V. & Fusek, M., 2008. Cathepsin D-Many functions of one aspartic protease. *Critical Reviews in Oncology/Hematology*, 68(1), pp.12–28.

Bergstrom, C. & Garcia-Valenzuela, E., 2009. Progressive Optical Coherence Tomography Deterioration in Chloroquine Maculopathy. *Retinal Cases & Brief Reports*, 3(2), pp.183–185.

Bharti, K. et al., 2012. A regulatory loop involving PAX6, MITF, and WNT signaling controls retinal pigment epithelium development. *PLoS Genetics*, 8(7).

Bharti, K. et al., 2006. The other pigment cell: Specification and development of the pigmented epithelium of the vertebrate eye. *Pigment Cell Research*, 19(5), pp.380–394.

Bharti, K., Miller, S.S. & Arnheiter, H., 2010. The new paradigm: retinal pigment epithelium cells generated from embryonic or induced pluripotent stem cells. *Pigment cell & melanoma research*, 24(1), pp.21–34.

Bhutto, I. & Lutty, G., 2012. Understanding age-related macular degeneration (AMD): Relationships between the photoreceptor/retinal pigment epithelium/Bruch's membrane/choriocapillaris complex. *Molecular Aspects of Medicine*, 33(4), pp.295–317.

Biasutto, L. et al., 2013. Retinal pigment epithelium (RPE) exosomes contain signaling phosphoproteins affected by oxidative stress. *Experimental Cell Research*, 319(13), pp.2113–2123.

Biccas Neto, L. & Mesquita, A.S. de, 2009. Toxic maculopathy caused by antimalarial drugs: detection using spectral domain OCT: case reports. *Arquivos brasileiros de oftalmologia*, 72(5), pp.710–714.

Blott, E.J. & Griffiths, G.M., 2002. Secretory Lysosomes. *Nature Reviews Molecular Cell Biology*, 3(2), pp.122–131.

Boulton, M. et al., 1994. Regional variation and age-related changes of lysosomal enzymes in the human retinal pigment epithelium. *The British journal of ophthalmology*, 78(2), pp.125–9.

Boulton, M.E., 2014. Studying melanin and lipofuscin in RPE cell culture models. *Experimental Eye Research*, 126, pp.61–67.

Bourdenx, M. et al., 2016. Nanoparticles restore lysosomal acidification defects: Implications for Parkinson and other lysosomal-related diseases. *Autophagy*, 12(3), pp.472–483.

Bourdenx, M. & Dehay, B., 2016. What lysosomes actually tell us about Parkinson's disease? *Ageing Research Reviews*, 32, pp.140–149.

Brandl, C. et al., 2014. In-depth characterisation of retinal pigment epithelium (RPE) cells derived from human induced pluripotent stem cells (hiPSC). *NeuroMolecular Medicine*, 16(3), pp.551–564.

Bright, N.A., Davis, L.J. & Luzio, J.P., 2016. Endolysosomes Are the Principal Intracellular Sites of Acid Hydrolase Activity. *Current Biology*, 26(17), pp.2233–2245.

Bright, N. a et al., 1997. Dense core lysosomes can fuse with late endosomes and are re-formed from the resultant hybrid organelles. *Journal of cell science*, 110 (Pt 1, pp.2027–2040.

Brown, W.J., Goodhouse, J. & Farquhar, M.G., 1986. Mannose-6-phosphate receptors for lysosomal enzymes cycle between the Golgi complex and endosomes. *Journal of Cell Biology*, 103(4), pp.1235–1247.

Buchholz, D.E. et al., 2013. Rapid and Efficient Directed Differentiation of Human Pluripotent Stem Cells Into Retinal Pigmented Epithelium. *STEM CELLS Translational Medicine*, 2(5), pp.384–393.

Burgoyne, T., Meschede, I.P. & Futter, C.E., 2016. New light on photoreceptor renewal. *Cell Cycle*, 15(11), pp.1389–1390.

Cabukusta, B. & Neefjes, J., 2018. Mechanisms of Lysosomal Positioning and Movement. *Traffic*.

Cano, M. et al., 2010. Cigarette smoking, oxidative stress, the anti-oxidant response through Nrf2 signaling, and Age-related Macular Degeneration. *Vision Research*, 50(7), pp.652–664.

Carmona-Gutierrez, D. et al., 2016. The crucial impact of lysosomes in aging and longevity. *Ageing Research Reviews*, 32, pp.2–12.

Carr, A.-J. et al., 2009. Molecular characterization and functional analysis of phagocytosis by human embryonic stem cell-derived RPE cells using a novel human retinal assay. *Molecular vision*, 15(January), pp.283–95.

Carr, A.J. et al., 2009. Protective effects of human iPS-derived retinal pigment epithelium cell transplantation in the retinal dystrophic rat. *PLoS ONE*, 4(12).

Carr, A.J.F. et al., 2013. Development of human embryonic stem cell therapies for age-related macular degeneration. *Trends in Neurosciences*, 36(7), pp.385–395.

Chang, J., Lee, S. & Blackstone, C., 2014. Spastic paraplegia proteins spastizin and spatacsin mediate autophagic lysosome reformation. *Journal of Clinical Investigation*, 124(12), pp.5249–5262.

Chen, C.S. et al., 2000. Probing the cathepsin D using a BODIPY FL-pepstatin A: Applications in fluorescence polarization and microscopy. *Journal of Biochemical and Biophysical Methods*, 42(3), pp.137–151.

Chen, H. et al., 2009. Dysfunction of the retinal pigment epithelium with age: Increased iron decreases phagocytosis and lysosomal activity. *Investigative Ophthalmology and Visual Science*, 50(4), pp.1895–1902.

Chen, M. et al., 2008. Characterization of a Spontaneous Mouse Retinal Pigment Epithelial Cell Line B6-RPE07. *Investigative Opthalmology & Visual Science*, 49(8), p.3699.

Chen, P.M., Gombart, Z.J. & Chen, J.W., 2011. Chloroquine treatment of ARPE-19 cells leads to lysosome dilation and intracellular lipid accumulation: Possible implications of lysosomal dysfunction in macular degeneration. *Cell and Bioscience*, 1(1), pp.1–10.

Choy, C.H. et al., 2018. Lysosome enlargement during inhibition of the lipid kinase PIKfyve proceeds through lysosome coalescence. *Journal of Cell Science*, p.jcs.213587.

Coffey, E.E. et al., 2014. Lysosomal alkalization and dysfunction in human fibroblasts with the alzheimer's disease-linked presenilin 1 A246E mutation can be reversed

with cAMP. *Neuroscience*, 263, pp.111–124.

Congdon, N., 2004. Causes and Prevalence of Visual Impairment among Adults in the United States. *Archives of Ophthalmology*, 122(4), pp.477–485.

Dahrouj, M. et al., 2015. Receptor mediated disruption of retinal pigment epithelium function in acute glycated-albumin exposure. *Experimental Eye Research*, 137, pp.50–56.

Dahrouj, M. et al., 2014. Vascular endothelial growth factor modulates the function of the retinal pigment epithelium in vivo. *Investigative Ophthalmology & Visual Science*, 55(4), p.IOVS-13-13334.

David E. Buchholz, S.T.H., 2009. Derivation of Functional Retinal Pigmented Epithelium from Induced. *Stem Cells*, 27, pp.2427–2434.

Davidson, S.M. & Vander Heiden, M.G., 2017. Critical Functions of the Lysosome in Cancer Biology. *Annual Review of Pharmacology and Toxicology*, 57(1), p.annurev-pharmtox-010715-103101.

Decressac, M. et al., 2013. TFEB-mediated autophagy rescues midbrain dopamine neurons from -synuclein toxicity. *Proceedings of the National Academy of Sciences*, 110(19), pp.E1817–E1826.

Dehay, B. et al., 2013. Lysosomal impairment in Parkinson's disease. *Movement Disorders*, 28(6), pp.725–732.

Delevoye, C. et al., 2011. Biogenesis of melanosomes - the chessboard of pigmentation. *Medecine sciences : M/S*, 27(2), pp.153–62.

DeSelm, C.J. et al., 2011. Autophagy Proteins Regulate the Secretory Component of Osteoclastic Bone Resorption. *Developmental Cell*, 21(5), pp.966–974.

Durchfort, N. et al., 2012. The enlarged lysosomes in beige j cells result from decreased lysosome fission and not increased lysosome fusion. *Traffic*, 13(1), pp.108–119.

de Duve, C., 2005. The lysosome turns fifty. *Nature cell biology*, 7(9), pp.847–9.

De Duve, C. et al., 1974. Lysosomotropic agents. *Biochemical Pharmacology*, 23(18), pp.2495–2531.

Eiraku, M. & Sasai, Y., 2012. Mouse embryonic stem cell culture for generation of three-dimensional retinal and cortical tissues. *Nature protocols*, 7(1), pp.69–79.

Elkin, S.R., Lakoduk, A.M. & Schmid, S.L., 2016. Endocytic pathways and endosomal trafficking: a primer. *Wiener Medizinische Wochenschrift*, 166(7–8), pp.196–204.

Esteve-Rudd, J. et al., 2014. In Vivo and in Vitro Monitoring of Phagosome Maturation in Retinal Pigment Epithelium Cells. In Springer, New York, NY, pp. 85–90.

Evans, J.R., 2001. Risk Factors for age-related macular degeneration. *Progress in Retinal and Eye Research*, 20(2), pp.227–253.

Fearnley, G.W. et al., 2016. VEGF-A isoforms program differential VEGFR2 signal transduction, trafficking and proteolysis. *Biology open*, 5(5), pp.571–83.

Feeney-Burns, L., Hilderbrand, E.S. & Eldridge, S., 1984. Aging human RPE: Morphometric analysis of macular, equatorial, and peripheral cells. *Investigative Ophthalmology and Visual Science*, 25(2), pp.195–200.

Ferguson, T.A. & Green, D.R., 2014. Autophagy and phagocytosis converge for better vision. *Autophagy*, 10(1), pp.165–167.

Ferrington, D.A., Sinha, D. & Kaarniranta, K., 2016. Defects in retinal pigment

epithelial cell proteolysis and the pathology associated with age-related macular degeneration. *Progress in Retinal and Eye Research*, 51, pp.69–89.

Florey, O. et al., 2015. V-ATPase and osmotic imbalances activate endolysosomal LC3 lipidation. *Autophagy*, 11(1), pp.88–99.

Folts, C.J. et al., 2016. Lysosomal Re-acidification Prevents Lysosphingolipid-Induced Lysosomal Impairment and Cellular Toxicity. *PLoS Biology*, 14(12), pp.1–39.

Ford, K.M. et al., 2011. Expression and role of VEGF in the adult retinal pigment epithelium. *Investigative Ophthalmology and Visual Science*, 52(13), pp.9478–9487.

Forest, D.L., Johnson, L. V & Clegg, D.O., 2015. Cellular models and therapies for age-related macular degeneration. *Disease models & mechanisms*, 8(5), pp.421–427.

Frost, L.S. et al., 2015. The Contribution of Melanoregulin to Microtubule-Associated Protein 1 Light Chain 3 (LC3) Associated Phagocytosis in Retinal Pigment Epithelium. *Molecular Neurobiology*, 52(3), pp.1135–1151.

Frost, L.S., Mitchell, C.H. & Boesze-Battaglia, K., 2014. Autophagy in the eye: Implications for ocular cell health. *Experimental Eye Research*, 124, pp.56–66.

Fuhrmann, S., 2010. Eye morphogenesis and patterning of the optic vesicle. *Current topics in developmental biology*, 93, pp.61–84.

Fuhrmann, S., Zou, C. & Levine, E.M., 2014. Retinal pigment epithelium development, plasticity, and tissue homeostasis. *Experimental Eye Research*, 123, pp.141–150.

Fung, A.E., Samy, C.N. & Rosenfeld, P.J., 2007. Optical coherence tomography findings in hydroxychloroquine and chloroquine-associated maculopathy. *Retinal cases & brief reports*, 1(3), pp.128–130.

Galloway, C.A. et al., 2017. Drusen in patient-derived hiPSC-RPE models of macular dystrophies. *Proceedings of the National Academy of Sciences*, p.201710430.

Galluzzi, L. et al., 2017. Molecular definitions of autophagy and related processes. *The EMBO Journal*, 36(13), pp.1811–1836.

Geisen, P. et al., 2006. Characterization of barrier properties and inducible VEGF expression of several types of retinal pigment epithelium in medium-term culture. *Current Eye Research*, 31(9), pp.739–748.

Goldman, S.D.B. & Krise, J.P., 2010. Niemann-Pick C1 functions independently of Niemann-Pick C2 in the initial stage of retrograde transport of membrane-impermeable lysosomal cargo. *Journal of Biological Chemistry*, 285(7), pp.4983–4994.

Golestaneh, N. et al., 2017. Dysfunctional autophagy in RPE, a contributing factor in age-related macular degeneration. *Cell Death and Disease*, 8(1), p.e2537.

Gonzalez-Cordero, A. et al., 2013. Photoreceptor precursors derived from three-dimensional embryonic stem cell cultures integrate and mature within adult degenerate retina. *Nat Biotechnol*, 31(8), pp.741–747.

Gross, A.K. & Bales, K.L., 2015. Aberrant protein trafficking in retinal degenerations: The initial phase of retinal remodeling. *Experimental eye research*.

Guerrin, M. et al., 1995. VasculotropinNascular Endothelial Growth Factor Is an Autocrine Growth Factor for Human Retinal Pigment Epithelial Cells Cultured In Vitro. *Journal of cellular physiology*, 394(2), pp.385–394.

Guha, S., Coffey, E.E., et al., 2014. Approaches for detecting lysosomal alkalinization

and impaired degradation in fresh and cultured RPE cells: Evidence for a role in retinal degenerations. *Experimental Eye Research*, 126, pp.68–76.

Guha, S. et al., 2013. Lysosomal alkalinization, lipid oxidation, and reduced phagosome clearance triggered by activation of the P2X7 receptor. *FASEB Journal*, 27(11), pp.4500–4509.

Guha, S., Liu, J., et al., 2014. Retinal Degenerative Diseases. , 854, pp.105–111.

Guha, S. et al., 2012. Stimulation of the D5 dopamine receptor acidifies the lysosomal pH of retinal pigmented epithelial cells and decreases accumulation of autofluorescent photoreceptor debris. *Journal of Neurochemistry*, 122(4), pp.823–833.

Hageman, G.S. et al., 1995. *Age-Related Macular Degeneration (AMD)*, University of Utah Health Sciences Center.

Hageman, G.S. et al., 2001. An integrated hypothesis that considers drusen as biomarkers of immune-mediated processes at the RPE-Bruch's membrane interface in aging and age-related macular degeneration. *Progress in Retinal and Eye Research*, 20(6), pp.705–732.

Halder, G., Callaerts, P. & Gehring, W.J., 1995. New perspectives on eye evolution. *Current Opinion in Genetics and Development*, 5(5), pp.602–609.

Hamdi, H.K. & Kenney, C., 2003. AGE-RELATED MACULAR DEGENERATION: A NEW VIEWPOINT. *Frontiers in Bioscience*, 8, pp.305–314.

Haruta, M. et al., 2004. In Vitro and In Vivo Characterization of Pigment Epithelial Cells Differentiated from Primate Embryonic Stem Cells. *Investigative Opthalmology & Visual Science*, 45(3), p.1020.

Hirami, Y. et al., 2009. Generation of retinal cells from mouse and human induced pluripotent stem cells. *Neuroscience Letters*, 458(3), pp.126–131.

Holz, F.G. et al., 2014. Fundus autofluorescence imaging in dry AMD: 2014 jules gonin lecture of the retina research foundation. *Graefe's Archive for Clinical and Experimental Ophthalmology*, 253(1), pp.7–16.

Hombrebueno, J.R. et al., 2014. Intravitreal Injection of Normal Saline Induces Retinal Degeneration in the C57BL/6J Mouse. *Translational Vision Science & Technology*, 3(2), p.3.

Housset, M. et al., 2013. Loss of Otx2 in the adult retina disrupts retinal pigment epithelium function, causing photoreceptor degeneration. *The Journal of neuroscience : the official journal of the Society for Neuroscience*, 33(24), pp.9890–904.

Hughes, A.L. & Gottschling, D.E., 2012. An early age increase in vacuolar pH limits mitochondrial function and lifespan in yeast. *Nature*, 492(7428), pp.261–265.

Huotari, J. & Helenius, A., 2011. Endosome maturation. *EMBO Journal*, 30(17), pp.3481–3500.

Huss, M. & Wieczorek, H., 2009. Inhibitors of V-ATPases: old and new players. *Journal of Experimental Biology*, 212(3), pp.341–346.

Idelson, M. et al., 2009. Directed Differentiation of Human Embryonic Stem Cells into Functional Retinal Pigment Epithelium Cells. *Cell Stem Cell*, 5(4), pp.396–408.

ImmunoChemistryTechnologies, 2002. Magic Red ™ Caspase Detection Kit. *Immunochemistry*, 7, pp.3–6.

Invitrogen, 2007. LysoTracker® and LysoSensor™ Probes. , pp.1–5.

Ivanina, T.A. et al., 1983. Ultrastructural alterations in rat and cat retina and pigment epithelium induced by chloroquine. *Graefe's archive for clinical and experimental ophthalmology = Albrecht von Graefes Archiv für klinische und experimentelle Ophthalmologie*, 220(1), pp.32–8.

Jin, Z.-B. et al., 2012. Integration-Free Induced Pluripotent Stem Cells Derived from Retinitis Pigmentosa Patient for Disease Modeling. *STEM CELLS Translational Medicine*, 1(6), pp.503–509.

Johnson, D.E. et al., 2016. The position of lysosomes within the cell determines their luminal pH. *Journal of Cell Biology*, 212(6), pp.677–692.

de Jong, P.T.V.M., 2006. Age-Related Macular Degeneration. *N Eng J Med*, 355(14), pp.1474–1485.

Jopling, H.M. et al., 2014. Endosome-to-Plasma Membrane Recycling of VEGFR2 Receptor Tyrosine Kinase Regulates Endothelial Function and Blood Vessel Formation. *Cells*, 3(2), pp.363–85.

Jopling, H.M. et al., 2009. Rab GTPase regulation of VEGFR2 trafficking and signaling in endothelial cells. *Arteriosclerosis, Thrombosis, and Vascular Biology*, 29(7), pp.1119–1124.

Juuti-Uusitalo, K. et al., 2017. Autophagy regulates proteasome inhibitor-induced pigmentation in human embryonic stem cell-derived retinal pigment epithelial cells. *International Journal of Molecular Sciences*, 18(5), p.1089.

Kamao, H. et al., 2014. Characterization of human induced pluripotent stem cell-derived retinal pigment epithelium cell sheets aiming for clinical application. *Stem Cell Reports*, 2(2), pp.205–218.

Kami, J. et al., 2008. Inhibition of choroidal neovascularization by blocking vascular endothelial growth factor receptor tyrosine kinase. *Japanese Journal of Ophthalmology*, 52(2), pp.91–98.

Kaufmann, A.M. & Krise, J.P., 2008. Niemann-Pick C1 functions in regulating lysosomal amine content. *Journal of Biological Chemistry*, 283(36), pp.24584–24593.

Kawasaki, H. et al., 2002. Generation of dopaminergic neurons and pigmented epithelia from primate ES cells by stromal cell-derived inducing activity. *Proceedings of the National Academy of Sciences of the United States of America*, 99(3), pp.1580–5.

Keeling, E. et al., 2018. Impaired Cargo Clearance in the Retinal Pigment Epithelium (RPE) Underlies Irreversible Blinding Diseases. *Cells*, 7(2), p.16.

Kellner, U., Kellner, S. & Weinitz, S., 2008. Chloroquine retinopathy: Lipofuscin- and melanin-related fundus autofluorescence, optical coherence tomography and multifocal electroretinography. *Documenta Ophthalmologica*, 116(2), pp.119–127.

Ketel, K. et al., 2016. A phosphoinositide conversion mechanism for exit from endosomes. *Nature*, 529(7586), pp.408–412.

Kevany, B.M., Palczewski, K. & Palczewsk, K., 2010. Phagocytosis of Retinal Rod and Cone Photoreceptors. *Physiology*, 25(60), pp.8–15.

Kim, G.H.E. et al., 2014. PIKfyve inhibition interferes with phagosome and endosome maturation in macrophages. *Traffic*, 15(10), pp.1143–1163.

Kim, J.Y. et al., 2013. Noncanonical autophagy promotes the visual cycle. *Cell*, 154(2),

pp.365–376.

Kissing, S. et al., 2015. Vacuolar ATPase in phagosome-lysosome fusion. *Journal of Biological Chemistry*, 290(22), pp.14166–14180.

Kissing, S., Saftig, P. & Haas, A., 2017. Vacuolar ATPase in phago(lyso)some biology. *International Journal of Medical Microbiology*, (June), pp.0–1.

Klaver, C.C. et al., 1998. Genetic association of apolipoprotein E with age-related macular degeneration. *American journal of human genetics*, 63(1), pp.200–206.

Klettner, A. et al., 2015. Basal and apical regulation of VEGF-A and placenta growth factor in the RPE / choroid and primary RPE. , (July), pp.736–748.

Klettner, A. et al., 2013. Regulation of constitutive vascular endothelial growth factor secretion in retinal pigment epithelium/choroid organ cultures: p38, nuclear factor κB, and the vascular endothelial growth factor receptor-2/phosphatidylinositol 3 kinase pathway. *Molecular vision*, 19(February), pp.281–91.

Klettner, A.K., Doths, J. & Roider, J., 2012. Nicotine reduces VEGF-secretion and phagocytotic activity in porcine RPE. *Graefe's Archive for Clinical and Experimental Ophthalmology*, 250(1), pp.33–38.

Klimanskaya, I. et al., 2004. Derivation and Comparative Assessment of Retinal Pigment Epithelium from Human Embryonic Stem Cells Using Transcriptomics. *Cloning and Stem Cells*, 6(3), pp.217–245.

Klumperman, J. & Raposo, G., 2014. The complex ultrastructure of the endolysosomal system. *Cold Spring Harbor Perspectives in Biology*, 6(10), p.a016857.

Kolb, H., 1995. *Simple Anatomy of the Retina*, Available at: http://webvision.med.utah.edu/book/part-i-foundations/simple-anatomy-of-the-retina/.

Korah, S. & Kuriakose, T., 2008. Optical coherence tomography in a patient with chloroquine-induced maculopathy. *Indian journal of ophthalmology*, 56(6), pp.511–513.

Korolchuk, V.I. et al., 2011. Lysosomal positioning coordinates cellular nutrient responses. *Nature cell biology*, 13(4), pp.453–60.

Korolchuk, V.I. & Rubinsztein, D.C., 2011. Regulation of autophagy by lysosomal positioning. *Autophagy*, (August), pp.927–928.

Korthagen, N.M. et al., 2015. Chloroquine and Hydroxychloroquine Increase Retinal Pigment Epithelial Layer Permeability. *Journal of Biochemical and Molecular Toxicology*, 29(7), pp.299–304.

Krohne, T.U. et al., 2010. Effects of lipid peroxidation products on lipofuscinogenesis and autophagy in human retinal pigment epithelial cells. *Experimental Eye Research*, 90(3), pp.465–471.

Krohne, T.U. et al., 2012. Generation of Retinal Pigment Epithelial Cells from Small Molecules and OCT4 Reprogrammed Human Induced Pluripotent Stem Cells. *STEM CELLS Translational Medicine*, 1(2), pp.96–109.

Kwan, K.M. et al., 2012. A complex choreography of cell movements shapes the vertebrate eye. *Development*, 139(2), pp.359–372.

Lagutin, O. V. et al., 2003. Six3 repression of Wnt signaling in the anterior neuroectoderm is essential for vertebrate forebrain development. *Genes and Development*, 17(3), pp.368–379.

Laurent-Matha, V. et al., 2006. Processing of human cathepsin D is independent of its catalytic function and auto-activation: Involvement of cathepsins L and B. *Journal of Biochemistry*, 139(3), pp.363–371.

Law, A.-L. et al., 2010. Annexin A2 Regulates Phagocytosis of Photoreceptor Outer Segments in the Mouse Retina. *Molecular Biology of the Cell*, 82(4), pp.327–331.

Leach, L.L. et al., 2015. Canonical/beta-catenin Wnt pathway activation improves retinal pigmented epithelium derivation from human embryonic stem cells. *Investigative ophthalmology & visual science*, 56(2), pp.1002–1013.

Leach, L.L. & Clegg, D.O., 2015. Concise Review: Making Stem Cells Retinal: Methods for Deriving Retinal Pigment Epithelium and Implications for Patients with Ocular Disease. *Stem Cells*, 33(8), pp.2363–2373.

Lehmann, G.L. et al., 2014. Plasma membrane protein polarity and trafficking in RPE cells: Past, present and future. *Experimental Eye Research*, 126, pp.5–15.

Lei, L. et al., 2017. Inhibition or stimulation of autophagy affects early formation of lipofuscin-like autofluorescence in the retinal pigment epithelium cell. *International Journal of Molecular Sciences*, 18(4), pp.1–18.

Lezmi, S. et al., 2013. Chloroquine causes similar electroretinogram modifications, neuronal phospholipidosis and marked impairment of synaptic vesicle transport in Albino and Pigmented Rats. *Toxicology*, 308, pp.50–59.

Li, X. et al., 2016. A molecular mechanism to regulate lysosome motility for lysosome positioning and tubulation. *Nature Cell Biology*, 18(4), pp.404–417.

Liu, J. et al., 2008. Restoration of Lysosomal pH in RPE Cells from Cultured Human and ABCA4 −/− Mice: Pharmacologic Approaches and Functional Recovery. *Investigative Opthalmology & Visual Science*, 49(2), p.772.

Longbottom, R. et al., 2009. Genetic ablation of retinal pigment epithelial cells reveals the adaptive response of the epithelium and impact on photoreceptors. *Proceedings of the National Academy of Sciences*, 106(44), pp.18728–18733.

Lööv, C. et al., 2015. Slow degradation in phagocytic astrocytes can be enhanced by lysosomal acidification. *Glia*, 63(11), pp.1997–2009.

Lopes, V.S., Wasmeier, C., et al., 2007. Melanosome maturation defect in Rab38-deficient retinal pigment epithelium results in instability of immature melanosomes during transient melanogenesis. *Molecular biology of the cell*, 18(10), pp.3914–3927.

Lopes, V.S., Ramalho, J.S., et al., 2007. The ternary Rab27a-Myrip-Myosin VIIa complex regulates melanosome motility in the retinal pigment epithelium. *Traffic*, 8(5), pp.486–499.

Lopes da Silva, M. et al., 2012. The host endocytic pathway is essential for plasmodium berghei late liver stage development. *Traffic*, 13(10), pp.1351–1363.

López-Otín, C. et al., 2013. The hallmarks of aging. *Cell*, 153(6).

Lu, B. et al., 2009. Long-term safety and function of RPE from human embryonic stem cells in preclinical models of macular degeneration. *Stem Cells*, 27(9), pp.2126–2135.

Lu, S. et al., 2017. Lysosomal adaptation: How cells respond to lysosomotropic compounds. *PLoS ONE*, 12(3), pp.1–22.

Luo, W. et al., 2016. TFEB regulates PER3 expression via glucose-dependent effects on

CLOCK/BMAL1. *International Journal of Biochemistry and Cell Biology*, 78, pp.31–42.

Luthert, P.J., 2011. Pathogenesis of age-related macular degeneration. *Diagnostic Histopathology*, 17(1), pp.10–16.

Luzio, J.P. et al., 2014. Lysosome-Related Organelles. , pp.1–17.

Luzio, J.P. et al., 2017. The Biogenesis of Lysosomes and Lysosome-Related Organelles. *Cold Spring Harbor Perspectives in Biology*, 6(9), pp.1–18.

Luzio, J.P., Pryor, P.R. & Bright, N.A., 2007. Lysosomes: Fusion and function. *Nature Reviews Molecular Cell Biology*, 8(8), pp.622–632.

Machado, E. et al., 2015. Regulated lysosomal exocytosis mediates cancer progression. *Science Advances*, 1(11), pp.e1500603–e1500603.

Mahon, G.J. et al., 2004. Chloroquine causes lysosomal dysfunction in neural retina and RPE: implications for retinopathy. *Current eye research*, 28(4), pp.277–284.

Mandai, M. et al., 2017. Autologous Induced Stem-Cell–Derived Retinal Cells for Macular Degeneration. *New England Journal of Medicine*, 376(11), pp.1038–1046.

Mannerström, M. et al., 2002. Evaluation of the cytotoxicity of selected systemic and intravitreally dosed drugs in the cultures of human retinal pigment epithelial cell line and of pig primary retinal pigment epithelial cells. *Toxicology in Vitro*, 16(2), pp.193–200.

Marmorstein, A.D., 2001. The polarity of the retinal pigment epithelium. *Traffic*, 2(12), pp.867–872.

Marneros, A.G. et al., 2005. Vascular endothelial growth factor expression in the retinal pigment epithelium is essential for choriocapillaris development and visual function. *American Journal of Pathology*, 167(5), pp.1451–1459.

Martina, J. et al., 2015. Novel roles for the MiTF/TFE family of transcription factors in organelle biogenesis, nutrient sensing, and energy homeostasis. *Cell Mol Life Sci*, (13), p.2483–2497.

Martinez-Morales, J.R. et al., 2001. Otx genes are required for tissue specification in the developing eye. *Development (Cambridge, England)*, 128(11), pp.2019–2030.

Martínez-Morales, J.R., Rodrigo, I. & Bovolenta, P., 2004. Eye development: A view from the retina pigmented epithelium. *BioEssays*, 26(7), pp.766–777.

Maruotti, J. et al., 2013. A Simple and Scalable Process for the Differentiation of Retinal Pigment Epithelium From Human Pluripotent Stem Cells. *Stem Cells Translational Medicine*, 2(5), pp.341–354.

Maxson, M.E. & Grinstein, S., 2014. The vacuolar-type H+-ATPase at a glance - more than a proton pump. *Journal of Cell Science*, 127(23), pp.4987–4993.

Mazzoni, F., Safa, H. & Finnemann, S.C., 2014. Understanding photoreceptor outer segment phagocytosis: Use and utility of RPE cells in culture. *Experimental Eye Research*, 126, pp.51–60.

Medina, D.L. et al., 2011. Transcriptional activation of lysosomal exocytosis promotes cellular clearance. *Developmental Cell*, 21(3), pp.421–430.

Mehta, S., 2015. Age-Related Macular Degeneration. *Primary Care - Clinics in Office Practice*, 42(3), pp.377–391.

Meyer, J.S. et al., 2009. Modeling early retinal development with human embryonic and induced pluripotent stem cells. *Proceedings of the National Academy of Sciences*,

106(39), pp.16698–16703.

Miao, Y. et al., 2015. A TRP channel senses lysosome neutralization by pathogens to trigger their expulsion. *Cell*, 161(6), pp.1306–1319.

Mindell, J.A., 2012. Lysosomal Acidification Mechanims. *Annual Review of Physiology*, (74), pp.69–86.

Mizushima, N. & Yoshimori, T., 2007. How to interpret LC3 immunoblotting. *Autophagy*, 3(6), pp.542–545.

Molino, D. et al., 2016. The journey of the autophagosome through mammalian cell organelles and membranes. *Journal of Molecular Biology*.

Moreno-García, A. et al., 2018. An Overview of the Role of Lipofuscin in Age-Related Neurodegeneration. *Frontiers in Neuroscience*, 12(July), pp.1–13.

Munro, S., 2002. Organelle identity and the targeting of peripheral membrane proteins. *Current Opinion in Cell Biology*, 14(4), pp.506–514.

Myllykangas, L. et al., 2005. Cathepsin D-deficient Drosophila recapitulate the key features of neuronal ceroid lipofuscinoses. *Neurobiology of Disease*, 19(1–2), pp.194–199.

Napolitano, G. & Ballabio, A., 2016. TFEB at a glance. *Journal of Cell Science*, 129(13), pp.2475–2481.

van Niel, G. et al., 2015. Apolipoprotein E Regulates Amyloid Formation within Endosomes of Pigment Cells. *Cell Reports*, 13(1), pp.43–51.

Okabe, K. et al., 2014. Neurons limit angiogenesis by titrating VEGF in retina. *Cell*, 159(3), pp.584–596.

Olson, A.J.F. et al., 1980. PIKfyve activity regulates reformation of terminal storage lysosomes from endolysosomes.

Osakada, F. et al., 2009. In vitro differentiation of retinal cells from human pluripotent stem cells by small-molecule induction. *Journal of cell science*, 122(Pt 17), pp.3169–79.

Osakada, F. et al., 2008. Toward the generation of rod and cone photoreceptors from mouse, monkey and human embryonic stem cells. *Nature Biotechnology*, 26(2), pp.215–224.

Pauwels, A.M. et al., 2017. Patterns, Receptors, and Signals: Regulation of Phagosome Maturation. *Trends in Immunology*, 38(6), pp.407–422.

Penn, J.S. et al., 2008. Vascular endothelial growth factor in eye disease. *Progress in Retinal and Eye Research*, 27(4), pp.331–371.

Pennington, B.O. et al., 2015. Defined Culture of Human Embryonic Stem Cells and Xeno-Free Derivation of Retinal Pigmented Epithelial Cells on a Novel, Synthetic Substrate. *Stem Cells Translational Medicine*, 4, pp.165–177.

Peters, S. et al., 2006. Inhibition of lysosomal degradation in retinal pigment epithelium cells induces exocytosis of phagocytic residual material at the basolateral plasma membrane. *Ophthalmic Research*, 38(2), pp.83–88.

Pires, C.F., 2014. *Cellular Reprogramming Strategies for Degenerative Disorders Involving*.

Pires, C.F. et al., 2012. Optimization of a Retinal Pigment Epithelium differentiation protocol driven by ectopic expression of eye transcription factors. In *Pigment Cell & Melanoma Research*.

Platt, F.M., Boland, B. & van der Spoel, A.C., 2012. Lysosomal storage disorders: The cellular impact of lysosomal dysfunction. *Journal of Cell Biology*, 199(5), pp.723–734.

Polito, V.A. et al., 2014. Selective clearance of aberrant tau proteins and rescue of neurotoxicity by transcription factor EB. *EMBO molecular medicine*, 6(9), pp.1142–60.

Pu, J. et al., 2015. BORC, a Multisubunit Complex that Regulates Lysosome Positioning. *Developmental Cell*, 33(2), pp.176–188.

Raghunath, A. & Perumal, E., 2015. Micro-RNAs and their roles in eye disorders. *Ophthalmic Research*, 53(4), pp.169–186.

Rakoczy, P.E. et al., 1996. Correlation between autofluorescent debris accumulation and the presence of partially processed forms of cathepsin D in cultured retinal pigment epithelial cells challenged with rod outer segments. *Experimental eye research*, 63(2), pp.159–67.

Rakoczy, P.E. et al., 1997. Modulation of cathepsin D activity in retinal pigment epithelial cells. *The Biochemical journal*, 324 (Pt 3(Pt 3), pp.935–40.

Rakoczy, P.E. et al., 2002. Progressive age-related changes similar to age-related macular degeneration in a transgenic mouse model. *The American journal of pathology*, 161(4), pp.1515–24.

Ramkumar, H.L., Zhang, J. & Chan, C.C., 2010. Retinal ultrastructure of murine models of dry age-related macular degeneration (AMD). *Progress in Retinal and Eye Research*, 29(3), pp.169–190.

Raposo, G. & Marks, M.S., 2007. Melanosomes - Dark organelles enlighten endosomal membrane transport. *Nature Reviews Molecular Cell Biology*, 8(10), pp.786–797.

Reddy, A., Caler, E. V. & Andrews, N.W., 2001. Plasma membrane repair is mediated by Ca2+-regulated exocytosis of lysosomes. *Cell*, 106(2), pp.157–169.

Reynolds, J. & Lamba, D., 2014. Human embryonic stem cell applications for retinal degenerations. *Exp. Eye Res.*, 123(6), pp.151–160.

Rimpelä, A.K. et al., 2016. Drug distribution to retinal pigment epithelium: Studies on melanin binding, cellular kinetics, and single photon emission computed tomography/computed tomography imaging. *Molecular Pharmaceutics*, 13(9), pp.2977–2986.

Rimpelä, A.K. et al., 2017. Implications of melanin binding in ocular drug delivery. *Advanced Drug Delivery Reviews*.

Riolobos, L. et al., 2013. HLA Engineering of Human Pluripotent Stem Cells. *Molecular Therapy*, 21(6), pp.1232–1241.

Rizzolo, L.J., 2014. Barrier properties of cultured retinal pigment epithelium. *Experimental Eye Research*, 126, pp.16–26.

Rodríguez, A. et al., 1997. Lysosomes behave as Ca2+-regulated exocytic vesicles in fibroblasts and epithelial cells. *Journal of Cell Biology*, 137(1), pp.93–104.

Rosenthal, A.R. et al., 1978. Chloroquine retinopathy in the rhesus monkey. *Investigative ophthalmology & visual science*, 17(12), pp.1158–1175.

Roska, B. & Sahel, J., 2018. Review Restoring vision.

Rózanowska, M., 2011. Properties and Functions of Ocular Melanins and Melanosomes. In *Melanins and Melanosomes: Biosynthesis, Biogenesis,*

Physiological, and Pathological Functions. Weinheim, Germany: Wiley-VCH Verlag GmbH & Co. KGaA, pp. 187–224.

Saeed, M.U., Gkaragkani, E. & Ali, K., 2013. Emerging roles for antiangiogenesis factors in management of ocular disease. *Clinical Ophthalmology*, 7, pp.533–543.

Saftig, P. & Klumperman, J., 2009. Lysosome biogenesis and lysosomal membrane proteins: Trafficking meets function. *Nature Reviews Molecular Cell Biology*, 10(9), pp.623–635.

Samie, M.A. & Xu, H., 2014. Lysosomal exocytosis and lipid storage disorders. *Journal of Lipid Research*, 55(6), pp.995–1009.

Sanjuan, M.A. et al., 2007. Toll-like receptor signalling in macrophages links the autophagy pathway to phagocytosis. *Nature*, 450(7173), pp.1253–1257.

Sardiello, M. et al., 2009. A gene network regulating lysosomal biogenesis and function. *Science*, 325(5939), pp.473–477.

Sardiello, M. et al., 2009. A Gene Network Regulating Lysosomal Biogenesis and Function Marco. *Science*, 325(July), pp.473–477.

Schink, K.O., Tan, K.-W. & Stenmark, H., 2016. Phosphoinositides in Control of Membrane Dynamics. *Annu. Rev. Cell Dev. Biol*, 322429(1), pp.1–24.

Schwartz, S.D. et al., 2012. Embryonic stem cell trials for macular degeneration: a preliminary report. *Lancet*, 379(9817), pp.713–20.

Schwartz, S.D. et al., 2015. Human embryonic stem cell-derived retinal pigment epithelium in patients with age-related macular degeneration and Stargardt's macular dystrophy: Follow-up of two open-label phase 1/2 studies. *The Lancet*, 385(9967), pp.509–516.

Segev, N., 2011. GTPases in intracellular trafficking: An overview. *Seminars in Cell and Developmental Biology*, 22(1), pp.1–2.

Settembre, C., Fraldi, A., et al., 2013. Signals from the lysosome: a control centre for cellular clearance and energy metabolism. *Nature Reviews Molecular Cell Biology*, 14(5), pp.283–296.

Settembre, C., De Cegli, R., et al., 2013. TFEB controls cellular lipid metabolism through a starvation-induced autoregulatory loop. *Nature Cell Biology*, 15(6), pp.647–658.

Settembre, C. & Ballabio, A., 2014. Lysosomal adaptation: How the lysosome responds to external cues. *Cold Spring Harbor Perspectives in Biology*, 6(6), pp.1–16.

Shang, P. et al., 2017. The amino acid transporter SLC36A4 regulates the amino acid pool in retinal pigmented epithelial cells and mediates the mechanistic target of rapamycin, complex 1 signaling. *Aging Cell*, 16(2), pp.349–359.

Singh, R., Phillips, M.J., et al., 2013. Functional analysis of serially expanded human iPS cell-derived RPE cultures. *Investigative Ophthalmology and Visual Science*, 54(10), pp.6767–6778.

Singh, R., Shen, W., et al., 2013. iPS cell modeling of best disease: Insights into the pathophysiology of an inherited macular degeneration. *Human Molecular Genetics*, 22(3), pp.593–607.

Sinha, D. et al., 2016. Lysosomes: Regulators of autophagy in the retinal pigmented epithelium. *Experimental Eye Research*, 144, pp.46–53.

Slade, L. & Pulinilkunnil, T., 2017. The MiTF/TFE Family of Transcription Factors:

Master Regulators of Organelle Signaling, Metabolism and Stress Adaptation. *Molecular Cancer Research*, (15), p.molcanres.0320.2017.

Song, D. & Dunaief, J.L., 2013. Retinal iron homeostasis in health and disease. *Frontiers in Aging Neuroscience*, 5(JUN), pp.1–13.

Song, J.X. et al., 2016. A novel curcumin analog binds to and activates TFEB in vitro and in vivo independent of MTOR inhibition. *Autophagy*, 12(8), pp.1372–1389.

Song, M.J. & Bharti, K., 2016. Looking into the future: Using induced pluripotent stem cells to build two and three dimensional ocular tissue for cell therapy and disease modeling. *Brain Research*, 1638, pp.2–14.

Sonoda, S. et al., 2009. A protocol for the culture and differentiation of highly polarized human retinal pigment epithelial cells. *Nature protocols*, 4(5), pp.662–73.

Spampanato, C. et al., 2013. Transcription factor EB (TFEB) is a new therapeutic target for Pompe disease. *EMBO Molecular Medicine*, 5(5), pp.691–706.

Sparrow, J.R., Hicks, D. & Hamel, C.P., 2010. The retinal pigment epithelium in health and disease. *Current molecular medicine*, 10(9), pp.802–23.

Steingrímsson, E., Copeland, N.G. & Jenkins, N.A., 2004. Melanocytes and the *Microphthalmia* Transcription Factor Network. *Annual Review of Genetics*, 38(1), pp.365–411.

Strauss, O., 2016. Pharmacology of the retinal pigment epithelium, the interface between retina and body system. *European Journal of Pharmacology*, 787, pp.84–93.

Strauss, O., 1995. *The Retinal Pigment Epithelium*, University of Utah Health Sciences Center.

Strauss, O., 2005a. The Retinal Pigment Epithelium in Visual Function. *Physiological Reviews*, 85(3), pp.845–881.

Strauss, O., 2005b. The Retinal Pigment Epithelium in Visual Function. *Physiological Reviews*, 85(3), pp.845–881.

Sundelin, S.P. & Terman, A., 2002. Different effects of chloroquine and hydroxychloroquine on lysosomal function in cultured retinal pigment epithelial cells. *APMIS*, 110(6), pp.481–489.

Sung, C.H. & Chuang, J.Z., 2010. The cell biology of vision. *Journal of Cell Biology*, 190(6), pp.953–963.

Szatmári-Tóth, M. et al., 2016. Clearance of autophagy-associated dying retinal pigment epithelial cells – a possible source for inflammation in age-related macular degeneration. *Cell Death and Disease*, 7(9), p.e2367.

Takahashi, K. & Yamanaka, S., 2006. Induction of Pluripotent Stem Cells from Mouse Embryonic and Adult Fibroblast Cultures by Defined Factors. *Cell*, 126(4), pp.663–676.

Tanga, L. et al., 2011. Retinal functional changes measured by frequency-doubling technology in patients treated with hydroxychloroquine. *Graefe's Archive for Clinical and Experimental Ophthalmology*, 249(5), pp.715–721.

Toimela, T., Tahti, H. & Salminen, L., 1995. Retinal pigment epithelium cell culture as a model for evaluation of the toxicity of tamoxifen and chloroquine. *Ophthalmic Res*, 27 Suppl 1(1), pp.150–153.

Tol, M.J. et al., 2018. HEPES activates a MiT/TFE-dependent lysosomal-autophagic

gene network in cultured cells: A call for caution. *Autophagy*, 14(3), pp.437–449.

Toops, K.A. & Lakkaraju, A., 2013. Let's play a game of chutes and ladders: Lysosome fusion with the epithelial plasma membrane. *Communicative and Integrative Biology*, 6(4), p.e24474.

Treusch, S. et al., 2004. Caenorhabditis elegans functional orthologue of human protein h-mucolipin-1 is required for lysosome biogenesis. *Proceedings of the National Academy of Sciences of the United States of America*, 101(13), pp.4483–8.

Trudeau, K.M. et al., 2016. Lysosome acidification by photoactivated nanoparticles restores autophagy under lipotoxicity. *Journal of Cell Biology*, 214(1), pp.25–34.

Tsunemi, T. et al., 2012. PGC-1a rescues Huntington's disease proteotoxicity by preventing oxidative stress and promoting TFEB function. *Science Translational Medicine*, 4(142), p.142ra97-142ra97.

Turk, B., Turk, V. & Turk, D., 1997. Structural and functional aspects of papain-like cysteine proteinases and their protein inhibitors. *Biological Chemistry*, 378(3–4), pp.141–150.

Valapala, M. et al., 2014. Lysosomal-mediated waste clearance in retinal pigment epithelial cells is regulated by CRYBA1/b3/A1-crystallin via V-ATPase-MTORC1 signaling. *Autophagy*, 10(3), pp.480–496.

Verity, C.M. et al., 2010. The epidemiology of progressive intellectual and neurological deterioration in childhood. *Archives of Disease in Childhood*, 95(5), pp.361–364.

Volland, S. et al., 2015. A comparison of some organizational characteristics of the mouse central retina and the human macula. *PLoS ONE*, 10(4), p.e0125631.

Vugler, A. et al., 2008. Elucidating the phenomenon of HESC-derived RPE: Anatomy of cell genesis, expansion and retinal transplantation. *Experimental Neurology*, 214(2), pp.347–361.

Wang, A.L. et al., 2009. Autophagy and exosomes in the aged retinal pigment epithelium: possible relevance to drusen formation and age-related macular degeneration. *PLoS one*, 4(1), p.e4160.

Wang, A.L. & Neufeld, A.H., 2010. Smoking mice: A potential model for studying accumulation of drusen-like material on Bruch's membrane. *Vision Research*, 50(7), pp.638–642.

Wang, H. et al., 2011. The role of RPE cell-associated VEGF189 in choroidal endothelial cell transmigration across the RPE. *Investigative Ophthalmology and Visual Science*, 52(1), pp.570–578.

Wartosch, L., Bright, N.A. & Luzio, J.P., 2015. Lysosomes. *Current Biology*, 25(8), pp.R315–R316.

Wavre-Shapton, S.T. et al., 2013. Conditional Ablation of the Choroideremia Gene Causes Age-Related Changes in Mouse Retinal Pigment Epithelium. *PLoS ONE*, 8(2), pp.1–11.

Wavre-Shapton, S.T. et al., 2014. Phagosome maturation during endosome interaction revealed by partial rhodopsin processing in retinal pigment epithelium. *Journal of Cell Science*, 127(17), pp.3852–3861.

Wolfe, D.M. et al., 2013. Autophagy failure in Alzheimer's disease and the role of defective lysosomal acidification. *European Journal of Neuroscience*, 37(12), pp.1949–1961.

Wozniacka, A., Carter, A. & Dp, M., 2002. Antimalarials in cutaneous lupus erythematosus : mechanisms of therapeutic bene t. *Lupus*, 11(2), pp.71–81.

Wu, J. et al., 2017. Autophagy regulates TGF-β2-induced epithelial-mesenchymal transition in human retinal pigment epithelium cells. *Molecular Medicine Reports*, pp.3607–3614.

Xiao, Q. et al., 2015. Neuronal-Targeted TFEB Accelerates Lysosomal Degradation of APP, Reducing A Generation and Amyloid Plaque Pathogenesis. *Journal of Neuroscience*, 35(35), pp.12137–12151.

Xu, J. et al., 2012. Mechanism of polarized lysosome exocytosis in epithelial cells. *Journal of Cell Science*, 125(24), pp.5937–5943.

Xu, P.T. et al., 1999. Sialylated human apolipoprotein E (apoE(s)) is preferentially associated with neuron-enriched cultures from APOE transgenic mice. *Neurobiology of Disease*, 6(1), pp.63–75.

Yang, J. et al., 2014. Validation of genome-wide association study (GWAS)-identified disease risk alleles with patient-specific stem cell lines. *Human Molecular Genetics*, 23(13), pp.3445–3455.

Yoshida, T. et al., 2005. The potential role of amyloid beta in the pathogenesis of age-related macular degeneration. *Journal of Clinical Investigation*, 115(10), p.2793.

Young, R.W., 1971. The renewal of rod and cone outer segments in the rhesus monkey. *Journal of Cell Biology*, 49(2), pp.303–318.

Yu, B. et al., 2018. Phagocytosed photoreceptor outer segments activate mTORC1 in the retinal pigment epithelium. *Sci. Signal.*, 11(532), p.eaag3315.

Yu, L. et al., 2010. Termination of autophagy and reformation of lysosomes regulated by mTOR. *Nature*, 465(7300), pp.942–946.

Zhan, J. et al., 2016. Crosstalk between the autophagy-lysosome pathway and the ubiquitin-proteasome pathway in retinal pigment epithelial cells. *Current molecular medicine*, 16(5), pp.487–495.

Zhang, D. et al., 2005. Correlation between inactive cathepsin D expression and retinal changes in mcd2/mcd2 tansgenic mce. *Investigative Ophthalmology and Visual Science*, 46(9), pp.3031–3038.

Zhao, G.Q. et al., 1993. TFEC, a basic helix-loop-helix protein, forms heterodimers with TFE3 and inhibits TFE3-dependent transcription activation. *Molecular and cellular biology*, 13(8), pp.4505–12.

Zhao, Z. et al., 2011. Age-related retinopathy in NRF2-deficient mice A. C. Y. Lo, ed. *PLoS ONE*, 6(4), p.e19456.

Zheng, L., 2012. *Lysosomal Involvement in the Pathogenesis of Alzheimer ' S Disease*,

Zhu, D. et al., 2011. Polarized secretion of PEDF from human embryonic stem cell-derived RPE promotes retinal progenitor cell survival. *Investigative ophthalmology & visual science*, 52(3), pp.1573–85.

Zhu, Y. et al., 2013. Three-Dimensional Neuroepithelial Culture from Human Embryonic Stem Cells and Its Use for Quantitative Conversion to Retinal Pigment Epithelium. *PLoS ONE*, 8(1).

CHAPTER 7

Supplementary Material

This chapter contains parts of the following manuscript in preparation.

"*VEGF titration by RabGTPase-regulated trafficking of VEGFR2 in RPE*"

M. Helena Cardoso[1], Inês P. Rodrigues[1], Sara Maia[1], Cristiana F. Pires[1], Martim D. Portal[1], Olaf Strauss[2], Miguel C. Seabra[1], José S. Ramalho[1#]
[1]CEDOC, Chronic Diseases Research Centre, NOVA Medical School|Faculdade de Ciências Médicas, Universidade NOVA de Lisboa 1169-056, Portugal.
[2]Experimental Ophthalmology, Eye Hospital, University Medical Center Regensburg, Regensburg, Germany.

[#]E-mail: jose.ramalho@nms.unl.pt

ABSTRACT

The Retinal Pigment Epithelium (RPE) is a highly specialized layer of cells, representing a fundamental component of the visual unit. A disturbance of the delicate balance of RPE functions can give rise to retinal degeneration with progression to blindness.
RPE's role in disease onset and progression has been shown critical, particularly regarding VEGF secretion control. VEGFR2, a known regulator of pro-angiogenic signaling in endothelial cells, is also expressed by RPE cells and its intracellular trafficking is regulated by RabGTPases. Through Rab-regulated endocytosis of VEGFR2, RPE cells are capable of titrating available VEGF in the retinal milieu.
Keywords: VEGF, RabGTPases, VEGFR2, RPE

INTRODUCTION

Our sense of vision relies on three highly interdependent layers of the retina: the neuroretina, the retinal pigment epithelium (RPE) and the choroid(Sung & Chuang 2010). The RPE in particular establishes a morphological and functional barrier, assuring the integrity and interaction of the entire visual unit (Song & Bharti 2016; Strauss 2005b). On the apical side, the RPE provides nutrients to the neuroretina, transports ions and metabolic waste and extends microvilli to phagocytose the photoreceptors' outer segments and recycle the visual pigment. On the basolateral side, the RPE contacts with the choroid capillaries through the Bruch's membrane, posing as the selective blood-retina barrier(Strauss 2005b). In order to communicate with the adjacent layers, the RPE secretes different factors and expresses several transmembrane receptors in a polarized manner(Marmorstein 2001).

The Vascular Endothelial Growth Factor (VEGF), namely VEGF-A, is one of such vital factors, both during retinal development and for choroid maintenance throughout life. VEGF has been a target of study, particularly due to its role in the pathogenesis of retinal degeneration disorders, as a mediator of neovascularization and barrier disruption(Knatokie M Ford et al. 2011; Penn et al. 2008). A disturbance of these tightly controlled processes can cause RPE degeneration, photoreceptor death and choriocapillaries atrophy or overgrowth, ultimately leading to blindness(Strauss 2005b).

RPE dysfunction has been shown crucial to retinal degenerative disorders onset and progression, particularly due to RPE's role in VEGF secretion control. It has been previously described that RPE cells express both VEGF and its receptors: VEGFR1 and VEGFR2(Knatokie M. Ford et al. 2011). Both these receptors contain an extracellular VEGF-binding domain, but while VEGFR1 has been suggested to be a "decoy" receptor that sequesters VEGF, VEGFR2 mediates pro-angiogenic signaling, culminating in survival, proliferation and migration of cells. This is true for endothelial cells, however, when considering the RPE, proliferation and migration are kept to a minimum throughout life, in healthy conditions(Fuhrmann et al. 2014). This suggests there could be another function and outcome of VEGF intake by RPE, such as titration of the extracellular soluble VEGF. Furthermore, we know Rab GTPases are key regulators of intracellular trafficking and have been described as molecular players in VEGFR2 endocytic trafficking, in endothelial cells(Jopling et al. 2009).

In an effort to explore the mechanisms by which the RPE controls VEGF secretion and uptake, we sought out to clarify the Rab-regulated endocytic pathway's involvement in this process.

Understanding how Rab proteins functions' disruption could affect VEGF secretion and uptake, possibly contributing to angiogenesis, would ultimately contribute to find new therapeutic agents. With this study we aim to shed light on the RPE role as VEGF regulator, through Rab-regulated endocytosis of VEGFR2, and open the door to possible new therapies, targeting specifically RPE cells and VEGFR2 trafficking.

B6-RPE07 as an RPE model to evaluate VEGF regulation

Expression and secretion of VEGF have been well documented, both in RPE primary culture cells and RPE cell lines(Geisen et al. 2006; Klettner et al. 2012). These cells have also been shown to express VEGFR2(Wang et al. 2011; Ford et al. 2011; Guerrin et al. 1995). Furthermore, research suggests a crucial role for VEGF/VEGFR2 interplay in fundamental RPE functions(Ablonczy & Crosson 2007; Dahrouj et al. 2015; Guerrin et al. 1995; Dahrouj et al. 2014), and clinical observations revealed RPE-derived VEGF to be essential to choroid health(Marneros et al. 2005; Penn et al. 2008).

B6-RPE07 mouse RPE cell line has previously been reported to produce cytokines and chemokines, including VEGF(Hombrebueno et al. 2014). The present study confirms not only expression and secretion of VEGF, but also expression of VEGFR2 and endocytic/recycling RabGTPases Rab4a, Rab4b, Rab5a, Rab5b, Rab7a, Rab11a and Rab11b (Fig.1).

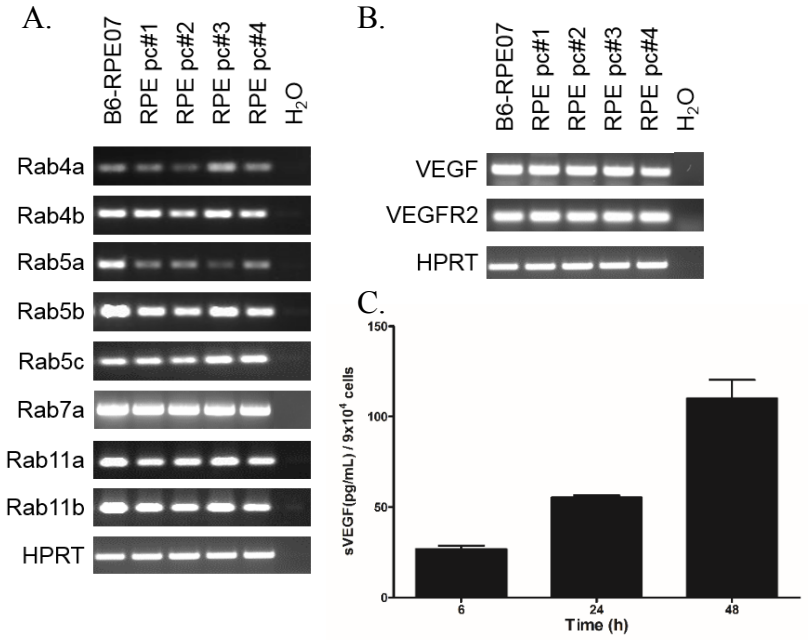

Figure 1- RPE cells express Rab4a, Rab4b, Rab5a, Rab5b, Rab5c, Rab7a, Rab11a, Rab11b and VEGF and VEGFR2. A. Electrophoretic analysis of RT-PCR products of Rab4a, Rab4b, Rab5a, Rab5b, Rab5c, Rab7a, Rab11a and Rab11b in B6-RPE07 cell line and RPE primary cultures. B. Electrophoretic analysis of RT-PCR products of VEGF and VEGFR2 in B6-RPE07 cell line and RPE primary cultures. HPRT expression was used as control transcript. C. Evaluation of VEGF secretion in the conditioned medium of B6-RPE07 cells along the time (n=4).

This set of RabGTPases was selected based on previous studies, and to further elucidate their potential involvement in soluble VEGF secretion by RPE cells. Rab expression levels were found similar to those of RPE primary culture lines, except for Rab5a and Rab5b, with B6-RPE07 displaying a relatively higher expression (Fig.1A). VEGF and VEGFR2 expression levels were similar for all cells tested (Fig.1B). Finally, B6-RPE07 were shown to secrete VEGF to the culture medium (Fig.1C), as soon as 6h after plating and in a regular manner up until 48h after plating, indicating B6-RPE07 as a suitable model for the study of VEGF and VEGFR2 regulation in the RPE.

miR-silencing adenoviruses efficiently knock down Rab GTPases

In order to evaluate RabGTPases' influence in VEGF intracellular trafficking, we first sought out to knock down (KD) each endocytic rab individually. To this end, ssDNA oligos, were designed and cloned into adenoviral vectors to create silencing molecular tools for the target proteins, as previously described in Material and Methods section. For each target protein, 1 to 3 sequences were designed. In order to efficiently reproduce the ability of infectious adenoviral vectors to create quantifiable biological events, all viral preparations were titrated prior to usage.

Adenoviruses were added and transduction was left to occur overnight. The next day, cells were fed with fresh serum-free medium for 8h, after which cells were given fresh medium with 1%FBS. 48h after, cells were harvested in lysis buffer and prepared for Western Blot analysis. All data are expressed as pg/ml of VEGF secreted by $9x10^4$ B6-RPE07 cells, referring to the initial cell seeding density. No evidence was found as to differences in proliferation or death between all conditions (data not shown). The level of endogenous Rab proteins' KD was assessed by probing membranes with specific polyclonal antibodies against each rab isoform and using either calnexin or βactin as loading control, as presented in Fig. 2.

For each individual rab, a representative western blot image is presented, showing a downregulation of that specific protein, relatively to a non-transduced cell lysate (NT) and also to a cell lysate from cells transduced with a control miR (Scr). Efficiency of KD was quantified by comparison of band intensities of endogenous Rab KD to negative control (Scr), by densitometric analysis. No significant differences were found between non-transduced (NT) and negative control cells (Scr). For all Rab proteins tested KD levels were 50% or higher. Note: polyclonal antibodies specific for every rab isoform were used, except for rab4; i.e. anti-rab4 antibody recognizes both rab4a and rab4b. Nonetheless, a statistically significant reduction of rab4 (either a or b isoforms) was detected, using the miR specifically designed to target each isoform. Therefore, it was considered that a precise knock down of each isoform was attained, detected by a decrease of expression of total Rab4 (to 20% for rab4a KD and 50% for rab4b KD).

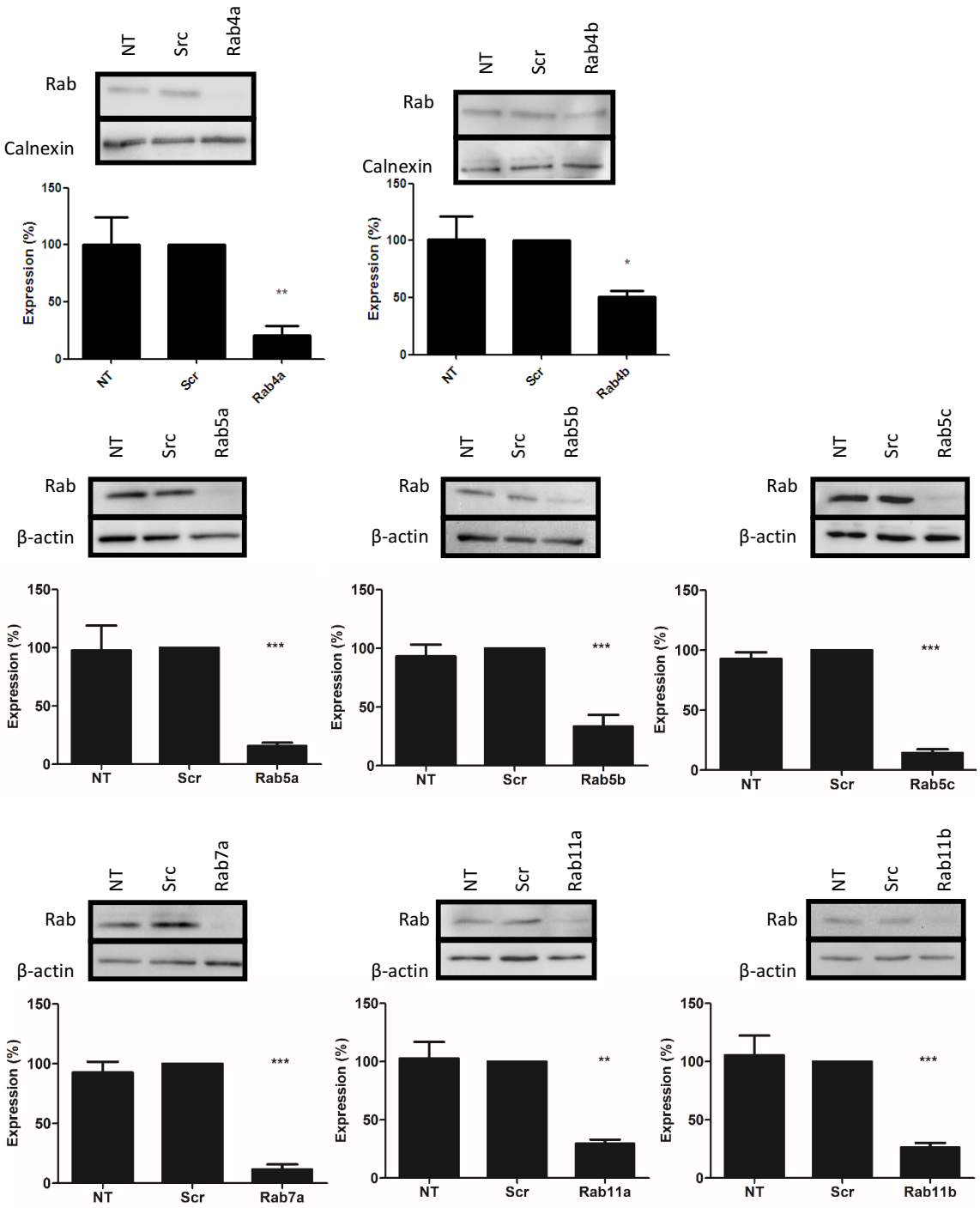

Figure 2 miR-silencing adenoviruses efficiently knock-down target Rab GTPases in RPE cells. Representative western blot image and densiometric evaluation of Rab expression, normalized for calnexin or β-actin. Data are expressed as percentage of expression (mean±SEM, n≥ 3). Significance was determined using One-way ANOVA. * P<0.05, **P<0.01, ***P<0.001. No significant changes were observed between non-transduced cells (NT) and cells transduced with an adenovirus expressing an irrelevant mir control (Scr). Rab4a (n=5), Rab4b (n=5), Rab5a (n=3), Rab5b (n=3), Rab5c (n=5), Rab7a (n=4), Rab11a (n= 3) and Rab11b (n=4)

Endocytic Rab GTPases in RPE negatively regulate extracellular sVEGF

Screening of individual Rab GTPases' involvement in VEGF secretion by B6-RPE07 cells was performed using the conditions described in *Experimental Procedures* section. Soluble VEGF (sVEGF) levels were measured by ELISA and normalized to total amount of protein. Cells transduced with miR-Negative adenovirus (Src) secreted VEGF in comparable amounts to non-transduced cells, indicating that miR-Negative adenovirus did not interfere with VEGF secretion (data not shown). Each endocytic rab KD resulted in an increase of VEGF detected in the conditioned medium. The amount of VEGF released to the medium upon rab KD increased significantly (between 1.3-2.3x fold increase), with Rab4b and Rab5c being the most striking examples of sVEGF upregulation (Fig.3).

The opposite experiment, where the same RabGTPases were individually overexpressed,

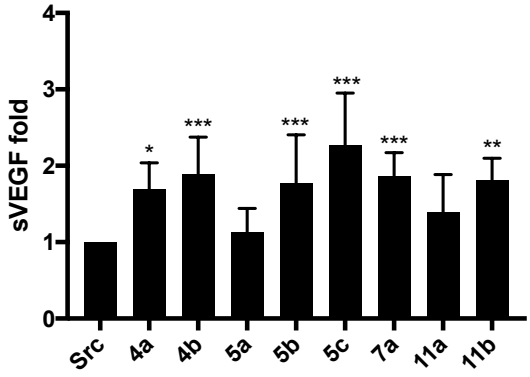

Figure 3 Knock-down of individual Rab GTPases increases secretion of VEGF by RPE cells. Data are expressed as fold change of VEGF secreted by 9 x10^4 B6-RPE07 cells (mean±SEM, n≥ 3). Significance was determined using One-way ANOVA. *P<0.05, **P<0.01, ***P<0.001. No significant changes were observed between non-transduced cells and cells transduced with an adenovirus expressing an irrelevant mir control (Scr).

revealed coherent results: a decrease in the conditioned medium's VEGF. B6-RPE07 cells were transduced overnight with adenovirus carrying a GFP-tagged version of Rab protein. Cell lysates were collected the next day and prepared for western blot analysis, to verify overexpression profiles. The use of these constructs has been described before (Lopes, Ramalho, et al. 2007; Lopes da Silva et al. 2012). Differences between non transduced cells and cells transduced with Ctr negative overexpression vector (containing GFP alone) affected cells, causing a 1.2x fold increase in measured VEGF in culture medium corresponding to Ctr (data not shown). Nevertheless, when comparing each rab's overexpression to Ctr, a consistent decrease of VEGF amounts in the conditioned medium was found. Specifically, 1.2x fold decrease (rab4a or rab5b) to 1.5x fold decrease (rab4b, or 11b).

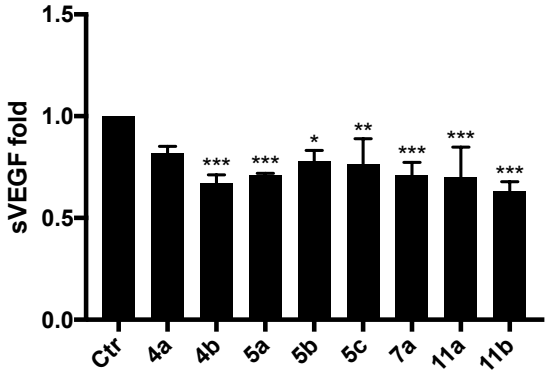

Figure 4 Overexpression of Rab GTPases diminishes the release of VEGF by RPE cells. Data are expressed as fold change of VEGF secreted by 9 x10^4 B6-RPE07 cells (mean±SEM, n = 3). Significance was determined using One-way ANOVA. *p<0.05, **P<0.01, ***P<0.001.

The less evident effect of overexpression of endocytic and recycling rabGTPases (as compared to their knockdown) can be attributed to the fact that in OE experiments, conditioned medium was collected the day after transduction, while in KD experiments, medium was collected ~3 days after adding the adenoviruses, as described. Moreover, the limiting rate of endocytosis/recycling pathways could influence the outcome, considering only one player is being overexpressed at a time; in the case of the KD experiments, when one player of the pathway is missing/reduced, the whole pathway is perturbed. Finally, there could be functional redundancy of isoforms, and thus the effect of a single KD or OE could be less evident. Altogether, these results propose an important role for endocytic and recycling Rab proteins on the regulation of VEGF secretion by RPE cells.

sVEGF is regulated by Rab-mediated trafficking of VEGFR2 in RPE

Immunofluorescence co-localization staining did not provide definitive evidence of direct involvement of these rab proteins in the trafficking of VEGF (data not shown). Moreover, KD of rabs caused VEGF up regulation (data not shown) and release (Fig. 3), suggesting a negative feedback effect.

Ultimately, the following hypothesis was proposed: RabGTPases act as indirect regulators of VEGF production and secretion, through intracellular trafficking of VEGFR2. The approach undertaken consisted in producing VEGFR2 KD B6-RPE07 cell lines. Lines #4162 and #4163 were constructed, using lentiviral vectors to deliver constitutive miR targeting specifically VEGFR2. Efficient VEGFR2 KD was confirmed by PCR (data not shown) and Westen Blot (Fig.5 A). As presented, VEGFR2 protein levels were reduced from 20% (#4162) to less than 10% (#4163), relatively to endogenous expression (B6).

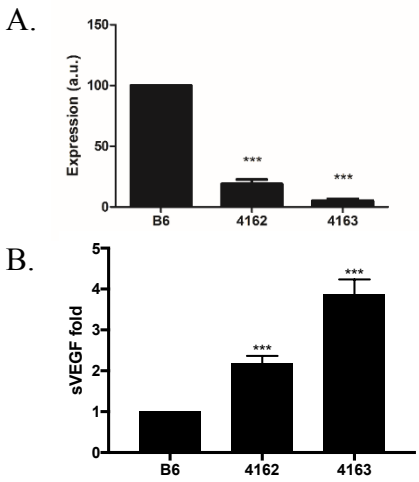

Figure 5 VEGFR2 knockdown leads to accumulation of secreted VEGF by RPE cells. A. Western blot representative image of stable VEGFR2 knockdown B6-RPE07 derived cell lines. Densiometric evaluation of VEGFR2 expression, normalized for β-actin. Data are expressed as percentage of expression (mean±SEM, n≥ 3). Significance was determined using One-way ANOVA (***P<0.001). B. Quantification of VEGF in the conditioned medium (sVEGF) of B6-REP07 cells (B6) and VEGFR2 knockdown lines. Data are expressed as fold increase of sVEGF produced by 9 x 10^4 cells (mean±SEM, n = 3). Significance was determined using One-way ANOVA (***P<0.001).

VEGF levels detected in the conditioned medium, by ELISA, were increased up to 3.8x fold when VEGFR2 was knocked down. Increased levels of detected sVEGF were proportional to VEGFR2 KD, meaning the less VEGFR2, the more sVEGF found in the medium. This suggests a direct causal effect of VEGFR2 KD and also correlates with the results found for rab KD. When each endocytic or recycling rab was individually knocked down, a similar, though weaker, result was observed. This lesser effect could be explained considering rab isoforms' functional redundancy as well as other compensatory mechanisms of endocytic/recycling trafficking pathways. Previous studies using endothelial cells corroborate the direct involvement of rab4, rab5, rab7 and rab11 in the trafficking of VEGFR2(Jopling et al. 2014; Jopling et al. 2009). The present findings, however, suggest different signaling pathways are activated in RPE, rather than

(endothelial cells') proliferation and migration. Here, there is indication of a VEGFR2 functional role as a sensor or negative regulator of sVEGF levels.

A relevant note should be taken as to the different functions of these rab proteins inside the cell: while rab4 and rab11 are generally considered as part of the fast and slow recycling pathways, respectively, rab5 is a marker for early endosomes and rab7 for late endosomes/lysosomes. Because each rab protein isoform was analyzed individually, no specific trend was observed as to their functional role in the pathway.

In order to further explore these results, a double KD was attained, by knocking down each of these endocytic/recycling rabGTPase in the VEGFR2 KD cell line B6-#4163. sVEGF levels detected by ELISA, in the conditioned medium, revealed no significant additive effect, with the exception of Rab5b (Fig.6).

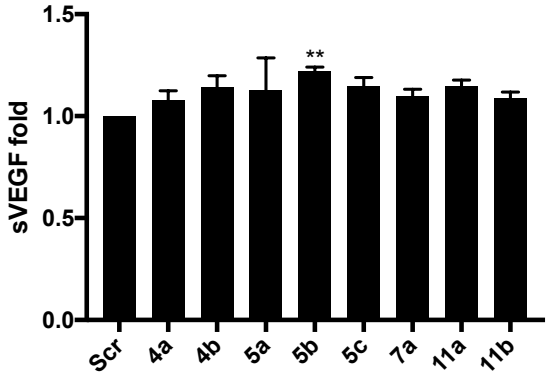

Figure 6 Knock-down of individual Rab GTPases on top of VEGFR2 KD (B6-#4163 line) increases secretion of VEGF by RPE cells. Data are expressed as fold increase of VEGF secreted by 9 x10^4 B6-#4163 cells (mean±SEM, n≥ 3). Significance was determined using One-way ANOVA. **P<0.01.

sVEGF levels measured during this experiment were notably higher (5x to 11x fold), comparing to the levels detected upon Rab KD on B6RPE07 original cell line. These large differences can be attributed to the accumulation of VEGF in the medium, since in KD experiments medium is collected ~3 days after adding the adenoviruses, and as observed previously, B6-#4163 secretes up to 3.8x fold comparing to B6 (Fig.5). As a result, the Rab knock down effect could be diluted, as it is less pronounced. Ultimately, VEGFR2 knock down is the determining factor contributing to soluble VEGF accumulation in the conditioned medium.

RPE regulates VEGF through VEGFR2 autocrine loop.

Retinal pigmented epithelium cells have been shown capable of sustaining their own basal growth by synthesizing and binding VEGF (Guerrin et al. 1995). More recently, Okabe and colleagues described retinal neurons using VEGF uptake as a means to titrate sVEGF, during development (Okabe et al. 2014). Additionally, in the mouse eye, while VEGFR2 expression is gradually decreased in the neuroretina, after 1 week post-birth(Okabe et al. 2014), VEGFR2 expression in RPE increases from postnatal days 6.5 to 8.5(Ford et al. 2011). Both these reports suggest an autocrine loop as a way of sensing VEGF through VEGFR2. In the developing retina, blood vessels grow, according to the VEGF gradient, determined first by neuronal cells and at later stages, by RPE. Loss of this VEGFR2 leads to overgrowth of blood vessels into the retina, and thus vision disturbance(Okabe et al. 2014; Ford et al. 2011). Like neuronal cells, we propose RPE to have a sensing mechanisms to titrate VEGF's availability and thus control how choroid blood vessels are limited to the outside of the RPE barrier.

Importantly, Klettner and colleagues reported that inhibition of VEGFR2 leads to a decrease of apical sVEGF(Klettner et al. 2015). VEGFR2 inhibition by SU1498, in this case, caused apical sVEGF decrease in RPE/choroid organ culture, but no effect in RPE cell culture alone. Even though our results seem contradictory, the two studies were preformed differently: on the one hand, a polarized RPE system was not used in the present study; on the other hand, the use of an RPE/choroid organ culture could be a confounding factor, since there could be paracrine regulation by choroidal endothelial cells or others (Klettner et al. 2013). Nevertheless, both studies coincide in the notion of an autocrine regulation of sVEGF, by RPE's apical expression of VEGFR2. As a future step, the present study would greatly benefit from the use of a polarized RPE system, with barrier function.

Polarized VEGF secretions is the result of apical sensing, through VEGFR2.

RPE has been shown to secrete more VEGF through its basolateral side than from the apical side(Klettner et al. 2015; Ablonczy & Crosson 2007; Ford et al. 2011). Furthermore, VEGFR2 has been shown to be expressed preferentially at the apical side of the polarized RPE monolayer((Ablonczy & Crosson 2007)).

When RPE is subjected to an increase in apical VEGF, its barrier function is compromised(Ablonczy & Crosson 2007; Dahrouj et al. 2014; Dahrouj et al. 2015). These studies suggest VEGF excess to be disruptive and possibly a trigger for RPE dismantlement. Another study, showed that VEGF neutralization causes degeneration of RPE and loss of fenestration of choriocapillaries(Ford et al. 2011).

Altogether, these studies reinforce the importance of a polarized VEGF regulation by the RPE.

By blocking endocytosis of VEGFR2, the RPE cannot sense VEGF

A recent study suggests that, for endothelial cells, if constitutive endocytosis of VEGFR2 is impaired, the receptor is cleaved at the plasma membrane, rendering less VEGF sensitivity to the cell(Basagiannis & Christoforidis 2016). One of the strategies used by these authors for the inhibition of endocytosis was the use of mutant forms of Rab5, either causing inhibition of endocytosis or retention of cargo at the early endosome. When VEGFR2 becomes trapped at the membrane, shedding occurs and thus, removal of the VEGF binding domain could cause the cell to become less sensitive to sVEGF amounts. Shedding of VEGFR2 could render RPE insensitive to sVEGF amounts and account for its increased secretion, as demonstrated in the present study. Furthermore, consequent events could trigger choroidal cells to invade the retina. In either case, VEGFR2 endocytic regulation is of utmost importance for homeostasis maintenance of the RPE and the whole visual unit.

Importance of new therapies

At the moment, there are three types of molecules being routinely used as therapeutic agents in retinal neovascular disease: 1. anti-VEGF-A antibody (bevacizumab), 2. a fragment of such an antibody (ranibizumab) or 3. an engineered protein that carries the binding domains of two VEGF

receptors, VEGFR1 and VEGFR2 (aflibercept) (Strauss 2016). In fact, anti-VEGF therapies constitute the first effective treatment for Age-related Macular Degeneration, as well as other retinal degenerative disorders. In fact, patients who receive this treatment show structural and functional retinal improvement, as measured by increased visual acuity and quality of life indices (Strauss 2016; Ford et al. 2011). Recent observations, however, raise questions about treatment efficacy after 2 years, as well as adverse effects, such as retinal tear, RPE atrophy and systemic circulation of VEGF-A neutralizing agents (Ford et al. 2011; Strauss 2016).

Although anti-VEGF therapy has been shown beneficial, it generally works to manage symptoms and disease progression, rather than treat or prevent vision loss.

By knowing more about the mechanisms by which the RPE regulates VEGF production and release, we would become more capable of interfering with it. i.e. by becoming able to target VEGFR2 function in the RPE, we can better understand disease and come up with better solutions to locally repair the damaged eye.

Cell culture

Mouse RPE cell line B6-RPE07 was kindly provided by Dr. Heping Xu (Queen's University Belfast, Ireland) (Chen et al. 2008) and cultured in Dulbecco's Modified Eagle Medium (DMEM) (Lonza) supplemented with 10% Fetal Bovine Serum (FBS) (Life Technologies), 100 U/mL penicillin and 100 µg/mL streptomycin (Life Technologies) (complete medium). Cells were maintained at a humidified cabinet at 37oC and 5% CO2.

Generation of adenoviruses

microRNA (miRNA) adenoviral constructs were engineered using an expression vector system (BLOCK-iT Pol II miR RNAi; Life Technologies) according to the manufacturer's protocol. Single-stranded oligonucleotides were designed and annealed to form an engineered pre-miRNA sequence structure that targets unique sequences in mouse Rab GTPases selected isoforms. Double-stranded oligonucleotides were cloned into pcDNA™6.2-GW/EmGFP-miR for generation of expression clones. As a negative control (miR-Negative) pcDNA™6.2-GW/EmGFP-miR-neg control plasmid (Life Technologies) was used. The resulting EmGFP-miRNA cassettes from expression constructs were subsequently cloned in the pAd/CMV/V5-DEST™ adenoviral vector (Life Technologies).

Adenoviruses were produced in a packaging cell line (293A) using ViraPower™ Adenoviral Gateway® Expression Kit; Life Technologies) according to the manufacturer's recommended protocol. Briefly, cells were transfected with 5 µg of *PacI*-digested vector using Lipofectamine 2000 as transfecting reagent (Life Technologies). Medium containing cells and mature adenoviral particles was collected when approximately 80% cytopathic effect was visible (10-13 days post-transfection). To obtain a crude viral lysate 3 cycles of freeze/thaw were performed, followed by centrifugation at 4100 g for 10 minutes to pellet cell debris. This first lysate was used to prepare re-amplifications of viral particles. The re-amplified supernatant was collected and prepared as the crude initial lysate.

Titration of adenoviral stocks was performed using B6-RPE07 cells. Cells were plated at a known density and transduced with serial dilutions of adenoviral stock. After 24 hours cells were harvested and washed in PBS/BSA 0.1%. Cell pellet was fixed in PBS/BSA 0.1%/PFA 0.4% and kept at 4oC until acquisition. The percentage of transduced cells was determined by counting GFP+ cells (total of 30000 events) using FACSCalibur (BD Biosciences). Data was analyzed with the program FlowJo (Tree Star) and the viral titer was expressed as green fluorescent units per mL (gfu/mL).

Western Blotting

Samples were mixed with Laemmli buffer in the appropriate ratio, sonicated for a few seconds, boiled for 5 minutes at 95ºC and subjected to SDS-PAGE. Polyvinylidene fluoride (PVDF) membranes were used for blotting (Immobilon, Millipore). The blots were blocked in 4% Ovalbumin/PBS-Tween20 0.02% (PBST buffer) for 60 minutes at room temperature. Primary antibodies were diluted as described in table I, in PBST.

Membranes were incubated for 60 minutes at room temperature or overnight at 4ºC. Proteins were visualized using HRP-conjugated secondary antibodies (Sigma, 1:20000) diluted in 4% nonfat dried milk/ PBS-Tween20 0.02% and ECL Plus Western Blotting Detection Reagent (GE Healthcare) in a ChemiDoc software (BioRad). Western Blot analysis was performed using Fiji software.

Table I

Antibody	Source	Catalog number	Raised in	Dilution
α-GFP	Sicgen	AB66-200	goat	1:500
α-calnexin	Sicgen	AB41-200	goat	1:2000
α-VEGF	Abcam	ab3109	mouse	1:200
α-VEGFR2	Sicgen	AB142-200	goat	1:500
α-Rab4	Sicgen	AB238239-200	goat	1:500
α-Rab5a	Sicgen	AB10-200	goat	1:500
α-Rab5b	Sicgen	AB12-200	goat	1:500
α-Rab5c	Sicgen	AB24-200	goat	1:500
α-Rab7a	Sicgen	AB33-200	goat	1:500
α-Rab11a	Sicgen	AB34a-200	goat	1:500
α-Rab11b	Sicgen	AB82-200	goat	1:500
α-actin	Sicgen	AB145-200	goat	1:2000

Real-time quantitative PCR

Total RNA was extracted using RNAse Mini kit (Qiagen) according to the manufacturer's instructions. One µg of RNA was converted into complementary DNA using random primers and SuperScript II reverse transcriptase (Life Technologies). Real-time quantitative PCR (RT-qPCR) was performed in ABI Prism 7900HT system using ABI Power SYBR Green PCR Master Mix (Applied Biosystems). Messenger RNA (mRNA) levels were normalized against actin. Results were expressed as the relative expression using the delta-delta Ct method. Experiments were performed in triplicate and results are presented as mean fold-increase ± SD.

sVEGF detection by ELISA

The concentration of secreted VEGF (sVEGF) in culture supernatant was determined quantitatively with a Quantikine ELISA kit (R&D Systems) according to the manufacturer's instructions. The capture antibody VEGF was diluted in PBS to 0.4 µg/mL and immobilized overnight in proper 96-well ELISA plates. The biotinylated detection antibody was used at a concentration of 100 ng/mL. Enzyme-catalyzed chromogen formation was quantified by measuring the visible absorbance at 45nm using a calibration curve plotted with recombinant mouse VEGF (in pg/mL, normalized to the total amount of protein). Experiments were performed at least 6 times and results are presented as mean average value ± SD. The bicinchoninic acid (BCA) colorimetric method was used for whole cell lysates proteins' quantification according to the manufacturer's instructions (Pierce). Optical density was measured at 595 nm (iMark, BioRad). RayBiotech mouse VEGF ELISA Kit (ELM-VEGF) was used in one of the experiments – rab KD in B6-#4163 cells –, and sample overlap was attained, in order to compare results from both kits. All reagents were prepared as described in the protocol. Supernatant sample dilution was 1:2. According to the instructions, optical density was measured at 450nm.

Generation of lentivirus for VEGFR2 knock down

Lentivirus were produced in a packaging cell line (STAR-Rdpro), by co-transfection of 3rd Generation Packaging System plasmids (Addgene) and pLenti/V5-GW/miR. The plasmids pMD2.G, pMDLg/pRPE and pRSV-Rev encode for more advanced packaging and envelope viral proteins and are crucial for the improvement of lentiviral stocks' quality. DNA mixture was prepared using 3ug of purified plasmid DNA of pLenti/V5-GW/miR expression construct, 1.5ug of pMD2.G, 2ug of pMDLg/pRPE and 1ug of pRSV-Rev. The DNA-liposomal complexes were set up and incubated at room temperature for 45 minutes. Transfection of confluent STAR-Rpro cells proceeded; supernatants were collected 72 hours post-transfection and centrifuged at 4100g for 10 minutes to pellet cell debris. Aliquots of viral stocks were stored at -80ºC. Two VEGFR2 knockdown B6-RPE07 cell lines were obtained: B6-#4162C28 and B6-#4163C34. Briefly, 90% confluent B6-RPE07 cells were transduced with lentiviral vectors carrying VEGFR2 miRNAs and a blasticidin resistance gene. After blasticidin selection of transduced cells, knockdown was verified by PCR and western blot.

References

Ablonczy, Z. & Crosson, C.E., 2007. VEGF modulation of retinal pigment epithelium resistance. *Experimental eye research*, 85(6), pp.762–71.

Basagiannis, D. & Christoforidis, S., 2016. Constitutive endocytosis of VEGFR2 protects the receptor against shedding. *Journal of Biological Chemistry*, 291(32), pp.16892–16903.

Chen, M. et al., 2008. Characterization of a spontaneous mouse retinal pigment epithelial cell line B6-RPE07. *Investigative ophthalmology & visual science*, 49(8), pp.3699–706.

Dahrouj, M. et al., 2015. Receptor mediated disruption of retinal pigment epithelium function in acute glycated-albumin exposure. *Experimental eye research*, 137, pp.50–6.

Dahrouj, M. et al., 2014. Vascular endothelial growth factor modulates the function of the retinal pigment epithelium in vivo. *Investigative ophthalmology & visual science*, 55(4), pp.2269–75.

Fearnley, G.W. et al., 2016. VEGF-A isoforms program differential VEGFR2 signal transduction, trafficking and proteolysis. *Biology open*, 5(5), pp.571–83.

Ford, K.M. et al., 2011. Expression and role of VEGF in the adult retinal pigment epithelium. *Investigative Ophthalmology and Visual Science*, 52(13), pp.9478–9487.

Ford, K.M. et al., 2011. Expression and role of VEGF in the adult retinal pigment epithelium. *Investigative ophthalmology & visual science*, 52(13), pp.9478–87.

Fuhrmann, S., Zou, C. & Levine, E.M., 2014. Retinal pigment epithelium development, plasticity, and tissue homeostasis. *Experimental Eye Research*, 123, pp.141–150.

Geisen, P. et al., 2006. Characterization of barrier properties and inducible VEGF expression of several types of retinal pigment epithelium in medium-term culture. *Current Eye Research*, 31(9), pp.739–48.

Gibbs, D., Kitamoto, J. & Williams, D.S., 2003. Abnormal phagocytosis by retinal pigmented epithelium that lacks myosin VIIa, the Usher syndrome 1B protein. *Proceedings of the National Academy of Sciences of the United States of America*, 100(11), pp.6481–6.

Guerrin, M. et al., 1995. VasculotropinNascular Endothelial Growth Factor Is an Autocrine Growth Factor for Human Retinal Pigment Epithelial Cells Cultured In Vitro. *Journal of cellular physiology*, 394(2), pp.385–394.

Hombrebueno, J.R. et al., 2014. Intravitreal Injection of Normal Saline Induces Retinal Degeneration in the C57BL/6J Mouse. *Translational vision science & technology*, 3(2), p.3.

Jopling, H.M. et al., 2014. Endosome-to-Plasma Membrane Recycling of VEGFR2 Receptor Tyrosine Kinase Regulates Endothelial Function and Blood Vessel Formation. *Cells*, 3(2), pp.363–85.

Jopling, H.M. et al., 2009. Rab GTPase regulation of VEGFR2 trafficking and signaling in endothelial cells. *Arteriosclerosis, thrombosis, and vascular biology*, 29(7), pp.1119–24.

Klettner, A. et al., 2015. Basal and apical regulation of VEGF-A and placenta growth factor in the RPE / choroid and primary RPE. , (July), pp.736–748.

Klettner, A. et al., 2013. Regulation of constitutive vascular endothelial growth factor secretion in retinal pigment epithelium/choroid organ cultures: p38, nuclear factor κB, and the vascular endothelial growth factor receptor-2/phosphatidylinositol 3 kinase pathway. *Molecular vision*, 19, pp.281–91.

Klettner, A.K., Doths, J. & Roider, J., 2012. Nicotine reduces VEGF-secretion and phagocytotic activity in porcine RPE. *Graefe's archive for clinical and experimental ophthalmology = Albrecht von Graefes Archiv für klinische und experimentelle Ophthalmologie*, 250(1), pp.33–8.

Lopes, V.S. et al., 2007. The ternary Rab27a-Myrip-Myosin VIIa complex regulates melanosome motility in the retinal pigment epithelium. *Traffic (Copenhagen, Denmark)*, 8(5), pp.486–99.

Lopes da Silva, M. et al., 2012. The host endocytic pathway is essential for Plasmodium berghei late liver stage development. *Traffic (Copenhagen, Denmark)*, 13(10), pp.1351–63.

Marmorstein, A.D., 2001. The polarity of the retinal pigment epithelium. *Traffic (Copenhagen, Denmark)*, 2(12), pp.867–72.

Marneros, A.G. et al., 2005. Vascular endothelial growth factor expression in the retinal pigment epithelium is essential for choriocapillaris development and visual function. *The American journal of pathology*, 167(5), pp.1451–9.

Okabe, K. et al., 2014. Neurons limit angiogenesis by titrating VEGF in retina. *Cell*, 159(3), pp.584–96.

Penn, J.S. et al., 2008. Vascular endothelial growth factor in eye disease. *Progress in retinal and eye research*, 27(4), pp.331–71.

Rattner, A. & Nathans, J., 2006. Macular degeneration: recent advances and therapeutic opportunities. *Nature reviews. Neuroscience*, 7(11), pp.860–72.

Stone, E.M., 2007. Macular Degeneration. *Annual Review of Medicine*, 58(1), pp.477–490.

Strauss, O., 2016. Pharmacology of the retinal pigment epithelium, the interface between retina and body system. *European Journal of Pharmacology*, 787, pp.84–93.

Strauss, O., 2005. The retinal pigment epithelium in visual function. *Physiological reviews*, 85(3), pp.845–81.

Sung, C.H. & Chuang, J.Z., 2010. The cell biology of vision. *Journal of Cell Biology*, 190(6), pp.953–963.

Wang, H. et al., 2011. The role of RPE cell-associated $VEGF_{189}$ in choroidal endothelial cell transmigration across the RPE. *Investigative ophthalmology & visual science*, 52(1), pp.570–8.